Neural Plasticity

Understanding Neuromuscular System Plasticity to Improve Motor Function in Health, Disease, and Injury

Guest Editors: Guang H. Yue, Brian C. Clark, Sheng Li, and David E. Vaillancourt

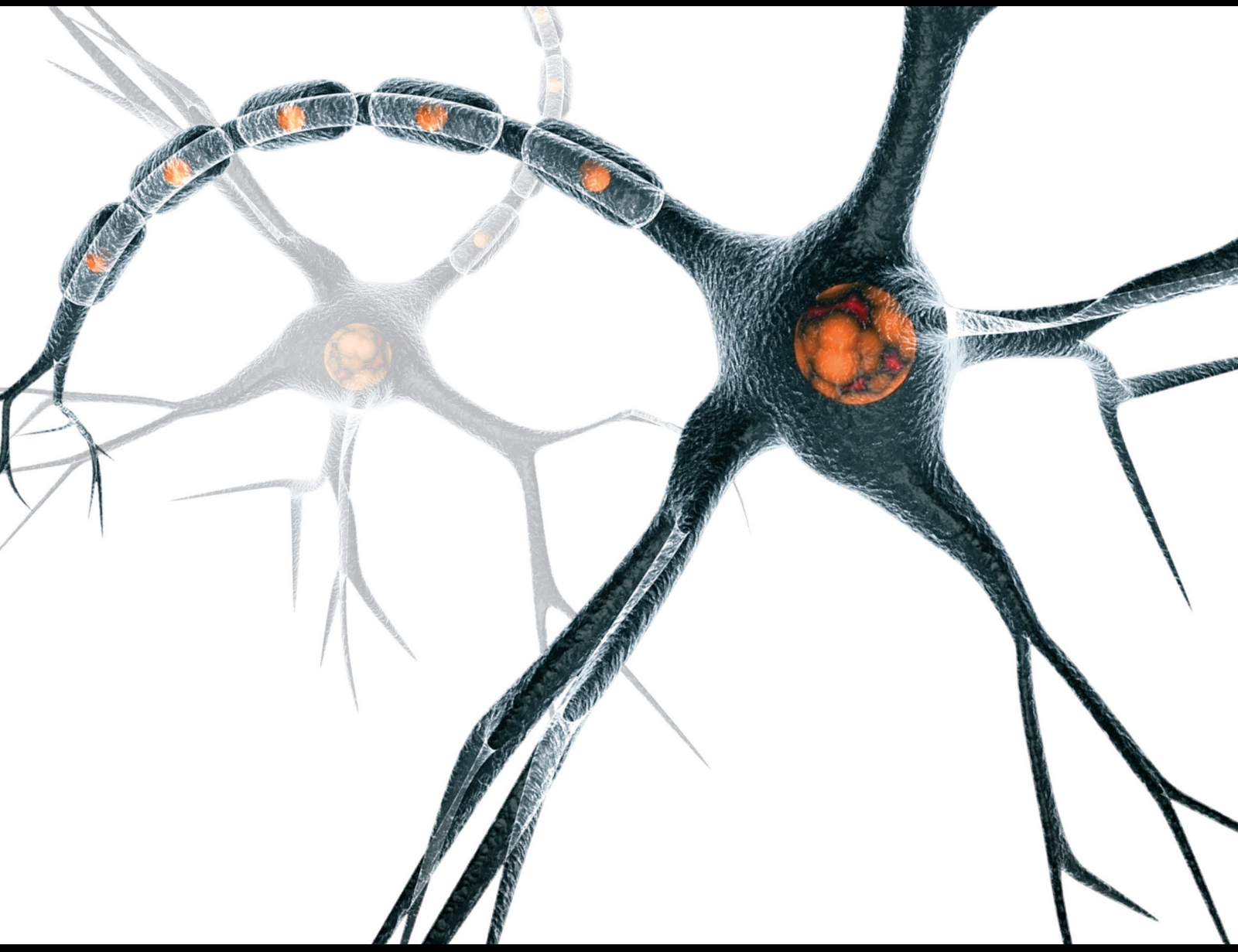

Understanding Neuromuscular System Plasticity to Improve Motor Function in Health, Disease, and Injury

Neural Plasticity

Understanding Neuromuscular System Plasticity to Improve Motor Function in Health, Disease, and Injury

Guest Editors: Guang H. Yue, Brian C. Clark, Sheng Li, and David E. Vaillancourt

Editorial Board

Contents

Understanding Neuromuscular System Plasticity to Improve Motor Function in Health, Disease, and Injury
Guang H. Yue, Brian C. Clark, Sheng Li, and David E. Vaillancourt
Volume 2017, Article ID 2425180, 2 pages

Navigated Transcranial Magnetic Stimulation: A Biologically Based Assay of Lower Extremity Impairment and Gait Velocity
Heather T. Peters, Kari Dunning, Samir Belagaje, Brett M. Kissela, Jun Ying, Jarmo Laine, and Stephen J. Page
Volume 2017, Article ID 6971206, 7 pages

Scale-Dependent Signal Identification in Low-Dimensional Subspace: Motor Imagery Task Classification
Qingshan She, Haitao Gan, Yuliang Ma, Zhizeng Luo,
Tom Potter, and Yingchun Zhang
Volume 2016, Article ID 7431012, 15 pages

EEG Source Imaging Guided by Spatiotemporal Specific fMRI: Toward an Understanding of Dynamic Cognitive Processes
Thinh Nguyen, Thomas Potter, Trac Nguyen,
Christof Karmonik, Robert Grossman, and Yingchun Zhang
Volume 2016, Article ID 4182483, 10 pages

Effects of a Single Session of High Intensity Interval Treadmill Training on Corticomotor Excitability following Stroke: Implications for Therapy
Sangeetha Madhavan, James W. Stinear, and Neeta Kanekar
Volume 2016, Article ID 1686414, 8 pages

Kinematic and EMG Responses to Pelvis and Leg Assistance Force during Treadmill Walking in Children with Cerebral Palsy
Ming Wu, Janis Kim, Pooja Arora, Deborah J. Gaebler-Spira, and Yunhui Zhang
Volume 2016, Article ID 5020348, 12 pages

Progressive FastICA Peel-Off and Convolution Kernel Compensation Demonstrate High Agreement for High Density Surface EMG Decomposition
Maoqi Chen, Ales Holobar, Xu Zhang, and Ping Zhou
Volume 2016, Article ID 3489540, 5 pages

Mirror Visual Feedback Training Improves Intermanual Transfer in a Sport-Specific Task: A Comparison between Different Skill Levels
Fabian Steinberg, Nils Henrik Pixa, and Michael Doppelmayr
Volume 2016, Article ID 8628039, 11 pages

Neuromuscular Plasticity: Disentangling Stable and Variable Motor Maps in the Human Sensorimotor Cortex
Dominic Kraus and Alireza Gharabaghi
Volume 2016, Article ID 7365609, 13 pages

Hindawi
Neural Plasticity
Volume 2017, Article ID 2425180, 2 pages
http://dx.doi.org/10.1155/2017/2425180

Editorial

Understanding Neuromuscular System Plasticity to Improve Motor Function in Health, Disease, and Injury

Guang H. Yue,[1] Brian C. Clark,[2] Sheng Li,[3] and David E. Vaillancourt[4]

[1]*Kessler Foundation and Rutgers University, West Orange, NJ, USA*
[2]*Ohio Musculoskeletal and Neurological Institute (OMNI), Ohio University, Athens, OH, USA*
[3]*Department of Physical Medicine and Rehabilitation, University of Texas Health Sciences Center at Houston, Houston, TX, USA*
[4]*Department of Applied Physiology and Kinesiology, University of Florida, Gainesville, FL, USA*

Correspondence should be addressed to Guang H. Yue; gyue@kesslerfoundation.org

Received 21 December 2016; Accepted 22 December 2016; Published 2 March 2017

Disease or injury of motor system components often leads to motor dysfunction, and the success of medical intervention, motor skill learning, exercise, or sports training is linked to plasticity in the neuromuscular system at both the central and peripheral levels. However, the neuroplasticity mechanisms underlying the therapeutic efficacy of motor function rehabilitation, exercise training, or motor learning on the neuromuscular system are not well understood. The lack of knowledge on plasticity at various levels of the central and peripheral motor systems, including the muscle, limits a good understanding of neural mechanisms provoking movement disorders and their recovery and hinders development of targeted therapies for effective treatment. In addition, understanding neuroplasticity linked to motor learning may help identify practice strategies to maximize the progressive plasticity and relearning of motor skills. In the field of sports training, profound insights into plasticity of the neuromuscular system may help develop unique training regimes to aid athletes reach their maximal potential and at the same time prevent injury. The special issue in this journal solicited high quality, original research articles as well as review articles focused on plasticity of central and/or peripheral motor systems, including the muscular system as a result of motor system disease, injury, and rehabilitation; motor skill learning; and exercise or sports training. Approximately half of the articles in this issue center on the development of new methodologies to evaluate neuroplasticity. More specifically, Q. She and colleagues report a novel method to identify classes of electroencephalography (EEG) signals during different motor imagery tasks, while T. Nguyen and colleagues report a novel multimodal EEG/MRI integration method to achieve high spatiotemporal accuracy. M. Chen and colleagues report that a novel progressive FastICA peel-off (PFP) framework technique for decomposing high density surface EMG signals into different motor units yields a high degree of agreement with the more common convolution kernel compensation (CKC) method, and they suggest that combination of the two methods may have the potential to further increase the decomposition yield. D. Kraus and A. Gharabaghi describe a novel projection, interpolation, and coregistration technique, which considers the individual gyral anatomy, to acquire TMS motor maps that demonstrated long-term, high test-retest reliability. Lastly, H. Peters and colleagues utilized transcranial magnetic stimulation to elicit motor evoked potentials (MEPs) from tibialis anterior and soleus muscles of thirty-five chronic stroke patients with lower extremity hemiparesis and observed that a prolonged MEP latency was associated with reduced lower extremity physical function. As such, they suggest that MEP latency could serve as a stroke-related biomarker.

The other articles center on interventional strategies to promote neuromuscular system plasticity. Here, S. Madhavan and colleagues report that a single session of high-intensity interval treadmill exercise suppresses corticomotor excitability in the paretic muscles of some (~65%) chronic stroke survivors and that when this exercise is preceded by

transcranial direct current stimulation in combination with a skill acquisition task, the asymmetry of between-hemisphere corticomotor excitability is reduced. M. Wu and colleagues report data suggesting that improved weight shifting induced by robotically applied pelvis assistance force during stance may facilitate stepping in children with cerebral palsy (CP) and that applying large leg swing assistance force during treadmill training may reduce the active participation of children with CP. Lastly, F. Steinberg and colleagues report data suggesting that mirror visual feedback facilitates intermanual transfer effects in sport, but only for participants that had experience with the movements being performed. As such, they introduce and discuss the role of skill level and task complexity in the field of mirror visual feedback.

Collectively, we hope this series of articles will, in the long term, help to advance our understanding of neural mechanisms (plasticity) of motor function disorders and will facilitate the development of targeted therapies to maximize the plasticity for effective treatment, leading to fast recovery of motor function.

Guang H. Yue
Brian C. Clark
Sheng Li
David E. Vaillancourt

Hindawi Publishing Corporation
Neural Plasticity
Volume 2017, Article ID 6971206, 7 pages
http://dx.doi.org/10.1155/2017/6971206

Research Article

Navigated Transcranial Magnetic Stimulation: A Biologically Based Assay of Lower Extremity Impairment and Gait Velocity

Heather T. Peters,[1,2] Kari Dunning,[3] Samir Belagaje,[4] Brett M. Kissela,[3] Jun Ying,[3] Jarmo Laine,[5] and Stephen J. Page[1,2]

[1]*Division of Occupational Therapy, The Ohio State University, Columbus, OH, USA*
[2]*B.R.A.I.N. (Better Rehabilitation and Assessment for Improved Neuro-recovery) Laboratory, Ohio State University, Columbus, OH, USA*
[3]*The University of Cincinnati, Cincinnati, OH, USA*
[4]*Department of Neurology, Emory University School of Medicine, Atlanta, GA, USA*
[5]*Nexstim, Ltd., Helsinki, Finland*

Correspondence should be addressed to Heather T. Peters; heather.tanksley@osumc.edu

Received 29 December 2015; Revised 10 October 2016; Accepted 6 December 2016; Published 24 January 2017

Academic Editor: Guang H. Yue

Objectives. (a) To determine associations among motor evoked potential (MEP) amplitude, MEP latency, lower extremity (LE) impairment, and gait velocity and (b) determine the association between the presence of a detectable MEP signal with LE impairment and with gait velocity. *Method*. 35 subjects with chronic, stable LE hemiparesis were undergone TMS, the LE section of the Fugl-Meyer Impairment Scale (LE FM), and 10-meter walk test. We recorded presence, amplitude, and latency of MEPs in the affected tibialis anterior (TA) and soleus (SO). *Results*. MEP presence was associated with higher LEFM scores in both the TA and SO. MEP latency was larger in subjects with lower LEFM and difficulty walking. *Conclusion*. MEP latency appears to be an indicator of LE impairment and gait. *Significance*. Our results support the precept of using TMS, particularly MEP latency, as an adjunctive LE outcome measurement and prognostic technique.

1. Introduction

Two-thirds of the growing stroke survivor population exhibits significantly diminished walking ability [1, 2], making walking retraining a major focus of stroke rehabilitation [3, 4]. Precise measurement of deficits is fundamental to characterizing patients' impairment and to planning cost effective, appropriate, lower extremity (LE) interventions [5]. Consequently, a variety of behavioral measures are deployed to quantify paretic LE outcomes [6–8].

Clinical assessment tools (e.g., Timed Up and Go and Dynamic Gait Index) provide clinicians with valuable insight into patients' ambulatory independence, which greatly influences the course and content of rehabilitative therapies. However, outcomes from such performance-based assessments are associated with extraneous (e.g., fear of falling [9, 10]) and/or peripheral variables (e.g., osteoarthritis [11]; diminished cardiorespiratory fitness [12, 13]), which can raise the likelihood of Type I and Type II errors. These instruments are also limited in that they are subjective and do not provide direct insight into central nervous system (CNS) response to restorative approaches, that is, a limitation, given that insufficient activation of the LE musculature is the primary impairment underlying walking deficits after stroke [14].

Volitional ambulation is activated by neural impulses travelling primarily via the corticospinal tract (CST) [15]. These descending CST pathways transmit signals primarily to the contralateral extremities, with a small percentage of signals transmitted ipsilaterally [16]. Poststroke motor evoked potentials (MEPs) reflect excitability of the lesioned areas, alterations in interhemispheric communication, and

resultant CST activity [17]. The presence of MEPs from upper extremity muscles is associated with a more favorable prognosis after stroke [18, 19], while MEP amplitude is correlated with upper extremity impairment [20]. MEPs have likewise been advocated as a biological method for measuring and predicting poststroke ambulation changes [21–23]. However, associations between MEPs and LE outcomes have not been investigated in stroke, aside from one case report during the acute phase [18, 20, 24], when considerable spontaneous recovery and multiple interventions are cooccurring.

Given the increasing prevalence of stroke survivors and diminishing length of stays in rehabilitative settings, assessment methods to direct LE treatment must be optimized. Could MEPs constitute a biologically based, objective, method to address this need? Our overall objective was to examine the association of MEPs with LE outcomes in a well-defined cohort of chronic, stable, stroke survivors. To accomplish this objective, the study had two primary aims: (1) to determine associations among tibialis anterior (TA) and soleus (SO) MEP characteristics (amplitude and latency) and scores on clinical measures; (2) to determine associations among the presence of a detectable MEP signal and scores on clinical measures. Within these two primary aims, we specifically examined the following associations: (a) TA and SO MEP amplitude/latency and scores on the LE FM; (b) TA and SO MEP amplitude/latency and gait; (c) presence of a MEP response and LE FM scores; and (d) presence of a MEP response and gait. To our knowledge, this was the first study to extensively examine MEPs as a measure of LE outcomes after stroke, as well as being one of the first studies to use navigated TMS in either the paretic upper or lower extremities to associate MEP presence with outcomes.

2. Methods

2.1. Subjects. Volunteers were recruited directly from local stroke support groups and by using advertisements placed in local outpatient stroke clinics. After signing an approved consent form, the following study criteria were applied to volunteers expressing interest in the study: *Inclusion criteria* were as follows: (a) ≥20 years of age; (b) unilateral stroke experienced ≥ 4 months prior to study enrollment, occurring in middle cerebral artery (MCA) territory involving the motor cortex (cortical stroke) or/and its corticospinal projections (subcortical stroke); (c) no other known brain abnormalities by history or by structural MRI. *Exclusion criteria* were as follows: (a) contraindications to neuroimaging as described in detail elsewhere [25] (e.g., seizure history; pregnancy; metal in head; implanted medical devices); (b) history of alcohol abuse and/or drug use; (c) history of mental illness; (d) personal or family history of epilepsy; (e) hypertensive or hypotensive condition; (f) any condition that would prevent the subject from giving voluntary informed consent; (g) taking any medication that interferes with the TMS measures; (h) enrolled in an interventional trial during this study; (i) a fixed contraction deformity in the paretic LE; (j) excessive spasticity in any joint of the affected LE as indicated by the Modified Ashworth Spasticity (MAS) Scale ≥ 2.

2.2. Instruments. Given that LE impairment was the primary study outcome, the primary outcome measure was the LE section of the *Fugl-Meyer Impairment Scale (FM)* [6]. The FM has a maximum score of 34, with individual items examining paretic LE reflexes, isolated movement at joints in the paretic LE, and speed of movement. Thus, the FM enabled our team to examine the influence of the CST on LE active movement in an iterative, quantified, way.

We also wished to determine whether isolated movements activated primarily by the CST affected functional outcomes. Gait velocity is a reliable, valid, and sensitive measure of poststroke mobility and function [26] that is highly correlated with recovery and independence [27]. Thus, we measured gait velocity during a *10-meter walk test*, administered at both a self-selected and fast speed. The 10-meter walk test is a commonly used measure of gait velocity and has shown excellent reliability [28] and validity [29] in the poststroke population. Gait velocity was assessed in a subset of our sample ($n = 26$) that could ambulate safely without use of an ankle foot orthosis (AFO) or adaptive equipment (e.g., a cane or walker), enabling more pure assessment of the association between CST integrity and ambulation without the mitigating impact of extraneous assistance. Difficulty to walk was a binary variable defined as those subjects who reported being unable to walk without AFO or had self-selected gait speed <60 cm/sec or had fast gait speed <80 cm/sec.

2.3. Testing Procedures. To obtain MEPs, transcranial magnetic stimulation (TMS) was used. Conventionally, TMS has consisted of applying an electromagnetic field to a particular cortical area believed to control a certain function (for a review see ref. [30]). However, a common challenge associated with conventional TMS is identifying the proper stimulation site on the cortex, as one must do so based on landmarks on the head and estimation of normal brain topography. Unlike the upper extremity representation, LE cortical representations are buried deep in the junction of central sulcus and longitudinal fissure and the variability of individual cortical gyri is considerable. Since the distance from coil to target LE representation is also larger than that of hand motor representations, optimal stimulation of LE cortex may also be challenging to estimate, in particular in patients with compromised function due to lesions such as stroke. Navigated brain stimulation (NBS) integrates a particular patient's brain MRI into his/her stimulation procedures. The MRI essentially acts as a "map," enabling real-time location of where the magnetic coil is located and the area being stimulated (Figure 1).

In the current study (and consistent with the above), a high-resolution 3-dimensional, T1 weighted MRI was first obtained for each subject's brain to use with the navigation system (Nexstim eXimia). Next, we performed each subject's brain to head coregistration by identifying 3 landmarks on the MRI (the tragus of the right and left ears; the bridge of

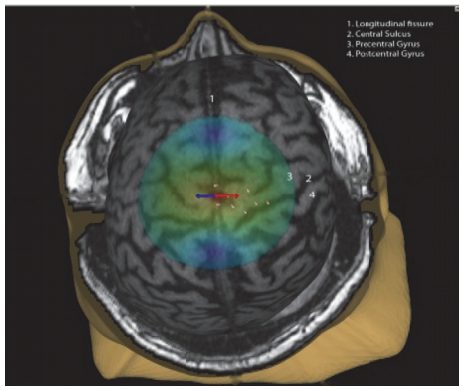

Figure 1: Example image obtained during stimulation of the paretic lower extremity cortical areas.

the nose) and marking them on the subject's head using a digitizing stylus.

TMS was applied through a figure-of-eight coil that was 70 mm in diameter (eXimia 3.2. stimulator, Helsinki, Finland). The motor threshold (MT) was defined as the lowest stimulation strength (in V/m) and in stimulator output (%) to produce a response of greater than 50 μV in the paretic abductor pollicis brevis muscle (APB) and to locate the central sulcus functionally. This information was used as a basis for LE mapping. Specifically, the TA and SO located near the central fissure were identified on each subject's brain and stimulated first with 110% of APB MT +20 V/m stimulation intensity at rest. This intensity was chosen as a starting point as it has been shown to be sufficient to elicit LE MEPs in healthy subjects [31]. Coil orientation was based on previous work by Groppa and colleagues [21] stating that coil placement should be perpendicular to the longitudinal fissure at the junction of central sulcus and central fissure with the coil angled to induce coronally oriented left-to-right current flow for the right LE or right-to-left current flow for the left LE. Stimulation was continued by following the longitudinal fissure 2 cm anteriorly and 2 cm posteriorly in steps with 2-3 mm spacing. Stimulation was also performed perpendicular to the uppermost part of central sulcus, 3 cm from the longitudinal fissure. If there was a positive muscle response during any of these attempts, the intensity was lowered −10 V/m until the response was 100–600 uV and the muscle (TA or SO) was mapped. If there was no response, the subject was asked to actively move the muscle (TA or SO). Intensity was increased in steps of +10 V/m until a 100–600 uV response was obtained or the maximum output of the stimulator was reached and the muscle (TA or SO) was mapped.

Presence of MEP responses in TA and SO muscles was tested and recorded for all locations. When the stimulation of the primary motor cortex (M1) of the affected hemisphere did not elicit a discernible, reproducible, MEP amplitude in at least five out of ten stimulations at any location, this was considered "no response" (coded as MEP response = 0). When the stimulation of the M1 of the affected hemisphere at a specific location elicited a discernible MEP amplitude in at least five out of ten stimulations, it was considered a "response" (coded as MEP response = 1). The latency was defined as the time from the onset of stimulus to the onset of MEP. For subjects with a MEP response, the peak-to-peak amplitude was measured. The average of amplitudes (or latencies) from observed trials was obtained as the outcome measure for each subject with response to a targeted TA (or SO) muscle. As an alternative method, the maximum of amplitudes (or its corresponded latency) was also considered as the outcome measure for the study.

2.4. Data Analyses. The binary measure of MEP response was compared of rates between affected side and unaffected side using McNemar's test. For numerical outcome measures of amplitude (AMP) and latency (LAT), they were log-transformed to correct right skewness before formal analysis. Log-transformed variables (called Ln_AMP and LN_LAT) were then compared between affected and healthy sides using a mixed effect model, after correcting for within person correlation using a random effect. For the affected TA and SO, mean LEFM score was compared between subjects with and without MEP responses using a two-sample t-test, and the rates of difficulty to walk were compared between groups using a Chi-square test. The Ln_AMP and Ln_LAT were assessed of their relationships to LEFM score using Pearson's correlation coefficients and compared of means between subjects with and without having difficulty to walk using two-sample t-tests.

The aforementioned unadjusted analyses were then repeated using multivariate mixed effect models to investigate the between-group means after adjusting for controlling covariates, such as age, gender, and duration of stroke. Results from both unadjusted and adjusted analyses were reported in this paper. The study also provided analyses on AMP and LAT measures using the maximum methods. Those results were not reported as the findings were consistent to the current (averaged AMP and LAT) method.

All statistical methods were performed using SAS 9.4 software (SAS, Cary, NC). p values < 0.05 were considered statistically significant.

3. Results

3.1. Subject Demographics. Using the aforementioned study criteria, 35 subjects were included (demographics depicted in Table 1).

3.2. Outcomes. As shown in Table 2, while the TMS input parameters stimulation intensity and electronic field (EF) were the same between affected and unaffected sides, MEP response rates were different. The affected side had significantly lower response compared to the unaffected side for both TA and SO. Among subjects with MEP responses, latency was longer (larger) in the affected side versus the unaffected side.

Table 3 shows that subjects with no MEP response in the affected side had lower LEFM scores in both TA and SO and they were more likely to have difficulty with walking.

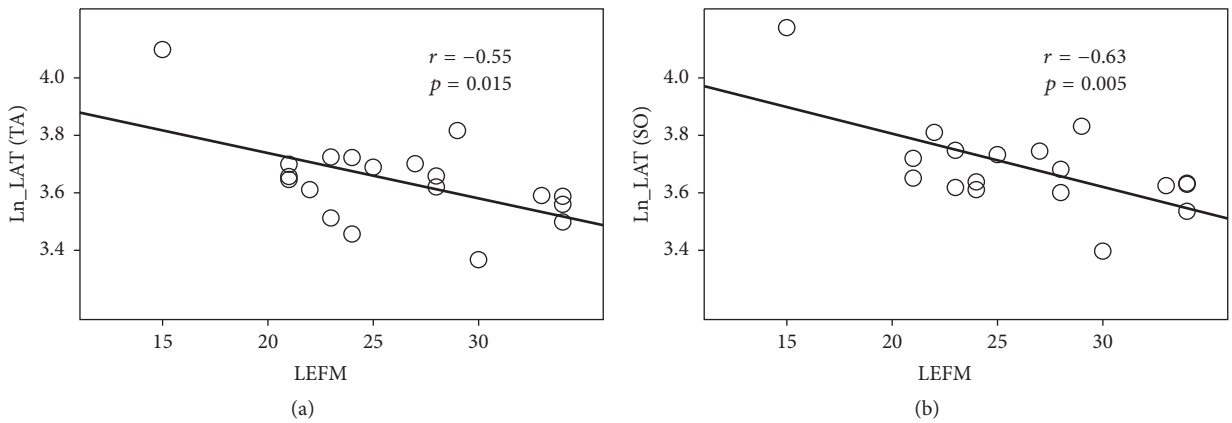

Figure 2: Plot of latency versus LEFM for SO and TA (Ln_LAT versus LEFM score). (a) Ln_LAT at TA. (b) Ln_LAT at SO.

Table 1: Summary of demographics and baseline characteristics ($N = 35$).

Variable	Category	Statistics
Age[†]		61.6 ± 8.2
Gender	Male[‡]	23 (65.7%)
Time after stroke (months)[†]		36 (2,332)[$]
Dominant_hand	Right[‡]	23 (64.7%)
Affected_side	Right[‡]	19 (54.3%)
Gait speed (cm/sec) without AFO (self-selected)	Able[‡*]	26 (74.3%)
	Speed[†] ($n = 26$)	81.6 ± 39.8
Gait speed (cm/sec) without AFO (fast)	Able[‡*]	25 (71.4%)
	Speed[†] ($n = 25$)	109.2 ± 49.5
Difficulty to walk	Yes[‡**]	16 (45.7%)
LEFM total[†]		23.5 ± 5.9

[†]Values in cells are median (range).
[‡]Values in cells are frequency (in %).
[*]"Able" to walk without AFO was self reported. Subjects were asked if they felt comfortable walking without the AFO. Gait speed without AFO was tested only for subjects who reported they felt comfortable ($n = 26$ were able to walk without AFO at self selected and $n = 25$ at fast speed).
[**]Difficulty to Walk is defined as "Yes" if a person reported not able to walk at either self or fast speed, or was observed below 60 at self-speed or below 80 at fast speed.
LEFM = Lower extremity Fugl Meyer
[$]Value in cell is median (min, max).

Table 2: TMS parameters on affected and healthy sides.

Variable	Affected side	Healthy side	p value
TA			
MEP[†]	19 (54.3%)	31 (88.6%)	0.003
Ln_AMP[‡]	4.85 ± 0.13 (4.87 ± 0.16)	5.38 ± 0.14 (5.39 ± 0.13)	0.035 (0.009)
Ln_LAT[‡]	3.64 ± 0.04 (3.63 ± 0.03)	3.54 ± 0.02 (3.53 ± 0.02)	0.011 (0.014)
SO			
MEP[†]	18 (51.4%)	30 (85.7%)	0.001
Ln_AMP[‡]	5.07 ± 0.18 (5.05 ± 0.17)	5.32 ± 0.13 (5.31 ± 0.14)	0.274 (0.214)
Ln_LAT[‡]	3.69 ± 0.04 (3.68 ± 0.03)	3.57 ± 0.02 (3.56 ± 0.02)	0.028 (0.002)

[†]Values in cells are frequency (in %); the p value is from McNemar's test.
[‡]Values in cells are mean ± standard error (SE) of log-transformed variables, based upon MEP response patients only. Values in parentheses are mean ± SE from multivariate mixed effect models after adjusting for age, gender, and duration of stroke.

As shown in Figure 2, latency was negatively related to LEFM score.

4. Discussion

Outcome measures quantifying poststroke LE impairments are vital to prescribing and gauging response to rehabilitation. To move toward the possibility of applying TMS as an adjunctive or stand-alone LE outcome measurement technique, the primary study objective was to examine associations among MEPs (specifically amplitude and latency) with LE impairment and with gait. Our data suggested that MEP latency is associated with both LE impairment and gait, whereas MEP amplitude was not associated with either metric. This may suggest that a less impaired subject would take a shorter amount of time to reach the amplitude peak, whereas MEPs in a more impaired subject would take a greater amount of time to reach such a peak. Introduced in 1975, the FM is the most established, and one of the most frequently used, instruments in neurorehabilitation. The high degree of agreement between MEP latency and this well-recognized measure supports the precept of using MEP latency as a surrogate LE outcome, per our overall objective. In contrast, the negative findings with regard to MEP amplitude were somewhat unsurprising given that MEP amplitudes have been found unreliable in smaller studies of healthy subjects [32] and in the lesioned hemispheres of chronic stroke subjects when the LE was stimulated [33]. Our results were also unsurprising given the nature of the measures to which MEP outcomes were being compared. As stated earlier, gait velocity can be confounded by a number of extraneous factors such as the patient's fear of falling,

Table 3: LEFM and difficulty to walk versus MEP response.

Variable	TA					SO				
	MEP response		Non-MEP response		p	MEP response		Non-MEP response		p
	N	Statistics†	N	Statistics†		N	Statistics†	N	Statistics†	
LEFM_Total	19	26.45 ± 1.17 (26.80 ± 1.15)	16	20.31 ± 1.30 (20.96 ± 1.31)	0.002 (0.002)	18	26.74 ± 1.18 (26.99 ± 1.16)	17	20.35 ± 1.24 (21.02 ± 1.27)	0.001 (0.001)
Difficulty to walk	19	26.3%	16	68.8%	0.012	18	22.2%	17	70.6%	0.004
Age	19	61.45 ± 2.22	16	62.13 ± 1.38	0.735	18	61.95 ± 2.28	17	61.53 ± 1.43	0.962

†Values in cells are mean ± SE for numerical variables and percentage for the binary variable. Values in parentheses are mean ± SE from multivariate fixed effect models after adjusting for age, gender, and duration of stroke.

strength, and range of motion of the affected extremity. In contrast, LE impairment is a rather pure measure in that it mostly reflects isolated movement of the extremity at targeted joints and is relatively less subject to extraneous factors. One would expect that this movement-based measure would be more closely associated with the activation of the networks modulating this movement. Although convincing and well founded, our findings with regard to MEPs need to be confirmed in a larger sample of subjects.

Our results also showed a direct relationship between the presence of MEPs and impairment as measured by the FM. Corroborating findings have been reported in other studies using nonnavigated TMS techniques. Most notably, Hendricks and colleagues [18] also examined the relationship between the presence of TA MEPs to LE FM scores in subacute stroke, reporting a positive odds ratio of 18 when MEPs were elicited. Although the result was similar to ours, the difference in the magnitude of the results between that study and ours may be related to the subjects' chronicity. Other prospective studies have similarly demonstrated that the presence of MEPs is predictive of LE movement, function [34], and dependence [35], providing additional support for the findings reported herein and impetus for their clinical implementation. While data from the first aim speak to the use of MEP latency as a viable outcome measure, findings from this second aim suggest that the presence of MEPs may offer prognostic value in terms of LE impairment. Taken together, these data provide credence to the notion that MEPs, measured as either the presence of a MEP or by MEP latency, could be coadministered with (or used instead of) impairment-based measures for the LE.

Although not a primary study aim, we also monitored the rate of MEP response in the less affected versus affected brain hemispheres. In the less affected hemisphere, MEP responses were obtained in 88.6% and 85.7% of subjects in the TA and SO, respectively. In contrast, MEP responses were obtained in 54.3% and 51.4% of subjects in the TA and SO, respectively, in the affected hemisphere. These differences were also unsurprising given outcomes of previous work comparing MEPs in the two hemispheres [33]. From a mechanistic standpoint, the differences between the affected and unaffected hemispheres are explainable, given that direct damage to cortical and subcortical neurons would be expected to cause less neuronal firing and, thus, smaller MEP amplitudes on the affected side. Similarly, longer latencies in the affected hemisphere would also be likely to occur due to a decrease in the amount of descending volleys with a subsequently longer period of time required to bring alpha motor neurons to firing threshold.

Stimulating the LE motor cortex accurately is a technically difficult undertaking. By the nature of its location on the homunculus, the LE representation is challenging to reach with a stimulation coil. Navigated TMS may, thus, be advantageous in identifying and stimulating the LE representation, possibly leading to a higher response rate than nonnavigated stimulation and enhanced ability to collect valuable prognostic and outcome data. Our data on responses in the affected and unaffected hemispheres provide preliminary support for this assertion: whereas a recent study using nonnavigated TMS in chronic stroke [36] reported that only 21% of subjects exhibited TA MEPs in the affected hemisphere, ours showed a substantially higher proportion of subjects using navigated TMS. Admittedly, though, this assertion still needs to be confirmed with larger samples. Future researchers may also wish to examine the associations of the MEPs of other LE muscles with impairment and velocity.

5. Conclusion

This constitutes the largest poststroke LE MEP study to date, the largest LE study to use navigated TMS, the first to examine associations between LE MEPs and established LE outcomes, and the first to report the parameters of the soleus muscle. The sample size was relatively small, which constitutes a possible study limitation. However this limitation is mitigated by the fact that the sample was well defined (due to relatively stringent study criteria). The contaminating effects of concurrent therapies or medications were taken into account by the study criteria. Moreover, subjects were in the chronic stage, meaning that no spontaneous recovery was occurring. Given these factors and the corroborating results of other studies, it is likely that our findings are valid, and they lay the basis for future work, including interventional studies that examine how MEPs are modulated by active therapy conditions and how these changes conspire with other outcomes to increase independence and quality of life.

Competing Interests

The authors certify that no party having a direct interest in the results of the research supporting this article has or will

confer a benefit on them or on any organization with which they are associated and, if applicable, certify that all financial and material support for this research (e.g., NIH or NHS grants) and work are clearly identified in the title page of the manuscript. The authors declare that there are no competing interests regarding the publication of this article.

Acknowledgments

This work was supported by grants from Nexstim, Ltd., the Drake Center Foundation, and the National Institutes of Health (R01AT004454-04; R03 HD062545-02).

References

[1] H. S. Jørgensen, H. Nakayama, H. O. Raaschou, and T. S. Olsen, "Recovery of walking function in stroke patients: the copenhagen stroke study," *Archives of Physical Medicine and Rehabilitation*, vol. 76, no. 1, pp. 27–32, 1995.

[2] D. T. Wade, V. A. Wood, A. Heller, J. Maggs, and R. Langton Hewer, "Walking after stroke. Measurement and recovery over the first 3 months," *Scandinavian Journal of Rehabilitation Medicine*, vol. 19, no. 1, pp. 25–30, 1987.

[3] R. B. Shepherd, "Exercise and training to optimize functional motor performance in stroke: driving neural reorganization?" *Neural Plasticity*, vol. 8, no. 1-2, pp. 121–129, 2001.

[4] K.-H. Mauritz, "Gait training in hemiplegia," *European Journal of Neurology*, vol. 9, supplement 1, pp. 23–29, 2002.

[5] M. K. Holden, K. M. Gill, M. R. Magliozzi, J. Nathan, and L. Piehl-Baker, "Clinical gait assessment in the neurologically impaired. Reliability and meaningfulness," *Physical Therapy*, vol. 64, no. 1, pp. 35–40, 1984.

[6] D. Podsiadlo and S. Richardson, "The timed 'Up & Go': a test of basic functional mobility for frail elderly persons," *Journal of the American Geriatrics Society*, vol. 39, no. 2, pp. 142–148, 1991.

[7] A. R. Fugl Meyer, L. Jaasko, and I. Leyman, "The post stroke hemiplegic patient. I. A method for evaluation of physical performance," *Scandinavian Journal of Rehabilitation Medicine*, vol. 7, no. 1, pp. 13–31, 1975.

[8] K. Berg, S. Wood-Dauphinee, J. I. Williams, and D. Gayton, "Measuring balance in the elderly: preliminary development of an instrument," *Physiotherapy Canada*, vol. 41, no. 6, pp. 304–311, 1989.

[9] J. Y. Lim, S. H. Jung, W.-S. Kim, and N.-J. Paik, "Incidence and risk factors of poststroke falls after discharge from inpatient rehabilitation," *PM&R*, vol. 4, no. 12, pp. 945–953, 2012.

[10] Å. G. Andersson, K. Kamwendo, and P. Appelros, "Fear of falling in stroke patients: relationship with previous falls and functional characteristics," *International Journal of Rehabilitation Research*, vol. 31, no. 3, pp. 261–264, 2008.

[11] P. Doruk, "The impact of knee osteoarthritis on rehabilitation outcomes in hemiparetic stroke patients," *Journal of Back and Musculoskeletal Rehabilitation*, vol. 26, no. 2, pp. 207–211, 2013.

[12] J. W. Gersten and W. Orr, "External work of walking in hemiparetic patients," *Scandinavian Journal of Rehabilitation Medicine*, vol. 3, no. 1, pp. 85–88, 1971.

[13] J. W. Gersten and W. Orr, "External work of walking in hemiparetic patients," *Scandinavian Journal of Rehabilitation Medicine*, vol. 3, no. 1, pp. 38–88, 1971.

[14] S. Mulroy, J. Gronley, W. Weiss, C. Newsam, and J. Perry, "Use of cluster analysis for gait pattern classification of patients in the early and late recovery phases following stroke," *Gait and Posture*, vol. 18, no. 1, pp. 114–125, 2003.

[15] D. Barthélemy, M. J. Grey, J. B. Nielsen, and L. Bouyer, "Involvement of the corticospinal tract in the control of human gait," *Progress in Brain Research*, vol. 192, pp. 181–197, 2011.

[16] H. Blumenfeld, *Corticospinal Tract and Other Motor Pathways. Neuroanatomy Through Clinical Cases*, Sinauer Associates, Sunderland, Mass, USA, 2002.

[17] P. M. Rossini, C. Calautti, F. Pauri, and J.-C. Baron, "Post-stroke plastic reorganisation in the adult brain," *Lancet Neurology*, vol. 2, no. 8, pp. 493–502, 2003.

[18] H. T. Hendricks, M. J. Zwarts, E. F. Plat, and J. Van Limbeek, "Systematic review for the early prediction of motor and functional outcome after stroke by using motor-evoked potentials," *Archives of Physical Medicine and Rehabilitation*, vol. 83, no. 9, pp. 1303–1308, 2002.

[19] A. Turton, S. Wroe, N. Trepte, C. Fraser, and R. N. Lemon, "Contralateral and ipsilateral EMG responses to transcranial magnetic stimulation during recovery of arm and hand function after stroke," *Electroencephalography and Clinical Neurophysiology—Electromyography and Motor Control*, vol. 101, no. 4, pp. 316–328, 1996.

[20] H. T. Hendricks, G. Hageman, and J. Van Limbeek, "Prediction of recovery from upper extremity paralysis after stroke by measuring evoked potentials," *Scandinavian Journal of Rehabilitation Medicine*, vol. 29, no. 3, pp. 155–159, 1997.

[21] S. Groppa, A. Oliviero, A. Eisen et al., "A practical guide to diagnostic transcranial magnetic stimulation: report of an IFCN committee," *Clinical Neurophysiology*, vol. 123, no. 5, pp. 858–882, 2012.

[22] J. Reis, O. B. Swayne, Y. Vandermeeren et al., "Contribution of transcranial magnetic stimulation to the understanding of cortical mechanisms involved in motor control," *Journal of Physiology*, vol. 586, no. 2, pp. 325–351, 2008.

[23] H. Peters, K. Dunning, S. Belagaje et al., "Navigated transcranial magnetic stimulation: a biologically-based assay of lower extremity impairment and gait velocity?" *Archives of Physical Medicine and Rehabilitation*, vol. 97, no. 10, article no. e113, 2016.

[24] S. H. Peurala, I. M. Tarkka, M. Juhakoski et al., "Restoration of normal cortical excitability and gait ability in acute stroke after intensive rehabilitation," *Cerebrovascular Diseases*, vol. 26, no. 2, pp. 208–209, 2008.

[25] S. Rossi, M. Hallett, P. M. Rossini et al., "Safety, ethical considerations, and application guidelines for the use of transcranial magnetic stimulation in clinical practice and research," *Clinical Neurophysiology*, vol. 120, no. 12, pp. 2008–2039, 2009.

[26] J. Perry, M. Garrett, J. K. Gronley, and S. J. Mulroy, "Classification of walking handicap in the stroke population," *Stroke*, vol. 26, no. 6, pp. 982–989, 1995.

[27] S. E. Lord, K. McPherson, H. K. McNaughton, L. Rochester, and M. Weatherall, "Community ambulation after stroke: how important and obtainable is it and what measures appear predictive?" *Archives of Physical Medicine and Rehabilitation*, vol. 85, no. 2, pp. 234–239, 2004.

[28] U.-B. Flansbjer, A. M. Holmbäck, D. Downham, C. Patten, and J. Lexell, "Reliability of gait performance tests in men and women with hemiparesis after stroke," *Journal of Rehabilitation Medicine*, vol. 37, no. 2, pp. 75–82, 2005.

[29] J.-H. Lin, M.-J. Hsu, H.-W. Hsu, H.-C. Wu, and C.-L. Hsieh, "Psychometric comparisons of 3 functional ambulation measures for patients with stroke," *Stroke*, vol. 41, no. 9, pp. 2021–2025, 2010.

[30] M. Hallett, "Transcranial magnetic stimulation: a primer," *Neuron*, vol. 55, no. 2, pp. 187–199, 2007.

[31] L. Säisänen, P. Julkunen, E. Niskanen et al., "Motor potentials evoked by navigated transcranial magnetic stimulation in healthy subjects," *Journal of Clinical Neurophysiology*, vol. 25, no. 6, pp. 367–372, 2008.

[32] N. H. Jung, I. Delvendahl, N. G. Kuhnke, D. Hauschke, S. Stolle, and V. Mall, "Navigated transcranial magnetic stimulation does not decrease the variability of motor-evoked potentials," *Brain Stimulation*, vol. 3, no. 2, pp. 87–94, 2010.

[33] L. A. Wheaton, F. Villagra, D. F. Hanley, R. F. Macko, and L. W. Forrester, "Reliability of TMS motor evoked potentials in quadriceps of subjects with chronic hemiparesis after stroke," *Journal of the Neurological Sciences*, vol. 276, no. 1-2, pp. 115–117, 2009.

[34] L. Piron, F. Piccione, P. Tonin, and M. Dam, "Clinical correlation between motor evoked potentials and gait recovery in poststroke patients," *Archives of Physical Medicine and Rehabilitation*, vol. 86, no. 9, pp. 1874–1878, 2005.

[35] L. D'Olhaberriague, J.-M. E. Gamissans, J. Marrugat, A. Valls, C. O. Ley, and J.-L. Seoane, "Transcranial magnetic stimulation as a prognostic tool in stroke," *Journal of the Neurological Sciences*, vol. 147, no. 1, pp. 73–80, 1997.

[36] C.-L. Yen, R.-Y. Wang, K.-K. Liao, C.-C. Huang, and Y.-R. Yang, "Gait training—induced change in corticomotor excitability in patients with chronic stroke," *Neurorehabilitation and Neural Repair*, vol. 22, no. 1, pp. 22–30, 2008.

Hindawi Publishing Corporation
Neural Plasticity
Volume 2016, Article ID 7431012, 15 pages
http://dx.doi.org/10.1155/2016/7431012

Research Article

Scale-Dependent Signal Identification in Low-Dimensional Subspace: Motor Imagery Task Classification

Qingshan She,[1] Haitao Gan,[1] Yuliang Ma,[1] Zhizeng Luo,[1] Tom Potter,[2] and Yingchun Zhang[2,3]

[1]*Institute of Intelligent Control and Robotics, Hangzhou Dianzi University, Hangzhou, Zhejiang 310018, China*
[2]*Department of Biomedical Engineering, University of Houston, Houston, TX 77204, USA*
[3]*Guangdong Provincial Work Injury Rehabilitation Center, Guangzhou 510000, China*

Correspondence should be addressed to Zhizeng Luo; luo@hdu.edu.cn

Received 22 June 2016; Revised 6 September 2016; Accepted 4 October 2016

Academic Editor: Guang H. Yue

Motor imagery electroencephalography (EEG) has been successfully used in locomotor rehabilitation programs. While the noise-assisted multivariate empirical mode decomposition (NA-MEMD) algorithm has been utilized to extract task-specific frequency bands from all channels in the same scale as the intrinsic mode functions (IMFs), identifying and extracting the specific IMFs that contain significant information remain difficult. In this paper, a novel method has been developed to identify the information-bearing components in a low-dimensional subspace without prior knowledge. Our method trains a Gaussian mixture model (GMM) of the composite data, which is comprised of the IMFs from both the original signal and noise, by employing kernel spectral regression to reduce the dimension of the composite data. The informative IMFs are then discriminated using a GMM clustering algorithm, the common spatial pattern (CSP) approach is exploited to extract the task-related features from the reconstructed signals, and a support vector machine (SVM) is applied to the extracted features to recognize the classes of EEG signals during different motor imagery tasks. The effectiveness of the proposed method has been verified by both computer simulations and motor imagery EEG datasets.

1. Introduction

Many people throughout the world live with a variety of clinical conditions, including stroke, spinal trauma, cerebral palsy, and multiple sclerosis. Unfortunately, these conditions frequently present with motor deficits, which greatly reduce the quality of life for those affected. Mental practice with motor imagery (MI) is currently considered a promising additional treatment to improve motor functions [1]—repetitive cognitive training exercise, during which the patient imagines performing a task or body movement without actual physical activity, has been shown to modulate the cerebral perfusion and neural activity in specific brain regions [2]. Interestingly, it has been suggested that the combination of robot-assisted training devices and brain-controlled limb assistive technology may help to induce neural plasticity, resulting in motor function improvement [3]. Despite recording noninvasively and on the same time scale as the sensorimotor control of the brain, the high-dimensional EEG data used in MI exercises faces many challenges [4]. More specifically, these signals are usually collected from multiple electrodes (or channels), which are inevitably contaminated by the noise from biological, environmental, and instrumental origins.

Dimensionality reduction plays a key role in many fields of data analysis [5]. Using this method, data from a high-dimensional space can be represented by vectors in a reduced, low-dimensional space in order to simplify problems without degrading performance. One of the most popular dimensionality reduction methods is principle component analysis (PCA) [6], which is theoretically guaranteed to discover the dimensionality of the subspace and produce a compact representation if the data is embedded in a linear subspace. In many real world problems, however, there is no evidence that the data is actually sampled from a linear subspace

[7, 8]. This has motivated researchers to consider manifold-based approaches for dimensionality reduction. Various manifold learning techniques, including ISOMAP, locally linear embedding (LLE), and Laplacian eigenmaps, have been proposed to reduce the dimensionality of fixed training sets in ways that maximally preserve certain interpoint relationships [9–11]. Unfortunately, these methods do not generally provide a functional mapping between the high- and low-dimensional spaces that is valid both on and off the training data [7]. Recently, spectral methods have also emerged as powerful tools for dimensionality reduction. Spectral regression (SR), based on regression and spectral graph analysis, can make efficient use of both labeled and unlabeled points to discover the intrinsic discriminant structure in the data [7, 8]. As a result, SR has been applied to supervised, semisupervised, and unsupervised situations across different pattern recognition tasks [12, 13] and has shown its superiority over traditional dimensional reduction methods.

Empirical mode decomposition (EMD) is a fully data-driven and adaptive analysis method that is widely applied within the field of biomedical signal processing [14–16]. It decomposes a raw signal into a set of intrinsic mode functions (IMFs) which represent the natural oscillatory modes contained within the original data. EMD does have some limitations in processing multichannel data, since the IMFs decomposed from different data channels are difficult to match in number and/or frequency [17, 18]. In order to resolve this problem, a noise-assisted multivariate EMD (NA-MEMD) [19] method has been proposed recently. This method applies the dyadic filter bank property of multivariate EMD [20] to white noise and is thereby capable of reducing the mode-mixing problem significantly, achieving favorable performance in the classification of MI EEG signals [21]. Although EMD and its extended versions have been widely researched and applied, there have been few studies on the selection of relevant IMF levels (scales), raising the question of how to select the information-bearing IMF components in an efficient way. Conventional approaches make use of prior knowledge in task-related domains: relevant IMFs are selected by calculating the average power spectra of the first several IMFs and comparing them to the frequency distributions of the *mu* (8–12 Hz) and *beta* rhythms (18–25 Hz) [21]. Similarly, in the neural beta-related oscillatory activities, the informative IMFs are chosen by examining the mean beta band frequency [22]. In [23], the relevant modes are selected by means of partial reconstruction and measures of similarity are calculated between the probability density function of the input signal and that of each mode extracted by EMD, though this is still insufficient to analyze multivariate data. Recently, a novel statistical approach has been proposed to recognize the information-bearing IMFs on each scale [24]. This method uses similarity measures to compare the IMFs to both the data and noise, yielding impressive results when applied to the multichannel local field potentials recorded from the cortices of monkeys during generalized flash suppressing (GFS) tasks.

In this work, we propose a novel method to identify the information-bearing components from EEG data in low-dimensional space, independent of prior knowledge. The proposed method first performs NA-MEMD on the input signal to obtain different scales of IMFs. Secondly, unsupervised kernel spectral regression is employed to map the decomposed IMFs into a low-dimensional subspace, avoiding the eigendecomposition of dense matrices and enabling the flexible incorporation of various regularizers into the regression framework [7, 8]. Thirdly, a Gaussian mixture model (GMM) is generated, informed by the IMFs from both the original signal and noise, and an optimal number of clusters and corresponding model parameters are estimated by the GMM clustering approach. Finally, the information-bearing IMFs from the input signal are discriminated on each scale. The GMM clustering algorithm is essentially similar to conventional clustering algorithms (e.g., K-means, performing a hard assignment of data points to clusters) except that it allows cluster parameters to be accurately estimated even when the clusters overlap substantially [25]. Compared to existing methods of identifying informative IMFs, the new method has several noteworthy aspects:

(1) Kernel spectral regression is employed to reduce the dimension of the decomposed IMFs by constructing a nearest neighbor graph to model their intrinsic structure.

(2) The probability density function of the composite IMFs is modeled by a mixture of Gaussian distributions and the number of clusters which best fits the composite IMFs is estimated and used to recognize the information-bearing components.

(3) The method does not depend on prior knowledge and can discriminate the informative IMFs from each signal channel on each scale.

The rest of the paper is organized as follows: Section 2 presents the materials and proposed signal identification method, consisting of the noise-assisted multivariate empirical mode decomposition of multichannel EEG signals, the spectral regression-based dimensionality reduction of the composite data created by combining the IMFs from signal and noise channels, and GMM clustering. It then briefly introduces the common spatial patterns-based feature extraction of the reconstructed signals from the identified information-bearing IMFs and support vector machine (SVM) classifier. Section 3 then demonstrates the experimental results, including simulation results and applications on real MI EEG datasets. Finally, we provide some concluding remarks and suggestions for future work in Section 4.

2. Materials and Methods

2.1. Subjects and Data Recording. In order to assess the proposed algorithm, the EEG data from nine subjects was obtained from two publicly available datasets. These datasets contain EEG signals recorded while subjects imagined limb movements, such as left/right hand or foot movements. They are described briefly as follows:

(1) BCI Competition IV Dataset I [26] was provided by the Berlin BCI group. EEG signals were recorded using 59 electrodes from four healthy participants (*a*,

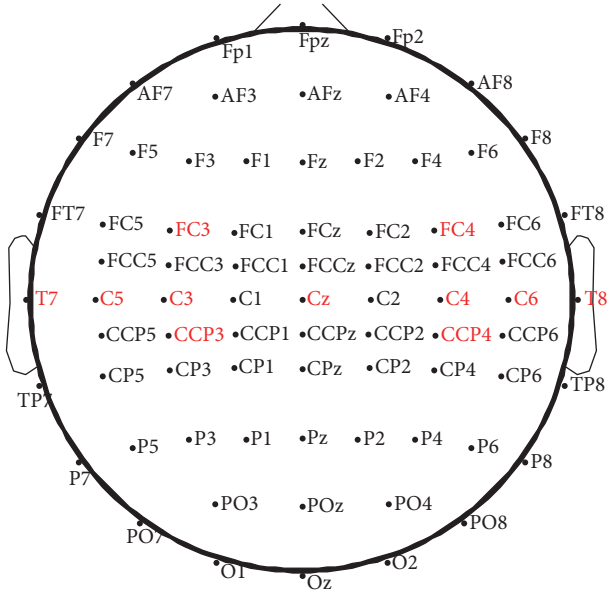

Figure 1: The positions of the chosen electrodes in the extended international 10–20 system.

b, *f*, and *g*) who performed two classes of MI tasks. More precisely, subjects *a* and *f* performed left hand and foot MI while subjects *b* and *g* carried out left hand and right hand MI. A total of 200 trials were available for each subject, including 100 trials for each class.

(2) BCI Competition III Dataset IVa [27] was provided by the Berlin BCI group. EEG signals were recorded using 118 electrodes from five healthy subjects (*aa*, *al*, *av*, *ay*, and *aw*) who performed right hand and foot MI. A training set and a testing set were available for each subject, though their size differed for each subject. In total, 280 trials were available for each subject, among which 168, 224, 84, 56, and 28 trials comprised the respective training sets for subjects *aa*, *al*, *av*, *ay*, and *aw*, with the remaining trials belonging to their testing sets.

Since the sensorimotor rhythms (SMRs) of motor imagery are primarily linked to the central area of the brain [28, 29], 11 EEG channels from the experimental data were used (FC3, FC4, Cz, C3, C4, C5, C6, T7, T8, CCP3, and CCP4, as recommended in [21]). The locations of these channels are shown in Figure 1.

2.2. Signal Identification in Low-Dimensional Subspace. Our goal is to identify the significant information-bearing IMFs on each scale for multichannel data. For each set of multivariate IMFs obtained by NA-MEMD, it is key to recognize the suitable IMFs bearing significant information associated with the MI EEG activities. In this section, we introduce a novel four-stage method to identify the informative IMFs. First, the NA-MEMD algorithm is performed on the original data to obtain a set of multivariate IMFs, from which the composite data is created by combining the IMFs from each signal channel with those from the noise channels on each scale. Secondly, the composite data is mapped into lower-dimensional subspace to extract feature vectors using unsupervised kernel spectral regression [7, 8]. Thirdly, a Gaussian mixture model is informed by exploiting the intrinsic discriminant structure of the probability distribution that generates the low-dimensional feature vectors. Then, for each group of feature vectors on each scale, the maximum likelihood classification is performed to distinguish them into classes after an optimal number of clusters and corresponding model parameters are estimated by the GMM clustering approach [25]. Finally, the informative IMFs from each signal channel on each scale are identified according to the clustering results. In the following sections, more details are provided for each stage of the proposed approach.

2.2.1. Noise-Assisted Multivariate Empirical Mode Decomposition. For multivariate signals, the MEMD method [20] is utilized by generating multidimensional envelopes, taking signal projections along different directions, and finally averaging these projections to obtain the local mean. Though it is valid in processing multivariate nonstationary signals, MEMD still inherits a degree of mode-mixing. This has led to the recent development of the NA-MEMD approach [19], which is performed by adding white noise as additional channels in the original signal. NA-MEMD then enjoys both the benefits of the quasi-dyadic filter bank structure of MEMD on white noise and the additional realizations of white noise, guaranteeing the separability of the IMFs that correspond to both the original signal and noise. Given an n-variate input neuronal signal $\{\mathbf{s}(t)\}_{t=1}^{L} = \{s_1(t), s_2(t), \ldots, s_n(t)\}$ with L samples per trial, MEMD produces J multivariate IMFs:

$$\mathbf{s}(t) = \sum_{j=1}^{J} \mathbf{d}_j(t) + \mathbf{r}(t), \tag{1}$$

where $\mathbf{d}_j(t)$ denotes the jth IMF of $\mathbf{s}(t)$ and $\mathbf{r}(t)$ represents the n-variate residual.

In practice, the sifting process for a multivariate IMF can be stopped when all the projected signals fulfill a stoppage criterion. For MEMD sifting, a combination of EMD stoppage criteria is employed as introduced in [30, 31]. The stoppage criterion in standard EMD requires that the number of extrema and zero crossings differ at most by one for τ consecutive iterations in the sifting algorithm [30]. By introducing the envelope amplitude $\rho(t) = 1/\kappa \sum_{k=1}^{\kappa} |e^{\theta_k}(t) - m(t)|$ and defining an evaluation function $f(t) = |m(t)/\rho(t)|$, where κ denotes the total number of direction vectors in MEMD decomposition, $e^{\theta_k}(t)$ represents the envelope curve along the kth ($k = 1, \ldots, \kappa$) set of directions given by angles $\theta_k = \{\theta_1^k, \theta_2^k, \ldots, \theta_{n-1}^k\}$, and $m(t)$ is the local mean signal, another stoppage criterion is proposed [31]. The sifting process is continued until the value of $f(t)$ is less than or equal to some predefined threshold γ. Similar to the given values in [20], $\tau = 5$ and $\gamma = 0.075$ were chosen in this paper.

2.2.2. Dimensionality Reduction by Spectral Regression. Spectral regression is an efficient method to reduce dimensionality

from the graph embedding viewpoint [7, 8]. Specifically, an affinity graph is first constructed to learn the responses for labeled or unlabeled data and then the ordinary regression is applied for learning the embedding function. In essence, SR performs regression after the spectral analysis of the graph.

Suppose we have N data points $\{\mathbf{x}_i\}_{i=1}^N \subset \mathbb{R}^L$, dimensionality reduction would aim to find a lower-dimensional representation $\{\mathbf{z}_i\}_{i=1}^N \subset \mathbb{R}^M$, $M \ll L$. Given a p-nearest neighbor graph G with N vertices, where the ith vertex corresponds to a data point $\mathbf{x}_i$, let $\mathbf{W}$ be a symmetric $N \times N$ matrix with W_{ij} having the weight of the edge joining vertices i and j. G and $\mathbf{W}$ can be defined to characterize certain statistical or geometric properties of the dataset.

Let $\mathbf{v} = [v_1, \ldots, v_N]^{\mathrm{T}}$ be the map from the graph to the real line, where T denotes a transposition. In the graph embedding approach [7], by introducing a linear function, $v_i = f(\mathbf{x}_i) = \mathbf{a}^{\mathrm{T}}\mathbf{x}_i$, we find $\mathbf{X}^{\mathrm{T}}\mathbf{a} = \mathbf{v}$, where $\mathbf{X} = [\mathbf{x}_1, \ldots, \mathbf{x}_N] \in \mathbb{R}^{L\times N}$ and $\mathbf{a} = [a_1, \ldots, a_N]^{\mathrm{T}}$. The optimal embedding, $\mathbf{v}$, is then given by the eigenvector corresponding to the maximum eigenvalue of the generalized eigenproblem

$$\mathbf{X}\mathbf{W}\mathbf{X}^{\mathrm{T}}\mathbf{a} = \lambda\mathbf{X}\mathbf{D}\mathbf{X}^{\mathrm{T}}\mathbf{a} \tag{2}$$

with the eigenvalue λ, where $\mathbf{D}$ is a diagonal matrix whose entries are the column sums of $\mathbf{W}$, $D_{ii} = \sum_j W_{ji}$. This optimization can be solved through regression by adopting the regularization technique [7], and its solution is then given by

$$\widehat{\mathbf{a}} = \arg\min_{\mathbf{a}} \sum_{i=1}^{N} \left(\left(\mathbf{a}^{\mathrm{T}}\mathbf{x}_i - v_i\right)^2 + \alpha \sum_{j=1}^{L} \left\|a_j\right\|_2^2 + \beta \sum_{j=1}^{L} \left|a_j\right| \right), \tag{3}$$

where v_i is the ith element of $\mathbf{v}$, the nonnegative regularization parameter α is used to control the amount of shrinkage, and some coefficients will be shrunk to exact zero if the nonnegative parameter β is large enough due to the nature of the L_1 penalty. When the number of features is larger than the number of samples, the sample vectors will typically be linearly independent; thus the solutions to the optimization problem in (3) are the eigenvectors of the eigenproblem in (2) as α and β decrease to zero [7, 8]. The largest M eigenvectors of $\mathbf{a}$ are obtained according to the expected dimensionality of the reduced subspace in real applications. In this way, a low-dimensional representation of the sample matrix $\mathbf{X}$ is obtained as $\mathbf{Z} = \mathbf{X}^{\mathrm{T}}\mathbf{a}$.

Similar to linear regression, by defining a nonlinear embedding function in reproducing kernel Hilbert space (RKHS), that is, $v = f(\mathbf{x}) = \sum_{i=1}^{N} a_i K(\mathbf{x}, \mathbf{x}_i) = K(\mathbf{x})^{\mathrm{T}}\mathbf{a}$, where $K(\mathbf{x}, \mathbf{x}_i)$ is the Mercer kernel of RKHS and $K(\mathbf{x}) = [K(\mathbf{x}, \mathbf{x}_1), \ldots, K(\mathbf{x}, \mathbf{x}_N)]^{\mathrm{T}}$, the linear spectral regression approach can be generalized to kernel spectral regression (KSR) [8].

2.2.3. Gaussian Mixture Model for Data Clustering. The Gaussian mixture model (GMM) is widely used as a probabilistic modeling approach to address unsupervised learning problems. Based on the expectation-maximization (EM) algorithm [32] and an agglomerative clustering strategy using Rissanen's minimum description length (MDL) criterion, a GMM-based clustering approach is developed [25]. The process begins with an initial number of clusters and a set of cluster parameters and iteratively combines the clusters until only one remains.

Let $\mathbf{Z} = [\mathbf{z}_1, \ldots, \mathbf{z}_N] \in \mathbb{R}^{M\times N}$ be a set of M-dimensional samples belonging to different subclasses or clusters and let $\mathbf{y} = [y_1, \ldots, y_N]$ be the subclass of each sample, where $y_i \in \{1, \ldots, c\}$ denotes which Gaussian distribution the sample $\mathbf{z}_i$ belongs to and c is the number of Gaussian components. The detailed steps of the GMM cluster algorithm are then given as follows.

(1) Initialize the parameters including the initial number of clusters c_o and the Gaussian model parameters $\boldsymbol{\Omega}^{(0)} = \{\{\pi_1^{(0)}, \boldsymbol{\mu}_1^{(0)}, \boldsymbol{\Sigma}_1^{(0)}\}, \ldots, \{\pi_c^{(0)}, \boldsymbol{\mu}_c^{(0)}, \boldsymbol{\Sigma}_c^{(0)}\}\}$, where $\boldsymbol{\mu}_k$ is the mean vector, $\boldsymbol{\Sigma}_k$ is the covariance matrix for the kth Gaussian distribution, and π_k denotes the prior probability of the data point generated from the kth component, $k = 1, \ldots, c$. The number of initial clusters in this case should be chosen to fit the number of data types for discrimination.

(2) Apply an iterative EM algorithm until the change in the MDL criterion (MDL$(K, \boldsymbol{\Omega})$) is less than a threshold ε, where $\varepsilon = 0.01 \times (1 + M + (M+1)M/2) \times \log(NM)$:

$$\mathrm{MDL}(c, \boldsymbol{\Omega}) = -\sum_{i=1}^{N} \log\left(\sum_{k=1}^{c} \pi_k p_{\mathbf{z}_i|y_i}\left(\mathbf{z}_i \mid k, \boldsymbol{\Omega}\right) \right) + \frac{1}{2} v \log(NM), \tag{4}$$

where $p_{\mathbf{z}_i|y_i}(\mathbf{z}_i \mid k, \boldsymbol{\Omega})$ is the Gaussian probability density function for the sample $\mathbf{z}_i$ given that $y_i = k$, $\log(\cdot)$ denotes the log-transformation and v is the number of continuously valued real numbers required to specify the model parameters $\boldsymbol{\Omega}$, $v < 1/(2NM)$.

(3) Record the model parameter $\boldsymbol{\Omega}^{(c,i_{\mathrm{final}})}$ and the value of the MDL$(c, \boldsymbol{\Omega}^{(c,i_{\mathrm{final}})})$, where i_{final} denotes the final iteration of the EM updating process for each value of c.

(4) If the number of clusters is greater than 1, apply a defined distance function [25] to reduce the number of clusters, set $c \leftarrow c - 1$, and repeat Step (2).

(5) Choose the value $\widehat{c}$ and the model parameters $\boldsymbol{\Omega}^{(\widehat{c},i_{\mathrm{final}})}$ which minimize the value of the MDL criterion.

(6) Based on the optimal parameters $\widehat{c}$ and $\boldsymbol{\Omega}^{(\widehat{c},i_{\mathrm{final}})}$ from Step (5), sample vectors are distinguished into $\widehat{c}$ classes using the maximum likelihood classification.

2.2.4. Identification Algorithm for Information-Bearing IMFs. In this section, we introduce our algorithm for discriminating between informative and noninformative IMFs. The detailed steps of our method (KSR-GMM) are described as follows.

(1) Generate $(n + l)$-channel multivariate signal consisting of the input n-channel signal and an l-channel uncorrelated Gaussian white noise time-series of the same length as the input and then perform the MEMD decomposition [20] on the multivariate signal, obtaining $(n + l)$-variate IMFs denoted by $(n + l) \times J \times L$ matrix, where J is the number

of decomposition scales and L is the length of samples per channel.

(2) On the jth ($j = 1, \ldots, J$) scale of the resulting multivariate IMFs from Step (1), combine the l-channel IMFs corresponding to the noise with the one-channel IMFs from the original signal, giving n-groups of $(l+1)$-variate composite data given by $n \times (l+1) \times L$ matrix.

(3) At a given (jth) scale, the unsupervised KSR algorithm is performed, respectively, on the ith ($i = 1, \ldots, n$) group of composite data obtained in Step (2), yielding n-groups of low-dimensional representation vectors denoted by $n \times (l+1) \times M$ matrix in the reduced subspace, where M is the number of reduced dimensions.

(4) At the given scale, for each group of representation vectors extracted in Step (3), the optimal number of clusters $\widehat{c}$ is estimated by the GMM clustering approach and, based on the value of $\widehat{c}$ and the corresponding model parameters, the representation vectors are then classified into $\widehat{c}$ classes using the maximum likelihood classification.

(5) At the given scale, the information-bearing IMFs are identified according to the clustering results in Step (4): if an IMF from any individual signal channel is clustered with the IMFs from noise channels, then IMF is rejected as noninformative. All remaining IMFs are considered to be significantly information-bearing.

In this work, the initial number of clusters is chosen to be two in the GMM clustering, since we only discriminate two kinds of data: informative and noninformative IMFs. Additionally, it should be noted that excessive noise levels can compromise the data-driven ability of the NA-MEMD, though there is no technical limit on the number of the noise channels that can be added. As a rule of thumb, the variance of the noise is required to be within 2–10% of the variance of the input signal to produce reliable results [20].

2.3. Common Spatial Patterns for Feature Extraction. In the context of EEG signal processing, the common spatial patterns (CSP) approach aims at finding linear spatial filters that maximize the variance of EEG signals from one class while minimizing their variance from others [33]. Mathematically, the spatial filters are the stationary points of the following optimization problem:

$$\begin{aligned} \max_{\mathbf{u}} \quad & J(\mathbf{u}) = \frac{\mathbf{u}^{\mathrm{T}}\mathbf{E}_1\mathbf{E}_1^{\mathrm{T}}\mathbf{u}}{\mathbf{u}^{\mathrm{T}}\mathbf{E}_2\mathbf{E}_2^{\mathrm{T}}\mathbf{u}} = \frac{\mathbf{u}^{\mathrm{T}}\mathbf{C}_1\mathbf{u}}{\mathbf{u}^{\mathrm{T}}\mathbf{C}_2\mathbf{u}} \\ \text{s.t.} \quad & \|\mathbf{u}\|_2 = 1, \end{aligned} \tag{5}$$

where $\mathbf{u}$ denotes a spatial filter, $\mathbf{E}_i$ represents the $n \times L$ data matrix from class i where n is the number of channels and L is the number of samples per channel, and $\mathbf{C}_i$ is the estimated spatial covariance matrix from class $i \in [1, 2]$. Using the Lagrange multiplier method, the solution can be obtained as the eigenvectors of the generalized eigenvalue decomposition: $\mathbf{C}_1\mathbf{u} = \zeta\mathbf{C}_2\mathbf{u}$, where ζ denotes the eigenvalue associated with $\mathbf{u}$. The spatial filters are then the eigenvectors of $\mathbf{C}_2^{-1}\mathbf{C}_1$, which correspond to the largest and lowest eigenvalues.

With the projection matrix $\mathbf{U} = [\mathbf{u}_1, \ldots, \mathbf{u}_n]$, the spatially filtered signal of a trial $\mathbf{E}$ is given as $\widehat{\mathbf{S}} = \mathbf{U}^{\mathrm{T}}\mathbf{E}$. For discriminating between two classes of MI tasks, the extracted feature vectors are the logarithm of the spatially filtered signal:

$$f_j = \log\left(\frac{\mathrm{var}\left(\widehat{\mathbf{s}}_j\right)}{\sum_{i=1}^{2m}\mathrm{var}\left(\widehat{\mathbf{s}}_i\right)}\right), \tag{6}$$

where $\widehat{\mathbf{s}}_j$ ($j = 1, \ldots, 2m$) denotes the m first and last rows of $\widehat{\mathbf{S}}$ and the symbol var$(\cdot)$ denotes the variance.

2.4. Support Vector Machine Classification of MI EEG. The support vector machine (SVM) algorithm [34] is believed to be a state-of-the-art classification method due to its robustness to outliers and favorable generalization capability. The central idea of SVM is to separate data by finding the hyperplane that produces the largest possible margin, which is the distance between nearest data points of different classes.

The detailed steps of EEG processing are outlined as follows:

(1) Preprocess the n-channel EEG data using a 5th-order Butterworth filter, obtaining filtered data with the frequency band 8–30 Hz.

(2) Perform the proposed identification method on the composite signals which are acquired by combining an additional l-channel Gaussian white noise with the n-channel EEG data obtained in Step (1), identifying the information-bearing IMFs on each scale.

(3) For the n-channel EEG data, the informative IMFs distinguished from Step (2) are added together to construct the band-pass filtered signals.

(4) Process the reconstructed signals from Step (3) with the CSP algorithm to extract the feature vectors for different motor imagery tasks.

(5) Employ the SVM classifier to identify the classes of EEG during different MI tasks based on the extracted feature vectors in Step (4).

3. Experimental Results and Discussion

In this section, several experiments on simulated data and real world EEG data were performed to show the effectiveness of our proposed method. The new algorithm was constructed based on the spectral regression code (http://www.cad.zju.edu.cn/home/dengcai/Data/data.html) and the GMM clustering code found in the software package (https://engineering.purdue.edu/~bouman/software/cluster/). We used the LIBSVM toolbox [35] to implement the SVM classification of EEG data. For all methods using kernel applications, a Gaussian kernel function is chosen due to its validity and stability in experiments, that is, $\exp(-\|\mathbf{x}_i - \mathbf{x}_j\|^2/2\eta^2)$, where the parameter η is the Gaussian kernel width. All the methods are implemented in MATLAB 2013a environment on a PC with a 2.5 GHz processor and 4.0 GB RAM.

3.1. Simulation Results. Our proposed method is first performed on the simulated data to verify its effectiveness. Unless otherwise specified, 15-channel noise data was generated using an uncorrelated Gaussian white noise time-series which has the same length as that of the input signal. Moreover, the variance of noise was set to be 6% of the variance of the input according to suggestions in [20]. Additionally, the number of nearest neighbors ($p = 5$) and the regularization parameters ($\alpha = 0.001$ for L_2 penalty and $\beta = 0.01$ for L_1 penalty) were chosen by cross-validation in this simulation.

In this experiment, the same simulated data was generated as in [24]. A 3-channel synthetic signal $[X(t), Y(t), Z(t)]$ with the length $N = 1000$ and the sampling rate $f_s = 1000$ Hz is

$$\begin{aligned} X(t) &= \sin\left(2\pi f_1 t\right) + \sin\left(2\pi f_2 t\right) + \sin\left(2\pi f_3 t\right) \\ &\quad + q_1(t), \quad t = 1, 2, \ldots, 1000 \\ Y(t) &= \sin\left(2\pi f_1 t\right) + \sin\left(2\pi f_3 t\right) + q_2(t), \\ &\qquad t = 1, 2, \ldots, 1000 \\ Z(t) &= \sin\left(2\pi f_2 t\right) + \sin\left(2\pi f_3 t\right) + q_3(t), \\ &\qquad t = 1, 2, \ldots, 1000, \end{aligned} \tag{7}$$

where $f_1 = 12/f_s$, $f_2 = 26/f_s$, $f_3 = 50/f_s$, and $q_1(t)$, $q_2(t)$, $q_3(t)$ represent Gaussian white noises.

(I) To study the clustering performance of our method. A set of 3-channel input signals with SNR = 20 dB was generated and an additional 15-channel white noise with SNR = 6.1 dB was added to the input signal to create the composite signal. Our method was then performed on the composite signal and the information-bearing IMFs on each scale were identified. Figure 2 shows a scatter plot with class labels of sixteen samples from a two-dimensional feature vector at the first seven scales, including one sample corresponding to one signal channel and fifteen samples from noise channels. Here, the data points corresponding to signal channels are represented by "$*$" while those corresponding to noise channels are displayed by "o" in blue.

It can be seen from Figure 2 that the composite data points on the 4th, 5th, and 6th scales in X-group are all clustered into two classes, with the same being true for the 4th and 6th scales in Y-group and the 4th and 5th scales in Z-group, while the composite data on the remaining scales of each channel falls into one class. According to the proposed method, these IMFs with two clusters are regarded as informative and the identification results are consistent with the IMFs containing the true frequency components decomposed by the NA-MEMD algorithm, as shown in Figure 3. The first seven IMFs are denoted as C_1–C_7 and the residuals are represented as C_{res}, which are the sums of the remaining scales of IMFs. It can be seen that the underlying frequency components occur in the 4–6th IMF components, which are displayed in red.

(II) To test the effect of noise with different SNRs on our method, it was necessary to verify this performance since measured data often suffers from noise contamination in real applications. Our method was compared with several approaches for identifying information-bearing components: (i) Hu's method [24], which uses the Wasserstein distance to assess the similarity between the reference IMFs from noise channels and the IMFs from signal channels and subsequently establishes a confidence interval (e.g. 95%) for the distance by employing a Monte-Carlo technique, denoted as WD-CI; and (ii) three algorithms for dimensionality reduction together with GMM clustering: PCA, kernel PCA (KPCA) [36], and L_1-norm PCA (L_1PCA) [6]. In order to facilitate performance comparison, two kinds of error were evaluated. These are defined as (1) Type I error, which is the failure to identify true IMF components bearing relevant information, and (2) Type II error, which is the improper identification of information-free IMF components.

First, different SNRs were varied by systematically changing the variance of the white noise superimposed in the input signal, combined with separate 15-channel white noise (SNR 6.1 dB) as reference channels. Overall, sixteen SNR levels were tested with 100 trials performed at each level. In each trial, the SNR of the white noise superimposed on the input signal was first changed, the relevant IMFs were identified by the different algorithms, and the corresponding error rates were calculated. The results from this test are shown in Figure 4. Low rates of Type I and Type II error were found at the higher SNR levels for all methods. On the whole, with the exception of Type I error rates in PCA-based approaches, increases in SNR led to decreases in error rates. When compared with other identification approaches, PCA-GMM, KPCA-GMM, and L_1PCA-GMM showed lower Type I error rates but higher Type II error rates, while WD-CI yielded the lowest Type II error rate. The proposed method showed an improved Type I error rate with a slightly higher Type II error rate than the WD-CI algorithm, though the overall Type II error rates of both the new method and the WD-CI algorithm remain very small, even at low SNRs. These results indicate that our method is able to effectively identify the information-bearing components at low SNRs and is highly resistant to white noise.

Next, considering that the noise contained in the signal channels is mismatched with the noise in the reference channels, the effects of red noises ($1/f^2$ noise) with different SNRs were tested on the proposed method. Figure 5 shows the identification error rates at different noise SNR levels. Results indicate that both the new method and the WD-CI algorithm work well even when there is a mismatch between the noise contained in the data and the noise in the reference channels. This further demonstrates the robustness of our method when identifying the informative components in noisy data at low SNRs.

3.2. MI EEG Classification Results. This section evaluates the performance of our proposed method on MI EEG datasets. It has already been shown that the greatest result of motor imagery is a modulation of the SMRs [27]. Differential modulations in the SMRs were decomposed using the NA-MEMD method with locally orthogonal and narrowband IMF bases. Based on the identified information-bearing IMFs, relevant

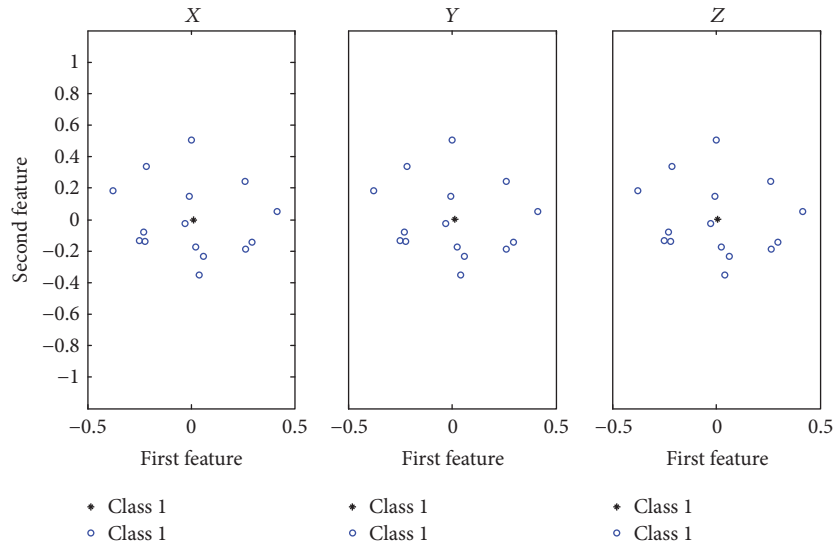

(a) Scale 1

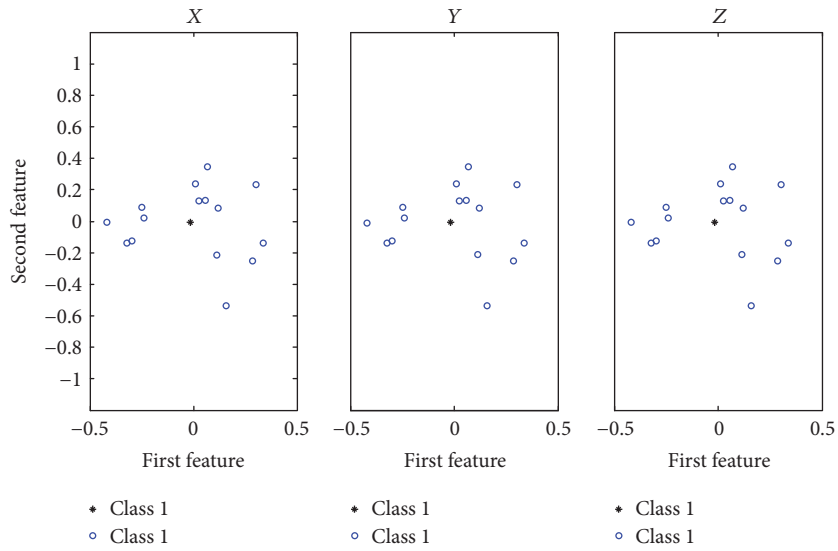

(b) Scale 2

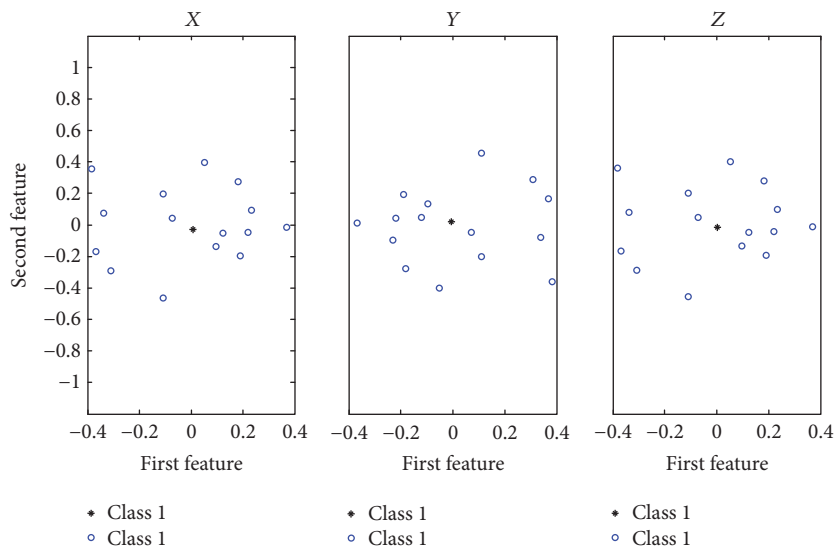

(c) Scale 3

Figure 2: Continued.

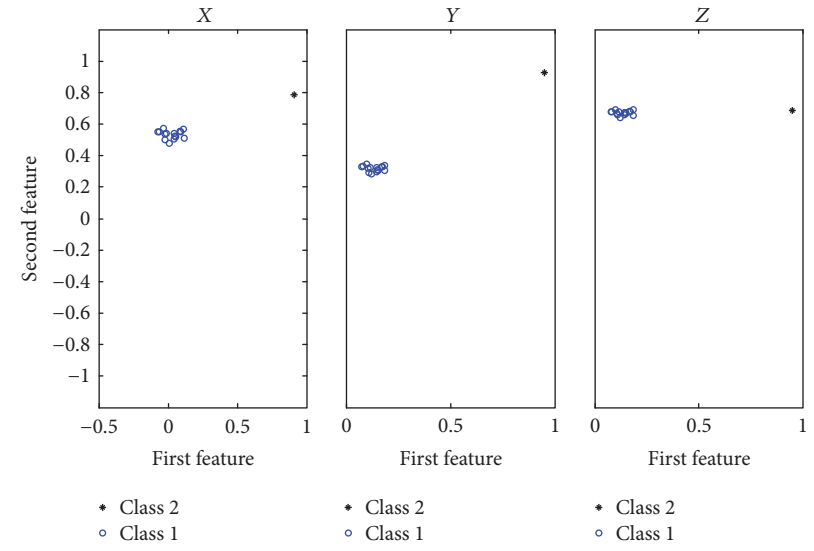

(d) Scale 4

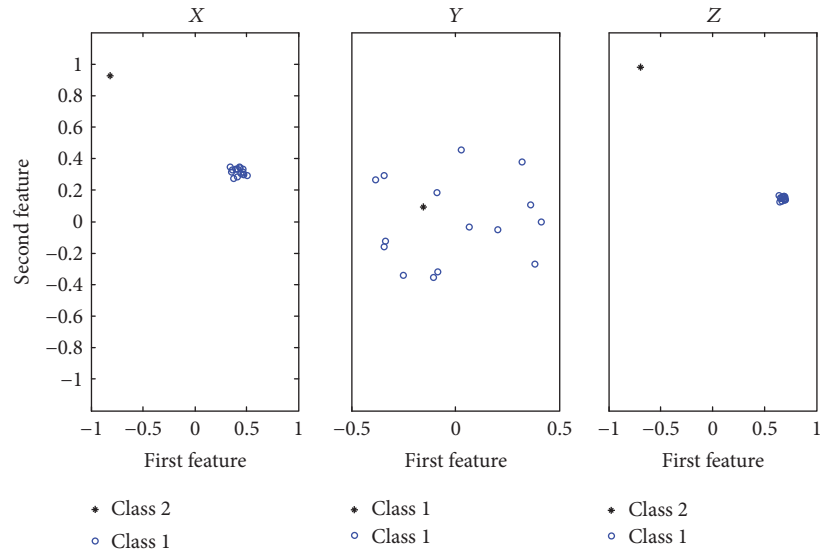

(e) Scale 5

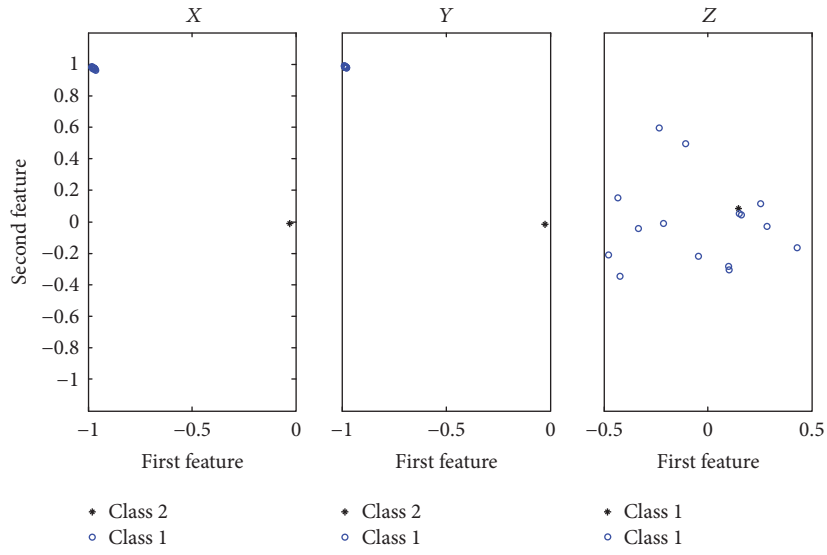

(f) Scale 6

Figure 2: Continued.

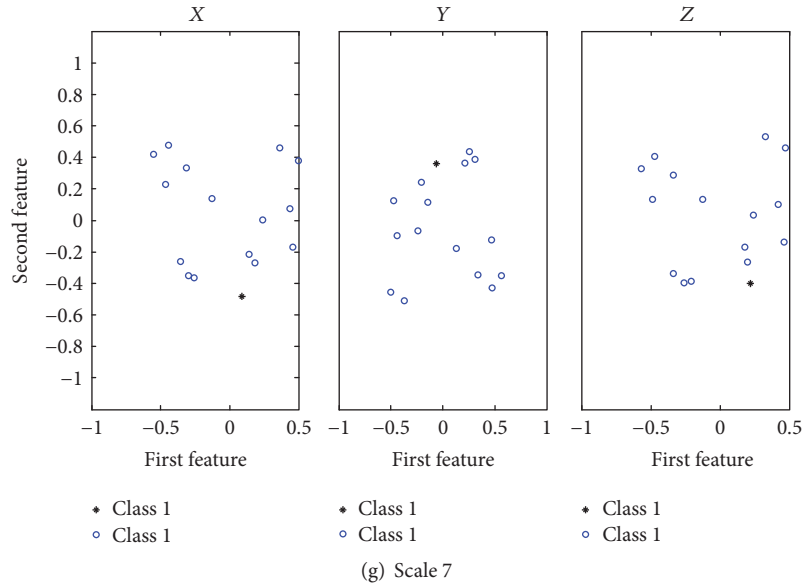

(g) Scale 7

Figure 2: Clustering results using the proposed method at first seven scales.

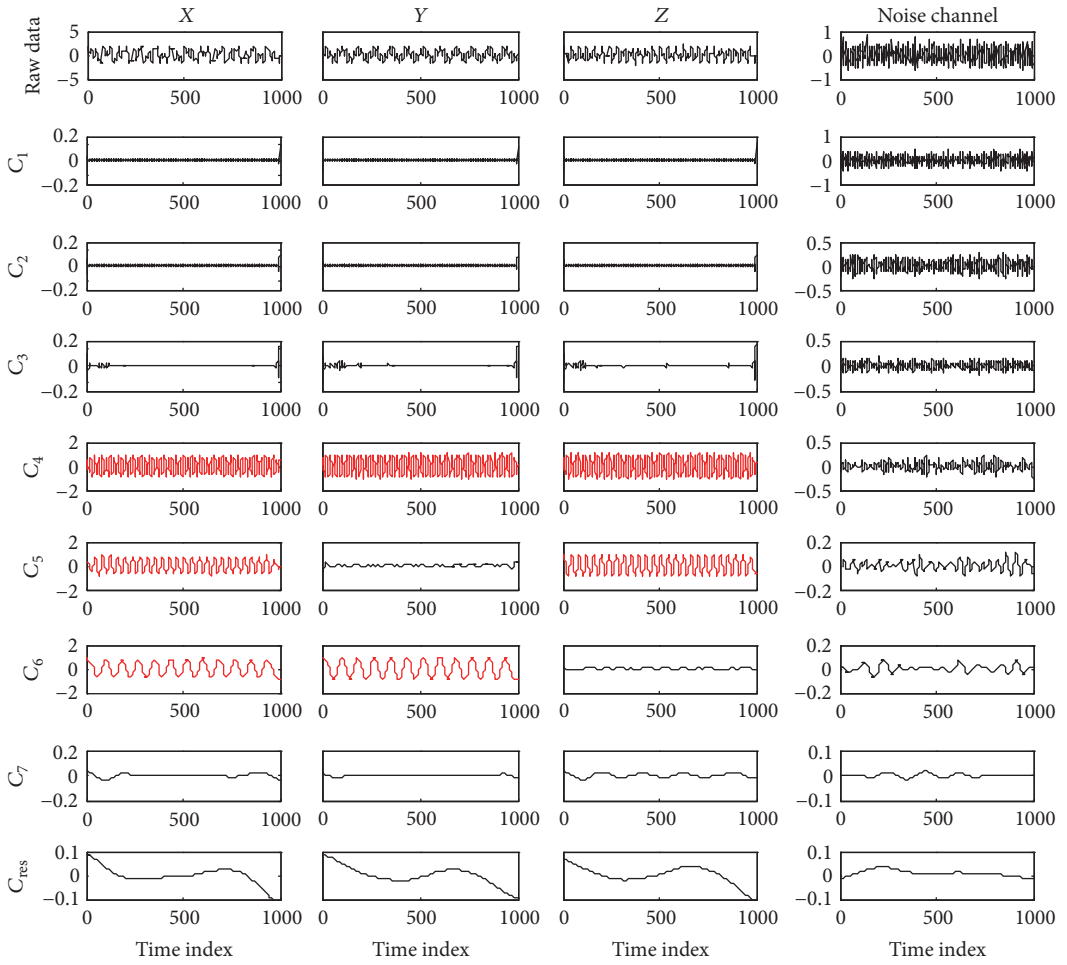

Figure 3: Decomposition results of the simulated data using the NA-MEMD algorithm.

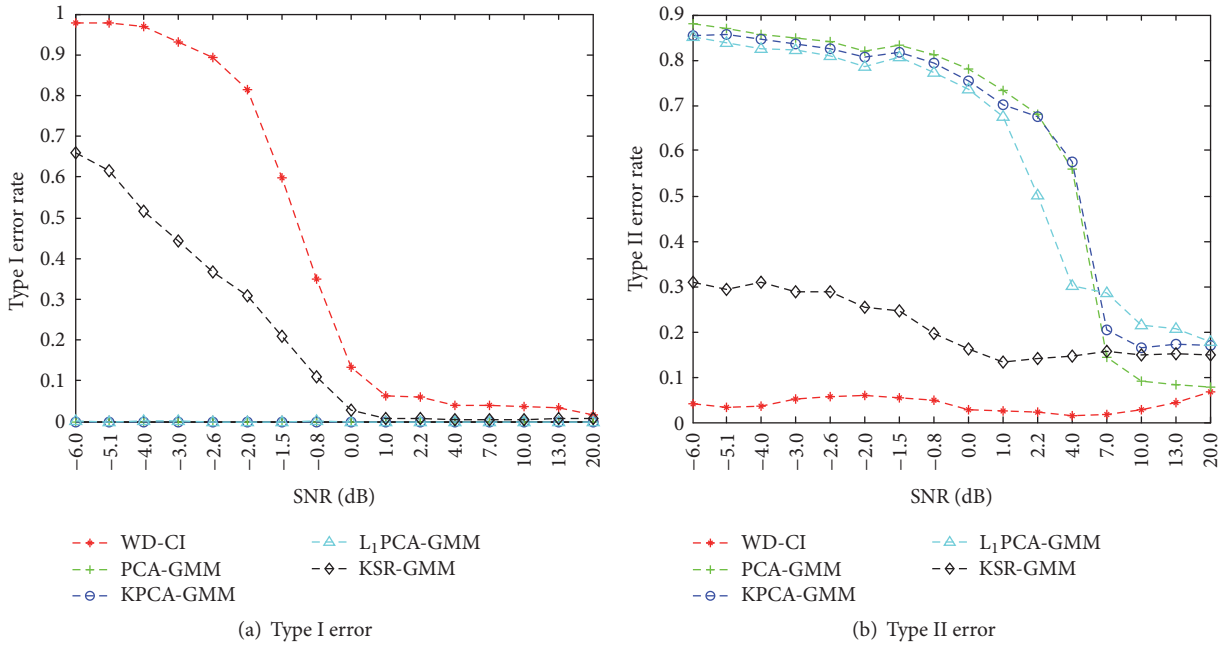

(a) Type I error (b) Type II error

Figure 4: Statistical results by different methods at different SNRs which are systematically varied by changing the variance of the white noise superimposed in the signal.

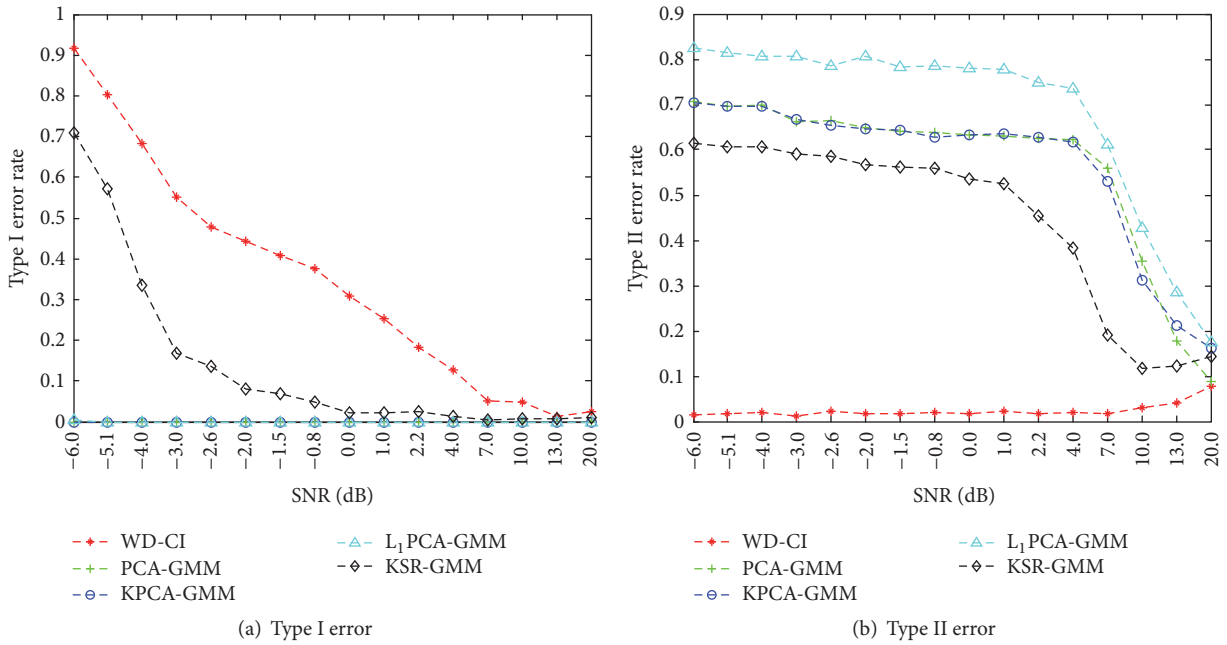

(a) Type I error (b) Type II error

Figure 5: Statistical results achieved by different methods at different SNRs. SNRs were systematically varied by changing the variance of the red noise superimposed on the signal.

IMFs from the same channel were summed to get the reconstructed signal, and CSP-based feature extraction and SVM-based classification were performed.

For each trial in the BCI Competition IV Dataset I, we selected the EEG data from 0–4 s after the initiation of MI, as performed in [21]. In contrast, the window from 0.5–2.5 s after initiation was used for the BCI Competition III Dataset IVa, as in [37]. The 11-channel EEG data was regarded as the input signal and combined with an additional 15-channel noise (SNR 20 dB). Several parameters chosen by cross-validation in our identification algorithm are $p = 5$, $\alpha = 0.1$, and $\beta = 0$. For both EEG datasets, the best model parameters were determined by fivefold cross-validation from $\{2^{-10}, \ldots, 2^{10}\}$ in SVM models. According to the

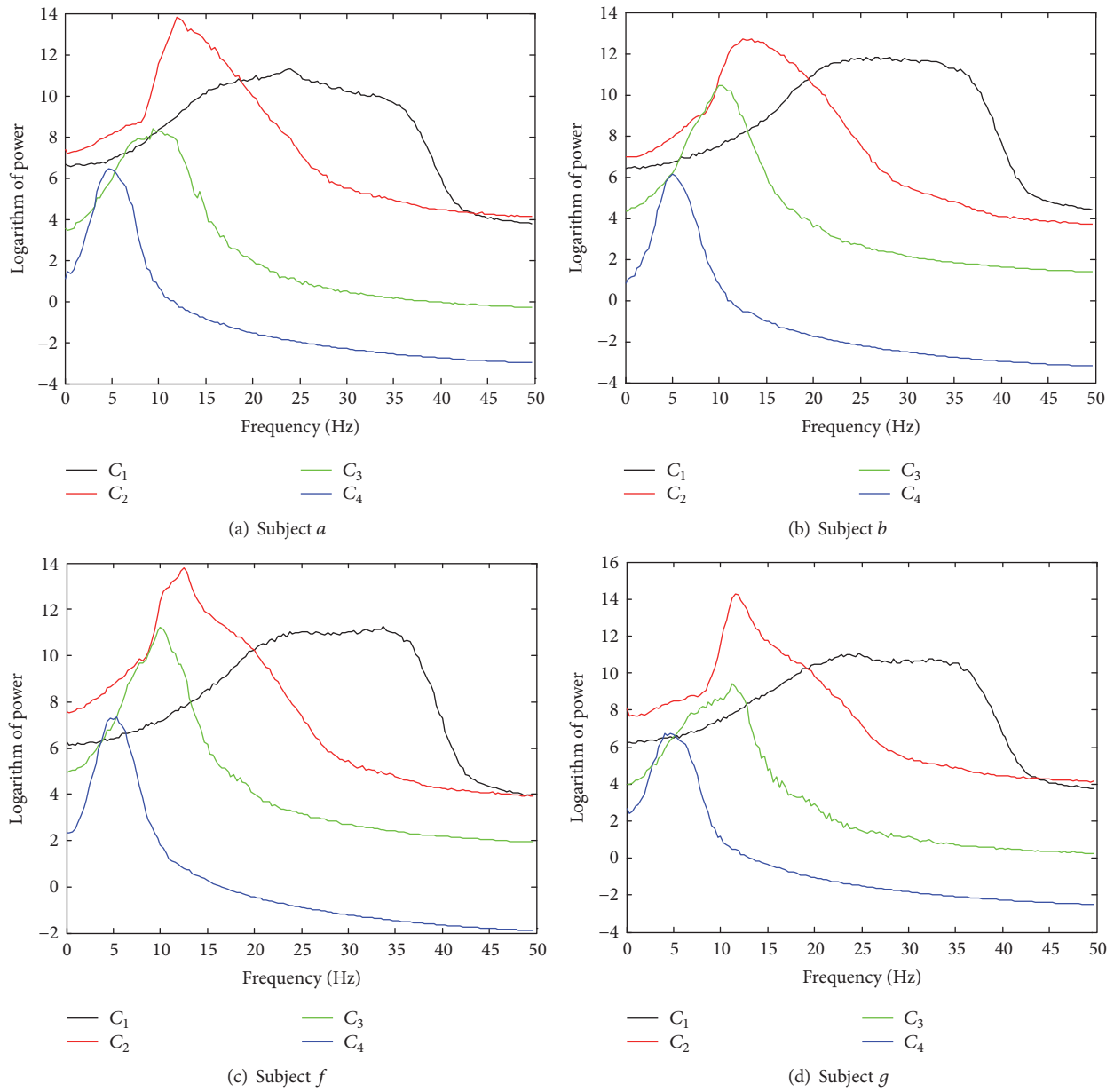

FIGURE 6: The average power spectra of $C_1 \sim C_4$ for all four subjects in BCI Competition IV Dataset I. Note that our method computes the average power spectra from the identified information-bearing IMFs at the first four scales for all 200 trials of each subject.

aforementioned steps, experimental results are presented as the following.

(I) To demonstrate the identification capability of the informative IMF components in EEG data using the proposed method: it is noted that, for EEG data, unlike the simulations, we do not know the ground truth of the IMFs that have been identified. For all 200 trials of each subject in the BCI Competition IV Dataset I, the average power spectra of the identified information-bearing IMFs were computed and then compared to those obtained using the existing method (NA-MEMD-PK) [21].

Figure 6 shows the logarithm of average power spectra for each subject using the new method. It can be seen that the *beta* and *mu* rhythms, which are contained in the 2nd (C_2) and 3rd IMFs (C_3), respectively, are separated clearly. Moreover, the frequency bandwidths in the 1st IMFs (C_1) are generally broad, containing some parts of the 15–30 Hz frequency band. Consequently, there is a trade-off in the choice of C_1; ignoring it would sacrifice some useful information, whereas conserving it could introduce noise. To resolve this problem, the role of the first scale is decided according to the optimal classification results combined with CSP-based feature extraction. For all four subjects, a paired t-test revealed no significant differences between the two approaches in the power spectra of all 200 trials at the first three IMFs but found a significant difference at the 4th IMF,

Table 1: p values comparing the power spectra of the first four IMFs identified by two approaches.

Subjects	1st IMFs	2nd IMFs	3rd IMFs	4th IMFs
a	0.581	0.995	0.536	0.007
b	0.899	0.989	0.866	0.004
f	0.656	0.998	0.958	0.030
g	0.540	1.000	0.777	0.010

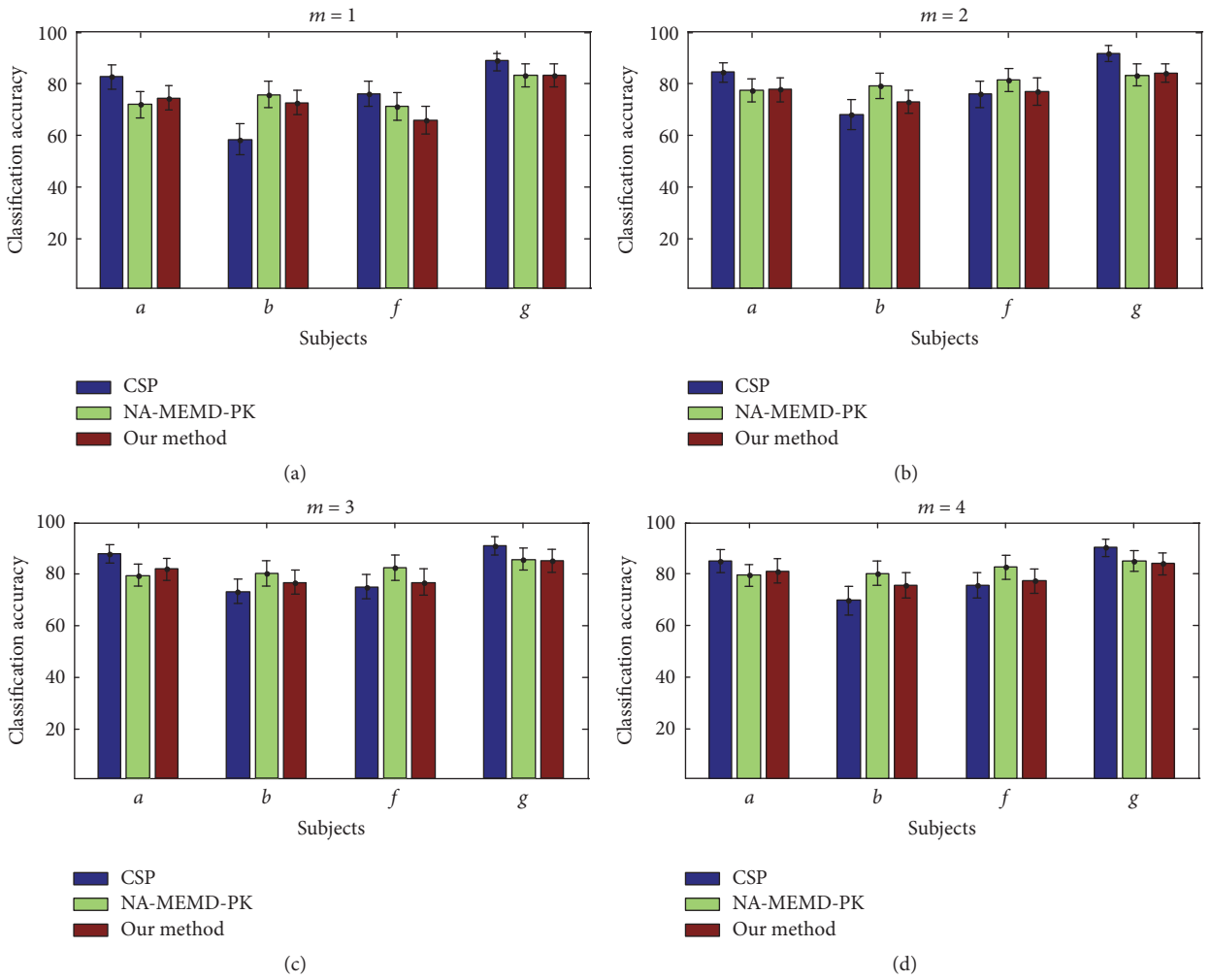

Figure 7: Classification accuracies (mean and standard deviation) obtained for the four subjects of BCI Competition IV Dataset I when $m = 1, 2, 3, 4$, respectively.

as shown in Table 1. This demonstrates the validity of the proposed approach when identifying information-bearing IMFs from real EEG data.

(II) An evaluation of the classification performance of the proposed method using a fivefold cross-validation study on two MI datasets: the classification process here was repeated 100 times using the new method, the NA-MEMD-PK algorithm [21], and the non-EMD based approach in which raw data is directly processed by CSP-based feature extraction and SVM-based classification for a varying number of spatial filters ($m = 1, 2, 3, 4$). The average accuracy and standard deviation were obtained for each method and used for direct comparison.

Considering the size of the total data for each subject in BCI Competition IV Dataset I, the number of EEG blocks was set at 140 for each training set and 60 for each testing set, as in [21]. To ensure a valid comparison between the different methods, the same data partitions were used in cross-validation. Figure 7 shows the classification performances for all four subjects from the BCI Competition IV Dataset I. The results show that the NA-MEMD-PK approach yielded the best averaged results, with an average classification accuracy of 81.01% for all four subjects—a 0.24% improvement over the CSP algorithm and a 1.81% improvement over the new method. The CSP method yielded the best performance among the three approaches in two subjects (a and g),

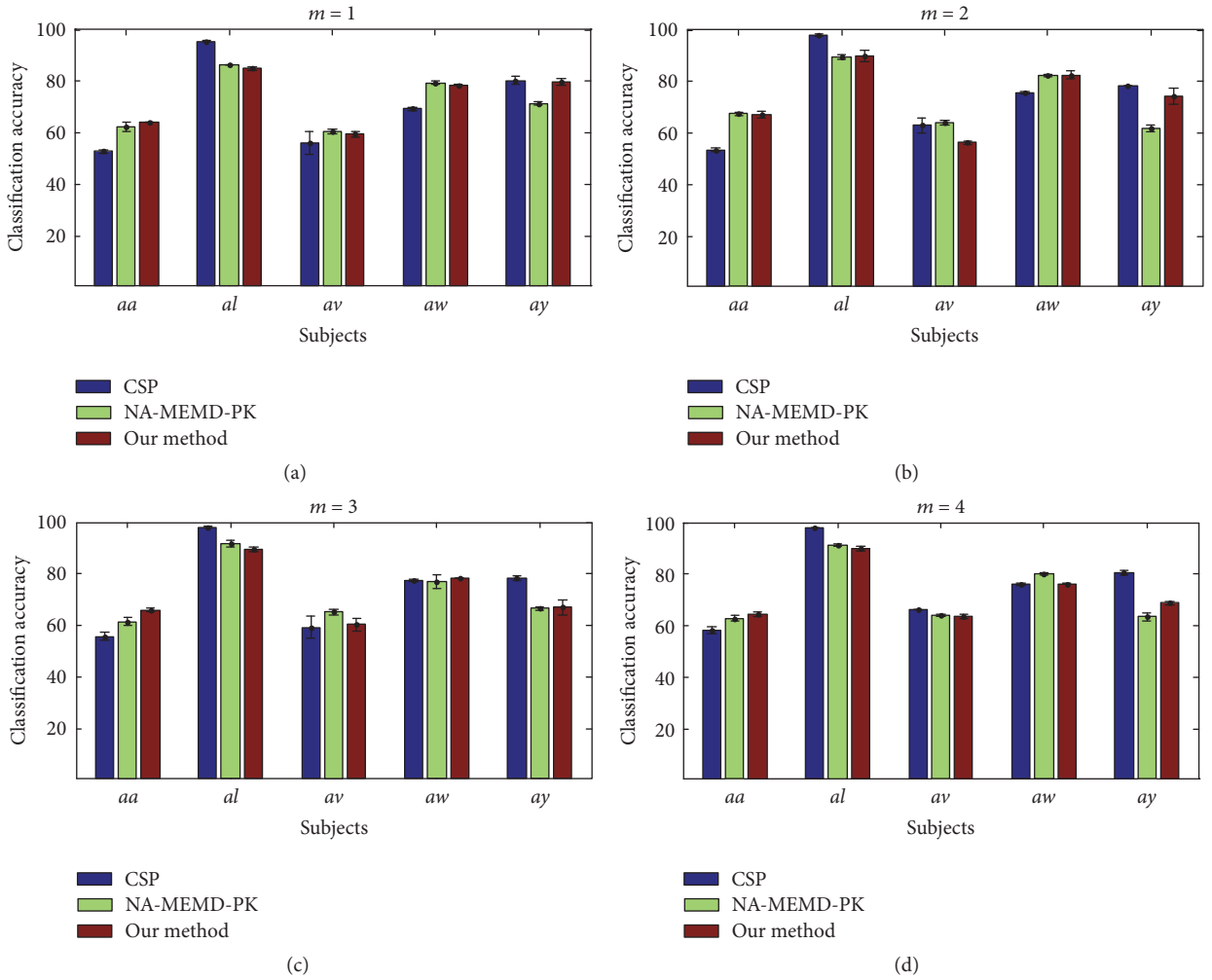

Figure 8: Classification accuracies (mean and standard deviation) obtained for the five subjects of BCI Competition III Dataset IVa when $m = 1, 2, 3, 4$, respectively.

whereas NA-MEMD-PK yielded the best mean accuracy in the two remaining subjects (b and f), while our method performed slightly higher than the CSP algorithm when $m = 2, 3$. Nevertheless, a paired t-test revealed no significant difference between our method and the NA-MEMD-PK algorithm ($p = 0.195, 0.096$ for $m = 2, 3$, resp.), no significant difference between our method and the CSP approach ($p = 0.074$ when $m = 2$), and a significant difference between our method and the CSP approach ($p = 0.003$ for $m = 3$). These results show that, when compared to the NA-MEMD-PK algorithm, our method can achieve similar results without the use of prior knowledge.

Finally, the classification performances for the five subjects from the BCI Competition III Dataset IVa are demonstrated. For each subject, the CSP filters and classifier models were trained on the available training sets. Figure 8 illustrates the classification accuracies (mean and standard deviation) obtained from these sets. The results showed that the average classification accuracy for all five subjects obtained by our method was 74.06%, yielding a 0.94% improvement over the NA-MEMD-PK approach. A paired t-test revealed no significant difference between our method and the NA-MEMD-PK algorithm ($p = 0.225, 0.027$ for $m = 2, 3$, resp.),and a significant difference between our method and the CSP approach (p values less than 0.01). When applied to the BCI Competition III data, the CSP method yielded the best performance among the three approaches in two subjects (*al* and *ay*), while the proposed algorithm performed the best in subject *aa* when $m = 1, 2, 3, 4$. Additionally, our method outperformed the NA-MEMD-PK approach in two subjects (*aa* and *ay*), whereas the NA-MEMD-PK algorithm performed better in two subjects (*al* and *av*) and yielded similar performance in subject *aw* for all four groups of spatial filters.

3.3. Discussion. In these experiments, the NA-MEMD algorithm exhibited an accurate localization of the task-specific frequency bands with favorable separability for feature extraction and classification, as demonstrated in its applications to MI EEG data. For the simulations, the new method was further shown to be robust to white and colored noises with different SNRs. When compared with other identification approaches (WD-CI, PCA-GMM, KPCA-GMM, and

L_1PCA-GMM), the proposed method obtained relatively improved performances in terms of both Type I and Type II error rates. For real EEG data, the information-bearing IMFs were discriminated clearly for nine subjects during MI tasks. When compared with the NA-MEMD-PK approach, which selects IMFs based on average power spectra, the proposed method yielded similar classification performance though it did not require prior knowledge to achieve such favorable results. Despite the favorable capability of the new algorithm when distinguishing the informative IMFs containing task-related frequency bands and classifying MI EEG signals, it should be recognized that individual subject differences may still have a great deal of influence on the recognition ability of the algorithm.

4. Conclusions

In this paper, we have shown how to discriminate the information-bearing components of motor imagery (MI) EEG independent of prior knowledge. The noise-assisted MEMD (NA-MEMD) algorithm was first performed on original datasets to obtain a set of multivariate IMFs, with the subsequent application of unsupervised kernel spectral regression (KSR) to generate low-dimensional feature vectors by mapping the decomposed IMFs into lower-dimensional subspace. For the low-dimensional feature vectors from each signal channel, a Gaussian mixture model (GMM) clustering approach was employed to estimate the optimal number of clusters and corresponding model parameters and then identify the information-bearing IMFs. The common spatial pattern (CSP) approach was exploited to train spatial filters to extract the task-related features from the reconstructed signals by adding the informative IMFs together. A support vector machine (SVM) classifier was applied to the extracted features and recognized the classes of EEG signals during different MI tasks. Using these techniques, we have demonstrated that our proposed method is effective at identifying the information-bearing IMF components in simulated data and MI EEG datasets and achieves excellent classification performance.

In conclusion, a novel method for scale-dependent signal identification in a low-dimensional subspace has been proposed for MI task classification. Although our method is independent of prior knowledge, entirely data-driven, and robust to different types of noise, several questions remain to be investigated in future work; the spectral regression-based dimensionality reduction approach selects the nearest neighbor graph; however this is not the only natural choice. Recently there has been a great deal of interest in exploring the different ways to construct a graph to model the intrinsic geometrical and discriminant structures within EEG datasets [38]. In addition, semisupervised clustering methods [39] have also yielded promising results when compared with the traditional unsupervised clustering approaches. To improve the clustering performance, it will be necessary to exploit the underlying manifold structure of the data along with additional knowledge from unlabeled data. Advancements such as these, in conjunction with the algorithm presented in this paper, will serve to improve the detection, classification, and evaluation of MI signals. This, in turn, can lead to improvements in EEG-based rehabilitation technologies, improving both the prediction and elicitation of motor recovery in a multitude of diseases worldwide [40].

Competing Interests

The authors declare that there is no conflict of interests regarding the publication of this article.

Acknowledgments

This work is supported by National Nature Science Foundation under Grants nos. 61201302, 61372023, 61671197, and 61601162 and Zhejiang Province Natural Science Foundation (LY15F010009). The authors would like to thank the providers of the BCI Competition IV Dataset I and BCI Competition III Dataset Iva which were used to test the algorithms proposed in this study.

References

[1] D. García Carrasco and J. Aboitiz Cantalapiedra, "Effectiveness of motor imagery or mental practice in functional recovery after stroke: a systematic review," *Neurologia*, vol. 31, no. 1, pp. 43–52, 2016.

[2] A. Faralli, M. Bigoni, A. Mauro, F. Rossi, and D. Carulli, "Noninvasive strategies to promote functional recovery after stroke," *Neural Plasticity*, vol. 2013, Article ID 854597, 16 pages, 2013.

[3] E. García-Cossio, M. Severens, B. Nienhuis et al., "Decoding sensorimotor rhythms during robotic-assisted treadmill walking for brain computer interface (BCI) applications," *PLoS ONE*, vol. 10, no. 12, Article ID e0137910, 2015.

[4] N. Jrad, M. Congedo, R. Phlypo et al., "sw-SVM: sensor weighting support vector machines for EEG-based brain-computer interfaces," *Journal of Neural Engineering*, vol. 8, no. 5, Article ID 056004, 2011.

[5] X.-W. Wang, D. Nie, and B.-L. Lu, "Emotional state classification from EEG data using machine learning approach," *Neurocomputing*, vol. 129, pp. 94–106, 2014.

[6] N. Kwak, "Principal component analysis based on L1-norm maximization," *IEEE Transactions on Pattern Analysis and Machine Intelligence*, vol. 30, no. 9, pp. 1672–1680, 2008.

[7] D. Cai, X. F. He, and J. W. Han, "Spectral regression: a unified approach for sparse subspace learning," in *Proceedings of the 7th IEEE International Conference on Data Mining (ICDM '07)*, pp. 73–82, IEEE, Omaha, Neb, USA, October 2007.

[8] D. Cai, *Spectral regression: a regression framework for efficient regularized subspace learning [Ph.D. thesis]*, University of Illinois at Urbana-Champaign, Champaign, Ill, USA, 2009.

[9] J. B. Tenenbaum, V. de Silva, and J. C. Langford, "A global geometric framework for nonlinear dimensionality reduction," *Science*, vol. 290, no. 5500, pp. 2319–2323, 2000.

[10] Y. Z. Pan, S. Z. S. Ge, and A. A. Mamun, "Weighted locally linear embedding for dimension reduction," *Pattern Recognition*, vol. 42, no. 5, pp. 798–811, 2009.

[11] M. Belkin and P. Niyogi, "Laplacian eigenmaps for dimensionality reduction and data representation," *Neural Computation*, vol. 15, no. 6, pp. 1373–1396, 2003.

[12] L. Wang, K. Wang, and R. F. Li, "Unsupervised feature selection based on spectral regression from manifold learning for facial expression recognition," *IET Computer Vision*, vol. 9, no. 5, pp. 655–662, 2015.

[13] Z. Xia, S. Xia, L. Wan, and S. Cai, "Spectral regression based fault feature extraction for bearing accelerometer sensor signals," *Sensors*, vol. 12, no. 10, pp. 13694–13719, 2012.

[14] N. E. Huang, Z. Shen, and S. R. Long, "The empirical mode composition and the Hilbert spectrum for nonlinear and non-stationary time series analysis," *Proceedings of the Royal Society of London Series A: Mathematical and Physical Sciences*, vol. 454, pp. 903–995, 1998.

[15] C.-H. Wu, H.-C. Chang, P.-L. Lee et al., "Frequency recognition in an SSVEP-based brain computer interface using empirical mode decomposition and refined generalized zero-crossing," *Journal of Neuroscience Methods*, vol. 196, no. 1, pp. 170–181, 2011.

[16] M. Hu and H. Liang, "Intrinsic mode entropy based on multivariate empirical mode decomposition and its application to neural data analysis," *Cognitive Neurodynamics*, vol. 5, no. 3, pp. 277–284, 2011.

[17] Z. Wu and N. E. Huang, "Ensemble empirical mode decomposition: a noise-assisted data analysis method," *Advances in Adaptive Data Analysis*, vol. 1, no. 1, pp. 1–41, 2009.

[18] N. Rehman, C. Park, N. E. Huang, and D. P. Mandic, "EMD via MEMD: multivariate noise-aided computation of standard EMD," *Advances in Adaptive Data Analysis*, vol. 5, no. 2, Article ID 1350007, 25 pages, 2013.

[19] N. ur Rehman and D. P. Mandic, "Filter bank property of multivariate empirical mode decomposition," *IEEE Transactions on Signal Processing*, vol. 59, no. 5, pp. 2421–2426, 2011.

[20] N. Rehman and D. P. Mandic, "Multivariate empirical mode decomposition," *Proceedings of The Royal Society of London. Series A. Mathematical, Physical and Engineering Sciences*, vol. 466, no. 2117, pp. 1291–1302, 2010.

[21] C. Park, D. Looney, N. Ur Rehman, A. Ahrabian, and D. P. Mandic, "Classification of motor imagery BCI using multivariate empirical mode decomposition," *IEEE Transactions on Neural Systems and Rehabilitation Engineering*, vol. 21, no. 1, pp. 10–22, 2013.

[22] H.-C. Chang, P.-L. Lee, M.-T. Lo, Y.-T. Wu, K.-W. Wang, and G.-Y. Lan, "Inter-trial analysis of post-movement beta activities in EEG signals using multivariate empirical mode decomposition," *IEEE Transactions on Neural Systems and Rehabilitation Engineering*, vol. 21, no. 4, pp. 607–615, 2013.

[23] A. Komaty, A.-O. Boudraa, B. Augier, and D. Dare-Emzivat, "EMD-based filtering using similarity measure between probability density functions of IMFs," *IEEE Transactions on Instrumentation and Measurement*, vol. 63, no. 1, pp. 27–34, 2014.

[24] M. Hu and H. Liang, "Search for information-bearing components in neural data," *PloS ONE*, vol. 9, no. 6, article e99793, 2014.

[25] C. A. Bouman, M. Shapiro, G. W. Cook et al., "Cluster: an unsupervised algorithm for modeling Gaussian mixtures," 2005, https://engineering.purdue.edu/~bouman/software/cluster/.

[26] B. Blankertz, G. Dornhege, M. Krauledat, K.-R. Müller, and G. Curio, "The non-invasive Berlin brain-computer interface: fast acquisition of effective performance in untrained subjects," *NeuroImage*, vol. 37, no. 2, pp. 539–550, 2007.

[27] G. Dornhege, B. Blankertz, G. Curio, and K.-R. Müller, "Boosting bit rates in noninvasive EEG single-trial classifications by feature combination and multiclass paradigms," *IEEE Transactions on Biomedical Engineering*, vol. 51, no. 6, pp. 993–1002, 2004.

[28] G. Pfurtscheller and F. H. L. Da Silva, "Event-related EEG/MEG synchronization and desynchronization: basic principles," *Clinical Neurophysiology*, vol. 110, no. 11, pp. 1842–1857, 1999.

[29] G. Pfurtscheller, C. Brunner, A. Schlögl, and F. H. Lopes da Silva, "Mu rhythm (de)synchronization and EEG single-trial classification of different motor imagery tasks," *NeuroImage*, vol. 31, no. 1, pp. 153–159, 2006.

[30] N. E. Huang, M. L. Wu, S. R. Long et al., "A confidence limit for the empirical mode decomposition and Hilbert spectral analysis," *Proceedings of Royal Society A*, vol. 459, no. 2037, pp. 2317–2345, 2003.

[31] G. Rilling, P. Flandrin, and P. Goncalves, "On empirical mode decomposition and its algorithms," in *Proceedings of the IEEE-EURASIP Workshop on Nonlinear Signal Image Processing (NSIP '03)*, vol. 3, pp. 8–11, Grado-Trieste, Italy, June 2003.

[32] A. P. Dempster, N. M. Laird, and D. B. Rubin, "Maximum likelihood from incomplete data via the EM algorithm," *Journal of the Royal Statistical Society. Series B. Methodological*, vol. 39, no. 1, pp. 1–38, 1977.

[33] H. Ramoser, J. Müller-Gerking, and G. Pfurtscheller, "Optimal spatial filtering of single trial EEG during imagined hand movement," *IEEE Transactions on Rehabilitation Engineering*, vol. 8, no. 4, pp. 441–446, 2000.

[34] V. N. Vapnik, *Statistical Learning Theory*, John Wiley & Sons, 1998.

[35] C.-C. Chang and C.-J. Lin, "LIBSVM: a library for support vector machines," 2001, http://www.csie.ntu.edu.tw/~cjlin/libsvm.

[36] C. M. Bishop, *Pattern Recognition and Machine Learning (Information Science and Statistics)*, Springer, New York, NY, USA, 2006.

[37] F. Lotte and C. T. Guan, "Regularizing common spatial patterns to improve BCI designs: unified theory and new algorithms," *IEEE Transactions on Biomedical Engineering*, vol. 58, no. 2, pp. 355–362, 2011.

[38] X. F. He, D. Cai, Y. L. Shao, H. Bao, and J. Han, "Laplacian regularized Gaussian mixture model for data clustering," *IEEE Transactions on Knowledge and Data Engineering*, vol. 23, no. 9, pp. 1406–1418, 2011.

[39] H. Gan, N. Sang, and R. Huang, "Manifold regularized semi-supervised Gaussian mixture model," *Journal of the Optical Society of America A*, vol. 32, no. 4, pp. 566–575, 2015.

[40] L. M. Alonso-Valerdi, R. A. Salido-Ruiz, and R. A. Ramirez-Mendoza, "Motor imagery based brain-computer interfaces: an emerging technology to rehabilitate motor deficits," *Neuropsychologia*, vol. 79, pp. 354–363, 2015.

Hindawi Publishing Corporation
Neural Plasticity
Volume 2016, Article ID 4182483, 10 pages
http://dx.doi.org/10.1155/2016/4182483

Research Article

EEG Source Imaging Guided by Spatiotemporal Specific fMRI: Toward an Understanding of Dynamic Cognitive Processes

Thinh Nguyen,[1] Thomas Potter,[1] Trac Nguyen,[1] Christof Karmonik,[2] Robert Grossman,[3] and Yingchun Zhang[1,4]

[1]*Department of Biomedical Engineering, Cullen College of Engineering, University of Houston, Houston, TX 77204, USA*
[2]*MRI Core, Houston Methodist Research Institute, Houston, TX 77030, USA*
[3]*Department of Neurosurgery, Houston Methodist Hospital and Research Institute, Houston, TX 77030, USA*
[4]*Guangdong Provincial Work Injury Rehabilitation Center, Guangzhou 510000, China*

Correspondence should be addressed to Yingchun Zhang; yzhang94@uh.edu

Received 27 June 2016; Revised 19 August 2016; Accepted 5 September 2016

Academic Editor: David E. Vaillancourt

Understanding the mechanism of neuroplasticity is the first step in treating neuromuscular system impairments with cognitive rehabilitation approaches. To characterize the dynamics of the neural networks and the underlying neuroplasticity of the central motor system, neuroimaging tools with high spatial and temporal accuracy are desirable. EEG and fMRI stand among the most popular noninvasive neuroimaging modalities with complementary features, yet achieving both high spatial and temporal accuracy remains a challenge. A novel multimodal EEG/fMRI integration method was developed in this study to achieve high spatiotemporal accuracy by employing the most probable fMRI spatial subsets to guide EEG source localization in a time-variant fashion. In comparison with the traditional fMRI constrained EEG source imaging method in a visual/motor activation task study, the proposed method demonstrated superior localization accuracy with lower variation and identified neural activity patterns that agreed well with previous studies. This spatiotemporal fMRI constrained source imaging method was then implemented in a "sequential multievent-related potential" paradigm where motor activation is evoked by emotion-related visual stimuli. Results demonstrate that the proposed method can be used as a powerful neuroimaging tool to unveil the dynamics and neural networks associated with the central motor system, providing insights into neuroplasticity modulation mechanism.

1. Introduction

Cognitive rehabilitation often involves and relies on the modulation of neuroplasticity to improve motor function. However, the neuroplasticity mechanisms associated with the central motor system remain poorly understood. While the brain regions involved in motor execution are well characterized, the detailed dynamics of these neural events and the underlying neural network changes still remain unclear. Neuroplasticity, the ability of the brain to alter neuronal connections, can be expressed on both anatomical and functional levels. The anatomical aspects of plasticity can be captured directly via structural imaging (e.g., MRI, DTI) [1, 2]. Accordingly, functional markers (delta waves, nonrapid eye movements, event related synchronization/desynchronization, etc.) of neural plasticity have also been identified in a variety of conditions [3–5]. Properly investigating these markers, however, remains a major challenge since it requires advanced imaging modalities with both high temporal and spatial resolution. Thoroughly characterizing the dynamic processes of the neuromuscular system, in both healthy and diseased brains, is the first step toward understanding the plastic changes that occur during neural diseases, injuries, and the treatment outcomes of different rehabilitation programs. Multiple noninvasive neuroimaging methods have been developed to achieve this goal, among which functional Magnetic Resonance Imaging (fMRI) and Electroencephalography (EEG) currently stand as prevailing techniques.

fMRI comprises one of the primary methods for observing neural activity. As an extension of anatomical MRI, fMRI utilizes a series of strong magnetic fields in concert

with native local inhomogeneities within the body to create a Blood Oxygen Level Dependent (BOLD) contrast that identifies regions with significantly different concentrations of oxygenated blood [6]. This serves as an indirect measure of underlying neuronal activity—the high metabolic demand of active brain regions requires an influx of oxygen-rich blood [7], increasing the intensity of voxels where activity can be observed [8]. Typical analysis for this convolves the detected timescale peaks with a hemodynamic response. The method continues by utilizing a general linear model that treats different conditions, motion parameters, and polynomial baselines as regressors to generate a map of significantly activated voxels [9, 10], ultimately creating a static but spatially accurate depiction of cortical BOLD fluctuations and, by extension, the underlying neural activity.

Beyond simple statistical tests, further analysis can be performed on fMRI data to elucidate networks of functional activity across the disparate brain regions. Instead of treating conditions as regressors, measures of correlation are calculated from the time courses of the BOLD signals of voxels and regions to identify highly correlated regions and the statistical dependencies between them [11, 12]. Correlations such as these can be applied in both the time and frequency domains and open the door for further analysis under graph theory, which creates a mathematical representation of functional networks by modeling voxels or regions as "nodes" and the connections between them as "edges." A variety of potential measures are available under this graph theory to describe the networks within the brain and their arrangement [13], each of which has shown use in different conditions or diseases, including the analysis of emotion processing [9, 14–20]. Together, these methods provide robust and varied methods for examining functional MRI data and the activity it reveals.

Electroencephalography (EEG), in contrast to fMRI, represents a method for directly detecting and recording electrical signals associated with neural activity from scalp electrodes. As signals are transduced from neuron to neuron, the postsynaptic potentials that result from neurotransmitter detection create electrical activity which, while individually weak, sums to produce larger voltage potentials [21]. With a series of electrodes measured against a reference at rapid sampling rate, EEG is able to generate temporally accurate measurements of these voltage differences on the scalp [22]. Unfortunately, the transduction of these signals through the brain, cerebrospinal fluid, skull, and scalp blurs the results, limiting the effective spatial resolution of the modality [23]. Source imaging methods have been developed to alleviate this limitation by modeling the intermediate layers and their conductivities and backwards calculating the origin of the sources [24]. However, this still poses a technical challenge, as the "inverse problem" in the source imaging methods is ill-posed: the number of variables vastly outnumber the available data [25]. Common source imaging analysis makes use of a pseudoinversion to circumvent this and results with focal spatial localization can be achieved by further minimizing a net current vector [26]. This solution, however, relies on a maximized likelihood instead of clear results and subsequently suffers from complex calculation and spatial imprecision.

EEG and fMRI can be viewed as complimentary imaging modalities. fMRI alone is limited as hemodynamic signals that only provide an indirect measure of the neuronal activity with a poor temporal resolution (second level). In contrast, EEG directly measures dynamic electrophysiological activity of the brain with a very high temporal resolution (millisecond level), but poor spatial resolution. These properties have led to multimodal approaches seeking to optimize the favorable properties from each [27]. Simultaneous EEG and fMRI allow the excellent temporal resolution of EEG to be combined with the high spatial accuracy of fMRI to overcome the limitations associated with unimodal fMRI or EEG.

Asymmetrical integration methods make use of EEG to inform fMRI [27] or fMRI BOLD maps as constraints to guide EEG localization [28, 29]. These methods, however, are subject to localization mismatch and bias [30]. Traditional EEG/fMRI integration and connectivity analysis starts with fMRI-informed EEG source localization. Usually, an fMRI-derived BOLD activation map is used to construct spatial constraints on the source space in the form of a source covariance matrix, whereas active sources not present in the fMRI are penalized [28, 29, 31]. The performance of this approach also relies on the accuracy of EEG source analysis, which could be spatially biased due to the use of fMRI BOLD activation map as "hard" constraints, in the sense that fMRI-derived spatial information is considered an absolute truth in guiding the EEG source analysis. As such, EEG source reconstruction could be strongly biased in the event of an EEG-fMRI mismatch [30] (due to neurovascular decoupling, signal detection failure, etc.).

The Bayesian framework has recently been developed [32–35] to perform fMRI-informed EEG source imaging utilizing fMRI information as "soft" constraints. In particular, two-level hierarchical empirical Bayesian models are used to model the EEG inverse problem, where parameters at the first level represent unknown source activity and the 2nd-level parameters (hyperparameters) model the prior distribution of the 1st-level parameters (equivalent to source covariance matrix). Model inversion is done using an Expectation Maximization (EM) technique that estimates the hyperparameters that would maximize the model evidence and, in turn, estimate the parameters of interest—EEG source activity (see [33, 36] for details on Bayesian model inversion scheme). These methods incorporate fMRI information as "soft" constraints, in which the fMRI-active map is modeled as a prior and its relative weighting is estimated via the hyperparameters. The hierarchical empirical Bayesian framework allows the fMRI information to be modeled as a weighted sum of multiple submaps, representing multiple priors, controlled by corresponding weighting hyperparameters, with values to be estimated. However, the issue of temporal mismatch between EEG-fMRI still persists.

In this study, we propose a spatiotemporal fMRI constrained EEG source imaging approach to address the issue of temporal mismatch between EEG-fMRI by calculating the optimal subset of fMRI priors (in terms of model evidence) based on a hierarchical Bayesian model. fMRI priors were computed in a data-driven manner from particular windows of interest in the EEG data, leading to time-variant

fMRI constraints. The proposed approach utilizes the high temporal resolution nature of EEG to compute a current density mapping of the cortical activity, informed by the high spatial resolution of fMRI in a time-variant, spatially selective manner, to accurately image dynamic neural activity. The high spatiotemporal features of this method then make it particularly desirable for studying the central motor system and functional aspects of plasticity as they relate to cognitive rehabilitation.

2. Methodology

2.1. Data Model. Considering a linear model of EEG data $Y \in \mathbb{R}^{m\times d}$ over m channels and d measurement samples:

$$Y = GJ + \varepsilon, \quad \varepsilon \sim N(0, C), \; J \sim N(0, R), \tag{1}$$

where $G \in \mathbb{R}^{m\times s}$ represents the lead field matrix and $J \in \mathbb{R}^{s\times d}$ represents the unknown source activity of d dipole sources in the source space. ε represents the noise component in the sensor space with its noise covariance matrix C. R represents the source covariance matrix. The current density J can be reconstructed according to (2) by applying the L_2-norm inversion scheme [26] to the model above.

$$J = RG^T \left(GRG^T + \lambda^C C\right)^{-1} Y. \tag{2}$$

The regularization parameter, λ^C, could be seen as the trade-off between model accuracy and complexity and is traditionally determined using the L-curve method. The source covariance matrix R represents prior knowledge about the distribution of J. R will be an identity matrix, I, if no prior assumption has been made to the distribution of J and R will be constructed according to the fMRI activation map in a EEG/fMRI integration approach [28]. Thus, the source space J is subjected to a prior spatial constraint based on the active voxels from the BOLD mapping. However, imposing such time-invariant fMRI constraints might not be appropriate for all time instances.

2.2. Spatiotemporal fMRI Constrained EEG Source Imaging

2.2.1. fMRI Data Analysis. The classical general linear model (GLM) is employed for statistical analysis of preprocessed fMRI data, and a map of the voxels that show statistically significant activity is achieved when contrasted between two or more conditions (e.g., task versus baseline). Voxel values in the fMRI map below a certain p value threshold ($p < 0.05$) are omitted, to ensure that only statistically significant voxels are used as constraints for the source imaging routine.

In this study, the fMRI activation map is further divided into multiple submaps based on clusters of neighboring locations or cortical functional regions for spatial flexibility in applying the fMRI information as a constraint.

2.2.2. The Source Covariance Matrix R. In our current framework, we employ the construction of R as follows:

$$R = \sum_{i=1}^{N} \lambda_i^R Q_i. \tag{3}$$

R is defined by the sum of N covariance components $Q = \{Q_1, \ldots, Q_N\}$, weighted by an unknown hyperparameter λ^R. Each covariance component, $Q_i = q_i q_i^T$, is formed from a subset q_i of the fMRI map as explained above.

2.2.3. Space Time Specific fMRI Priors. Given EEG data Y, an optimized weighted combination of these N priors via their respective λ_i^R is determined by maximizing the log model evidence $\ln p(Y \mid \lambda)$, where $\lambda = \{\lambda^C, \lambda^R\}$.

$$\begin{aligned} \ln p(Y \mid \lambda) &= \ln \int p(Y, J \mid \lambda)\, dJ, \\ \ln p(Y \mid \lambda) &= F + D\left(q(J) \parallel p(J \mid Y, \lambda)\right), \end{aligned} \tag{4}$$

where F is the variational free energy and a lower bound on the evidence. Maximizing this boundary would minimize the Kullback-Leibler divergence $D(q(J) \parallel p(J \mid Y, \lambda))$, so that the free energy approximates the log-evidence, $F \approx \ln p(Y \mid \lambda)$.

F can then be calculated as

$$\begin{aligned} F = &-\frac{1}{2}\mathrm{tr}\left(\Sigma\left(\mu^\lambda\right)^{-1} YY^T\right) - \frac{1}{2}\ln\left|\Sigma\left(\mu^\lambda\right)\right| - \frac{1}{2}\ln(2\pi) \\ &+ \frac{1}{2}\ln\left|\Sigma^\lambda\right| - \frac{1}{2}\left(\mu^\lambda - \eta\right)^T \Pi\left(\mu^\lambda - \eta\right), \end{aligned} \tag{5}$$

where $\Sigma(\mu^\lambda) = GRG^T + C$ and the conditional density of the hyperparameters is $q(\lambda) = N(\mu^\lambda, \Sigma^\lambda)$ with its prior $p(\lambda) = N(\eta, \Pi^{-1})$, where $\eta = -32$, $\Pi = 256$ (for a detailed derivation and discussion of the free energy F, see [33, 36]).

Given this model, F is equivalent to a ReML objective function and can be maximized using a classical ReML algorithm. The maximization of F yields $(\mu^\lambda, \Sigma^\lambda)$ and a model evidence which could further be used for model comparison. When $\lambda = \mu^\lambda$, an optimal weighted combination of fMRI priors $\{q_1, q_2, \ldots, q_N\}$ is determined and the corresponding source dynamics J can be solved for the given time window of interest.

2.2.4. EEG Source Imaging. EEG data is divided into different time windows. EEG information in each time window is then used to estimate the hyperparameter λ^R by estimating the model evidence $\ln p(Y \mid \lambda)$ via maximizing the variational free energy (4). The source covariance matrix R is determined from the estimated hyperparameter λ^R using (3) for each time window. The dynamic activity of the source J, constrained by R, is calculated in (2). Figure 1 shows a schematic of the approach described above. Instead of applying a static fMRI map as a constraint for all time instances, multiple subsets of the fMRI information are employed as spatial priors in a weighted manner and the weighting factors are determined by the EEG data in each specific time period. As such, EEG source imaging constrained by fMRI in spatiotemporal specific fashion is achieved.

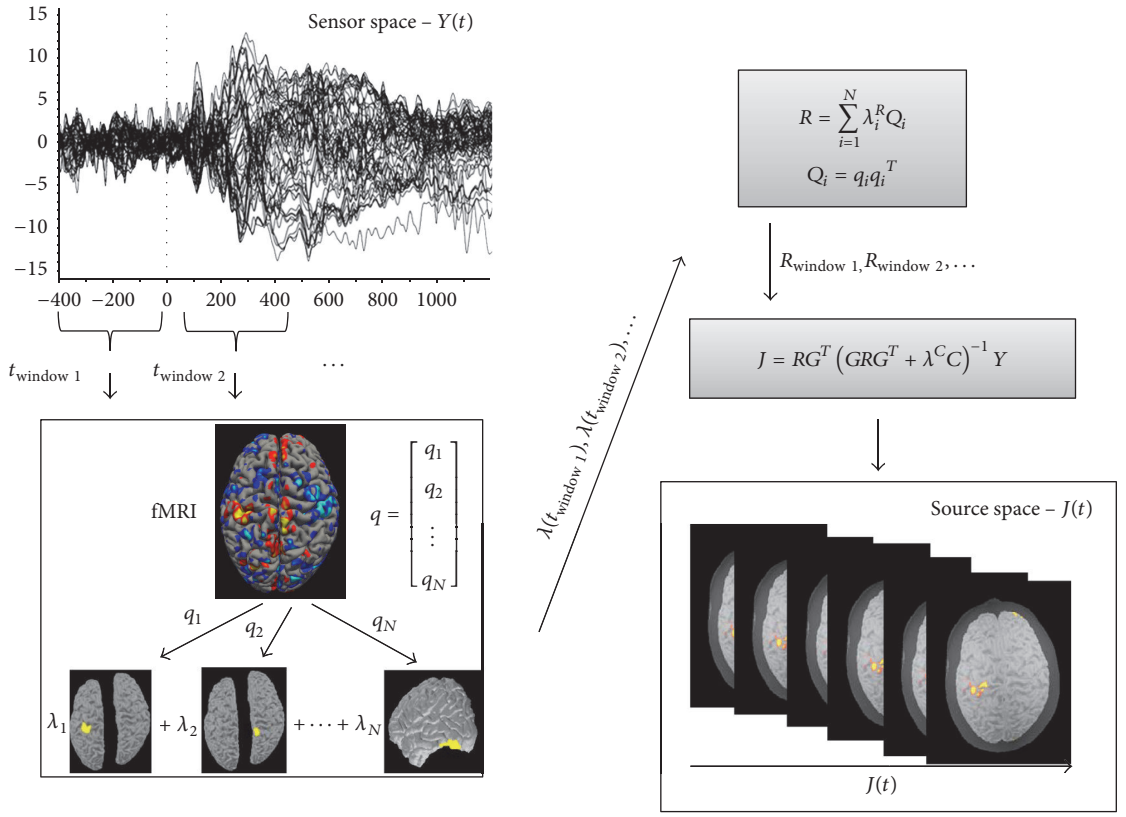

Figure 1: Schematic of the spatiotemporal fMRI constraints on EEG source imaging.

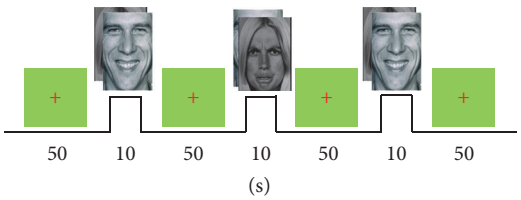

Figure 2: Experimental paradigm—rest state: subjects were shown a green background (50 seconds); active state: display of face image (two categories: unpleasant and pleasant); subjects are to squeeze a ball with right hand for 10 seconds if image was perceived as unpleasant.

2.3. Experimental Setup and Data Processing

2.3.1. The Paradigm. EEG and fMRI data were acquired from three healthy male subjects (age 22 to 26 years) participating in a visual stimulus/motor response experiment under a research protocol approved by the local ethic committee. The paradigm consisted of a series of visual stimuli, each belonging to one of two categories: pleasant faces and unpleasant faces as illustrated in Figure 2. In each trial, a 50-second green screen baseline was first shown, followed by a categorically randomized 10-second visual stimulus. The subject was instructed to squeeze a rubber ball with his right hand for the entire duration the stimulus image was shown if he perceived the presented face as unpleasant, while remaining at rest if the image was perceived as pleasant. The fMRI data from 5 pleasant and 5 unpleasant trials were collected while the EEG data from 40 pleasant and 40 unpleasant trials were collected outside the MRI room using the same experimental paradigm.

2.3.2. Anatomical and Functional MRI Data Acquisition. EEG and fMRI scans were performed during different sessions for each subject. fMRI data acquisition (Philips Ingenia 3.0T) was performed using gradient echo Echo-Planar Imaging, with repetition time (TR) of 1500 ms, echo time (TE) of 35 ms, and voxel size of 3 × 3 × 5 mm. fMRI data underwent a conventional fMRI preprocessing pipeline: realignment, slice timing correction, motion correction, coregistration, segmentation, normalization, and spatial smoothing (FWHM of 3 mm) were applied. The structural MRI for each subject was also obtained for fMRI coregistration and subject-specific head model generation. A T1-weighted MRI image was acquired using gradient echo, with TR = 8.1 ms, TE = 3.7, and voxel size 0.9 × 0.9 × 1 mm.

T1-weighted structural MRI images for each subject underwent full reconstruction procedure using the Freesurfer image analysis suite (publicly available at: http://surfer.nmr.mgh.harvard.edu/), resulting in generation of a high-definition cortical layer and brain-skull-skin layer. The high-density cortical layer mesh was downsampled to ~10,000

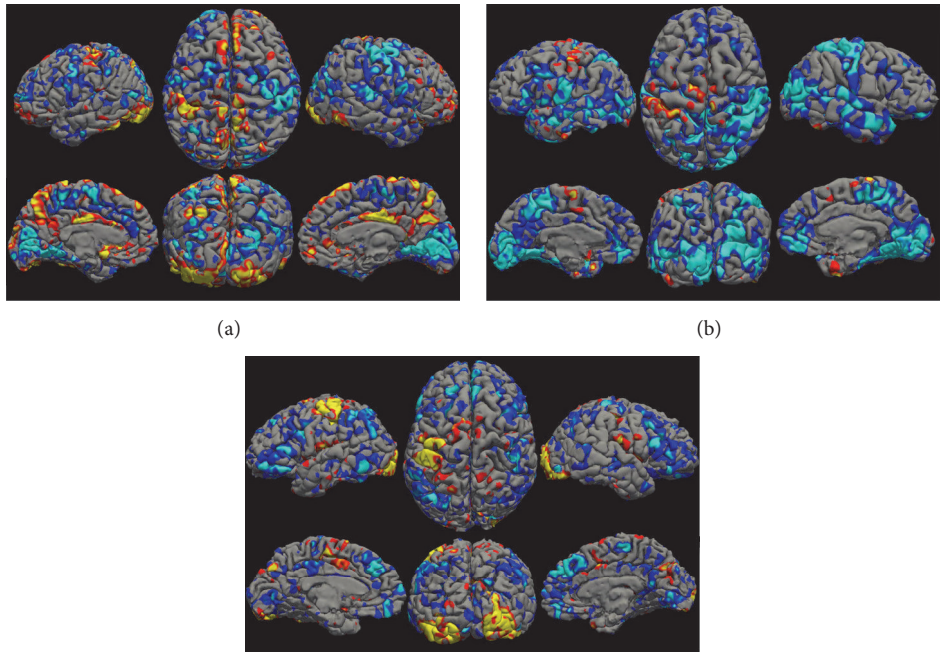

(a) (b)

(c)

Figure 3: Unpleasant-face response versus baseline fMRI activation map showing regions of high BOLD signal for subjects #1, #2, and #3 in (a), (b), and (c), respectively.

vertices per hemisphere and used as the source space, where each vertex location corresponds to a dipole source oriented perpendicular to the surface. A lead field matrix G was computed via a forward calculation using the cortical source space, a 3-layer head model, and 64-channel electrode locations coregistered to the model.

2.3.3. fMRI-EEG Data Acquisition and Processing. fMRI data analysis was performed using the Freesurfer software suite. Spatial blurring was applied using a Gaussian kernel with a 3 mm full width at half maximum (fwhm). The hemodynamic response was modeled using a 0th derivative canonical SPM hemodynamic response function. The two experimental conditions and six motion parameters were used as regressors in the general linear model (GLM) for the statistical analysis of the fMRI data, with a 2nd-order nuisance regressor included to correct for noise. Statistical t-maps contrasting experimental conditions against baseline were generated for each subject. Correction for multiple comparisons was performed by controlling the Family Wise Error Rate (FWER). A cluster-based FWE-corrected p value of 0.05 was set, such that only clusters large enough to surpass the $p < 0.05$ threshold were considered activated. Individual fMRI maps were translated to corresponding subject-specific cortical models and a 4-voxel cluster-extent threshold was applied to account for any erroneous voxel activity resulting from the translation process. EEG recordings were performed with a sampling rate of 5 kHz using a 64-channel EEG recording system (Brain Products, Germany). EEG data was preprocessed using BrainVision Analyzer 2.0 (Brain Products, Germany). Rereferencing to a linked mastoid and a band pass filter from 0.5 Hz to 50 Hz were employed along with a notch filter at 60 Hz. EKG artifacts were removed by means of template subtraction; ocular artifacts and movement-related artifacts were further removed by independent component analysis (ICA). The EEG data with unexpected artifacts and/or noise were removed, resulting in an EEG data set consisting of 36 pleasant trials and 37 unpleasant trials. Single-trial EEG data were employed and segmented from 400 ms prior to the visual stimulus onset (at 0 ms) to 1200 ms after the onset. Ball squeezing occurred at an average time of 600 ms (ranging from 500 ms to 800 ms) after visual stimulus onset. Each epoch was baseline corrected using a baseline measured from −400 ms to 0 ms. EEG data were segmented evenly to yield 40 individual time windows in this study. A window length of 40 ms was employed to maintain high specificity and accommodate the timeline of anticipated ERPs associated with the experimental paradigm with a minimal risk of clipping evoked potentials (VEP, P300, MEP, etc.) [37, 38].

3. Results

3.1. fMRI. The fMRI BOLD activation map shows statistically significant regions of cortical activity during the visually evoked and motor responses of the participant responding to the unpleasant-face stimulus (see Figure 3). The dominant activated regions were found to be in the bilateral visual cortices, left motor cortex, fusiform face area, supplementary motor area, and posterior cingulate cortex.

3.2. Model Comparison. The model evidence $p(Y \mid \lambda)$ describes how well a given model can explain the measured

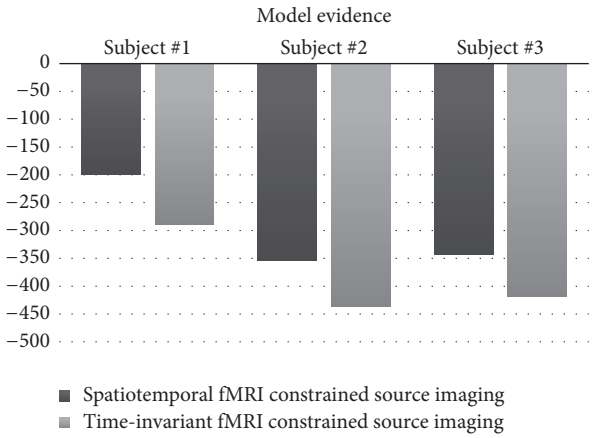

Figure 4: Model comparison between two methods: time-invariant fMRI constraints and spatiotemporal fMRI constraints source imaging for three subjects. Model comparison, given in terms of log model evidence $\ln p(Y \mid \lambda)$, serves as a relative metric to compare performance of different data models, with higher value depicting better model.

data; the absolute value itself is arbitrary and should only be interpreted as a relative metric to compare the performance of different models. The average log-evidence $\ln p(Y \mid \lambda)$ was computed across the time course of each epoch, comparing two models: the spatial and temporal variant fMRI-based prior model and the time-invariant fMRI constraints model. The results suggest better performance using the spatiotemporal variant fMRI model consistently across all three subjects as shown in Figure 4.

3.3. Validation. Two source imaging methods, that is, the traditional time-invariant fMRI constraints source imaging and spatiotemporal fMRI constrained EEG source imaging methods, were implemented and compared in terms of the performance in characterizing source dynamics in the brain. Source analysis was performed in a single-trial manner. For each trial, EEG data was divided into multiple time windows of interest and the weights for source priors were determined. Dynamic source activity for each time window was then computed using the calculated weights (as described in Section 2).

Figure 5 compares the neural activity at two time points of interest, as calculated by classical time-invariant algorithm (left; subfigures (1) and (2)) and the new spatiotemporal algorithm (right; subfigures (3) and (4)). For the subjects and the trials analyzed, both methods showed the increase of current density consistently in the bilateral visual cortices and left motor cortex. For subject #1, visual cortex activation was found at 260 ms (Figures 5(a1) and 5(a3)) with motor cortex activation at 610 ms (Figures 5(a2) and 5(a4)), and the subject response time was 592 ms. For subject #2, visual cortex activation was found at 125 ms (Figures 5(b1) and 5(b3)) and motor cortex activation was seen at 680 ms (Figures 5(b2) and 5(b4)), with a subject response time of 612 ms. Similarly, activity at visual cortex on subject #3 was found at 110 ms (Figures 5(c1) and 5(c3)) and the motor cortex

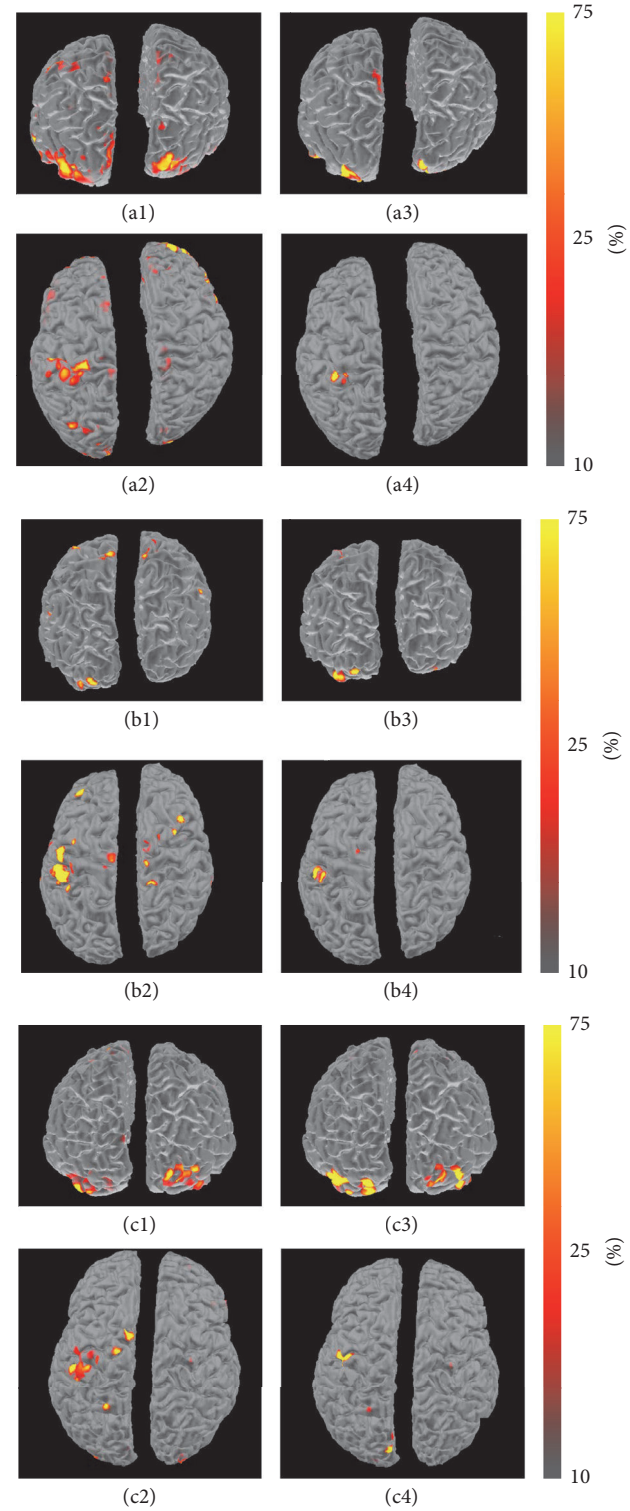

Figure 5: Source imaging results comparing two EEG/fMRI integration approaches: time-invariant fMRI constraints ((a1), (a2); (b1), (b2); (c1), (c2)) and spatiotemporal fMRI constraints ((a3), (a4); (b3), (b4); (c3), (c4)) at two time instances to demonstrate visual activation ((a1), (a3); (b1), (b3); (c1), (c3)) and motor activation ((a2), (a4); (b2), (b4); (c2), (c4)). Source activity shown is color coded as a percentage of its maximum.

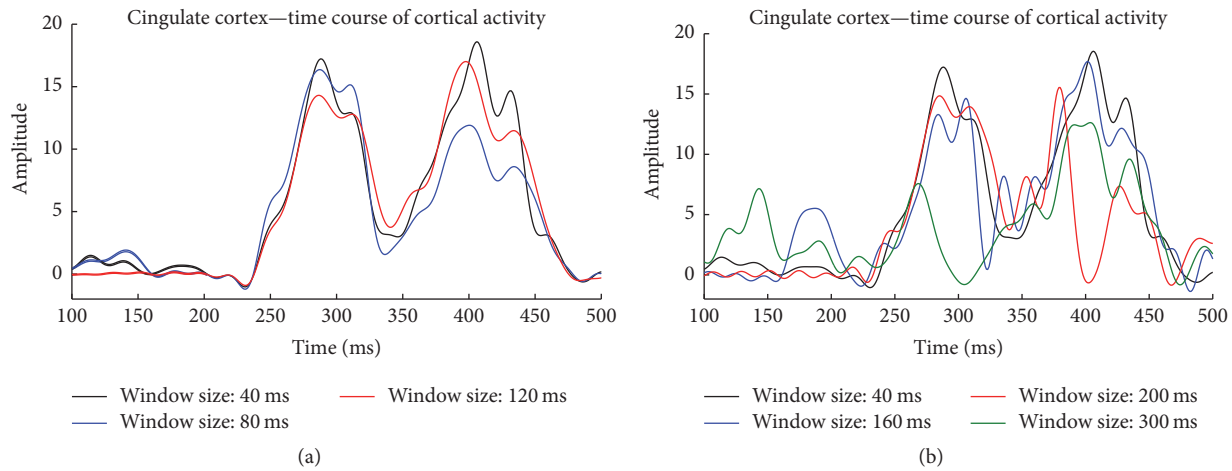

Figure 6: Cortical activity of the cingulate cortex calculated with different window sizes. Results with smaller window sizes show a great similarity (correlation $R > 0.95$) in (a); and results with larger window sizes show a greater disparity (correlation $R < 0.7$) in (b).

activity peaked at 800 ms (subject #3 had a response time of 704 ms). However, it can be observed that the source activity reconstructed using the proposed method yielded sparser, more localized results when compared to the conventional time-invariant fMRI-informed source imaging method.

The stability of the proposed method was investigated by examining how the reconstructed source activity changes with changes in the window size. Figure 6 shows the change in the activity time course for a source in the cingulate cortex when reconstructed with different window sizes. For window sizes below 120 ms, EEG source localization results showed minimal changes, as shown in Figure 6(a). The results began to lose detail and specificity, however, when window sizes increased above 120 ms (Figure 6(b)). While there is no limitation regarding the minimum window size used in the proposed algorithm, reducing the window size below 40 ms is not necessary as the changes in the estimated hyperparameter (λR) became very small, yet the cost of computational effort increases dramatically.

3.4. Transition Period. Examining the results of our algorithm in the transition period (Figure 7), several trends can be ascertained. Subjects showed an early peak of visual activation, followed by activation in the cingulate cortex and fusiform face area. Subsequently, activation can be observed in the motor cortex, followed by second peak of activity. Interestingly, the early activity in the motor cortex can be observed well before any physical motor activity is initiated. Squeezing of the ball is related to the second peak of the motor cortex activation. When comparing the specific source imaging with the time-invariant counterpart, the new algorithm consistently results in more precise and focused results. Areas of moderate activation (orange) are greatly reduced, creating results that are both sparse and high in contrast.

4. Discussion

A new method has been developed in this study to utilize a time-variant fMRI constraint in conjunction with EEG source imaging to produce a more precise and focused depiction of neural activity without amplifying erroneous signals. The Bayesian framework has been recently developed [32–35] to improve fMRI-informed EEG source imaging results by utilizing "soft" fMRI constraints, but the issue of temporal mismatch between EEG-fMRI still persists. This is especially problematic for neurological studies that explore the dynamic brain activity during the rapid transition periods between cognitive tasks—transition periods that may contain valuable information regarding the presentation of neural plasticity markers and how stimulus processing changes under various conditions. Furthermore, many paradigms do not allow for EEG data to be averaged over multiple occurrences or epochs, in cases where responses change over time (habituation) or are not time-locked (i.e., latency between stimulus and response). Difficulty in these cases may be further accentuated by the relatively static nature of utilized fMRI data. While EEG signals vary in a time dependent nature, BOLD signals remain static regardless of condition or timing and could potentially amplify irrelevant or erroneous sources in a multimodal framework. The proposed spatiotemporal fMRI constrained EEG source imaging approach utilizes the EEG data in a selected time window to determine the best-fit source prior from the fMRI BOLD activation map. The resulting fMRI priors are in turn utilized in fMRI-informed EEG source localization in order to solve the timing mismatch between EEG and fMRI.

The proposed approach was implemented and tested in an EEG/fMRI study on motor activation in response to emotionally evocative visual stimuli. The processed windowed EEG signals were analyzed to select the temporally relevant areas of fMRI activity, which were used to inform EEG source localization calculation. The results were compared against traditional fMRI-informed EEG approaches to demonstrate the spatiotemporal variant fMRI priors feature as well as the performance of the developed method.

The initial results from fMRI alone support our hypothesis that the task would involve visual stimulation, facial recognition, decision making, and motor responses,

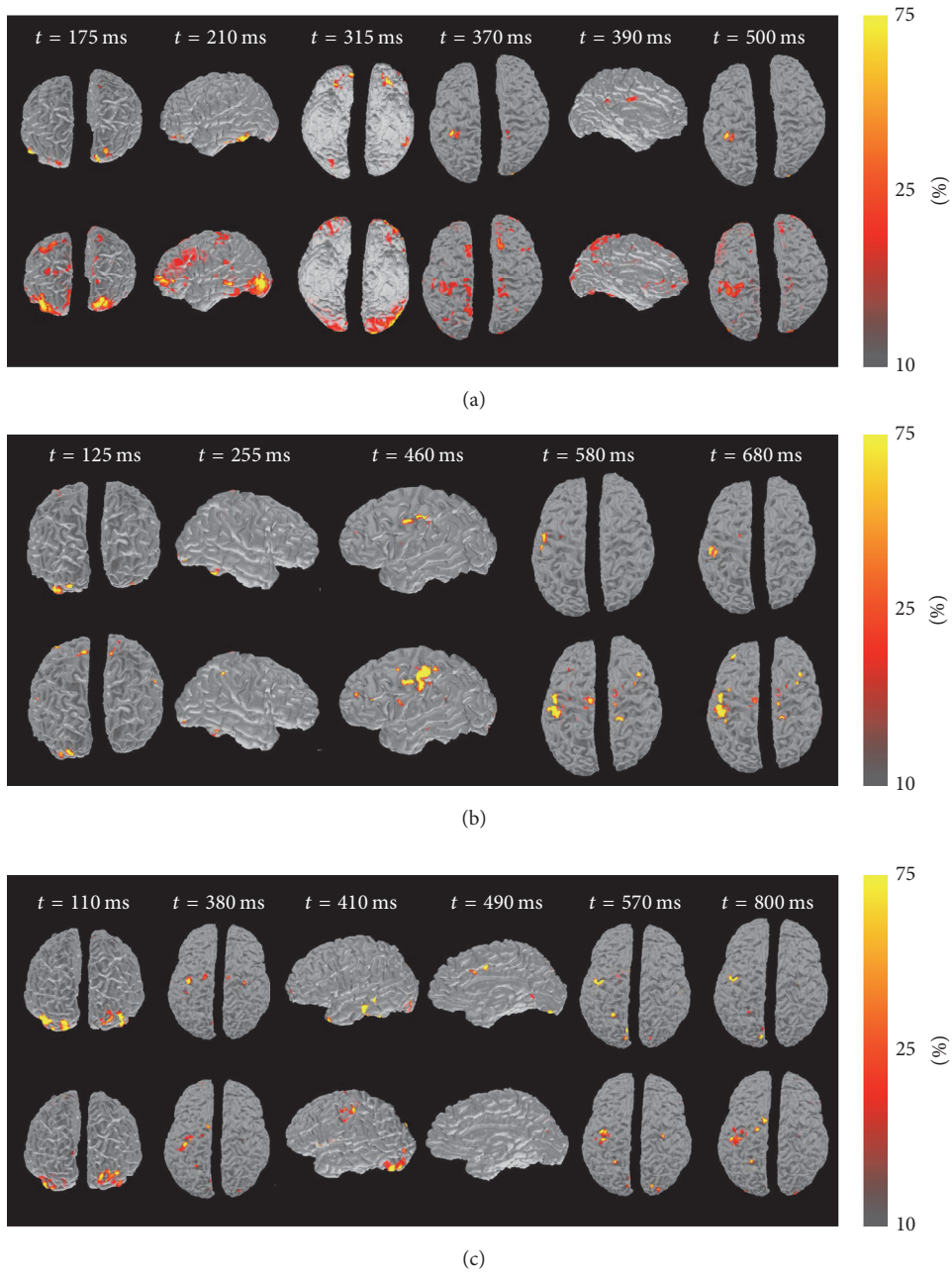

FIGURE 7: Transition period source imaging results for subjects #1, 2, and 3 in (a), (b), and (c), respectively. In each subfigure, top panel represents source imaging results using spatiotemporal fMRI constrained method, while bottom panel shows time-invariant fMRI constrained method. Results highlight cortical activity at different time instances during the period of time transitioning between a visual input to subject's response via motor output. Time stamps shown are with respect to the visual stimulus onset timing (at $t = 0$ ms). Source activity shown is color coded as a percentage of its maximum.

highlighting these as areas of interest for the new algorithm. The fMRI alone, however, still faces difficulty as no dynamic neural pathways relating to these events could be inferred from the BOLD activation map. Similarly, though EEG has the requisite temporal resolution to examine any potential pathways, the need for localization algorithms limits its use.

The new algorithm was compared to the traditional time-invariant fMRI constrained EEG source imaging method in a visual-motor response paradigm. The results showed similar areas of activation in the motor cortex, visual cortex, fusiform face area, supplementary motor area, and posterior cingulate cortex. While similar areas were highlighted under both conditions, the new algorithm produced results that are more spatially precise, with fewer areas showing moderate or low amplitude results. In contrast with the precise results from spatiotemporal fMRI constrained EEG source imaging method, the dispersed source imaging results seen in the traditional method were likely caused by the spatial bias of

using time-invariant fMRI constraints, as the same fMRI spatial information might not be valid for all time instances. It should further be noted that while the same general areas can be observed, the exact location of activity within these regions may be slightly shifted under the time-variant constraints (Figure 5).

With reference to the performed test, results are consistent with areas expected to be activated in a face-based visual-motor paradigm. Activation could first be observed in the visual cortex and fusiform face area at 100–175 ms after stimulus onset. As faces were utilized as the primary stimuli, activation in these regions is expected and aligns with findings in current literature [39, 40]. Following the visual activation, activity can be observed within the hand regions of the premotor and motor cortices (370–460 ms). While these sources do appear in predictable regions, their timing makes them a significant point of interest: motor response for the subjects is not observed until 500–570 ms after stimulus presentation. The hand region also shows activity at these times, and the early peak in activity may represent a previously unidentified premotor activation. Following this premotor wave, activity can be seen in the cingulate cortex, which is often associated with the emotional processing of the happy and sad stimuli and again fits with a previous report [41]. Finally, strong activation was observed in the motor cortex as motor activity took place. The results achieved in the performed task are overall consistent with our expectations. Aside from being spatially consistent, the time course of activation also indicates a dynamic neural pathway that is integral to the stimulus detection and response, starting in the visual cortex and proceeding to the motor cortex.

It is a grand challenge in the field to accurately and noninvasively detect and localize neural activity, let alone the transient markers associated with cortical plasticity. Though many technologies have been developed to accomplish this task, there has yet to be a complete solution that allows for both favorable temporal and spatial resolution. While fMRI constrained EEG source imaging seeks to accomplish this task, the static nature of the time-invariant fMRI constraint may unintentionally amplify inaccurate or erroneous results. By creating a time-variant constraint, it is believed that the new algorithm presented here advances current imaging technology by increasing imaging precision and specificity and will thereby enhance our ability to diagnose and treat neural diseases.

5. Conclusion

Plasticity manifests in both the physical and functional aspects of the brain. Identifying and understanding the dynamic changes in brain activity that accompany this plasticity stands as one of the major frontiers of biomedical research. Given the limitations in unimodal imaging methods as previously described, a new EEG/fMRI integration method is proposed utilizing fMRI information in a spatially and temporally varying manner to alleviate the sources of error encountered by its predecessor. The performance of the proposed spatiotemporal fMRI constrained source imaging approach was evaluated by comparing against the traditional time-invariant fMRI constrained EEG source imaging in a visual-motor task. Results demonstrated the capability of the proposed approach to noninvasively characterize internal brain activity with high level of spatiotemporal detail. The precision in imaging dynamic brain activity is essential in the study of neuromuscular plasticity mechanisms, characterization of the neuroplastic changes of functional networks in the brain, and evaluation of the progress of cognitive rehabilitation treatments.

Competing Interests

The authors declare that they have no competing interests.

Acknowledgments

This work was supported in part by NIH DK082644 and the University of Houston.

References

[1] B. Draganski, C. Gaser, G. Kempermann et al., "Temporal and spatial dynamics of brain structure changes during extensive learning," *The Journal of Neuroscience*, vol. 26, no. 23, pp. 6314–6317, 2006.

[2] Y. Sagi, I. Tavor, S. Hofstetter, S. Tzur-Moryosef, T. Blumenfeld-Katzir, and Y. Assaf, "Learning in the fast lane: new insights into neuroplasticity," *Neuron*, vol. 73, no. 6, pp. 1195–1203, 2012.

[3] G. Assenza and V. Di Lazzaro, "A useful electroencephalography (EEG) marker of brain plasticity: delta waves," *Neural Regeneration Research*, vol. 10, no. 8, pp. 1216–1217, 2015.

[4] B. Penolazzi, C. Spironelli, C. Vio, and A. Angrilli, "Brain plasticity in developmental dyslexia after phonological treatment: a beta EEG band study," *Behavioural Brain Research*, vol. 209, no. 1, pp. 179–182, 2010.

[5] S. G. Romero, D. J. McFarland, R. Faust, L. Farrell, and A. T. Cacace, "Electrophysiological markers of skill-related neuroplasticity," *Biological Psychology*, vol. 78, no. 3, pp. 221–230, 2008.

[6] N. K. Logothetis, "The underpinnings of the BOLD functional magnetic resonance imaging signal," *The Journal of Neuroscience*, vol. 23, no. 10, pp. 3963–3971, 2003.

[7] H. Girouard and C. Iadecola, "Neurovascular coupling in the normal brain and in hypertension, stroke, and Alzheimer disease," *Journal of Applied Physiology*, vol. 100, no. 1, pp. 328–335, 2006.

[8] M. Bélanger, I. Allaman, and P. J. Magistretti, "Brain energy metabolism: focus on astrocyte-neuron metabolic cooperation," *Cell Metabolism*, vol. 14, no. 6, pp. 724–738, 2011.

[9] G. K. Aguirre, E. Zarahn, and M. D'Esposito, "Empirical analyses of BOLD fMRI statistics. II. Spatially smoothed data collected under null-hypothesis and experimental conditions," *NeuroImage*, vol. 5, no. 3, pp. 199–212, 1997.

[10] E. Zarahn, G. K. Aguirre, and M. D'Esposito, "Empirical analyses of BOLD fMRI statistics. I. Spatially unsmoothed data collected under null-hypothesis conditions," *NeuroImage*, vol. 5, no. 3, pp. 179–197, 1997.

[11] K. Li, L. Guo, J. Nie, G. Li, and T. Liu, "Review of methods for functional brain connectivity detection using fMRI," *Computerized Medical Imaging and Graphics*, vol. 33, no. 2, pp. 131–139, 2009.

[12] K. J. Friston, "Functional and effective connectivity in neuroimaging: a synthesis," *Human Brain Mapping*, vol. 2, no. 1-2, pp. 56–78, 1994.

[13] M. Rubinov and O. Sporns, "Complex network measures of brain connectivity: uses and interpretations," *NeuroImage*, vol. 52, no. 3, pp. 1059–1069, 2010.

[14] E. Damaraju, E. A. Allen, A. Belger et al., "Dynamic functional connectivity analysis reveals transient states of dysconnectivity in schizophrenia," *NeuroImage: Clinical*, vol. 5, pp. 298–308, 2014.

[15] A. G. Garrity, G. D. Pearlson, K. McKiernan, D. Lloyd, K. A. Kiehl, and V. D. Calhoun, "Aberrant 'default mode' functional connectivity in schizophrenia," *The American Journal of Psychiatry*, vol. 164, no. 3, pp. 450–457, 2007.

[16] P. J. Nestor, P. Scheltens, and J. R. Hodges, "Advances in the early detection of Alzheimer's disease," *Nature Medicine*, vol. 10, pp. S34–S41, 2004.

[17] E. J. Sanz-Arigita, M. M. Schoonheim, J. S. Damoiseaux et al., "Loss of 'Small-World' networks in Alzheimer's disease: graph analysis of fMRI resting-state functional connectivity," *PLoS ONE*, vol. 5, no. 11, article e13788, 2010.

[18] L. Wang, Y. Zang, Y. He et al., "Changes in hippocampal connectivity in the early stages of Alzheimer's disease: evidence from resting state fMRI," *NeuroImage*, vol. 31, no. 2, pp. 496–504, 2006.

[19] L.-L. Zeng, H. Shen, L. Liu et al., "Identifying major depression using whole-brain functional connectivity: a multivariate pattern analysis," *Brain*, vol. 135, part 5, pp. 1498–1507, 2012.

[20] J. Kinnison, S. Padmala, J.-M. Choi, and L. Pessoa, "Network analysis reveals increased integration during emotional and motivational processing," *The Journal of Neuroscience*, vol. 32, no. 24, pp. 8361–8372, 2012.

[21] P. Olejniczak, "Neurophysiologic basis of EEG," *Journal of Clinical Neurophysiology*, vol. 23, no. 3, pp. 186–189, 2006.

[22] C. M. Michel, M. M. Murray, G. Lantz, S. Gonzalez, L. Spinelli, and R. G. de Peralta, "EEG source imaging," *Clinical Neurophysiology*, vol. 115, no. 10, pp. 2195–2222, 2004.

[23] C. Ramon, P. H. Schimpf, and J. Haueisen, "Influence of head models on EEG simulations and inverse source localizations," *Biomedical Engineering Online*, vol. 5, article 10, 2006.

[24] J. C. Mosher, M. E. Spencer, R. M. Leahy, and P. S. Lewis, "Error bounds for EEG and MEG dipole source localization," *Electroencephalography and Clinical Neurophysiology*, vol. 86, no. 5, pp. 303–321, 1993.

[25] R. D. Pascual-Marqui, "Review of methods for solving the EEG inverse problem," *International Journal of Bioelectromagnetism*, vol. 1, no. 1, pp. 75–86, 1999.

[26] M. S. Hämäläinen and R. J. Ilmoniemi, "Interpreting magnetic fields of the brain: minimum norm estimates," *Medical & Biological Engineering & Computing*, vol. 32, no. 1, pp. 35–42, 1994.

[27] R. J. Huster, S. Debener, T. Eichele, and C. S. Herrmann, "Methods for simultaneous EEG-fMRI: an introductory review," *The Journal of Neuroscience*, vol. 32, no. 18, pp. 6053–6060, 2012.

[28] A. K. Liu, J. W. Belliveau, and A. M. Dale, "Spatiotemporal imaging of human brain activity using functional MRI constrained magnetoencephalography data: monte Carlo simulations," *Proceedings of the National Academy of Sciences of the United States of America*, vol. 95, no. 15, pp. 8945–8950, 1998.

[29] F. Babiloni, F. Carducci, F. Cincotti et al., "Linear inverse source estimate of combined EEG and MEG data related to voluntary movements," *Human Brain Mapping*, vol. 14, no. 4, pp. 197–209, 2001.

[30] M. J. Rosa, J. Daunizeau, and K. J. Friston, "EEG-fMRI integration: a critical review of biophysical modeling and data analysis approaches," *Journal of Integrative Neuroscience*, vol. 9, no. 4, pp. 453–476, 2010.

[31] Z. Liu, L. Ding, and B. He, "Integration of EEG/MEG with MRI and fMRI," *IEEE Engineering in Medicine and Biology Magazine*, vol. 25, no. 4, pp. 46–53, 2006.

[32] J. Daunizeau, C. Grova, J. Mattout et al., "Assessing the relevance of fMRI-based prior in the EEG inverse problem: a Bayesian model comparison approach," *IEEE Transactions on Signal Processing*, vol. 53, no. 9, pp. 3461–3472, 2005.

[33] K. Friston, C. Chu, J. Mourão-Miranda et al., "Bayesian decoding of brain images," *NeuroImage*, vol. 39, no. 1, pp. 181–205, 2008.

[34] K. Friston, L. Harrison, J. Daunizeau et al., "Multiple sparse priors for the M/EEG inverse problem," *NeuroImage*, vol. 39, no. 3, pp. 1104–1120, 2008.

[35] M.-A. Sato, T. Yoshioka, S. Kajihara et al., "Hierarchical Bayesian estimation for MEG inverse problem," *NeuroImage*, vol. 23, no. 3, pp. 806–826, 2004.

[36] K. Friston, J. Mattout, N. Trujillo-Barreto, J. Ashburner, and W. Penny, "Variational free energy and the Laplace approximation," *NeuroImage*, vol. 34, no. 1, pp. 220–234, 2007.

[37] F. Di Russo, A. Martínez, M. I. Sereno, S. Pitzalis, and S. A. Hillyard, "Cortical sources of the early components of the visual evoked potential," *Human Brain Mapping*, vol. 15, no. 2, pp. 95–111, 2002.

[38] J. Polich, "Updating P300: an integrative theory of P3a and P3b," *Clinical Neurophysiology*, vol. 118, no. 10, pp. 2128–2148, 2007.

[39] D. A. Jeffreys and J. G. Axford, "Source locations of pattern-specific components of human visual evoked potentials. II. Component of extrastriate cortical origin," *Experimental Brain Research*, vol. 16, no. 1, pp. 22–40, 1972.

[40] M. Seeck and O.-J. Grüsser, "Category-related components in visual evoked potentials: photographs of faces, persons, flowers and tools as stimuli," *Experimental Brain Research*, vol. 92, no. 2, pp. 338–349, 1992.

[41] T. Yamazaki, K.-I. Kamijo, A. Kenmochi et al., "Multiple equivallent current dipole source localization of visual event-related potentials during oddball paradigm with motor response," *Brain Topography*, vol. 12, no. 3, pp. 159–175, 2000.

Hindawi Publishing Corporation
Neural Plasticity
Volume 2016, Article ID 1686414, 8 pages
http://dx.doi.org/10.1155/2016/1686414

Research Article

Effects of a Single Session of High Intensity Interval Treadmill Training on Corticomotor Excitability following Stroke: Implications for Therapy

Sangeetha Madhavan,[1] James W. Stinear,[2] and Neeta Kanekar[1]

[1]*Department of Physical Therapy, University of Illinois at Chicago, Chicago, IL, USA*
[2]*Department of Exercise Sciences, University of Auckland, Auckland, New Zealand*

Correspondence should be addressed to Sangeetha Madhavan; smadhava@uic.edu

Received 16 May 2016; Revised 13 July 2016; Accepted 26 July 2016

Academic Editor: Sheng Li

Objective. High intensity interval treadmill training (HIITT) has been gaining popularity for gait rehabilitation after stroke. In this study, we examined the changes in excitability of the lower limb motor cortical representation (M1) in chronic stroke survivors following a single session of HIITT. We also determined whether exercise-induced changes in excitability could be modulated by transcranial direct current stimulation (tDCS) enhanced with a paretic ankle skill acquisition task. *Methods*. Eleven individuals with chronic stroke participated in two 40-minute treadmill-training sessions: HIITT alone and HITT preceded by anodal tDCS enhanced with a skill acquisition task (e-tDCS+HIITT). Transcranial magnetic stimulation (TMS) was used to assess corticomotor excitability of paretic and nonparetic tibialis anterior (TA) muscles. *Results*. HIIT alone reduced paretic TA M1 excitability in 7 of 11 participants by ≥ 10%. e-tDCS+HIITT increased paretic TA M1 excitability and decreased nonparetic TA M1 excitability. *Conclusions*. HIITT suppresses corticomotor excitability in some people with chronic stroke. When HIITT is preceded by tDCS in combination with a skill acquisition task, the asymmetry of between-hemisphere corticomotor excitability is reduced. *Significance*. This study provides preliminary data indicating that the cardiovascular benefits of HIITT may be achieved without suppressing motor excitability in some stroke survivors.

1. Introduction

High intensity interval treadmill training (HIITT) is gaining popularity in the fitness industry and as a promising stroke rehabilitation protocol to improve cardiovascular and motor outcomes [1]. It involves short bursts of high effort alternated with longer recovery periods to maximize efficacy of training [2]. Treadmill training at high speeds results in improved overground gait speeds, facilitates a more normal walking pattern, and improves cardiovascular efficiency [2–5]. Although previous studies have examined the effects of HIITT on gait parameters and cardiovascular outcomes after stroke, no study has examined the effects of HIITT on corticomotor excitability after stroke. Despite the promising effects of HIITT (noted above), it is not known whether HIITT induces central fatigue in the corticomotor system. This is an important question to answer because people with stroke have a high reported incidence of central fatigue [6–8]. Insufficient central drive and an imbalance of between-hemisphere symmetry of corticomotor exitability (CME) are a well-established benchmark after stroke [9, 10]. People with stroke exercising at a high intensity may develop central neural fatigue that could compromise their ability to drive descending motor output [11–13]. Hence, the primary purpose of this study was to examine the short-term changes in CME of the lower limb M1 following a single session of HIITT. We hypothesized that a single session of HIITT would decrease CME of paretic lower limb muscles and create a further imbalance of between-hemisphere cortical excitability in stroke survivors. We also wanted to know if increasing lower limb corticomotor excitability prior to a session of HIITT could mitigate these changes. We chose transcranial direct current stimulation (tDCS) combined with a visuomotor ankle-tracking task that we had previously demonstrated to

Table 1: Baseline characteristics of participants.

	Mean (SEM)
Age (years)	58 (2.7)
Height (cm)	165 (2.7)
Weight (lbs)	178 (9.4)
Time after stroke (years)	9 (1.8)
Type of stroke	
Ischemic	7
Hemorrhagic	4
Gender	
Male	4
Female	7
Affected limb	
Right	7
Left	4
Fugl-Meyer	
Paretic	23.6 (0.6)
Nonparetic	29.4 (0.3)
MMSE	28 (0.7)

be a robust facilitator of lower limb skill acquisition and CME assessed in the paretic limb tibialis anterior (TA) muscle [14]. At the risk of limiting the conclusions that could be drawn from the study, we did not include additional sessions of skill acquisition alone and tDCS alone for this group of people with stroke and included two sessions: HIITT alone and HIITT plus anodal tDCS enhanced with ankle-tracking (e-tDCS+HIITT). The goal of the present study was, therefore, to provide preliminary data to inform future research that would examine in more detail whether the physiological and functional benefits of HIITT are limited by the induction of central fatigue.

2. Methods

2.1. Participants. Eleven individuals with chronic stroke participated in the study (see Table 1 for demographics). This was a carefully selected homogenous sample as these individuals had participated in a previous nonintervention study in the laboratory. These individuals were selected because transcranial magentic stimulaion (TMS) induced motor evoked potentials (MEPs) could be induced in their paretic leg muscles and demonstrated 5 degrees or more of active paretic ankle dorsiflexion necessary to perform our tDCS-enhanced ankle motor task. In addition, participants were able to walk independently (with or without an assistive device) for at least 10 minutes, a criterion necessary to fully participate in HIITT. Participants did not have contraindications to TMS, such as metallic implants in the head region, a history of seizures, implanted cardiac pacemakers, and medications known to alter central nervous system excitability. The Mini Mental State Examination (MMSE) was used to assess cognitive impairment, and those with a score of less than 24 (out of 30) were excluded. All the participants signed a written informed consent form approved by the Institutional Review Board of the University of Illinois at Chicago.

2.2. Experimental Protocol. Each individual participated in two treadmill training sessions, HIITT alone and e-tDCS+HIITT, the sessions being one week apart and pseudorandomized to avoid order effects. Prior to and at the end of each session, participants performed two trials of the overground 10-meter fast walking test (using their walking aid, e.g., cane and ankle foot orthosis if required). Baseline (pre-) and post-training corticomotor excitability measures were obtained for TA muscles bilaterally using single-pulse TMS. During the e-tDCS+HIITT session, participants received anodal tDCS over the lesioned lower limb M1 prior to treadmill training. During anodal tDCS, participants performed a visuomotor tracking task with their paretic ankle for 15 minutes while receiving tDCS. In order to match the e-tDCS+HIITT session duration with the HIITT only session, participants in the latter were asked to remain seated quietly for fifteen minutes prior to treadmill training. Blood pressure (BP) and heart rate (HR) were monitored during the fifteen minutes of tDCS and during the fifteen minutes of rest. No differences in BP and HR were noted during these seated sessions.

2.3. Electromyography (EMG). Muscle activity was recorded bilaterally from the TA using surface Ag/AgCl electrodes (Delsys Bagnoli 8, MA, USA) placed over the muscle belly after standard skin preparation. The ground electrode was placed over C7 spinous process. Two maximum voluntary isometric contractions (MVIC) were obtained for each muscle with the participants seated on a chair with knee flexed to 90° and the ankle in the neutral position and stabilized by a metal bar placed firmly and comfortably over the foot and secured to a wooden board to prevent movement of the foot. Pre- and post-training TMS measures were obtained, while participants produced a target EMG contraction corresponding to 10% MVIC for each muscle. EMG data were sampled at 2000 Hz, with a gain of 1000, and band-pass filtered (10–500 Hz). Spike2 software (Cambridge Electronic Design, Cambridge, UK) was used to collect the EMG data.

2.4. Transcranial Magnetic Stimulation. Single-pulse TMS at 0.25 Hz was delivered using a Magstim 200 stimulator (Magstim, Dyfed, Wales, UK) via a double-cone coil (diameter 110 mm) oriented to induce a posterior-anterior current flow in the cortex. Spike2 software was used to trigger the stimulator and also to record the trigger pulses. TMS was used to generate MEPs with the coil positioned contralateral to the TA muscle being tested (the nonparetic TA was tested first). A tightly fitted linen cap was placed on the participant's head and the position of the vertex (intersection of the lines connecting the nasion-inion and the two tragi) was marked. The TMS coil was placed on the cap at the vertex and then moved systematically to determine the hotspot for each muscle. The location of the hotspot for each TA was marked on the cap and the position was checked constantly by the experimenter during data collection to ensure that

the coil was in the same position throughout. During TMS, participants were given visual feedback of muscle activity and asked to maintain a tonic contraction of the TA that represented 10% of MVIC. Active motor threshold (AMT) was determined as the stimulus intensity resulting in identifiable MEPs of at least 0.4 mV peak-to-peak in 50% of ten successive trials from the contralateral TA [14, 15]. Responses were obtained at seven TMS intensities corresponding to 80–140% of AMT (randomized order) to generate a recruitment curve for each TA muscle. Six MEPs were recorded for each intensity at pre- and post-training. The same intensities were used to collect post-training responses (five minutes after treadmill training). For the e-tDCS+HIITT session, the hotspot of the paretic TA was first determined by placing the TMS coil directly over the scalp. The active tDCS electrode was then placed on the scalp, over which the cap was tightly fixed, and the hotspot procedure repeated.

2.5. Anodal tDCS. tDCS was delivered using a constant current stimulator (Chattanooga Iontophoresis System, Hixon, TN, USA) via an 8 cm^2 oblong saline-soaked sponge anode placed directly on the scalp over the hotspot for the paretic leg M1 and a self-adhesive carbonized reference cathode (35 cm^2) placed on the forehead above the contralateral orbit. A 1 mA current was applied for fifteen minutes, while the participant performed the motor training task [16].

For the motor training task, participants performed visuomotor tracking with their paretic ankle. Details of the motor training task have been previously reported [14, 15, 17, 18]. In brief, participants were required to track, as accurately as possible, a computer-generated sinusoidal waveform using a voltage generated by an electrogoniometer attached to their paretic ankle, while they performed continuous ankle dorsiflexion and plantarflexion movements for 15 minutes. They were given 1 minute of rest after every 4 minutes of tracking. Our previous study found that tDCS strongly facilitated corticomotor excitability and enhanced fine motor control of the ankle approximately 3-fold compared with tracking practice alone [14]. This finding is supported by other research that demonstrated that tDCS during a motor task is more effective in increasing corticomotor excitability than tDCS administered during rest [18, 19].

2.6. Treadmill Training. All participants participated in the HIITT protocol. The training was modified based on the protocol used by Pohl and colleagues [3]. The protocol consisted of 40 minutes (5 minutes warm-up, 30 minutes walking, and 5 minutes cooldown) of treadmill walking with a structured increase in walking speed. The treadmill was set at 0% incline and participants were fitted in a harness for safety with no body weight support. Participants were given no assistance with walking. Heart rate (HR) and rate of perceived exertion (RPE) using the modified Borg Scale were continuously monitored. Age-predicted HR was determined using the formula (220 − age) and 80% of the age-predicted HR was set as the upper cut-off safety limit while increasing the belt speed. The maximum overground walking speed was determined from the 10 m fast walking test performed at the start of each session. The participants then conducted a five-minute warm-up on the treadmill at a speed half of their maximum overground walking speed. After the warm-up, the first speed-dependent training interval began. During a period of 2 minutes, the belt speed was increased, within the participant's tolerance, to the highest speed at which the participant could walk safely and without stumbling. At the end of the two-minute interval, this maximum achieved belt speed was held for ten seconds. This was followed by a recovery period when the participant walked at the warm-up speed until a time at which the participant's HR and RPE returned to the levels reached during the warm-up phase. If the participant maintained the speed and felt safe during the ten seconds at the end of the first-training interval, the speed was then increased by 10% during the next interval. This speed was again held for ten seconds at the end of the second interval and followed by another recovery period. During any fast walking phase, if the participant was unable to maintain the speed and felt unsafe, or the HR reached the cut-off safety limit, the speed was reduced by 10% for the next interval. At the end of thirty minutes of structured walking, a five-minute cooldown phase was provided. The participants performed the training similarly during HIITT and e-tDCS+HIITT sessions and were able to increase their speed by a factor of 3 to 5 during each session. After the forty minutes of treadmill training, participants were given five minutes to rest before TMS measures were taken. BP, HR, and RPE were recorded during this time. An example of one participant's treadmill training speeds, distance walked, and heart rate is provided in Figure 1.

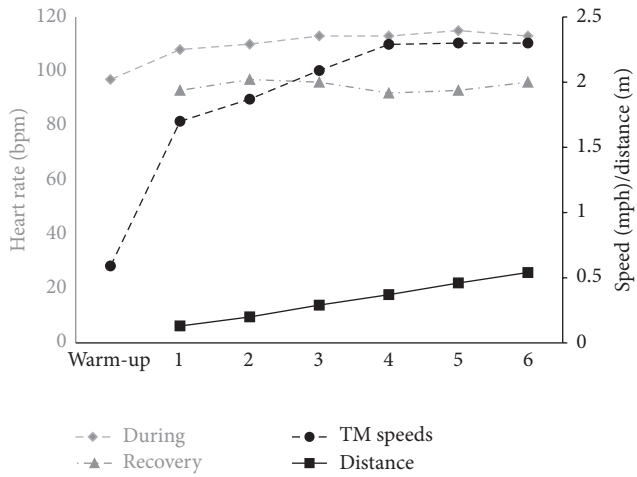

Figure 1: Representative example from one participant (number 2) during HIITT showing heart rate during training (gray diamonds), heart rate during recovery (gray triangles), treadmill speeds achieved at each interval (black circles), and composite distance (black squares). Heart rate (beats per minute) is represented on the primary left y-axis. Speed (miles per hour) and distance (miles) are presented on the secondary right y-axis. x-axis represents the time scale during treadmill training: 5 minute warm-up, the six walking intervals that the participant achieved during the session or in the case of the recovery HR, and the six recovery intervals that the participant needed to restore the HR to baseline.

2.7. Data Analyses

2.7.1. Gait Speed. An average pre- and post-training gait speed was calculated from the two pre- and two post-10 m fast trials for each participant for each session. A change in gait speed was calculated for each individual.

2.7.2. MEP Analyses. Spike2 software was used to analyze all MEP data. MEP amplitude was chosen as the primary measure to capture changes in corticomotor excitability. A MEP window was established for each muscle for each participant, for the pre- and post-training TMS trial during each session, by finding the onset and offset latencies of a large MEP in response to the highest TMS intensity (140% AMT). A window of identical width was set prior to the TMS stimulus to measure the tonic background contraction. The same MEP and background windows were then applied to analyze all the MEPs within a given session. MEP amplitude was calculated as the peak-to-peak magnitude of EMG activity within the MEP window and averaged across the six MEPs for each TMS intensity, each trial (pre and post), each muscle, and participant. The average MEP response was plotted against the corresponding stimulus intensity, and a linear function was used to fit this recruitment curve. The slope of this recruitment curve was calculated and a change in CME (gain) was determined for the nonparetic (NP) and paretic (P) TA muscles using the following equation:

$$\text{Percent change in CME} = \frac{(\text{Postslope} - \text{Preslope})}{\text{Preslope}} * 100. \quad (1)$$

A physiological measure of interhemispheric symmetry of corticomotor excitability was calculated as follows: paretic slope/nonparetic slope. This ratio yields a value between 0 and 1 where values close to 1 indicate well-balanced interhemispheric symmetry and as values decrease towards zero, they indicate increasing levels of asymmetry [20]. This was used to establish the baseline level of interhemispheric symmetry for all participants.

2.8. Statistical Analyses. SPSS software (IBM software version 22, Armonk, NY) was used to perform all statistical analyses. A two-way repeated-measures ANOVA (session by time) was used to compare RPE, HR, and overground gait speeds between the two sessions. Four levels of time (warm-up, during training, cooldown, and after training) were analyzed for RPE and HR. Two levels of time (pre and post) were analyzed for overground gait speeds. Paired two-tailed t-tests were performed to compare differences between the baseline MEP slopes of the two sessions for each limb. Intraclass correlations (ICC) were also performed to examine test-retest reliability of baseline MEP slopes of the two sessions for each limb.

A two-way repeated-measures ANOVA (session by limb) was used to examine changes in CME as an effect of the training session on the two limbs (paretic and nonparetic). Significant main effects and interactions were followed up with t-tests corrected for multiple comparisons. Participants were classified as "responders" based on change in the paretic TA CME after training. A participant who showed a change of +5% compared to baseline was considered as a responder and the number of responders for each session are reported. A correlation analysis between change in CME of the P TA during the e-tDCS-HIITT and HIITT sessions was conducted to determine whether a relationship between the extent of response to HIITT alone was related to the extent of change during e-tDCS-HIITT. Statistical significance was set at $p < 0.05$. Greenhouse-Geisser correction was used when data violated sphericity assumptions. Values are reported as mean ± SE (standard error).

3. Results

All participants completed the training. No adverse effects of e-tDCS or treadmill training were reported. On average, participants started at a treadmill belt speed of 2.0 ± 0.12 mph and most were able to increase and/or maintain their speeds for 5–7 intervals. The highest belt speed achieved was on average 2.6 ± 0.16 mph. Details of treadmill speeds, number of intervals, and distance covered by each participant are provided in Table 2. Two-way repeated-measures ANOVA on RPE revealed a significant interaction for RPE ($F_{3,24} = 4.24$, $p = 0.015$). Paired t-tests for RPE at each level of time to compare the two sessions revealed a significant difference ($p = 0.05$) during "cooldown" (Figure 2(b)). On average, RPE increased from 2 during warm-up to 8 during the speed intervals. The RPE remained slightly elevated at 4.62 for the HIITT session compared to 3.04 for the e-tDCS+HIITT session. Two-way repeated-measures ANOVA on HR revealed a significant main effect of time for HR. HR changed similarly across both sessions and was found to be significantly different between the four time points ($F_{3,27} = 101.768$, $p < 0.0001$, Figure 2(a)). All participants were able to complete their treadmill training sessions without a need to discontinue.

3.1. Overground Gait Speed. No significant main effects or interactions were noted for overground gait speeds. Baseline gait speeds were similar for both sessions and a trend for improvement (change of 0.04 m/s) was noted after treadmill training (Table 3).

3.2. Change in Corticomotor Excitability. No significant differences were noted for the baseline MEP slopes for the NP TA ($p = 0.38$) and P TA ($p = 0.43$) between the two sessions. Differences were found between the baseline slopes for the NP and P TA within each session. The mean baseline NP TA slope was significantly steeper than the mean P TA slope for the HIITT (73%, $p = 0.016$) and e-tDCS+HIITT (79%, $p = 0.013$) sessions. Excellent ICC values were found between the baseline values of the NP TA ($R = 0.83$, $p < 0.05$) and the P TA ($R = 0.94$, $p < 0.05$) between both sessions. The average interhemispheric symmetry ratio for both baseline sessions was 0.49 ± 0.36, establishing a tendency towards an imbalance in interhemispheric symmetry for all participants.

The two-way ANOVA revealed a significant session × limb interaction ($F_{1,10} = 5.647$, $p = 0.039$). Post hoc analyses

Table 2: Treadmill speeds and distance covered for each participant during treadmill training.

	Overground gait speed (m/s)	e-tDCS+HIITT				HIITT			
		First interval (mph)	Last interval (mph)	Number of intervals	Total distance (miles)	First interval (mph)	Last interval (mph)	Number of intervals	Total distance (miles)
1	1.08	2	2.4	7	2.95	2.3	2.7	6	2.24
2	0.47	1.8	2.6	7	2.1	1.7	2.3	6	1.99
3	0.42	1.1	1.4	5	1	1	1.4	7	0.78
4	0.84	2	2.4	5	1.22	2	2.4	4	1.26
5	0.69	2	2.6	6	2.29	2	2.6	5	1.53
6	0.86	1.7	1.7	5	1.7	1.7	2.1	4	1.24
7	0.72	1.9	2.3	5	1.63	1.9	2.3	5	1.21
8	1.29	2.3	2.5	5	2.56	2.3	2.5	5	2.63
9	1.08	2.4	2.8	6	2.69	2.4	2.8	5	2.31
10	1.15	2.3	2.5	5	1.11	2.3	2.9	5	2.20
11	1.37	2.4	2.8	5	2.68	2.4	2.8	5	2.74

m/s: meters/second; mph: miles per hour.

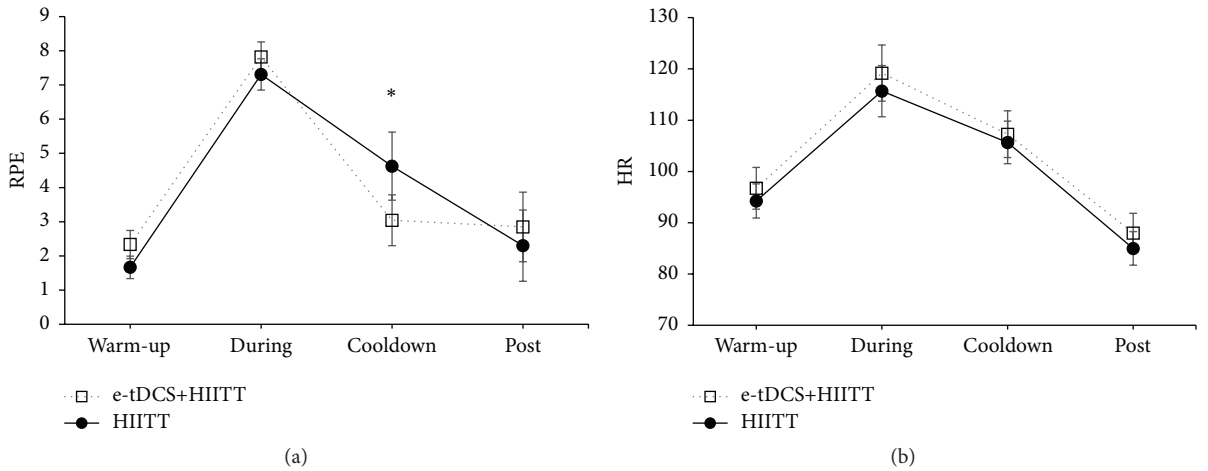

Figure 2: Rating of perceived exertion (RPE) and heart rate (HR; beats per minute (bpm)) are shown in Figures 2(a) and 2(b), respectively. y-axis represents 4 different time points at which these measurements were taken. Data are means and error bars are standard errors. There was a significant difference between the two sessions during cooldown for the RPE. A significant effect of time was noted for HR. $^{*}p < 0.05$.

Table 3: Overground fast walking speed.

Mean (SEM) gait velocity in m/s	Pre	Post
e-tDCS+HIITT	0.93 (0.09)	1.02 (0.09)
HIITT	0.93 (0.08)	0.96 (0.08)

m/s: meters/second.

with corrected paired t-tests to compare the two sessions within each limb revealed significant effects for both the NP TA ($p = 0.04$) and P TA ($p = 0.05$) (Figure 3). For the NP TA, a decrease in CME was revealed following the e-tDCS+HIITT session ($-19 \pm 7\%$) compared to the increase in CME for the HIITT session ($5 \pm 11\%$). There was an increase in CME for the P TA following the e-tDCS+HIITT session ($29 \pm 14\%$) compared to a decrease in the HIITT session ($-9 \pm 37\%$). Single sample t-tests were used to check whether CME means differed from zero. The change in CME for the NP TA and P TA in the e-tDCS+HIITT group differed significantly from zero ($p = 0.027$ and 0.023, resp.). The change was not significant in either limb following HIITT alone. For the latter, small changes in means were accompanied by large variances (NP TA $5 \pm 11\%$; P TA $-9 \pm 37\%$). Inspection of data revealed that only 2 of 11 participants had increased their P TA CME after HIITT, while the remaining 9 had decreased P TA CME. The mean reduction for the P TA for these 9 participants was $-22 \pm 6\%$, which differed from zero ($p = 0.004$). In the e-tDCS+HIITT group, 8 out 11 participants were classified as responders. The mean increase for the P TA for these 8 participants was $48 \pm 13\%$, which differed from zero ($p < 0.005$). With all participants' data included, there was a negative correlation between reduced P TA CME during HIITT alone and change in CME during e-tDCS+HIITT ($R^2 = 0.34$, $p = 0.05$) (Figure 4).

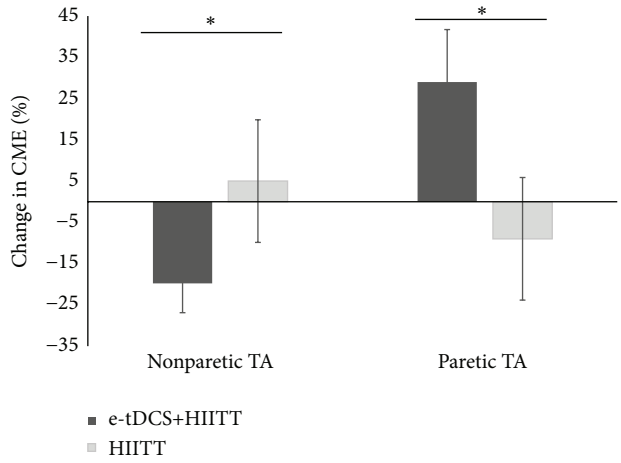

Figure 3: Percentage change in corticomotor excitability (CME) for the e-tDCS+HIITT (dark bars) and HIITT (light bars) groups. Corticomotor excitability was examined by calculating the change in linear slopes of the TMS recruitment curve before and after training for the bilateral tibialis anterior (TA) muscles. There were significant differences between the groups for the nonparetic and paretic TA muscles. $^{*}p < 0.05$.

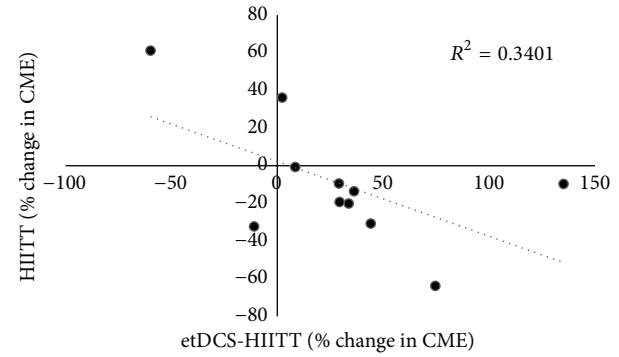

Figure 4: Relationship between percentage changes in corticomotor excitability of the paretic tibialis anterior muscle between the two sessions for all participants. Dashed line represents the negative linear relationship ($R^2 = 0.34$, $p = 0.05$) suggesting that those who were facilitated during e-tDCS+HIITT showed the most inhibition during HIITT alone.

4. Discussion

The objective of this study was to investigate the short-term effects of a single session of HIITT on corticomotor excitability in individuals with chronic stroke, and whether this modulation is affected by priming the motor cortex with tDCS and an ankle-tracking task prior to the exercise. HIITT alone resulted in small mean decreases in CME of the paretic TA and small mean increases in CME of the nonparetic TA, but the changes were not statistically significant. However, HIITT alone decreased CME in the majority of participants (9 of 11). When HIITT was preceded by the priming protocol (e-tDCS+HIITT), significant modulation was observed. After training, e-tDCS+HIITT induced an increase in CME of the paretic TA and a corresponding decrease in CME of the nonparetic TA. Interestingly, the correlation analysis revealed that participants with a greater CME downregulation also upregulated CME to a greater extent following priming with e-tDCS, indicating a possible shared neuroplastic mechanism. Both HIITT and e-tDCS+HIITT sessions showed a trend towards improved overground gait speeds (change of 0.03 and 0.09 m/s, resp.) after training. However, the change in gait speeds did not differ statistically between the two sessions.

This is the first study to examine the effects of HIITT on corticomotor excitability after stroke. Pohl et al. [3] and Sullivan et al. [4] independently investigated the effects of training at high treadmill velocities and demonstrated significant improvements in overground walking speeds with speed-dependent treadmill training compared to conventional therapy or at slow speeds. Faster speeds have also been shown to facilitate a more normal walking pattern after stroke without concomitant increases in common gait compensations, such as circumduction [5, 21]. Walking at progressively higher speeds not only requires increased cardiovascular activity but also increases neuromuscular demands to maintain the continuous stepping.

Another finding of this study is that CME of the paretic lower limb was augmented following e-tDCS+HIITT compared to HIITT alone. The fact that these changes were observed with a single session of training is promising and adds to the literature that forms the basis for investigating the effects of long-term training using cortical priming. An increase in CME of the P TA muscle was revealed following cortical stimulation-enhanced treadmill training. Interestingly, this increase in paretic TA CME was most evident in those who responded to HIITT with a downregulation of their paretic TA CME. The finding could indicate that exercise-induced neuroplastic mechanisms in some individuals make them candidates for motor priming protocols such as tDCS. Whether this acute increased neural drive is a predictor for long-term functional improvement is an interesting and important question for future studies.

The upregulation of CME in the e-tDCS+HIITT group was also accompanied by a decrease in CME of the NP TA. These results are consistent with previous studies that have revealed downregulation of the nonlesioned hemisphere along with an upregulation of the lesioned hemisphere [14, 16, 22]. There is support for the idea that upregulation of CME in the lesioned hemisphere is associated with a concomitant downregulation of the nonlesioned hemisphere via interhemispheric inhibition [9, 23]. Therefore, many upper limb studies have used noninvasive brain stimulation to suppress the nonlesioned hemisphere to produce an opposite modulation in the lesioned hemisphere (see [24] for review). However, in this pilot study, we did not provide behavioral data to support that the increase in paretic TA and decrease in the nonparetic TA are a positive functional outcome. Our hypothesis is supported by previous studies which have shown that a balanced CME is associated with less impairment and better function in stroke survivors [25–27].

The increase in neural excitability was not associated with a concomitant increase in gait speed. This is not surprising as it is unlikely that a single session of treadmill training would

produce significant improvements in overground walking. Nevertheless, the trend towards improvement in gait speed is concurrent with other long-term training studies that have reported improvements in gait speeds with treadmill training [26, 28, 29].

RPE during cooldown from e-tDCS+HIITT was observed to be significantly lower than RPE from HIITT alone. RPE data were collected to detect the effects of tDCS on perceived exertion. The time course of RPE changes from warm-up to cooldown were similar for HIITT and e-tDCS+HIITT sessions. The slightly lower cooldown RPE mean for e-tDCS+HIITT may indicate a more rapid decrease in RPE for the e-tDCS+HIITT than the HIITT session. Further elegant physiological studies are needed to corroborate this finding because the primary outcome measure of this study is related to CME.

4.1. Limitations. Because this was a preliminary study, it has several limitations. First, a homogenous sample that we had previously found to have MEPs in the paretic TA was recruited. In addition, the people in this sample of stroke survivors were relatively fast ambulators (average gait speed of 0.93 m/s) who had the necessary strength and endurance to complete the HIIT protocol. These are unavoidable limitations. Second, the sample size was small ($n = 11$) and only a subset of this sample provided support for our hypothesis. Another study with a larger sample size would be necessary to confirm our results, and the inclusion of a measure of oxygen consumption may answer the question not addressed in the present study of whether the suppression of CME we observed in some of our participants was the result of greater physiological effort. Third, to avoid making the study unwieldy, we chose to compare the effects of HIITT alone with our robust tDCS+tracking task. The absence of tDCS-only and tracking-only control conditions prevents us from understanding which element of the intervention promoted the reduction in asymmetry of between-hemisphere CME. Hence, our results should be interpreted with caution. Fourth, we did not compare our results with other excitability boosting priming paradigms or to a standard form of therapy. Regardless of these limitations, our results are intriguing and can be used to support future studies that explore the impact on stroke survivors' motor function that might result from a HIITT-induced suppression of corticomotor excitability.

5. Conclusions

This is the first study to report that a single session of HIITT has the potential to exacerbate suppressed corticomotor excitability of paretic lower limb muscle representations in some individuals with stroke. Future studies are needed in order to optimize gait rehabilitation by examining the effectiveness of repetitive long-term HIITT with and without the inclusion of cortical excitability enhancing protocols.

Additional Points

Highlights. (i) Corticomotor excitability (CME) following high intensity interval treadmill training (HIITT) has not been examined in stroke. (ii) A single session of HIITT reduces CME of the lesioned hemisphere in some stroke survivors. (iii) Motor priming with task-enhanced transcranial direct current stimulation (tDCS) prior to HIITT reduces this suppression and improves the between-hemisphere symmetry of CME.

Disclosure

The content is solely the responsibility of the authors and does not necessarily represent the official views of the National Institutes of Health.

Competing Interests

None of the authors have potential competing interests to be disclosed.

Acknowledgments

The authors would like to acknowledge support from the National Institutes of Health under Award no. R01HD075777 (SM).

References

[1] P. Boyne, K. Dunning, D. Carl, M. Gerson, J. Khoury, and B. Kissela, "High-intensity interval training in stroke rehabilitation," *Topics in Stroke Rehabilitation*, vol. 20, no. 4, pp. 317–330, 2013.

[2] T. Guiraud, A. Nigam, V. Gremeaux, P. Meyer, M. Juneau, and L. Bosquet, "High-intensity interval training in cardiac rehabilitation," *Sports Medicine*, vol. 42, no. 7, pp. 587–605, 2012.

[3] M. Pohl, J. Mehrholz, C. Ritschel, and S. Rückriem, "Speed-dependent treadmill training in ambulatory hemiparetic stroke patients: a randomized controlled trial," *Stroke*, vol. 33, no. 2, pp. 553–558, 2002.

[4] K. J. Sullivan, B. J. Knowlton, and B. H. Dobkin, "Step training with body weight support: effect of treadmill speed and practice paradigms on poststroke locomotor recovery," *Archives of Physical Medicine and Rehabilitation*, vol. 83, no. 5, pp. 683–691, 2002.

[5] C. M. Tyrell, M. A. Roos, K. S. Rudolph, and D. S. Reisman, "Influence of systematic increases in treadmill walking speed on gait kinematics after stroke," *Physical Therapy*, vol. 91, no. 3, pp. 392–403, 2011.

[6] D. Christensen, S. P. Johnsen, T. Watt, I. Harder, M. Kirkevold, and G. Andersen, "Dimensions of post-stroke fatigue: a two-year follow-up study," *Cerebrovascular Diseases*, vol. 26, no. 2, pp. 134–141, 2008.

[7] N. A. Flinn and J. E. Stube, "Post-stroke fatigue: qualitative study of three focus groups," *Occupational Therapy International*, vol. 17, no. 2, pp. 81–91, 2010.

[8] V. L. Barbour and G. E. Mead, "Fatigue after stroke: the patient's perspective," *Stroke Research and Treatment*, vol. 2012, Article ID 863031, 6 pages, 2012.

[9] N. Murase, J. Duque, R. Mazzocchio, and L. G. Cohen, "Influence of interhemispheric interactions on motor function in chronic stroke," *Annals of Neurology*, vol. 55, no. 3, pp. 400–409, 2004.

[10] J. Duque, F. Hummel, P. Celnik, N. Murase, R. Mazzocchio, and L. G. Cohen, "Transcallosal inhibition in chronic subcortical stroke," *NeuroImage*, vol. 28, no. 4, pp. 940–946, 2005.

[11] S. C. Gandevia, G. M. Allen, J. E. Butler, and J. L. Taylor, "Supraspinal factors in human muscle fatigue: evidence for suboptimal output from the motor cortex," *Journal of Physiology*, vol. 490, no. 2, pp. 529–536, 1996.

[12] J. L. Taylor and S. C. Gandevia, "A comparison of central aspects of fatigue in submaximal and maximal voluntary contractions," *Journal of Applied Physiology*, vol. 104, no. 2, pp. 542–550, 2008.

[13] A. Kuppuswamy, E. V. Clark, I. F. Turner, J. C. Rothwell, and N. S. Ward, "Post-stroke fatigue: a deficit in corticomotor excitability?" *Brain*, vol. 138, pp. 136–148, 2015.

[14] S. Madhavan, K. A. Weber II, and J. W. Stinear, "Non-invasive brain stimulation enhances fine motor control of the hemiparetic ankle: implications for rehabilitation," *Experimental Brain Research*, vol. 209, no. 1, pp. 9–17, 2011.

[15] S. Madhavan, L. M. Rogers, and J. W. Stinear, "A paradox: after stroke, the non-lesioned lower limb motor cortex may be maladaptive," *European Journal of Neuroscience*, vol. 32, no. 6, pp. 1032–1039, 2010.

[16] S. Madhavan and J. W. Stinear, "Focal and bidirectional modulation of lower limb motor cortex using anodal transcranial direct current stimulation," *Brain Stimulation*, vol. 3, no. 1, pp. 42–50, 2010.

[17] B. Shah, T. T. Nguyen, and S. Madhavan, "Polarity independent effects of cerebellar tDCS on short term ankle visuomotor learning," *Brain Stimulation*, vol. 6, no. 6, pp. 966–968, 2013.

[18] A. Sriraman, T. Oishi, and S. Madhavan, "Timing-dependent priming effects of tDCS on ankle motor skill learning," *Brain Research*, vol. 1581, pp. 23–29, 2014.

[19] C. J. Stagg, G. Jayaram, D. Pastor, Z. T. Kincses, P. M. Matthews, and H. Johansen-Berg, "Polarity and timing-dependent effects of transcranial direct current stimulation in explicit motor learning," *Neuropsychologia*, vol. 49, no. 5, pp. 800–804, 2011.

[20] O. Omiyale, C. R. Crowell, and S. Madhavan, "Effect of wii-based balance training on corticomotor excitability post stroke," *Journal of Motor Behavior*, vol. 47, no. 3, pp. 190–200, 2015.

[21] A. Lamontagne and J. Fung, "Faster is better: implications for speed-intensive gait training after stroke," *Stroke*, vol. 35, no. 11, pp. 2543–2548, 2004.

[22] G. Jayaram and J. W. Stinear, "The effects of transcranial stimulation on paretic lower limb motor excitability during walking," *Journal of Clinical Neurophysiology*, vol. 26, no. 4, pp. 272–279, 2009.

[23] R. Traversa, P. Cicinelli, P. Pasqualetti, M. Filippi, and P. M. Rossini, "Follow-up of interhemispheric differences of motor evoked potentials from the 'affected' and 'unaffected' hemispheres in human stroke," *Brain Research*, vol. 803, no. 1-2, pp. 1–8, 1998.

[24] J.-P. Lefaucheur, "Stroke recovery can be enhanced by using repetitive transcranial magnetic stimulation (rTMS)," *Neurophysiologie Clinique*, vol. 36, no. 3, pp. 105–115, 2006.

[25] C. M. Stinear, P. A. Barber, J. P. Coxon, M. K. Fleming, and W. D. Byblow, "Priming the motor system enhances the effects of upper limb therapy in chronic stroke," *Brain*, vol. 131, no. 5, pp. 1381–1390, 2008.

[26] C.-L. Yen, R.-Y. Wang, K.-K. Liao, C.-C. Huang, and Y.-R. Yang, "Gait training-induced change in corticomotor excitability in patients with chronic stroke," *Neurorehabilitation and Neural Repair*, vol. 22, no. 1, pp. 22–30, 2008.

[27] K.-C. Lin, Y.-H. Huang, Y.-W. Hsieh, and C.-Y. Wu, "Potential predictors of motor and functional outcomes after distributed constraint-induced therapy for patients with stroke," *Neurorehabilitation and Neural Repair*, vol. 23, no. 4, pp. 336–342, 2009.

[28] L. Koski, T. J. Mernar, and B. H. Dobkin, "Immediate and long-term changes in corticomotor output in response to rehabilitation: correlation with functional improvements in chronic stroke," *Neurorehabilitation and Neural Repair*, vol. 18, no. 4, pp. 230–249, 2004.

[29] L. W. Forrester, D. F. Hanley, and R. F. Macko, "Effects of treadmill exercise on transcranial magnetic stimulation-induced excitability to quadriceps after stroke," *Archives of Physical Medicine and Rehabilitation*, vol. 87, no. 2, pp. 229–234, 2006.

Hindawi Publishing Corporation
Neural Plasticity
Volume 2016, Article ID 5020348, 12 pages
http://dx.doi.org/10.1155/2016/5020348

Research Article

Kinematic and EMG Responses to Pelvis and Leg Assistance Force during Treadmill Walking in Children with Cerebral Palsy

Ming Wu,[1,2] Janis Kim,[1] Pooja Arora,[1] Deborah J. Gaebler-Spira,[1] and Yunhui Zhang[1]

[1]*Sensor Motor Performance Program, Rehabilitation Institute of Chicago, Chicago, IL 60611, USA*
[2]*Department of Physical Medicine and Rehabilitation, Northwestern University Medical School, Chicago, IL 60611, USA*

Correspondence should be addressed to Ming Wu; w-ming@northwestern.edu

Received 27 March 2016; Revised 21 July 2016; Accepted 2 August 2016

Academic Editor: Sheng Li

Treadmill training has been used for improving locomotor function in children with cerebral palsy (CP), but the functional gains are relatively small, suggesting a need to improve current paradigms. The understanding of the kinematic and EMG responses to forces applied to the body of subjects during treadmill walking is crucial for improving current paradigms. The objective of this study was to determine the kinematics and EMG responses to the pelvis and/or leg assistance force. Ten children with spastic CP were recruited to participate in this study. A controlled assistance force was applied to the pelvis and/or legs during stance and swing phase of gait through a custom designed robotic system during walking. Muscle activities and spatial-temporal gait parameters were measured at different loading conditions during walking. In addition, the spatial-temporal gait parameters during overground walking before and after treadmill training were also collected. Applying pelvis assistance improved step height and applying leg assistance improved step length during walking, but applying leg assistance also reduced muscle activation of ankle flexor during the swing phase of gait. In addition, step length and self-selected walking speed significantly improved after one session of treadmill training with combined pelvis and leg assistance.

1. Introduction

Cerebral palsy (CP) is the most prevalent physical disability originating in childhood with an incidence of 2-3 per 1,000 live births [1]. Up to 90% of children with CP have difficulty in walking [2, 3]. Reduced walking speed and endurance are two of the main functional problems, particularly in children with more severe disabilities [4]. Locomotion plays a central role in healthy bone development [5] and children who are able to ambulate are more accomplished in activities of daily living and social roles, such as participation in the community, than children who use a wheelchair [6]. Thus, improving walking function is one key focus of clinical therapeutic interventions for children with CP.

Treadmill training has been used as a promising technique for improving locomotor function in children with cerebral palsy (CP) [7, 8]. However, while statistically significant improvements in walking function after treadmill training have been shown, the functional gains are relatively small [9, 10]. In addition, treadmill training requires a high level of involvement from a physical therapist [11]. In order to reduce therapist labor levels, several robotic gait training systems have been developed to provide robotic gait training to children with CP [12, 13]. These robotic systems are effective in reducing therapist labor during locomotor training but show relatively limited functional gains for some children with CP. For instance, a recent randomized study indicated that only a modest improvement in gait speed was obtained following a prolonged (20 sessions) robotic treadmill training using the pediatric Lokomat [14], suggesting a need for improving the efficacy of current treadmill training paradigm. Possible reasons why treadmill training may not be optimally effective for improving gait speed in children with CP include limitations of the current robotic systems, such as the lack of mediolateral movement of the pelvis, which may constrain the mediolateral movement of the pelvis during treadmill walking [15].

Weight shifting in the mediolateral direction is of one of key components of human locomotion [16]. However, this weight shifting ability is often impaired in children with CP

compared to children who go through the normal stages of development [17]. For instance, children with CP were less efficient at weight shifting (demonstrated by a shorter range of motion of the center of pressure and slower velocity of the center of pressure displacement during visually guided weight shifting) than children with normal development. This impairment in weight shifting in children with CP may be related to weakness of hip abductors/adductors, which are suggested to play a crucial role in maintaining lateral balance during locomotion [18]. While the importance of weight shifting during locomotion of children with CP has been acknowledged, it remains unclear whether applying an assistance force to the pelvis during stance phase of gait will facilitate weight shifting and improve stepping.

Short step length is one of the key factors contributing to reduced walking speed of children with CP. Thus, in a clinical setting, assistance force is provided to the legs by physical therapists or robotic arms to facilitate leg swing during treadmill training in children with CP [9, 12]. While applying leg assistance may help to increase the step length of children with CP during treadmill training, applying too much assistance to the legs may be suboptimal to locomotor training because it may encourage passive instead of active participation of the subject; that is, the central neural system may reduce the motor output of subject in response to the assistance applied for the sake of the optimization of energy cost [19]. However, there is no evidence whether the muscle activation of the hip and/or ankle flexors of children with CP will be reduced when an assistance force is applied to legs during swing phase of gait.

In this study, we tested the spatial-temporal gait parameters and EMG responses to pelvis assistance applied during stance phase and leg assistance forces applied during swing phase in children with CP. We hypothesized that applying a lateral assistance load to the pelvis during the stance phase of gait will facilitate weight shifting, which will trigger an enhanced muscle activation of the hip abductors to stabilize the pelvis during the stance phase of gait, and applying a leg swing assistance force may reduce muscle activation of the hip flexors/ankle flexors during the swing phase of gait because the central nervous system may optimize energy output. In addition, we hypothesized that applying both leg assistance and pelvis assistance might improve step length and/or step height during treadmill walking. Furthermore, we tested the transfer of motor adaptation from the treadmill to overground walking after one session of robotic treadmill training. We hypothesized that the motor adaptation would be transferred from the treadmill to overground walking.

2. Methods

2.1. Subjects. Ten children (3 girls) with spastic CP were recruited to participate in this study. Mean age was 11±3 years old. According to the Gross Motor Function Classification System (GMFCS) [20], 2 of them were classified as level I, 4 of them were classified as level II, and 4 of them were classified as level III; see Table 1 for details.

Inclusion criteria were as follows: (a) age 7–16 years old; (b) spastic CP; (c) without Botulinum toxin treatment or surgery within 3 months before the onset of the study; (d) GMFCS levels that were I to III; (e) ability to signal pain, fear, or discomfort reliably; (d) ability to ambulate for at least 10 meters with/without assistive device.

Exclusion criteria were as follows: (a) severe lower extremity contractures, fractures, osseous instabilities, and osteoporosis; (b) unhealed skin lesions in the lower extremities; (c) thromboembolic diseases, cardiovascular instability, and aggressive or self-harming behaviors.

2.2. Apparatus. A custom designed 3D cable-driven gait training system was used to apply controlled assistance forces to the pelvis and legs, to facilitate weight shifting and leg swing, respectively, during treadmill walking; see Figure 1. The cable-driven robotic gait training system for leg assistance has been reported previously [21]. In brief, four nylon-coated stainless-steel cables (diameter 1.6 mm), which are driven by four motors and cable spools (two of them are located at the frontal of the treadmill and other two motors are located at the back of the treadmill), are affixed to custom braces that are strapped to the subject's legs to provide a controlled assistance (pulling forward) forces to legs. In this study, additional two motors (AKM33H, Kollmorgen, Drive amplifier, Servostar 30661), which are attached to the frame located at the side of treadmill, were used to provide controlled assistance forces at the pelvis in the mediolateral direction. Additionally, two sets of custom designed 3D position sensors were attached to the pelvis and legs above ankle through a strap and were used to record the pelvis and leg positions. Specifically, each position sensor consists of a detector bar and three potentiometers. One linear potentiometer (SP-2, Celesco, Chatsworth, CA) was used to measure the linear movement of the bar and the other two rotational potentiometers (P2201, Novotechnik, Southborough, MA) were used to measure rotational movements of the bar in the anterior-posterior and medial-lateral directions [21]. The cable driven system is compliant and highly backdrivable [21], which allows subjects to freely move their pelvis and legs through a natural gait pattern.

2.3. Protocol. An overhead harness was used while subjects walked on a treadmill. Body weight support was provided for one subject to prevent knee buckling or toe dragging and no body weight support was provided for other 9 subjects. The treadmill speed was set at each subject's comfortable speed determined at the beginning of experiment. Subjects were allowed to hold onto the bar in front of them for the sake of safety and to wear their orthosis. Each subject participated in two test sessions. Specifically, in session 1, subjects walked on a treadmill without a load for one minute, that is, baseline. Then, subjects walked on a treadmill with 3 loading conditions, that is, (1) pelvis assistance load only, (2) leg assistance load only, and (3) combined pelvis and leg assistance load. The order of these three loading conditions was randomized across subjects. Subjects walked for 3 minutes in each loading condition with a one-minute standing break inserted in between two test conditions. The peak value of the pelvis assistance force was set at ~14% of body weight, and the peak leg assistance force was set at ~6% of body

Table 1: Subject information indicating age, type of CP, weight, gender, GMFCS level, and orthosis and/or assistive devices used by subjects at the time of the study. RRW: reverse rolling walker; AFO: ankle-foot orthosis.

Number	Age (year)	Body weight (kg)	Gender	GMFCS level	Type of CP	Orthosis and assistive devices
1	7	22.5	M	III	Spastic diplegia	Bilateral AFO/crutches
2	10	27.0	M	II	Spastic diplegia	Bilateral AFO/none
3	11	34.7	M	III	Spastic diplegia	Bilateral AFO/RRW
4	16	58.5	F	I	Spastic diplegia	None/none
5	12	47.3	M	II	Spastic diplegia	Bilateral AFO/none
6	14	42.3	M	II	Spastic diplegia	Bilateral AFO/none
7	10	25.2	M	I	Spastic diplegia	None/none
8	9	27.5	F	III	Spastic diplegia	Bilateral AFO/RRW
9	9	43.7	M	II	Spastic diplegia	Orthotics/none
10	12	54.4	F	III	Spastic diplegia	Bilateral AFO/RRW

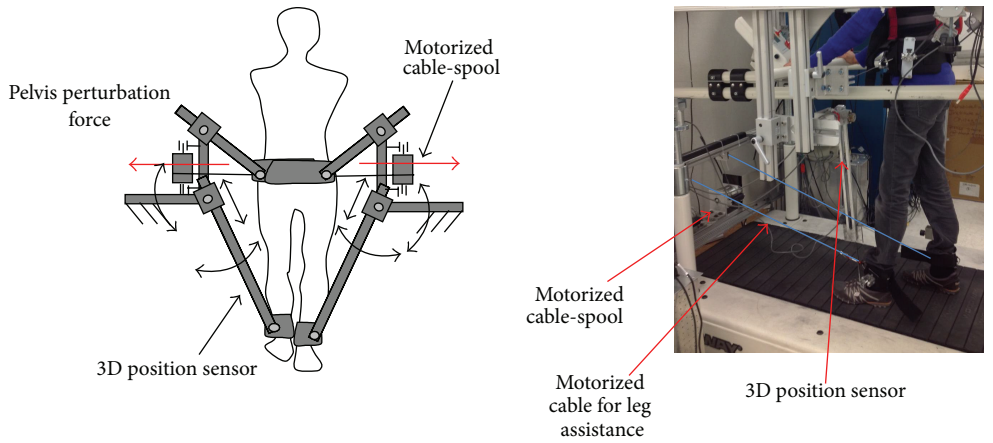

Figure 1: This figure illustrates the 3D cable-driven apparatus that was used with a treadmill and body weight support system. Four cables driven by four motors, pulleys, and cable spools were used to apply pelvis and leg assistance loads during treadmill walking. A personal computer was used to control the loads produced by four motors, applying controlled forces at targeted phase of gait.

weight, although these peak forces were adjusted based on the tolerance of each subject (i.e., to make sure they felt some challenges but not too overwhelming when the force was applied); see Table 2. The ankle position signals were used to trigger pelvis and ankle loading at targeted phases of gait. Specifically, toe-off was defined as the time during which the ankle position, which was measured using ankle position sensor, changed its moving direction from backward to forward; heel-contact was defined as the time during which the ankle position changed its moving direction from forward to backward [22, 23]. The leg assistance load was applied bilaterally to the ankle starting from toe-off to mid-swing, and the pelvis assistance load was applied bilaterally in the lateral direction (for facilitating weight shifting) starting at heel contact to mid-stance of the ipsilateral leg, determined based on signals recorded by ankle position sensors.

After subjects completed all the test conditions of session 1, subjects were given a 5-minute sitting break. Then, session 2 was initiated, in which subjects walked on a treadmill while a controlled assistance load was applied to both the pelvis and leg for another 20 minutes using a protocol similar to condition 3 of session 1. Short standing breaks were allowed as necessary depending on the tolerance of each subject during the test. Self-selected and fast (i.e., subjects were instructed to walk as fast as they could without running) overground walking speeds were tested using the GaitRite (CIR Systems Inc., Sparta, NJ), a 4.3 m long mat with embedded pressure sensors for measuring spatiotemporal gait parameters, before and after treadmill training. Three trials were tested for each speed and were averaged across the 3 trials for each test condition. Spatiotemporal parameters, including step length, stance time, and swing time, during self-selected and fast overground walking were also calculated using the GaitRite software and averaged across the three trials and two legs. The kinematics of the pelvis and legs during treadmill walking were recorded using two sets of custom-designed positional sensors, mentioned previously, and sampled at 500 Hz using a data acquisition card (National Instruments, Austin, TX,

Table 2: Testing parameters indicating body weight support, test speed, and average peak assistance forces applied to the leg at the ankle and pelvis. BW: body weight.

Number	Treadmill speed (m/s)	Pelvis assistance force (N)	Leg assistance force (N)	Body weight support (% BW)
1	0.37	52 (23.6%)	17 (7.7%)	0
2	0.48	41 (15.5%)	22 (8.3%)	0
3	0.18	52 (15.3%)	22 (6.4%)	30%
4	0.76	66 (11.5%)	22 (3.8%)	0
5	0.46	40 (8.6%)	23 (5.0%)	0
6	0.36	41 (9.9%)	23 (5.5%)	0
7	0.23	48 (19.4%)	20 (8.1%)	0
8	0.51	43 (15.9%)	17 (6.3%)	0
9	0.78	51 (11.9%)	27 (6.3%)	0
10	0.30	46 (8.6%)	28 (5.2%)	0
Mean	0.44 ± 0.20	48.0 ± 7.9 (14.0 ± 4.9%)	22.1 ± 3.6 (6.3 ± 1.4%)	

USA) on a personal computer. Custom LabVIEW (National Instruments) software was used for controlling the data acquisition and sending motor commands to the motor drivers at targeted phase of gait, which was determined using a custom designed ankle positional sensor.

The EMG activity of the right Tibialis Anterior (TA), Medial Gastrocnemius (MG), Soleus (SO), Vastus Medialis (VM), Rectus Femoris (RF), Medial Hamstrings (MH), hip Adductors (ADD), and Abductors (ABD) was recorded for all the testing sessions during treadmill walking (for the convenience of setup, only the right leg's muscle activities were recorded, although pelvis and leg assistance forces were applied bilaterally). Active Delsys electrodes (Model De-2.1, Delsys Inc. Boston, MA, USA) were applied to lightly abraded, degreased skin over the respective muscle belly. The leads were attached to a preamplifier/filter system (amplification ×1,000) and all signals were band-passed filtered (20–450 Hz), and sampled at 500 Hz on a personal computer, which was synchronized with the computer used for recording kinematic data.

2.4. Data Analysis. All kinematic data were smoothed using a 4th order Butterworth low-pass filter (cut-off frequency: 8 Hz) with zero lag (The MathWorks, Natick, Massachusetts). Step length and step height during treadmill walking were derived from subject's ankle trajectory, which were recorded using two ankle position sensors [24]. Step length was quantified as the horizontal distance between the two legs' ankle positions at the timing of heel-contact. Step height was quantified as the vertical difference between the leg's highest ankle position and lowest ankle position during a gait cycle. Swing time was quantified as the time between toe-off and heel-contact normalized to the gait cycle time. Weight shifting in the frontal plane during treadmill walking was quantified using the minimal lateral distance between the center of the pelvis and ankle position of the supporting leg, which was calculated using signals recorded by a set of pelvis and leg positional sensors. The spatial temporal parameters of the last 10 steps during treadmill walking of each loading condition were averaged and further averaged across both legs.

The EMG signals were notch filtered at 55 Hz to 65 Hz using 4th order Butterworth filter and rectified. Then, these data were segmented into step cycle from heel contact to next heel contact, dependent on the measured ankle position using the position sensor. The last ten steps of each condition were used for analysis. Due to the variability in step duration from cycle to cycle, the data from each cycle were interpolated and resampled and then averaged across 10 steps to create a mean EMG pattern, which were smoothed using low-pass filter at 40 Hz using 4th order Butterworth filter. The EMG data of each muscle from each condition were normalized to the average peak value of that muscle's activation pattern for the condition with maximum treadmill walking speed of each participant. Smoothed EMGs were integrated for the targeted period of the gait cycle, that is, from late stance (~10% gait cycle before toe off) to mid-swing and from heel contact to mid-stance. Spatial-temporal gait parameters during overground walking were obtained using data collection software of GaitRite (CIR Systems Inc., Sparta, NJ).

Repeated measures ANOVAs were used for the effect of different loading conditions on the spatial-temporal gait parameters and integrated EMG areas during treadmill walking, with significance noted at $p < 0.05$. If the ANOVA revealed significant differences, Tukey-Kramer post hoc tests were used to identify specific differences between different conditions, again with significance noted at $p < 0.05$. In addition, the spatial-temporal parameters and gait speeds during overground walking were also compared before and after treadmill walking to identify the transfer effect, again, with significance noted at $p < 0.05$.

3. Results

Applying controlled pelvis assistance facilitated weight shifting, indicated as a reduced minimal lateral distance between the pelvis and the supporting leg during stance phase. The displacements of the center of the pelvis in the mediolateral

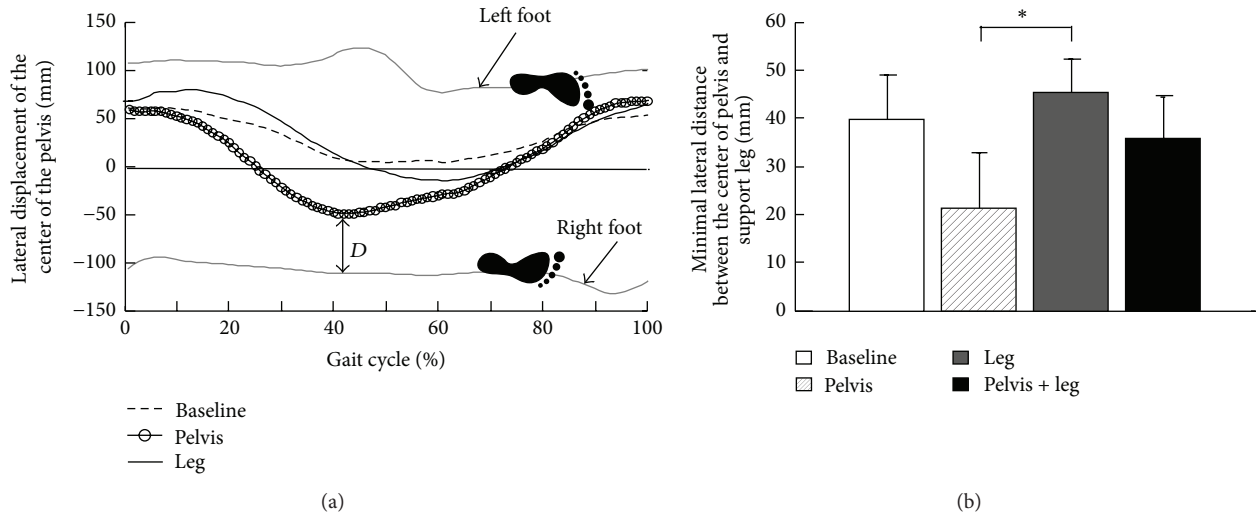

(a) (b)

Figure 2: Displacement of the center of the pelvis in the mediolateral direction while subjects walking on a treadmill. (a) Displacement of the center of the pelvis from one child with CP with no load, that is, baseline, with pelvis assistance, and leg assistance. Displacements of the center of the pelvis shown in the figure were average of 10 strides for each condition. Gray curves located at the top and the bottom indicated the trajectories of the left and right feet during treadmill walking. All the displacements of the center of the pelvis were normalized to the gait cycle, starting from heel strike of the right leg. "D" indicates the minimal distance in the mediolateral direction between the center of the pelvis and supporting leg during stance. (b) Group average of the minimal distance between the center of the pelvis and supporting leg across 9 subjects at 4 different loading conditions. The bar and error bar indicate the mean and standard deviation of the minimal distance across 10 subjects for each loading condition. Asterisk (∗) indicates significant effect of loading conditions.

direction, from one child with CP, with no load, that is, baseline, and with pelvis or leg assistance load are shown in Figure 2(a). We observed a greater lateral shifting of the center of mass (estimated using the center of the pelvis) to a position closer to the lateral limit of the base of support of the right leg when a pelvis assistance load was applied but a modest change in lateral shifting of the center of the mass in comparison with the baseline when a leg assistance load was applied. Results from all subjects indicated that loading condition had a significant impact on the minimal lateral distance between the center of the pelvis and ankle position of the supporting leg during stance ($p = 0.02$, $n = 9$, ANOVA, data from one child was excluded because the pattern of data across different load conditions was distinct from all other subjects due to unclear reasons). Post hoc tests indicated significant differences in the minimal lateral distance between the conditions with pelvis assistance only versus leg assistance only ($p = 0.01$) but indicated no significant difference between the conditions with baseline versus leg assistance only ($p = 0.85$), the conditions with baseline versus pelvis assistance only ($p = 0.08$), and the conditions with baseline versus combined pelvis and leg assistance ($p = 0.99$), Figure 2(b).

Applying a controlled pelvis and/or leg assistance force during treadmill walking had impact on the step length and height of children with CP. Ankle trajectories in the sagittal plane, from one child with CP, with no load, and with pelvis assistance or leg assistance load are shown in Figure 3(a). We observed an increase in step height when pelvis assistance was applied and an increase in step length when leg assistance was applied; see Figure 3(a). Results from a group of children with CP indicated that applying a controlled pelvis and/or leg assistance force had a significant impact on the step height ($p = 0.01$, $n = 9$, the step height from 1 subject was excluded because the data point was classified as an outlier, defined as a magnitude that was >3 SD above the population mean). Post hoc tests indicated significant differences in step height between baseline and the condition with pelvis assistance only (55.7% increase, $p = 0.04$) and between baseline and the condition with combined pelvis and leg assistance (68.0% increase, $p = 0.01$) but no significant difference between baseline and the condition with leg assistance only (31.6% increase, $p = 0.44$) (Figure 3(b)). In addition, group results indicated that pelvis and/or leg assistance loads had a significant impact on step length of children with CP ($p = 0.01$, $n = 10$, ANOVA). Post hoc tests indicated significant differences in step length between baseline and the condition with combined pelvis and leg assistance (9.2% increase, $p = 0.03$) and between baseline and the condition with leg assistance only (8.2% increase, $p = 0.01$) but no significant difference between baseline and the condition with pelvis assistance only (5.4% increase, $p = 0.28$); see Figure 3(c). Group results indicated that applying pelvis and/or leg assistance had no significant impact on the swing time ($p = 0.70$) (Figure 3(d)).

Applying a controlled pelvis and/or leg assistance force induced changes in the leg muscle activity pattern. Specifically, applying a leg assistance force induced a decrease in the magnitude of TA during swing phase of gait and a slight decrease in magnitude of MG during stance phase of gait; see Figure 4. In addition, applying a pelvis assistance force induced an increase in the magnitude of ABD during stance

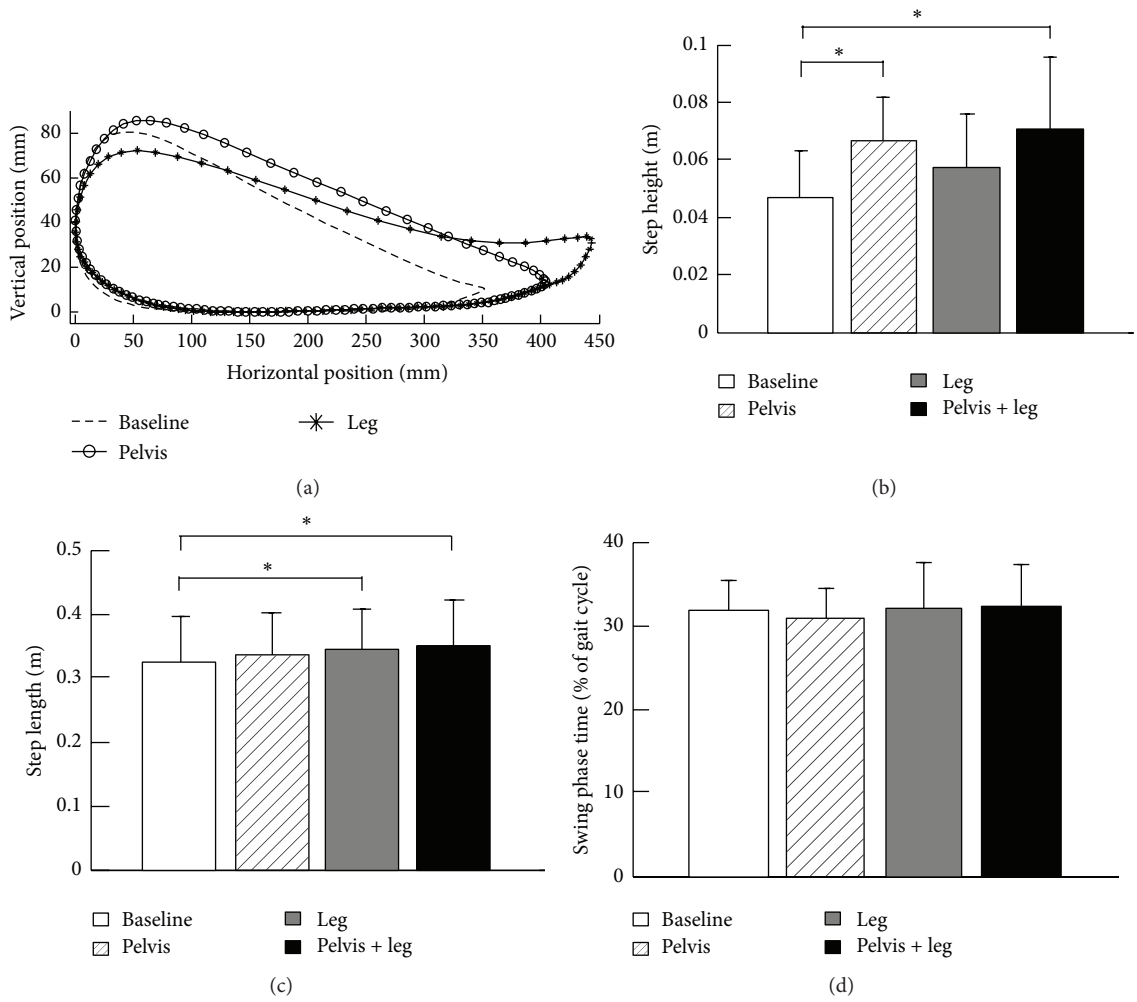

Figure 3: (a) Ankle trajectories in the sagittal plane are shown for one child with CP during treadmill walking with no load, that is, baseline, with pelvis and leg assistances. The ensemble-average trajectories across 10 strides are shown for each loading condition. Group averages of step height (b), step length (c), and swing time (d) during treadmill walking with different loading conditions. The bar and error bar indicate the mean and standard deviation of spatial and temporal gait parameters across 10 subjects for each loading condition. Asterisk (∗) indicates significant effect of loading conditions.

phase of gait but had a modest impact on the muscle activities of ADD; see Figure 4. A group average of integrated muscle activities during the early stance phase (from heel contact to mid-stance) and early swing phase (from late stance to mid-swing) are shown in Figure 5. The loading condition had a significant impact on the integrated muscle activity of TA during swing phase ($p = 0.002$). Post hoc tests indicated a significant decrease in muscle activity of TA from baseline to the conditions with leg assistance ($p = 0.006$) and with combined pelvis and leg assistance ($p = 0.003$). The loading condition had no significant impact on the integrated muscle activity of other muscles during swing phase ($p = 0.55$ for MG, $p = 0.32$ for SOL, $p = 0.14$ for VM, $p = 0.08$ for RF, $p = 0.85$ for MH, $p = 0.76$ for ADD, and $p = 0.14$ for ABD). In addition, loading condition had a significant impact on the integrated muscle activity of TA during stance phase of gait ($p = 0.04$). Post hoc tests indicated a significant decrease in muscle activity of TA from baseline to the condition with combined pelvis and leg assistance ($p = 0.03$). The loading condition had a significant impact on the integrated muscle activity of MG ($p = 0.02$) and ADD ($p = 0.02$) during the stance phase of gait, although post hoc tests indicated no significant differences between the other two conditions for these two muscles ($p > 0.05$). The loading condition had a significant impact on the integrated muscle activity of SOL during stance phase of gait ($p = 0.01$). Post hoc tests indicated a significant difference between baseline versus combined pelvis and leg assistance ($p = 0.02$) and pelvis only versus combined pelvis and leg assistance ($p = 0.04$). No significant differences were observed between the other two conditions ($p > 0.05$). Loading condition had no significant impact on the integrated muscle activity of VM during stance phase of gait ($p = 0.48$). The loading condition had a significant impact on the integrated muscle activity of RF during the stance phase of gait ($p = 0.04$). Post hoc tests indicated a significant decrease in muscle activity of RF from baseline to

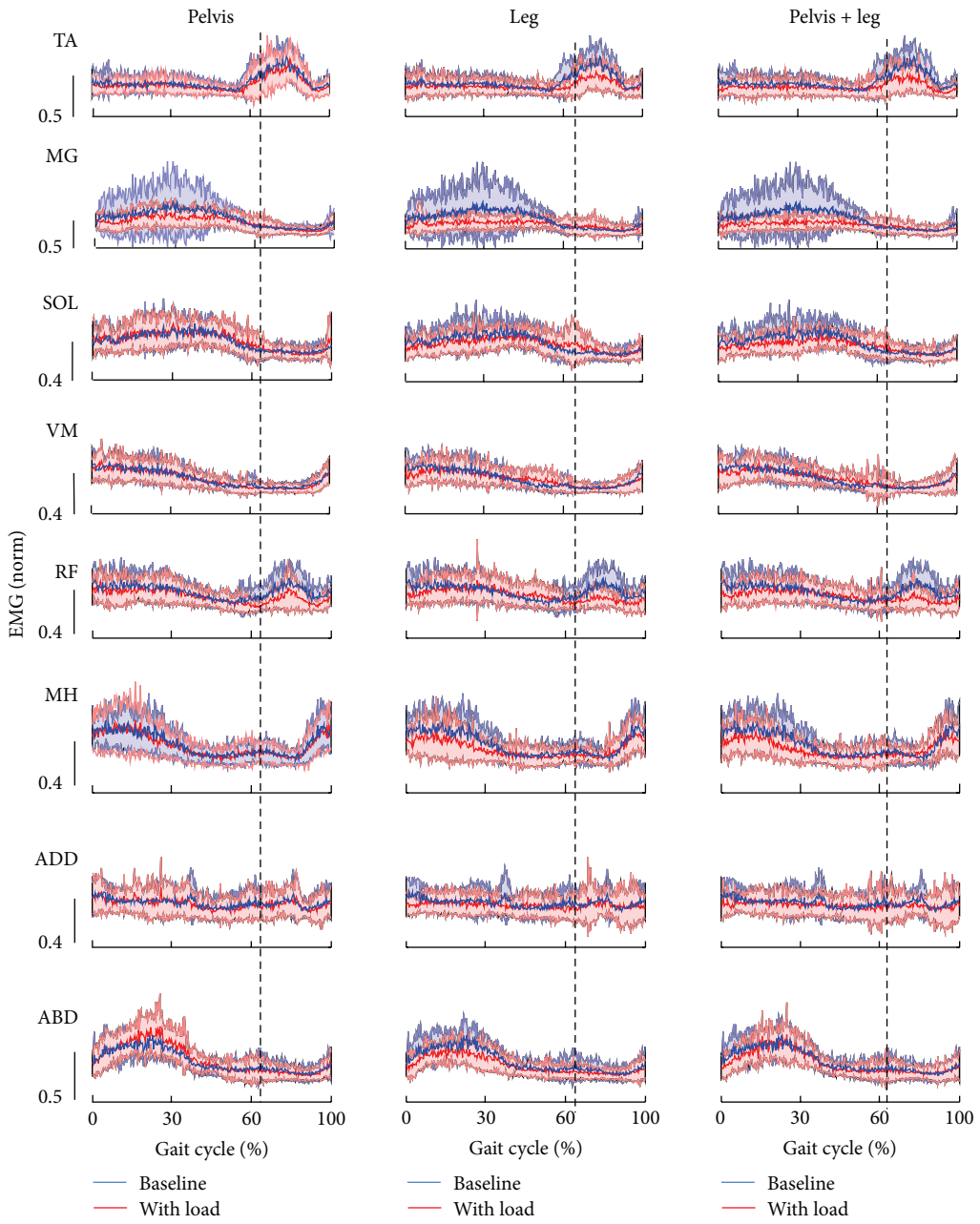

Figure 4: EMG activity patterns from 8 muscles of the right leg during treadmill walking with 3 different loading conditions, that is, pelvis assistance only, leg assistance only, and combined pelvis and leg assistance, in comparison with baseline condition in children with CP are shown. EMG patterns were averaged over the last 10 steps with load for each subject and were further averaged across 10 subjects for all 8 muscles except for MG ($n = 9$). EMG data of MG from one subject were excluded from average because the data was considered as an outlier. In all graphs, thick lines with surrounding thin lines represent the mean and standard deviation of EMG data. EMG data were normalized to the peak values of each muscle with subjects walking on a treadmill with maximum walking speed of each subject. All EMG signals were normalized in time to 100% of the gait cycle. Dashed vertical line indicates the onset of the swing phase of gait.

the condition with combined pelvis and leg assistance ($p = 0.03$). No significant differences were observed between other conditions ($p > 0.05$). The loading condition had a significant impact on the integrated muscle activity of MH during the stance phase of gait ($p < 0.001$). Post hoc tests indicated significant differences between baseline versus combined pelvis and leg assistance ($p < 0.001$), baseline versus leg assistance only ($p < 0.001$), pelvis versus leg assistance only ($p = 0.002$), and pelvis versus combined pelvis and leg assistance only ($p = 0.002$). No significant differences were observed between other conditions ($p > 0.05$). The loading condition had a significant impact on the integrated muscle activity of ABD during the stance phase of gait ($p < 0.001$). Post hoc tests indicated significant differences between baseline versus

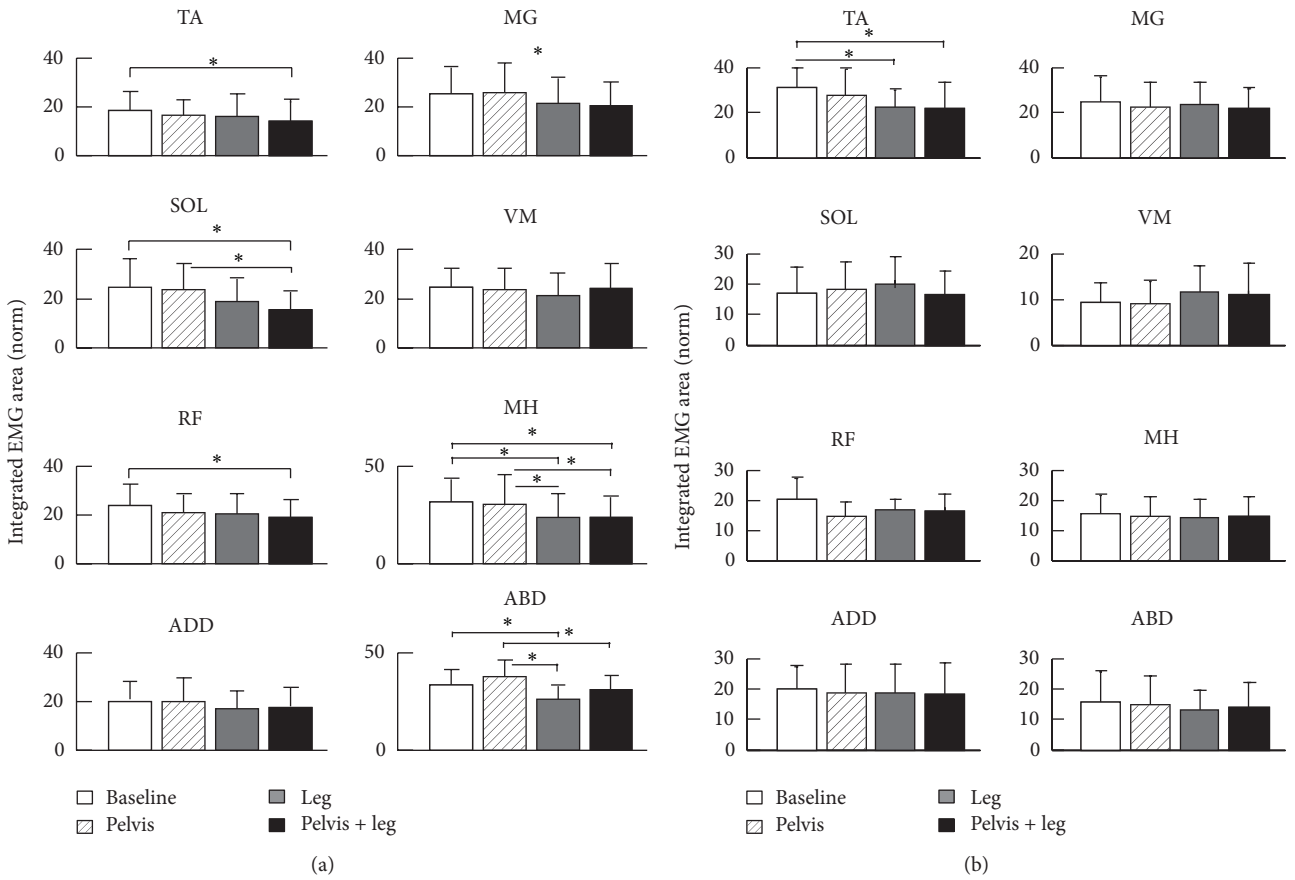

Figure 5: Average of integrated EMG area during stance phase (i.e., from heel strike to mid-stance, when the pelvis assistance force was applied), (a), and during swing phase (i.e., from late stance, 10% before toe-off, to mid-swing), (b), at 4 different loading conditions, that is, baseline, pelvis assistance only, leg assistance only, and combined pelvis and leg assistance, is shown. The bar and error bar indicate the mean and standard deviation of the integrated EMG area across subjects for each load condition. Asterisk (∗) indicates significant effect of treatment.

leg assistance only ($p = 0.02$), pelvis assistance only versus leg assistance only ($p < 0.001$), and pelvis assistance only versus combined pelvis and leg assistance ($p = 0.02$). No significant differences were observed between the other two conditions ($p > 0.05$).

Step length during overground walking at a self-selected speed significantly increased (9.6% increase) after one session of treadmill training (~20 minutes) with combined pelvis and leg assistance force ($p = 0.02$), suggesting that a potential transfer of motor skills occurred from robotic-assisted treadmill training to overground walking in children with CP; see Figure 6(a). Swing phase time (normalized to gait cycle time, $p = 0.01$) and step cadence ($p = 0.001$) during overground walking at a self-selected speed also significantly increased after one session of treadmill training; see Figures 6(b) and 6(c). In addition, self-selected overground walking speed significantly increased (22.2%) after one session of treadmill training with combined pelvis and leg assistance ($p = 0.001$); see Figure 6(d).

Step length during overground walking with fast speed had no change (1.7% increase) after one session of treadmill training with a controlled pelvis and leg assistance force ($p = 0.55$); see Figure 6(a). In addition, there were no significant changes in swing phase time during overground walking at a fast speed after one session of treadmill training ($p = 0.66$); see Figure 6(b). Fast walking speed had no significant change (8.3% increase, $p = 0.22$) after treadmill training; see Figure 6(d).

4. Discussion

Applying a controlled pelvis assistance force improved step height, and applying a controlled leg assistance force improved step length in children with CP, although leg assistance reduced muscle activation of leg flexors and pelvis assistance tended to increase muscle activation of hip abductors. Furthermore, we observed a significant increase in step length and self-selected walking speed of children with CP during overground walking after one session of treadmill training in which controlled forces were applied to the pelvis and leg, suggesting a potential transfer of motor adaptation from the treadmill to overground walking.

Improved weight shifting facilitated by the pelvis assistance force during treadmill walking may improve stepping in children with CP. To the best of our knowledge, this is the first study that provided direct evidence that applying lateral

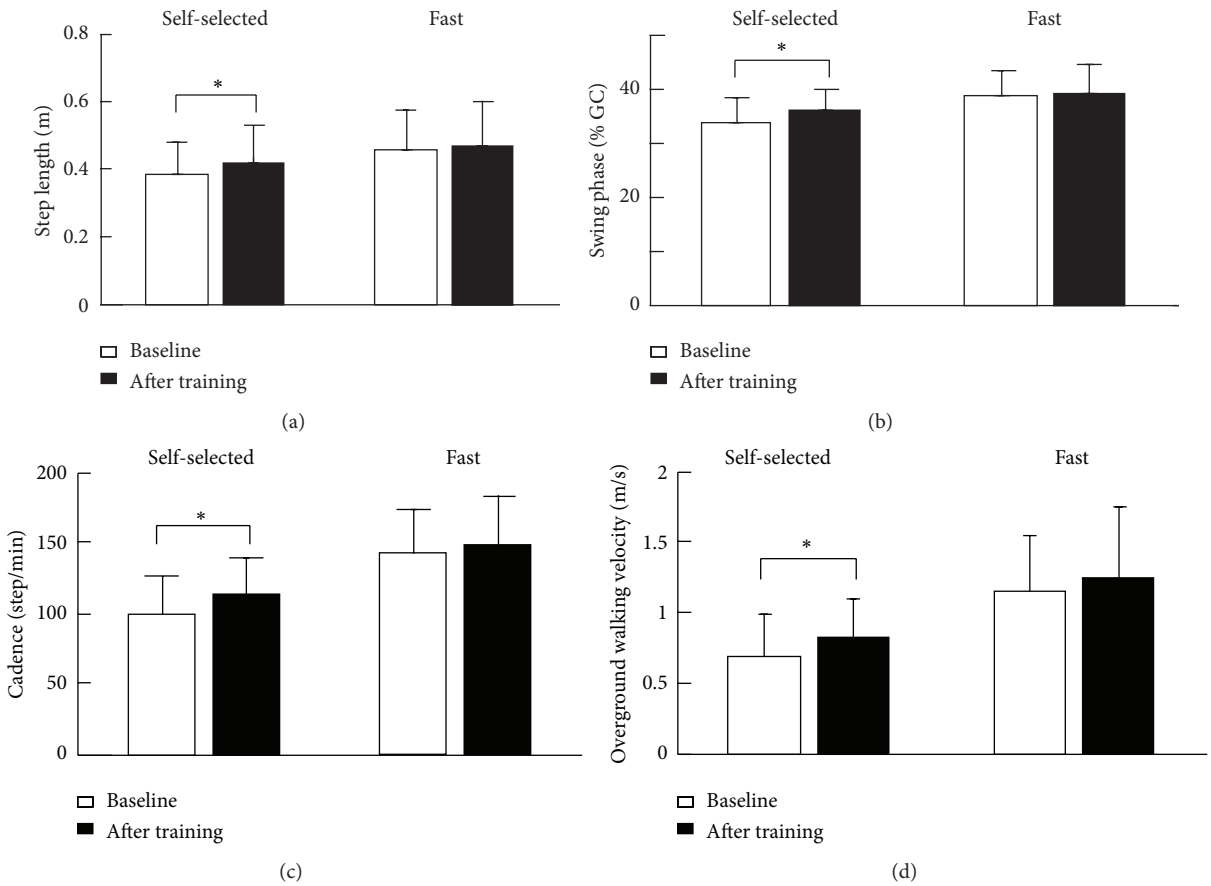

Figure 6: Step length, (a), self-selected and fast overground walking speeds, (b), step frequency (c), swing phase ratio, (d), and single leg support time, (d), in children with CP before and after treadmill training with controlled assistance forces applied to the pelvis and legs through the 3D cable-driven robot. The bar and error bar indicate the mean and standard deviation of the spatial and temporal gait parameters across 10 subjects. Asterisk (∗) indicates significant effect of treatment.

pelvis assistance to facilitate weight shifting in children with CP may improve step height in children with CP. Many children with CP have impairments in weight shifting [25, 26], which has been shown to be correlated to their walking speed [25]. One possible reason for insufficient weight shifting in children with CP may be due to muscle weakness of the hip abductors and adductors [27, 28], which have been suggested to play crucial roles in maintaining lateral balance control during locomotion [18]. The hip abductors and adductors serve as a stabilizer for the ipsilateral lower extremity during single leg stance. Therefore, weakness of the hip abductors and adductors may limit a child with CP to bear weight on one leg for a prolonged period of time, which may result in a shortened swing time and step length on the contralateral leg. In addition, a child with CP may have a limited capacity to laterally shift their center of mass to a position closer to the lateral limit of the base of support in children with CP when weakness in the hip abductors and adductors is present. Insufficient weight shifting to the ipsilateral leg may induce an inefficient unloading of the contralateral leg, a key afferent component for modulating transition from stance to swing [29, 30]. In the current study, an assistance load applied to the pelvis during stance also triggered enhanced muscle activity of the hip abductors (16% increase) (Figure 4), although this was not significant due to variability of integrated muscle activity across subjects ($p = 0.3$); see Figure 5. Thus, it is feasible that the controlled assistance force applied to the pelvis in the mediolateral direction may facilitate weight shifting in children with CP during the stance phase of gait, indicated as a reduction in minimal distance in the mediolateral direction between the center of the pelvis and supporting leg during stance, although this was not significant due to large variability across subjects. One mechanism through which gait pattern improvements in children with CP may occur is that an improvement in weight shifting to the ipsilateral leg (i.e., standing leg) may facilitate unloading of the contralateral leg (i.e., swing leg). Unloading afferent input from the swing leg may facilitate leg swing [29, 30]. We observed significant improvements in step height and step length, in children with CP with the application of a pelvis assistance force.

The central nervous system of children with CP may adapt to an external assistance force applied to the leg(s) during the swing phase of gait. In the current study, the

muscle activity of the TA of the ipsilateral leg (during swing phase) and MH and ABD of the contralateral leg (during stance phase) significantly decreased (the integrated muscle activity decreased 24.4%, for TA, 29.3%, for MH, and 18.4% for ABD, resp., in comparison to baseline) when a controlled assistance force was applied to both legs during the swing phase. This reduction in muscle activity suggests that the central neural system of children with CP recalibrated the motor output of the leg muscles in response to the externally applied leg assistance force, probably due to the optimization of the energy cost [19]. This is consistent with previous studies in which an ankle assistance force induced a reduction in muscle activity when an assistance force was applied to assist ankle dorsiflexion of healthy adults [31]. Given that the activity of the central neural system of children with CP may decrease when an external assistance force is applied, a large leg assistance force (e.g., with the magnitude of force at 6% of body weight) may be suboptimal for motor learning during locomotor training in children with CP because it may encourage passive rather than active training. Previous studies have indicated that active training is more effective than passive training [32, 33]. This is also consistent with a previous clinical study, which indicated that only a modest increase in the gait speed of children with CP was observed after robotic training in which a passive guidance force was applied to both legs [14].

The locomotor skills obtained during robotic treadmill training may partially transfer to overground walking in children with CP. While differences in the kinetics between treadmill and overground walking have been observed [34], the differences in the kinematics [35] between these two walking conditions are generally small in children with CP. The neural circuits controlling locomotion during treadmill and overground walking may be partially overlapped [36]. Thus, the motor skills obtained during treadmill training may partially transfer to overground walking in children with CP, which is consistent with previous studies in patients with spinal cord injury [24] and patients after stroke [36]. However, many other factors may influence the transfer of motor skills from training tasks to application tasks. For instance, visual information is quite different between treadmill and overground walking. During overground walking, subjects are moving through space and visual information is changing, whereas this is not happening during treadmill walking. In addition, subjects held on to a static bar during treadmill walking but used a walker/crutch or no assistive device during overground walking, which can affect the subject's stability and therefore walking pattern. In this study, the increase in step length during overground walking (9.6%) at a self-selected walking speed is comparable to the increase in step length during treadmill walking (9.2%) with combined pelvis and leg assistance versus baseline, suggesting that a majority of motor skills may be transferred from treadmill training to overground walking in children with CP.

In addition, while no significant change was seen in swing time with combined pelvis and legs assistance during treadmill walking, significant increase was observed during overground walking after robotic treadmill training. The increase in swing time, suggesting an improvement in balance of the support leg, after treadmill training may be due to the training effect of the mediolateral assistance force applied to the pelvis during treadmill training. The pelvis assistance force may facilitate weight shifting and children with CP may be forced to use more of the hip abductor/adductors, which provide crucial contributions to frontal plane balance control during walking [18], during robotic treadmill training. Thus, repetitive exposure to a pelvis assistance force during treadmill training may be helpful for improving motor control of the hip abductor/adductors. An increase in swing time may allow children with CP to take a longer step, paired with an increase in cadence, resulting an improvement in walking speed after robotic treadmill training.

This study may have some potential clinical applications. For instance, results from this study indicate that applying an assistance force to the pelvis during the stance phase of gait may facilitate weight shift and improve stepping in children with CP. Thus, it would be helpful for physical therapists to apply assistance forces to the pelvis of children with CP (even for these patients with GMFM level at I to III) during treadmill training. On the other hand, results from this study indicated that a leg assistance that is too large (e.g., at 6% of body weight) is suboptimal to encourage active participation of children with CP during treadmill training and may instead result in a decrease in leg muscle activity. Thus, results from this study suggest that physical therapists refrain from applying a large (e.g., 6% of body weight) leg assistance during treadmill training in order to encourage active participation of children with CP.

This study has several limitations. For instance, we did not test the retention of the improvements observed in step length and walking speed after 20 minutes of treadmill training with combined pelvis and leg assistance. We do not know how long these improvements will be retained, but we expect that long-term (e.g., 6 weeks) treadmill training using the 3D cable-driven robotic system may induce functional improvements in walking speed and endurance in children with CP. We do not know whether the magnitude, the timing, and the duration of force were optimal for each subject. Further studies are warranted to examine the effect of these parameters of the force perturbation on the kinematics of the pelvis and leg and EMG responses in children with CP. We did not collect the information about the level of spasticity of subjects who participated in this study. Thus, we do not know to what extent the level of spasticity had an impact on the gait performance of these subjects we tested [37]. We did not measure muscle activities during overground walking. In addition, the functional level of children with CP may also have an impact on improvements in walking speeds and step length after training. In this study, the subjects' GMFCS levels were I to III and all subjects could ambulate with/without assistive device. We do not know whether subjects with lower functional levels, such as GMFCS levels IV, and subjects who cannot ambulate will also have responses similar to those observed in this study. Subject's age may also impact the improvements in walking speeds and step length/step height after training. For instance, older healthy children may be faster to adapt gait than younger children [38]. However, we observed no correlation between the changes in step length

and height and the age of subjects ($p = 0.45$ for step length, $p = 0.74$ for step height), although we observed a trend that older children with CP had more improvements in overground walking speed after robotic treadmill training than younger children with CP, but this was not significant; that is, $p = 0.07$. Thus, other factors, such as functional level of subjects, might also have impact on these functional gains.

5. Conclusion

Improved weight shifting induced by a robotically applied pelvis assistance force during stance may facilitate stepping in children with CP during treadmill walking. In addition, applying a large leg swing assistance force (e.g., with the magnitude more than 6% of body weight) during treadmill training may reduce the active participation of children with CP. In particular, motor skills obtained during treadmill training may partially transfer to overground walking in children with CP. Results from this study may be used to develop a robotic gait training paradigm for improving walking function in children with CP through long-term robotic gait training in clinical settings.

Additional Points

Highlights. (1) Applying a pelvis assistance force may facilitate weight shifting and improve step height. (2) Applying leg assistance may improve step length but also may reduce muscle activation of the leg flexors. (3) Motor skills obtained during treadmill training may transfer to overground walking in children with CP.

Competing Interests

The authors declared no potential conflict of interests with respect to the research, authorship, and/or publication of this article.

Acknowledgments

This work is supported by NIDRR/RERC, H133E100007, and, in part, by the NIH, 1R21HD066261. The authors thank Ms. Jill Landry for her thoughtful comments.

References

[1] M. G. Rosen and J. C. Dickinson, "The incidence of cerebral palsy," *American Journal of Obstetrics & Gynecology*, vol. 167, no. 2, pp. 417–423, 1992.

[2] J. L. Hutton, P. O. D. Pharoah, and L. Rosenbloom, "Effects of cognitive, motor, and sensory disabilities on survival in cerebral palsy," *Archives of Disease in Childhood*, vol. 86, no. 2, pp. 84–89, 2002.

[3] P. O. D. Pharoah, T. Cooke, M. A. Johnson, R. King, and L. Mutch, "Epidemiology of cerebral palsy in England and Scotland, 1984–1989," *Archives of Disease in Childhood: Fetal and Neonatal Edition*, vol. 79, no. 1, pp. F21–F25, 1998.

[4] C. M. Duffy, A. E. Hill, A. P. Cosgrove, I. S. Corry, and H. K. Graham, "Energy consumption in children with spina bifida and cerebral palsy: A Comparative Study," *Developmental Medicine and Child Neurology*, vol. 38, no. 3, pp. 238–243, 1996.

[5] S. Wilmshurst, K. Ward, J. E. Adams, C. M. Langton, and M. Z. Mughal, "Mobility status and bone density in cerebral palsy," *Archives of Disease in Childhood*, vol. 75, no. 2, pp. 164–165, 1996.

[6] C. Lepage, L. Noreau, and P.-M. Bernard, "Association between characteristics of locomotion and accomplishment of life habits in children with cerebral palsy," *Physical Therapy*, vol. 78, no. 5, pp. 458–469, 1998.

[7] D. L. Damiano and S. L. DeJong, "A systematic review of the effectiveness of treadmill training and body weight support in pediatric rehabilitation," *Journal of Neurologic Physical Therapy*, vol. 33, no. 1, pp. 27–44, 2009.

[8] K. L. Willoughby, K. J. Dodd, and N. Shields, "A systematic review of the effectiveness of treadmill training for children with cerebral palsy," *Disability and Rehabilitation*, vol. 31, no. 24, pp. 1971–1979, 2009.

[9] K. J. Dodd and S. Foley, "Partial body-weight-supported treadmill training can improve walking in children with cerebral palsy: a clinical controlled trial," *Developmental Medicine and Child Neurology*, vol. 49, no. 2, pp. 101–105, 2007.

[10] K. L. Willoughby, K. J. Dodd, N. Shields, and S. Foley, "Efficacy of partial body weight-supported treadmill training compared with overground walking practice for children with cerebral palsy: a randomized controlled trial," *Archives of Physical Medicine and Rehabilitation*, vol. 91, no. 3, pp. 333–339, 2010.

[11] M. R. Schindl, C. Forstner, H. Kern, and S. Hesse, "Treadmill training with partial body weight support in nonambulatory patients with cerebral palsy," *Archives of Physical Medicine and Rehabilitation*, vol. 81, no. 3, pp. 301–306, 2000.

[12] A. Meyer-Heim, C. Ammann-Reiffer, A. Schmartz et al., "Improvement of walking abilities after robotic-assisted locomotion training in children with cerebral palsy," *Archives of Disease in Childhood*, vol. 94, no. 8, pp. 615–620, 2009.

[13] N. Smania, P. Bonetti, M. Gandolfi et al., "Improved gait after repetitive locomotor training in children with cerebral palsy," *American Journal of Physical Medicine and Rehabilitation*, vol. 90, no. 2, pp. 137–149, 2011.

[14] M. Druzbicki, W. Rusek, S. Snela et al., "Functional effects of robotic-assisted locomotor treadmill thearapy in children with cerebral palsy," *Journal of Rehabilitation Medicine*, vol. 45, no. 4, pp. 358–363, 2013.

[15] J. M. Hidler and A. E. Wall, "Alterations in muscle activation patterns during robotic-assisted walking," *Clinical Biomechanics*, vol. 20, no. 2, pp. 184–193, 2005.

[16] V. Inman, H. J. Ralston, and F. Todd, *Human Walking*, Williams and Wilkins, Baltimore, Md, USA, 1981.

[17] L. Ballaz, M. Robert, A. Parent, F. Prince, and M. Lemay, "Impaired visually guided weight-shifting ability in children with cerebral palsy," *Research in Developmental Disabilities*, vol. 35, no. 9, pp. 1970–1977, 2014.

[18] D. A. Winter, C. D. MacKinnon, G. K. Ruder, and C. Wieman, "An integrated EMG/biomechanical model of upper body balance and posture during human gait," *Progress in Brain Research*, vol. 97, pp. 359–367, 1993.

[19] D. J. Reinkensmeyer, O. Akoner, D. P. Ferris, and K. E. Gordon, "Slacking by the human motor system: computational models and implications for robotic orthoses," in *Proceedings of the Annual International Conference of the IEEE Engineering in Medicine and Biology Society*, pp. 2129–2132, 2009.

[20] R. Palisano, P. Rosenbaum, S. Walter, D. Russell, E. Wood, and B. Galuppi, "Development and reliability of a system to classify gross motor function in children with cerebral palsy,"

Developmental Medicine and Child Neurology, vol. 39, no. 4, pp. 214–223, 1997.

[21] M. Wu, T. G. Hornby, J. M. Landry, H. Roth, and B. D. Schmit, "A cable-driven locomotor training system for restoration of gait in human SCI," *Gait & Posture*, vol. 33, no. 2, pp. 256–260, 2011.

[22] F. Alton, L. Baldey, S. Caplan, and M. C. Morrissey, "A kinematic comparison of overground and treadmill walking," *Clinical Biomechanics*, vol. 13, no. 6, pp. 434–440, 1998.

[23] J. A. Zeni Jr., J. G. Richards, and J. S. Higginson, "Two simple methods for determining gait events during treadmill and overground walking using kinematic data," *Gait and Posture*, vol. 27, no. 4, pp. 710–714, 2008.

[24] S.-C. Yen, B. D. Schmit, J. M. Landry, H. Roth, and M. Wu, "Locomotor adaptation to resistance during treadmill training transfers to overground walking in human SCI," *Experimental Brain Research*, vol. 216, no. 3, pp. 473–482, 2012.

[25] H.-F. Liao, S.-F. Jeng, J.-S. Lai, C.-K. Cheng, and M.-H. Hu, "The relation between standing balance and walking function in children with spastic diplegic cerebral palsy," *Developmental Medicine and Child Neurology*, vol. 39, no. 2, pp. 106–112, 1997.

[26] C. Stackhouse, P. A. Shewokis, S. R. Pierce, B. Smith, J. McCarthy, and C. Tucker, "Gait initiation in children with cerebral palsy," *Gait and Posture*, vol. 26, no. 2, pp. 301–308, 2007.

[27] A. J. Dallmeijer, E. A. Rameckers, H. Houdijk, S. de Groot, V. A. Scholtes, and J. G. Becher, "Isometric muscle strength and mobility capacity in children with cerebral palsy," *Disability and Rehabilitation*, 2015.

[28] N. Thompson, J. Stebbins, M. Seniorou, and D. Newham, "Muscle strength and walking ability in Diplegic Cerebral Palsy: implications for assessment and management," *Gait & Posture*, vol. 33, no. 3, pp. 321–325, 2011.

[29] V. Dietz, R. Müller, and G. Colombo, "Locomotor activity in spinal man: significance of afferent input from joint and load receptors," *Brain*, vol. 125, no. 12, pp. 2626–2634, 2002.

[30] K. G. Pearson, J. E. Misiaszek, and K. Fouad, "Enhancement and resetting of locomotor activity by muscle afferents," *Annals of the New York Academy of Sciences*, vol. 860, pp. 203–215, 1998.

[31] P.-C. Kao, C. L. Lewis, and D. P. Ferris, "Short-term locomotor adaptation to a robotic ankle exoskeleton does not alter soleus Hoffmann reflex amplitude," *Journal of NeuroEngineering and Rehabilitation*, vol. 7, article 33, 2010.

[32] A. Kaelin-Lane, L. Sawaki, and L. G. Cohen, "Role of voluntary drive in encoding an elementary motor memory," *Journal of Neurophysiology*, vol. 93, no. 2, pp. 1099–1103, 2005.

[33] M. Lotze, C. Braun, N. Birbaumer, S. Anders, and L. G. Cohen, "Motor learning elicited by voluntary drive," *Brain*, vol. 126, no. 4, pp. 866–872, 2003.

[34] M. M. van der Krogt, L. H. Sloot, A. I. Buizer, and J. Harlaar, "Kinetic comparison of walking on a treadmill versus over ground in children with cerebral palsy," *Journal of Biomechanics*, vol. 48, no. 13, pp. 3586–3592, 2015.

[35] M. M. van der Krogt, L. H. Sloot, and J. Harlaar, "Overground versus self-paced treadmill walking in a virtual environment in children with cerebral palsy," *Gait and Posture*, vol. 40, no. 4, pp. 587–593, 2014.

[36] D. S. Reisman, R. Wityk, K. Silver, and A. J. Bastian, "Split-belt treadmill adaptation transfers to overground walking in persons poststroke," *Neurorehabilitation and Neural Repair*, vol. 23, no. 7, pp. 735–744, 2009.

[37] L. Bar-On, G. Molenaers, E. Aertbeliën, D. Monari, H. Feys, and K. Desloovere, "The relation between spasticity and muscle behavior during the swing phase of gait in children with cerebral palsy," *Research in Developmental Disabilities*, vol. 35, no. 12, pp. 3354–3364, 2014.

[38] E. V. L. Vasudevan, G. Torres-Oviedo, S. M. Morton, J. F. Yang, and A. J. Bastian, "Younger is not always better: development of locomotor adaptation from childhood to adulthood," *The Journal of Neuroscience*, vol. 31, no. 8, pp. 3055–3065, 2011.

Hindawi Publishing Corporation
Neural Plasticity
Volume 2016, Article ID 3489540, 5 pages
http://dx.doi.org/10.1155/2016/3489540

Research Article

Progressive FastICA Peel-Off and Convolution Kernel Compensation Demonstrate High Agreement for High Density Surface EMG Decomposition

Maoqi Chen,[1,2] Ales Holobar,[3] Xu Zhang,[1] and Ping Zhou[2,4,5]

[1] *Biomedical Engineering Program, University of Science and Technology of China, Hefei, China*
[2] *Guangdong Work Injury Rehabilitation Center, Guangzhou, China*
[3] *Faculty of Electrical Engineering and Computer Science, University of Maribor, Maribor, Slovenia*
[4] *Department of Physical Medicine and Rehabilitation, University of Texas Health Science Center at Houston, Houston, TX, USA*
[5] *TIRR Memorial Hermann Research Center, Houston, TX, USA*

Correspondence should be addressed to Ping Zhou; ping.zhou.1@uth.tmc.edu

Received 30 March 2016; Accepted 1 August 2016

Academic Editor: Brian C. Clark

Decomposition of electromyograms (EMG) is a key approach to investigating motor unit plasticity. Various signal processing techniques have been developed for high density surface EMG decomposition, among which the convolution kernel compensation (CKC) has achieved high decomposition yield with extensive validation. Very recently, a progressive FastICA peel-off (PFP) framework has also been developed for high density surface EMG decomposition. In this study, the CKC and PFP methods were independently applied to decompose the same sets of high density surface EMG signals. Across 91 trials of 64-channel surface EMG signals recorded from the first dorsal interosseous (FDI) muscle of 9 neurologically intact subjects, there were a total of 1477 motor units identified from the two methods, including 969 common motor units. On average, 10.6 ± 4.3 common motor units were identified from each trial, which showed a very high matching rate of 97.85 ± 1.85% in their discharge instants. The high degree of agreement of common motor units from the CKC and the PFP processing provides supportive evidence of the decomposition accuracy for both methods. The different motor units obtained from each method also suggest that combination of the two methods may have the potential to further increase the decomposition yield.

1. Introduction

The motor unit (which contains a spinal motor neuron, its axon, and the muscle fibers it innervates) is the final common pathway for neuromuscular control and provides a basic structure-function framework for neuromuscular system examination. Motor unit plasticity refers to motor unit adaptation or the ability of motor unit physical and functional changes as a result of activity, neurologic injury, age, rehabilitation training, and other factors. Motor unit plasticity can be assessed in different ways including by analyzing electromyogram (EMG) and muscle force output. Among various EMG signal processing methods, EMG decomposition provides a unique approach to observing the behavior of spinal motor neurons and its adaptation or alteration in human subjects by monitoring motor unit recruitment and firing rates.

EMG decomposition has been routinely performed with invasive needle electrodes [1–5]. The primary challenges of surface EMG decomposition arise from large number of active motor units, similar motor unit action potential (MUAP) waveforms for different motor units, and heavy MUAP superposition. With amplification technology developments, high density surface EMG relying on electrode arrays (comprised of up to hundreds of closely spaced tiny probes) has greatly advanced surface EMG decomposition. Various signal processing techniques using high density surface electrode arrays have been proposed for the decomposition purpose [6–9], among which the convolution kernel

compensation (CKC) has achieved distinguished yield for high density surface EMG decomposition [10–12]. The CKC approach has been tested using both simulated and experimental surface EMG signals [13–15], including the "two-source" validation with simultaneous intramuscular EMG recordings [13].

Very recently, we have developed a progressive FastICA peel-off (PFP) framework for high density surface EMG decomposition and tested this novel framework with both simulated and experimental surface EMG signals [16]. Given that both the CKC and PFP methods are designed for high density surface EMG recordings, they can be applied to the same set of data. This provides a strategy to assess the decomposition performance for both methods by comparing the discharge instants of the common motor units from independent CKC and PFP decompositions. The objective of the current study was to use such a strategy to compare the decomposition yield from the two different methods. We hypothesized that when processing the same set of high density surface EMG signals, high agreement can be achieved when comparing the decomposition results, thus providing supportive evidence of the decomposition performance for both CKC and PFP methods.

2. Methods

2.1. Data Model. Different from most of the other blind source separation technologies in surface EMG, both PFP and CKC use a shift-invariant model to describe multichannel surface EMG signal [10, 16], which allows MUAP shapes of a specific motor unit that vary in different channels but share the same discharge instants. Assuming N active motor units recorded by M surface electrodes: $\mathbf{x} = [x_1, x_2, \ldots, x_M]^T$, the signal on each channel can be described as

$$x_i(t) = \sum_{j=1}^{N} \sum_{\tau=0}^{L-1} a_{ij}(\tau)\, s_j(t-\tau) + n_i(t); \quad i = 1, 2, \ldots, M,\ t = 0, 1, \ldots, T. \tag{1}$$

In CKC, (1) can also be viewed as a convolutive linear time-invariant multiple-input multiple-output (MIMO) model, where $n_i(t)$ represents the additive white, zero-mean Gaussian noise in the ith channel. Each model input $s_j(t) = \sum_k \delta(t - T_j(k))$ is a sparse binary motor unit discharge pattern (i.e., its values are either 0 or 1) that indicates whether the jth motor unit discharges at a specific time t. $T_j(k)$ is the kth discharge time of the jth motor unit, whereas δ represents Dirac Delta function. The channel response a_{ij} stands for the waveform of the jth motor unit in the ith channel; L is the length of the waveform. It is assumed that $T_j(k+1) - T_j(k) > L$ for each k.

The model in (1) can be rewritten in matrix form:

$$\mathbf{x}(t) = \mathbf{A}\bar{\mathbf{s}}(t) + \mathbf{n}(t), \tag{2}$$

where $\bar{\mathbf{s}}(t) = [s_1(t), s_1(t-1), \ldots, s_1(t-L+1), \ldots, s_N(t), \ldots, s_N(t-L+1)]^T$ stands for an extended form of a sample vector $\mathbf{s}(t)$ and $\mathbf{n}(t) = [n_1(t), n_2(t), \ldots, n_M(t)]^T$ is a noise vector. The unknown matrix $\mathbf{A}$ comprises all the MUAPs as detected by the different surface electrodes (for details, please refer to [10, 16]).

2.2. Introduction of CKC and PFP. The CKC method first blindly estimates the cross-correlation vector between the discharge pattern of one motor unit and the EMG measurements. Then the unknown mixing matrix $\mathbf{A}$ (i.e., the convolution kernel) is partially compensated by calculating an estimation of the discharge patterns of this motor unit using the estimated cross-correlation vector and the correlation matrix of the EMG signal. As the convolution kernel is compensated gradually a number of motor units can be estimated. More details on CKC processing can be found in [10].

The PFP framework can be viewed as a process of progressively expanding the set of spike trains. In the framework, FastICA is used to estimate motor unit spike trains. A "peel-off" procedure is employed to estimate the MUAPs of all the identified motor units and subtract them from the original signal. Such a procedure mitigates the effect of the already identified motor units on the FastICA convergence, so more motor units can emerge when processing the residual signal. In order to ensure the reliability of the decomposition, a constrained FastICA is applied to assess the newly extracted discharge patterns and correct possible erroneous or missed spikes. These features work together to promote the decomposition yield. More details on PFP processing can be found in [16].

2.3. Data Description. The surface EMG signals used for testing the proposed framework were acquired from the first dorsal interosseous (FDI) muscle of nine healthy subjects. The procedures were approved by the local Institutional Review Board. All the subjects gave their written consent before the experiment. Subjects were seated upright in a mobile Biodex chair (Biodex, Shirley, NY). A standard 6 degrees of freedom load cell (ATI Inc., Apex, NC) setup was used to accurately record the isometric contraction force of the FDI muscle during index finger abduction. Standard procedures were followed to minimize spurious force contributions from unrecorded muscles as described in [17]. Surface EMG signals were recorded using a flexible two-dimensional 64-channel (8 × 8, individual recording probe 1.2 mm in diameter, center-to-center distance of 4 mm) surface electrode array (TMS International BV, Netherlands). The maximum voluntary contraction (MVC) was first measured; after that, each subject was asked to generate an isometric contraction force of the FDI muscle at different contraction levels. The subject was asked to maintain the force as stable as possible for at least 3 s (preferably more than 5 s). The actual percent MVC for each contraction was calculated afterwards by normalizing the force measurement (averaged from the stable force period) to each subject's MVC. A Refa128 amplifier (TMS International BV, Netherlands) was used to record surface EMG signals. The signals were sampled at 2 kHz per channel, with a bandpass filter setting at 10–500 Hz. Totally 91 experimental surface EMG signals (35 ± 27% MVC, range: ~1% to ~100% MVC) were decomposed by PFP and CKC, respectively. The two decomposition processes

were independent of each other and they were operated by two different operators. The decomposition by CKC was first processed by an automatic program, and a manual motor unit selecting process was used to ensure the reliability of the results. In particular, recently introduced pulse-to-noise ratio (PNR) metrics [18] has been employed to assess the accuracy of motor unit identification and only the motor units with PNR $\geq$ 30 dB (sensitivity in identification of motor unit discharges $\geq$ 90%) were kept whereas all the other motor units were discarded. For the PFP, manual monitoring was used to guarantee the reliability when using constrained FastICA to assess the identified spike trains.

2.4. Data Analysis. The matching rate (MR) was calculated to precisely measure the matching degree of the commonly identified motor units from the two decomposition methods. For each common motor unit, the matching rate between two decompositions was calculated as

$$\mathrm{MR} = \frac{2 \cdot N_{\mathrm{COM}}}{N_{\mathrm{CKC}} + N_{\mathrm{PFP}}} \cdot 100\%, \tag{3}$$

where N_{COM} stands for the number of discharges of a motor unit that were identified by both decomposition techniques (i.e., the number of corresponding discharges within time tolerance of $\pm$1 ms). N_{CKC} and N_{PFP} are the total number of discharges which were identified by CKC and PFP, respectively. Note that if either of the two spike trains is considered as the "standard" spike train, MR is actually an F1-score measure [19]. In this study we consider a motor unit as a common one only when MR between the two decomposition methods is higher than 90%.

A cross-correlation function method introduced in [16] was used to facilitate the identification of coupling discharge spike trains from the two decomposition algorithms and calculate MR. The following parameters were calculated:

$$\begin{aligned}
\rho_i^* &= \max_j \left\{ \max_t \left\{ \frac{R_{s_{C,i}, s_{P,j}}(t)}{\sqrt{R_{s_{C,i}, s_{C,i}}(0) \cdot R_{s_{P,j}, s_{P,j}}(0)}} \right\} \right\}, \\
j_i^* &= \arg\max_j \left\{ \max_t \left\{ \frac{R_{s_{C,i}, s_{P,j}}(t)}{\sqrt{R_{s_{C,i}, s_{C,i}}(0) \cdot R_{s_{P,j}, s_{P,j}}(0)}} \right\} \right\}, \\
t_i^* &= \arg\max_t \left\{ \frac{R_{s_{C,i}, s_{P,j_i^*}}(t)}{\sqrt{R_{s_{C,i}, s_{C,i}}(0) \cdot R_{s_{P,j_i^*}, s_{P,j_i^*}}(0)}} \right\},
\end{aligned} \tag{4}$$

where $R_{\cdot,\cdot}(t)$ represents cross-correlation function, $s_{C,i}$ stands for the ith spike train identified from CKC, and $s_{P,j}$ is the jth spike train identified from PFP. ρ_i^* is the maximum cross-correlation coefficient between $s_{C,i}$ and $s_{P,j}$. If $\rho_i^* \geq 0.3$, we accepted potential existence of a spike train coupling between $s_{C,i}$ and $s_{P,j}$. For the identified "coupling", j_i^* was used as the indicator of the corresponding spike train and the value of MR was used to determine whether the two spike trains really correspond or not. For this purpose, the corresponding delay t_i^* has been estimated and $s_{C,i}$ and $s_{P,j}$ aligned in time. After such a time shift, MR has been calculated as defined in (3).

3. Results

Figure 1 shows an example of discharge instants for motor units identified from an isometric contraction at the level of approximately 18% MVC. The red spike trains represent the results obtained by the CKC, and the blue ones are the results obtained by the PFP. In this example, 19 common motor units were identified, whose discharge patterns are aligned together in the figure. Black dots represent few locations where the two methods generated inconsistent discharge instants. In addition, each method also identified two different motor units, respectively, as shown in the figure.

Ninety-one trials of 9 subjects were processed with signal duration ranged from 3.2 to 11.2 s (7.9 $\pm$ 1.8 s), from which the matching rate was calculated. There were a total of 1477 motor units identified from the two methods, including 969 common motor units. On average, 10.6 $\pm$ 4.3 common motor units were identified from each trial, which showed a very high matching rate of 97.85 $\pm$ 1.85%. We did not observe a clear dependence of the number of common motor units and the matching rate on the contraction level. In addition to the common motor units which accounted for the majority of the decomposition yield, the two methods also identified a relatively small number of different motor units, such as those demonstrated in Figure 1, where 4 different motor units were identified from the two methods. Across the 91 trials, there were 5.6 $\pm$ 2.8 different motor units identified per trial from the two methods.

4. Discussion

Both CKC and PFP methods are designed for high density surface EMG decomposition, using blind source separation approaches based on a sparse shift-invariant model. The sparsity assumption for the motor unit discharge patterns ensures the algorithm can obtain sufficient information to separate the motor units. Unlike most of other decomposition methods primarily relying on MUAP template matching, the two algorithms focus on the underlying discharge patterns (i.e., the sparse components) in the EMG signal. The key iterative rules of the two algorithms also have a similar structure. Because of these similarities, the two methods achieved high agreement for high density surface EMG decomposition, as demonstrated in this study.

When comparing the decomposition yield from CKC and PFP methods, we only focused on the motor unit discharge instants, from which the MUAP waveforms can be estimated using spike triggered averaging (actually, during the PFP decomposition, the MUAP waveforms already emerge). Thus, if high agreement can be achieved in motor unit discharge instants between the two methods, high agreement in MUAP waveforms can also be expected.

In addition to the majority of common motor units, the two methods also identified a relatively small portion of different motor units. This might be due to differences between the PFP and CKC methods, such as in cost function and motor unit searching strategy (in dealing with the local convergence problem in gradient-based algorithm). For example, the CKC acts on original signal and each time the initial value is properly selected (at motor unit discharge

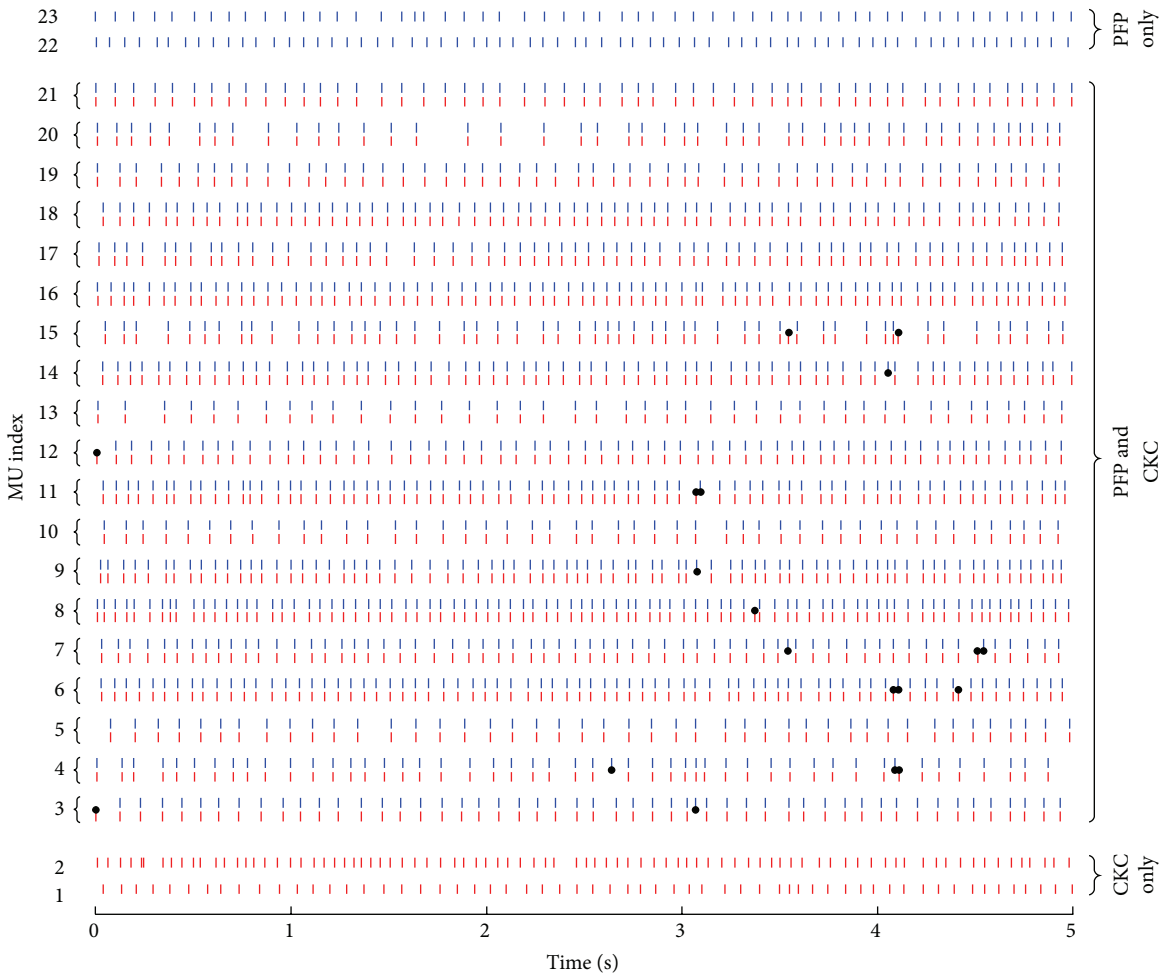

Figure 1: An example of discharge instants for motor units identified from an isometric contraction at ~18% MVC. The red spike trains represent the results obtained by the CKC, and the blue ones represent the results obtained by the PFP. Black dots represent the locations where the two methods generated inconsistent discharge instants.

instants) to ensure that the algorithm can converge to reliable results. Furthermore, the CKC adopts a probabilistic strategy, by blindly running the algorithm multiple times (e.g., 100 runs) and Gram-Schmidt orthogonalization of separation vectors to allow the algorithm to have sufficient probability to find those difficult convergent solutions and finally integrate all the results. Conversely, PFP adopts a different deflation strategy. When new solutions are obtained, the algorithm uses the information from discharge patterns of the already identified or validated motor units to estimate their MUAP trains and subtract them from the original signal and then applies FastICA to the residual signal to search other motor units. Such a deflation strategy mitigates the effect of the already identified motor units on the FastICA convergence, so extra motor units can emerge. However, it may lead to a cumulative error problem; that is, the early estimation error will be accumulated and magnified in the later process (this is why the constrained FastICA is used to ensure the accuracy of the identified spike trains).

Given that the CKC based surface EMG decomposition has been extensively validated in different situations [13–15], the high degree of agreement of common motor units between the decomposition results to some extent supports the accuracy of the PFP decomposition (and the accuracy of the CKC decomposition as well). To further confirm the accuracy of the PFP decomposition, simultaneous intramuscular EMG recording is necessary so a two-source validation can be performed.

Finally, it is noteworthy that some components of one method can be combined with the other. For example, the PFP can use the probability strategy (as used in the CKC) during each iteration to achieve more solutions. The CKC can adopt the MUAP estimation and the motor unit spike train validation mechanism similar to the constrained FastICA. Such a combination of CKC and PFP methods needs further investigation and might have a potential to increase the decomposition yield.

Competing Interests

The authors declare that they have no competing interests.

Acknowledgments

This study was supported by the National Natural Science Foundation of China under Grant 81271658, the National Institutes of Health of the US Department of Health and Human Services under Grant R01NS080839, and Slovenian Research Agency (Project J2-7357).

References

[1] D. Stashuk, "EMG signal decomposition: how can it be accomplished and used?" *Journal of Electromyography and Kinesiology*, vol. 11, no. 3, pp. 151–173, 2001.

[2] H. Parsaei, D. W. Stashuk, S. Rasheed, C. Farkas, and A. Hamilton-Wright, "Intramuscular EMG signal decomposition," *Critical Reviews in Biomedical Engineering*, vol. 38, no. 5, pp. 435–465, 2010.

[3] K. C. McGill, Z. C. Lateva, and H. R. Marateb, "EMGLAB: an interactive EMG decomposition program," *Journal of Neuroscience Methods*, vol. 149, no. 2, pp. 121–133, 2005.

[4] C. J. De Luca, "Decomposition of the EMG signal into constituent motor unit action potentials," *Muscle and Nerve*, vol. 18, no. 12, pp. 1492–1494, 1995.

[5] S. H. Nawab, R. P. Wotiz, and C. J. De Luca, "Decomposition of indwelling EMG signals," *Journal of Applied Physiology*, vol. 105, no. 2, pp. 700–710, 2008.

[6] B. U. Kleine, J. P. van Dijk, B. G. Lapatki, M. J. Zwarts, and D. F. Stegeman, "Using two-dimensional spatial information in decomposition of surface EMG signals," *Journal of Electromyography and Kinesiology*, vol. 17, no. 5, pp. 535–548, 2007.

[7] I. Gligorijević, J. P. van Dijk, B. Mijović, S. van Huffel, J. H. Blok, and M. De Vos, "A new and fast approach towards sEMG decomposition," *Medical and Biological Engineering and Computing*, vol. 51, no. 5, pp. 593–605, 2013.

[8] G. A. Garcia, R. Okuno, and K. Azakawa, "A decomposition algorithm for surface electrode-array electromyogram," *IEEE Engineering in Medicine and Biology Magazine*, vol. 24, no. 4, pp. 63–72, 2005.

[9] F. J. Theis and G. A. García, "On the use of sparse signal decomposition in the analysis of multi-channel surface electromyograms," *Signal Processing*, vol. 86, no. 3, pp. 603–623, 2006.

[10] A. Holobar and D. Zazula, "Multichannel blind source separation using convolution kernel compensation," *IEEE Transactions on Signal Processing*, vol. 55, no. 9, pp. 4487–4496, 2007.

[11] A. Holobar and D. Zazula, "Correlation-based decomposition of surface electromyograms at low contraction forces," *Medical and Biological Engineering and Computing*, vol. 42, no. 4, pp. 487–495, 2004.

[12] A. Holobar, D. Farina, M. Gazzoni, R. Merletti, and D. Zazula, "Estimating motor unit discharge patterns from high-density surface electromyogram," *Clinical Neurophysiology*, vol. 120, no. 3, pp. 551–562, 2009.

[13] H. R. Marateb, K. C. McGill, A. Holobar, Z. C. Lateva, M. Mansourian, and R. Merletti, "Accuracy assessment of CKC high-density surface EMG decomposition in biceps femoris muscle," *Journal of Neural Engineering*, vol. 8, no. 6, Article ID 066002, 2011.

[14] A. Holobar, M. A. Minetto, A. Botter, F. Negro, and D. Farina, "Experimental analysis of accuracy in the identification of motor unit spike trains from high-density surface EMG," *IEEE Transactions on Neural Systems and Rehabilitation Engineering*, vol. 18, no. 3, pp. 221–229, 2010.

[15] R. Merletti, A. Holobar, and D. Farina, "Analysis of motor units with high-density surface electromyography," *Journal of Electromyography and Kinesiology*, vol. 18, no. 6, pp. 879–890, 2008.

[16] M. Chen and P. Zhou, "A novel framework based on FastICA for high density surface EMG decomposition," *IEEE Transactions on Neural Systems and Rehabilitation Engineering*, vol. 24, no. 1, pp. 117–127, 2016.

[17] X. Li, A. Suresh, P. Zhou, and W. Z. Rymer, "Alterations in the peak amplitude distribution of the surface electromyogram poststroke," *IEEE Transactions on Biomedical Engineering*, vol. 60, no. 3, pp. 845–852, 2013.

[18] A. Holobar, M. A. Minetto, and D. Farina, "Accurate identification of motor unit discharge patterns from high-density surface EMG and validation with a novel signal-based performance metric," *Journal of Neural Engineering*, vol. 11, no. 1, Article ID 016008, 2014.

[19] C. Goutte and E. Gaussier, "A probabilistic interpretation of precision, recall and *F*-score, with implication for evaluation," in *Advances in Information Retrieval*, D. E. Losada and J. M. Fernández-Luna, Eds., vol. 3408 of *Lecture Notes in Computer Science*, pp. 345–359, Springer, Berlin, Germany, 2005.

Hindawi Publishing Corporation
Neural Plasticity
Volume 2016, Article ID 8628039, 11 pages
http://dx.doi.org/10.1155/2016/8628039

Research Article

Mirror Visual Feedback Training Improves Intermanual Transfer in a Sport-Specific Task: A Comparison between Different Skill Levels

Fabian Steinberg, Nils Henrik Pixa, and Michael Doppelmayr

Institute of Sport Science, Department of Sport Psychology, Johannes Gutenberg University Mainz, Mainz, Germany

Correspondence should be addressed to Fabian Steinberg; fabian.steinberg@uni-mainz.de

Received 26 April 2016; Revised 21 July 2016; Accepted 31 July 2016

Academic Editor: Brian C. Clark

Mirror training therapy is a promising tool to initiate neural plasticity and facilitate the recovery process of motor skills after diseases such as stroke or hemiparesis by improving the intermanual transfer of fine motor skills in healthy people as well as in patients. This study evaluated whether these augmented performance improvements by mirror visual feedback (MVF) could be used for learning a sport-specific skill and if the effects are modulated by skill level. A sample of 39 young, healthy, and experienced basketball and handball players and 41 novices performed a stationary basketball dribble task at a mirror box in a standing position and received either MVF or direct feedback. After four training days using only the right hand, performance of both hands improved from pre- to posttest measurements. Only the left hand (untrained) performance of the experienced participants receiving MVF was more pronounced than for the control group. This indicates that intermanual motor transfer can be improved by MVF in a sport-specific task. However, this effect cannot be generalized to motor learning per se since it is modulated by individuals' skill level, a factor that might be considered in mirror therapy research.

1. Introduction

It is well known that training both limbs facilitates performance through intermanual transfer from one limb to the other. For example, the training of a specific skill with one hand can improve the performance of the other hand [1–3]. These well documented transfer effects, originally handled under the term "cross-education," have been described for a range of fine motor skills [1, 2], sport-specific skills (e.g., [4, 5]), and muscle strength transfer [6, 7].

Several models have been put forward to explain empirical observations of intermanual transfer effects. Those theories are primarily based on studies that investigated transfer effects by the use of behavioral, neuroimaging, or brain modulation methods [6–11]. According to a recent review by Ruddy and Carson (2013) [11], two different theoretical models can be distinguished: the bilateral access (also known as the callosal access) model and the cross-activation model. The bilateral access model supports the idea that motor engrams, evolved after unilateral training in the dominant hemisphere, can be accessed by the opposite hemisphere via the corpus callosum, which leads to increased task performance of the contralateral limb [12]. The cross-activation model is supported by observations that unilateral motor executions evoke increased neuronal excitability of both the contra- and ipsilateral motor cortices, leading to neural plasticity in *both* hemispheres (cf. [8]). However, the underlying neurophysiology of bilateral transfer effects remains unclear. One possible mechanism was summarized from a recent review on neuroimaging studies in which it is argued that the mirror neural system (MNS) could be involved during bilateral transfer [7]. The MNS has been identified as the neuroanatomical basis that matches observed actions with an internal motor representation of the observed action such that the respective neuronal structures are active when movements are observed (own or others), imitated, imagined, or executed [13, 14]. Zult et al. (2014) [7] argued that imitation plays a role in motor learning during intermanual transfer paradigms, which is

supported by studies observing increased activations of brain areas during cross-education that overlap with areas containing mirror neurons [15–17].

Given the positive possibilities of intermanual transfer effects, in the recent past, interest emerged regarding a method that facilitates motor learning and intermanual transfer in the clinical context, known as mirror therapy [18]. This therapy uses a mirror that is placed in the midsagittal plane of a patient in order to provide visual feedback of an intact hand that is performing a motor task while the performer directs their gaze and attention onto the mirror. Simultaneously, the nontraining hand is hidden behind the mirror in a similar position. This superimposition provides an online visual illusion as if the contralateral nontraining limb (and impaired limb in patients) is moving as efficiently as the training limb. This therapy was originally used to treat phantom limb pain [19] and is currently thought to be supportive in patients with hemiparesis [20] and complex regional pain syndrome [21] and in stroke [22, 23]. The advantage of such a method is especially valuable for patients whose control of one hand is impaired or immobilized since in motor recovery programs the additional mirror visual feedback (MVF) can facilitate the recovery process [20]. In addition, the use of this novel technique has been repeatedly demonstrated to facilitate motor learning not only in patients practicing bilaterally, but also in healthy people performing unilateral motor training. Intermanual transfer was more pronounced by the use of MVF compared to other feedback modalities [24–26].

Those studies indicate that augmented visual feedback through a mirror facilitates intermanual transfer effects, while the underlying mechanisms remain unclear. Based on neuroimaging data, a recent review by Deconinck et al. (2015) [20] found that MVF-related neural activation patterns have substantial overlap with regions related to attention and action monitoring processes, both of which are strongly related to motor learning. Additionally and in line with another review on cross-education, increased neural activity of ipsilateral brain areas that are associated with the mirror neural system was reported in mirror training [6]. Since motor execution that is concurrently observed through a mirror (i.e., providing an illusion of movement of the contralateral hand, although not active) is a special kind of movement observation, it appears to be reasonable that the MNS could be involved [6, 7]. Therefore, the involvement of the MNS-related brain areas not only is proposed to play a role in intermanual transfer but also might be synergistically involved in the augmented transfer effects supported by visual feedback through a mirror [6].

So far, most studies concerning mirror-feedback are solely based on fine motor skills, so it remains unclear whether facilitation of intermanual transfer through MVF might also occur in tasks that require more complex (and sport-specific) motor abilities. It has been repeatedly claimed that the impact of augmented feedback methods depends on task complexity and skill level [27, 28], but MVF studies did not consider whether skill level or task complexity might influence the beneficial performance gains through MVF (i.e., whether performance gains differ in terms of experienced versus unexperienced or high versus low level of expertise in a complex motor skill). In sport science and other fields of expertise research, it is well established that skill level modulates motor execution [29–31], neural activity of the action observation network [32–34], action anticipation [35], focus of attention [36], and gaze behavior [37]. Moreover, experts MNS activation is differently with higher involvement of the MNS when observed movements are familiar compared to nonfamiliar (i.e., are part of their existing motor repertoire) [38, 39].

Therefore, the present study explores whether MVF may have beneficial effects on intermanual transfer in a sport-specific task and if it is modulated by skill level. To this end, we adapted the mirror therapy test apparatus and test protocol as reported by Hamzei et al. (2012) in order to allow participants of high and low proficiency in ball dribbling to perform a dribble task while they received either visual feedback of the trained hand through a mirror (i.e., visual illusion of the left hand) or direct feedback of the trained hand. Based on the existing literature on intermanual transfer effects, for which MVF has been shown to be supportive, we hypothesized that in a more complex sport-specific task we will find intermanual transfer effects that will be increased through MVF. More specifically, due to well-known novice-expert differences and the differential activation of the MNS, we hypothesized that athletes with experience in ball dribbling will profit more than novices from MVF.

2. Methods

2.1. Participants. Initially 84 right handed participants took part in this study, but four of them were not able to complete the whole training program due to injury or other engagements. The remaining 80 participants were 24.87 ± 4.14 years old (41 females). Of the sample, 39 participants (20 females) had experience in dribbling as evidenced by actively playing either handball or basketball in a club including participation in competitions. We recruited the sample from four teams within three different German sport clubs that participated in divisions that can be classified in the midrange of the amateur level. Two teams (one female team) were two levels below the professional division and the other two (one female team) were three divisions below the professional divisions of the German division system. This expertise level could be expressed in numbers when considering that the highest division ("1. Bundesliga") is one and the lowest eight for male and seven for female. Males had a mean expertise level of 3.9 ± 0.87, females had a mean level of 4.1 ± 0.55, and the whole sample had a mean level of 4.05 ± 0.71. The other forty-one participants (21 females) had no competition or sport club experience in sports requiring dribbling skills. However, novice participants were recruited from physical education students who are required to have at least minimal ball dribbling skills to fulfill course objectives. Given our test design (see below), minimal ball dribbling skills were needed to perform the task properly. Prior to the experiment, all participants were fully informed of the purpose of the study. The test protocol was in accordance with the Helsinki declaration and approved by the ethics committee of the Deutsche Gesellschaft für Psychologie.

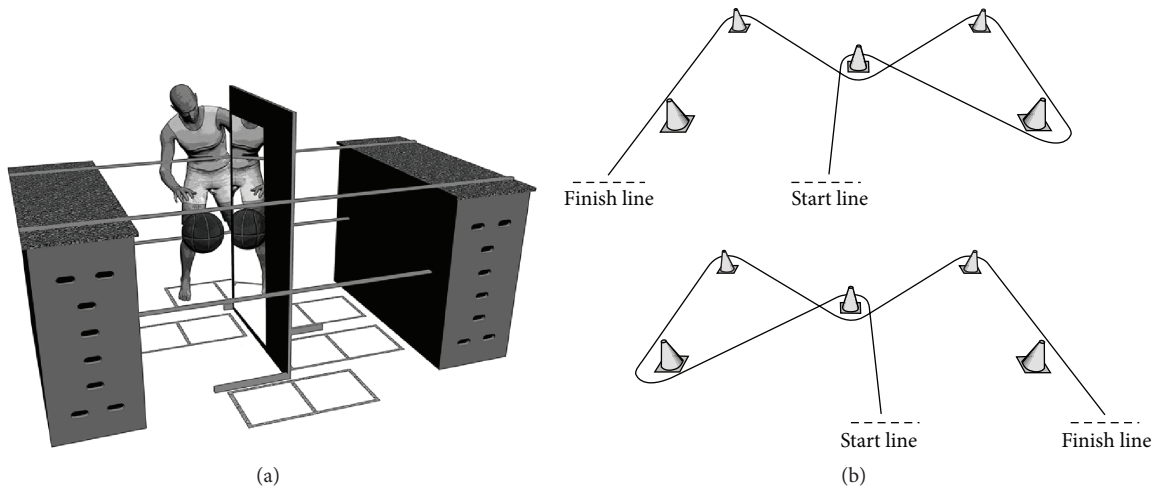

Figure 1: (a) The mirror box apparatus with the mirror being in the midsagittal plane of a participant; details in the text. (b) The slalom course setup for right hand dribbling (bottom) and for left hand dribbling (top).

2.2. Mirror Training and Slalom Course Setup. The mirror apparatus used in the present study was based on a typical mirror therapy box (e.g., Hamzei et al. 2012) [26] and was modified for the purpose of the present study. As depicted in Figure 1(a), a 120×50 cm mirror was attached to a 1.70-meter wooden wall that was placed in the middle of the construction. In front of the mirror, two marked-out fields indicated the positioning of the feet, guaranteeing that the mirror was in the midsagittal line of the participant. To the left and right of the mirror, two 34×34 cm fields made of wooden beams served as the target fields in which a basketball could be dribbled. These fields were designed to allow three different task executions: dribbling with the right hand with visual feedback through a mirror, dribbling with the right hand without MVF (i.e., direct feedback), and dribbling with the left hand without MVF. To ensure standardized task execution and comparability between individuals, a predefined range of hand and arm motions during dribbling was defined by two ropes that were stretched between two vaulting boxes at 80 cm and 130 cm.

In addition to the mirror task, participants had to perform a dribbling slalom course (Figure 1(b)), which served as a transfer task. This course was constructed to allow participants to dribble through pylons, including five directional changes with the starting line also being the finish line. This course was constructed once for right hand dribbling (Figure 1(b), bottom) and once in a mirrored fashion for left hand dribbling (Figure 1(b), top).

2.3. Motor Tasks. Participants had to perform a stationary dribble task at the mirror box construction and a dynamic slalom dribble task at the slalom course. In the stationary dribble task, participants assumed a standing position with their feet placed in the respective positions (see Figure 1) and were asked to dribble a basketball (sized appropriately for their gender) with either the right or the left hand as often as possible in the two target fields in a predefined sequence, which was as follows: they were free to begin in either the left or the right field by dribbling two times in the respective field, then two times in the neighboring field, then going back again, and so on. In case of a dribbling error, which occurred when the basketball touched the wooden beams, they were instructed to proceed with dribbling and ignore the error if possible. However, in the case of a complete loss of ball control, they could take a new basketball from a box, which was directly positioned beside them, and proceed with dribbling in the respective field where the error happened. Participants' resting hand had to be positioned behind the wall at the same height and position as the other hand. The task lasted 45 seconds, and successful dribbling was defined as the ball being dribbled in a field in the instructed sequence. They were not allowed to hold the ball or to bring the hand completely under the ball. In the slalom dribbling course, the task was to dribble the ball using only one hand while running as fast as possible through the cones that were placed on the floor as depicted in Figure 1.

2.4. Procedure. The experiment was executed in a sports hall. After arriving and receiving instruction as to the purpose of the study, participants were pseudorandomly assigned to either the mirror visual feedback (MVF) or the control (direct feedback) group. This pseudorandomization was separated into novice and experienced (according to dribbling expertise) participants, resulting in two groups (41 novice versus 39 experienced). In the expertise group 19 participants were assigned to the MVF and 20 to the control condition, while in the novice group 20 went to MVF and 21 to the control condition. Each participant began the experiment after an individual warm-up with the dynamic slalom dribbling task. For task familiarization, verbal instructions for the slalom course were provided first and then each participant was allowed to complete the slalom course two times in a self-paced manner. In a counterbalanced order within each group, participants started the first trial with either right hand or left hand dribbling while the time for course completion was recorded

via a handheld stop watch. Three trials were performed with each hand.

Subsequently, participants were instructed to the stationary dribbling task at the mirror box. For task familiarization, participants were allowed to perform the task three times (45 sec) with rest breaks of 45 sec between trials for each hand. After familiarization, baseline measurements (pretest) included three trials of 45 sec with rest breaks of 45 sec between trials for each hand performed in a counterbalanced order with the right and the left hand.

In the first training block, which followed the baseline measurements, participants performed 10 trials of 45 sec of the motor task with the right hand with rest breaks of 45 sec between each trial. In the control training condition, participants learned the motor task in the same way as was requested in the baseline measurements, with direct visual feedback of the right hand while dribbling the basketball. In the MVF training group, participants were requested to direct their gaze and attention onto the mirror while performing the motor task so that the mirror provided an illusion as if the left hand was dribbling the ball. In all, each participant performed four training blocks with the right hand as described for the first training session. The training period as well as posttest measurements were completed in a two-week interval, and only one training block was allowed per day. After the training blocks, posttest measurements were conducted on a separate day in the same way as the baseline measurements.

2.5. Data Analysis. Pre- and posttest trials were recorded with an HD video camera directed at the target fields for subsequent analysis of scores and errors. An investigator blinded to expertise level analyzed the video material and assigned scores as defined above (i.e., one point was given for successfully dribbling in a target field). Moreover, the error score was counted as well, such as a loss of ball control. Thus, dribbling scores (further called "dribbling performance") for the three trials with their respective errors (further called "dribbling error") could be analyzed for the pre- and the posttest and for each hand. Likewise, the three scores of the three trials were measured for the pre- and posttests of the slalom course (further called "slalom performance") for both hands. Statistical analysis presented here was performed by taking the mean values of the three pre- and posttest trials. We took the mean values since we could not find any statistical differences when we performed the same analysis using the median score or the best score.

2.6. Statistical Analysis. Shapiro-Wilks tests were used to check all variables for normal distribution; all scores of the stationary dribbling at the mirror box (i.e., dribbling performance) were normally distributed. However, error scores of the dribbling task at the mirror box (i.e., dribbling error) as well as times for the slalom course (i.e., slalom performance) were not normally distributed. Thus, ANOVAs and t-tests were used for normally distributed variables (i.e., only for the dribbling performance at the mirror test setup for the right and the left hand), while for the others Mann-Whitney U test were computed (see below). Before result presentation of the training effects, a section (statistics on baseline performance) is included to check for baseline differences between conditions (MVF versus control) by calculating independent t-tests or U-tests for each variable separated for each expertise level (i.e., within the experienced and within the novice group). Moreover, we compared the baseline scores of our parameters (dribbling performance, dribbling error, and slalom performance) by independent t-tests or U-test between experienced and novice group to check if pretest values mirror our group delineation (i.e., novices versus experienced participants). Effect sizes of t-test were estimated as Cohen's d, where $d > 0.2$ indicates a small effect, $d > 0.05$ a medium effect, and $d > 0.8$ a large effect [40]. Effect sizes based on z-scores computed by the U-tests were estimated by Pearson's correlation coefficients, where $r > 0.1$ indicates a small effect, $r > 0.3$ a medium effect, and $r > 0.5$ a large effect [40].

Three-way ANOVAs with repeated measures "TIME" (Pre/Post) on the between-factor "CONDITION" (MVF/Control) and "EXPERTISE" (Novice/Experienced) were calculated separately for left and right hand performance to observe whether the feedback modalities (MVF versus active) influence a different performance improvement in the two expertise groups. Wherever sphericity was violated, Greenhouse-Geisser adjusted values were reported and p values below the 5% thresholds were considered statistically significant. Effect sizes of ANOVAs were estimated as partial eta-squares (η_p^2), where $\eta_p^2 > 0.01$ indicates a small, $\eta_p^2 > 0.06$ a medium, and $\eta_p^2 > 0.14$ a large effect [40], and these were reported whenever significance dropped below 5%.

Finally, for the not-normally distributed variables (dribbling error and slalom performance), an index for performance changes was calculated by subtracting post- from prevalues. For these variables, between-subject performances changes between the MVF and control groups were analyzed by Mann-Whitney U tests separately for novice and experienced participants.

2.7. Statistics on Baseline Performance. Since in the following analysis several between-subject analyses were performed and body height might influence dribbling behavior at a test setup not adjusted to body height, we calculated ANOVAs with the between-factor CONDITION and EXPERTISE for body height to determine whether experimental groups systematically differ in these variables. However, no effects emerged (all $p > 0.05$). t-tests (for dribbling performance) and U-tests (for dribbling error and slalom performance) for baseline (pretest) scores revealed that, for all three test variables (i.e., left and right hand dribbling performance, dribbling error, and slalom performance), no significant difference between control and MVF (all $p > 0.05$) within the novice group or between control and MVF of the experienced group (all $p > 0.05$) emerged. This indicates that the control groups compared to the MVF groups did not start at different performance levels and thus different learning rates cannot be attributed to different baseline values.

We additionally tested whether our a priori group delineation criteria (active engagement in basketball or handball competition) were able to separate experienced from novice

Table 1: Performance scores for all test variables for experts and novices independent of condition. Shown are mean values along standard deviations.

Expertise level	Task/variable	Pretest		Posttest	
		Right hand	Left hand	Right hand	Left hand
Novice	Dribbling performance	85.52 ± 18.76	68.78 ± 16.63	104.33 ± 23.31	84.83 ± 20.98
Experienced		105.32 ± 15.39	95.60 ± 14.67	123.42 ± 18.07	107.15 ± 15.87
Novice	Dribbling error	2.52 ± 1.79	4.59 ± 2.74	1.23 ± 1.11	3.09 ± 2.30
Experienced		1.66 ± 1.84	2.99 ± 2.46	0.80 ± 0.93	1.93 ± 1.39
Novice	Slalom performance (sec)	9.09 ± 1.52	9.58 ± 1.69	8.80 ± 1.45	9.04 ± 1.57
Experienced		8.47 ± 1.01	8.61 ± 1.13	8.01 ± 0.87	8.11 ± 0.86

participants, that is, if it is mirrored in different baseline measures of our three outcome variables: Table 1 (values separated by the factor EXPERTISE) depicts the values of baseline (pretest) left and right hand performance from which one can see that left hand ($t(78) = 7.63$; $p < 0.001$; $d = 1.70$) as well as right hand ($t(78) = 5.14$; $p < 0.001$; $d = 1.15$) dribbling performance of the experienced participants was significantly higher than that of novices with high effect sizes. U-test revealed that (not-normally distributed variables) this pattern was mirrored in different dribbling error scores in the left hand ($z = -2.82$; $p < 0.01$; $r = -0.31$) and right hand ($z = -2.58$; $p < 0.05$; $r = -0.28$). Finally, we found expertise differences in the time for slalom performance in the left hand ($z = -2.63$; $p < 0.01$; $r = -0.29$) as well as in the right hand ($z = -2.00$; $p < 0.05$; $r = -0.22$) with better scores for the experience group compared to the novice group. These differences indicate that our delineation criteria were successful in separating novices from experienced participants for our sport-specific motor tasks.

3. Results

3.1. Global Analysis on the Central Parameter Dribbling Performance. As expected after four training sessions, a three-way ANOVA for the right hand dribbling performance revealed a highly significant performance improvement for the factor TIME ($F(1,76) = 178.31$; $p < 0.001$; $\eta_p^2 = 0.701$), while all other factors and their interactions remained nonsignificant (all $p > 0.05$). Thus, right hand performance improvements did not differ whether the right hand was trained at a mirror or whether the participant was novice or experienced. A three-way ANOVA for the parameter left hand dribbling performance revealed significant main and interaction effects. There was a highly significant effect for the factor TIME, meaning performance improved from pre- to posttest measurements ($F(1,76) = 175.37$; $p < 0.001$; $\eta_p^2 = 0.698$). A medium, significant effect was found for the interaction TIME ∗ CONDITION ($F(1,76) = 5.09$; $p < 0.05$; $\eta_p^2 = 0.063$). Another small but significant two-way interaction effect appeared between the factors TIME ∗ EXPERTISE ($F(1,76) = 4.32$; $p < 0.05$; $\eta_p^2 = 0.054$). Finally, a significant threefold interaction of TIME ∗ CONDITION ∗ EXPERTISE was noted ($F(1,76) = 7.27$; $p < 0.01$; $\eta_p^2 = 0.087$), indicating that performance improvements from pre- to posttests were differently effected by the kind of training (i.e., MVF versus active feedback training) and by the expertise level (i.e., experts versus novices). Since our participant group consisted of male and female participants that were almost evenly distributed across groups we exploratively included GENDER (male/female) as an additional factor in the ANOVA model but could not detect any significant GENDER effects (all $p > 0.05$).

3.2. Left Hand Dribbling Performance Improvements between Conditions. Due to the twofold and threefold interactions for left hand performance, we performed separate ANOVAs, one for the novice and one for the experienced group (since no interaction effects for right hand appeared, no further analyses were performed for right hand; see data analysis). As depicted in Figure 2(c), for the novice group a significant improvement for the factor TIME in left hand performance emerged ($F(1,39) = 96.48$; $p < 0.001$; $\eta_p^2 = 0.712$), but the interaction between TIME ∗ CONDITION was not significant ($p > 0.05$, see Figure 2(c)). A reversed pattern emerged for the experienced group in left hand performance improvement. As shown in Figure 2(a), the ANOVA for left hand dribbling indicated a significant effect for the factor TIME ($F(1,37) = 82.30$; $p < 0.001$; $\eta_p^2 = 0.690$) and a highly significant TIME ∗ CONDITION effect ($F(1,37) = 16.21$; $p < 0.001$; $\eta_p^2 = 0.305$). Although there were no interaction effects for right hand dribbling, performance measures for this hand are depicted in Figure 2 as well (Figures 2(b) and 2(d)) to account for the significant TIME effects.

3.3. Post Hoc Measures for Left Hand Dribbling Performance Improvements. For post hoc analysis to further elucidate the significant TIME ∗ CONDITION and TIME ∗ CONDITION ∗ EXPERTISE effects, we calculated a performance improvement score (posttest minus pretest). As clearly indicated by Figure 3 and relative improvements (in %) depicted in Table 2, Bonferroni-corrected independent t-tests revealed that only left hand performance gains in the experienced group significantly differed between MVF and control group ($t(37) = -4.02$; $p < 0.01$; $d = -1.29$), with higher improvements for the MVF group. Novices' performance improvements did not differ significantly between control and MVF ($p > 0.05$). Moreover, the novice control group improved significantly more than the control group of experienced participants ($t(39) = -3.11$; $p < 0.05$; $d = -0.97$), while the MVF groups did not differ significantly ($p > 0.05$).

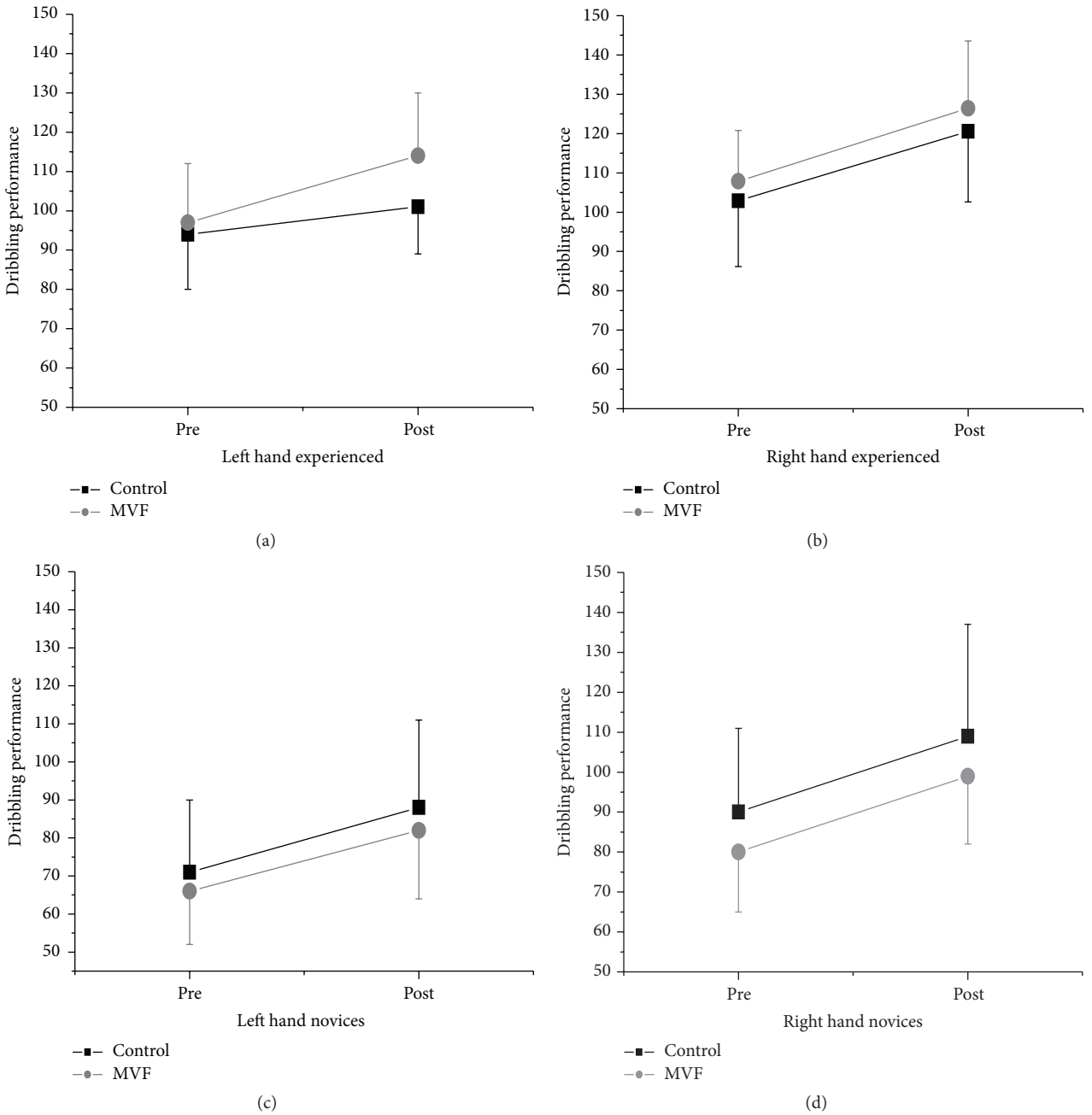

Figure 2: Interaction plots for the main outcome variable (dribbling performance) separated for novice and experienced groups and for left and right hand. Mean absolute scores are depicted and error bars indicate standard deviations; statistics are explained in the text.

For a complete overview of test results, right hand performance improvements are shown in Figure 3.

3.4. Dribbling Error Improvements between Groups. To observe whether the MVF group's dribbling error decrease from pre- to posttest measures (i.e., performance improvements) differed from the control groups, we compared the difference in the pre- and posttest measures separated for the factors CONDITION ∗ EXPERTISE. Table 2 depicts absolute and relative error decreases (%) of all dependent measures, while Figure 4 shows only the error decrease (note that a positive value indicates error decrease, not increase). However, for the right and left hand, error decreases (i.e., error improvements) did not differ between MVF and control (both $p > 0.05$) or for novices and experienced participants (both $p > 0.05$); thus the dribbling error decrease was constant across experimental groups.

3.5. Comparison of Slalom Performance Improvements between Groups. To detect whether the MVF group's performance improvements in slalom dribbling were more pronounced than the control groups, we compared the

Table 2: Absolute and relative performance improvements for all test variables separated by CONDITION ∗ EXPERTISE. Shown are mean values along standard deviations.

CONDITION ∗ EXPERTISE	Task/variable	Performance improvements		Performance improvements* (%)	
		Right hand	Left hand	Right hand	Left hand
Control novice	Dribbling performance	19.06 ± 15.33	16.50 ± 11.41	17.23	11.80
MVF novice		18.55 ± 9.79	15.58 ± 9.33	14.91	10.27
Control experienced		17.70 ± 11.48	6.50 ± 8.94	18.21	6.11
MVF experienced		18.51 ± 11.93	16.87 ± 11.93	19.97	16.41
Control novice	Dribbling error	−1.06 ± 1.45	−1.82 ± 2.02	40.66	40.80
MVF novice		−1.53 ± 1.45	−1.14 ± 1.75	42.99	24.35
Control experienced		−1.35 ± 2.07	−1.18 ± 2.25	63.81	35.91
MVF experienced		−0.65 ± 1.13	−0.70 ± 1.38	37.68	28.61
Control novice	Slalom performance (sec)	−0.25 ± 0.64	−0.64 ± 0.75	6.68	2.61
MVF novice		−0.33 ± 0.39	−0.42 ± 0.42	4.43	3.63
Control experienced		−0.42 ± 0.51	−0.28 ± 0.39	3.41	4.93
MVF experienced		−0.58 ± 0.83	−0.65 ± 0.52	7.53	6.90

*Note that the relative improvements, for example, 63.81% for the experienced control group (right hand), appear to be very high. Participants' error scores were generally relatively low, so reducing error from two errors in the pretest up to only one error in the posttest is already a 100% change.

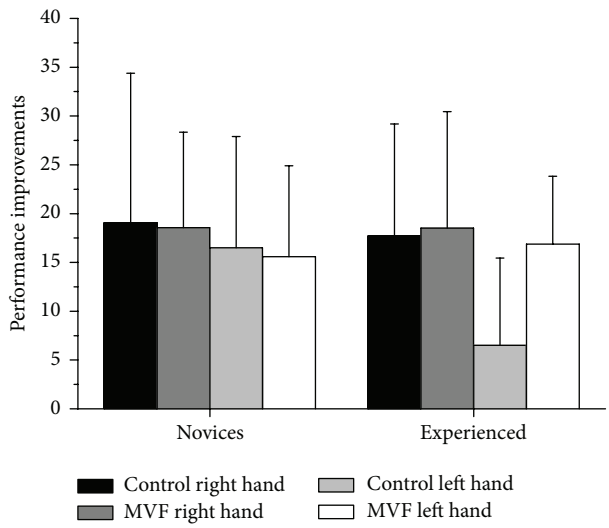

Figure 3: Shown are the performance improvements for the main outcome variable (dribbling performance) calculated by subtracting prevalues from postvalues and separated for novice and experienced groups. Scores depicted are absolute means, and error bars indicate standard deviations. The higher the value, the greater the improvement; statistics are explained in the text.

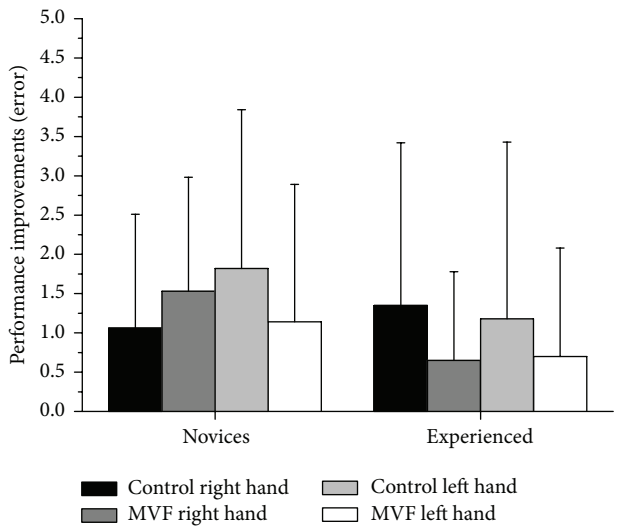

Figure 4: Shown are the performance improvements for the dribbling error, which was assessed for the dribbling task performed at the mirror box. Error improvements were calculated by subtracting prevalues from postvalues and are depicted separately for novice and experienced groups. Illustrated scores are absolute means, and error bars indicate standard deviations. Note that a positive value indicates improvement; statistics are explained in the text.

difference scores from pre- to posttest measures separated for the factors CONDITION ∗ EXPERTISE. Since the slalom dribbling performance scores were not normally distributed, instead of ANOVAs, nonparametric tests were computed (U-tests; see statistic section) and r-values indicate effects size estimations based on z-values [40]. Table 2 depicts absolute and relative performance improvements (%) of all dependent measures; Figure 5 shows only the slalom dribbling performance improvements.

We found no differences between MVF and control in right hand improvements, neither for experienced nor for novice participants (both $p > 0.05$). However, for left hand performance, comparison of the improvements between MVF and control in the experienced group yielded significance, with the MVF group improvement greater than that of the control group ($z = -2.529$; $p < 0.05$; $r = -0.58$), while the novice MVF group did not significantly improve performance with the left hand ($p > 0.05$).

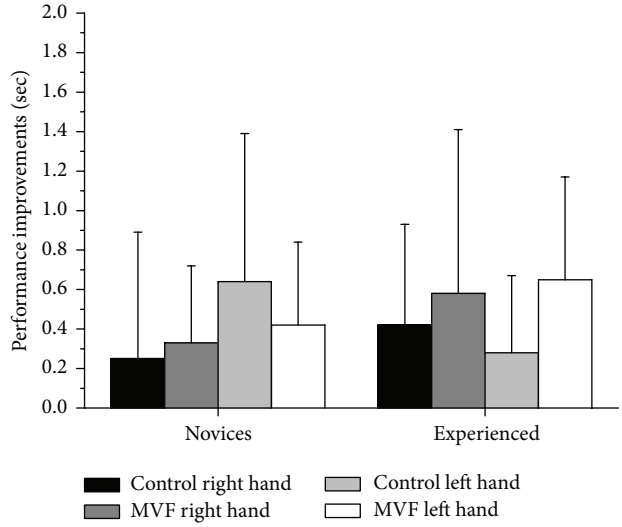

Figure 5: Shown are the performance improvements in the time for slalom dribbling parkour execution (i.e., slalom performance) calculated by subtracting prevalues from postvalues and separated for novice and experienced groups. These scores are absolute means, and error bars indicate standard deviations. The higher the value, the greater the improvement; statistics are explained in the text.

4. Discussion

The purpose of the present approach was to find out whether mirror visual feedback is applicable within a sport-scientific context and whether the well-known improvements of motor learning through MVF are modulated by skill level. Intermanual transfer effects were found, such as all groups, regardless of proficiency level or feedback modality, improving performance with the nontraining hand. Compared to direct feedback, superior left hand performance gains of MVF participants were significant in the experienced group only, while performance gains in novice participants did not differ between feedback modalities. Interestingly, this pattern of observations was accompanied by the same effects in a (nontrained) transfer task in which dynamic instead of stationary dribbling was requested. The results support our first hypothesis, which predicted intermanual transfer effects in the present motor task, which will be increased through MVF. However, this hypothesis has to be modified, as MVF effects depend on skill level. Consequently, our second hypothesis that experts will profit more from MVF than novices has to be rejected in its current formulation, since only experienced players showed improvement. A comparable decrease in error scores across groups indicates that a change in the speed and accuracy relationship cannot account for our findings. Moreover, we could not find any differences between male or female participants, which, however, should be handled cautiously due to the limited participant number for each gender and factor.

4.1. Intermanual Transfer. The intermanual transfer effects observed in the present study are in line with other studies that observed transfer effects of different motor tasks. For example, transfer effects were found in several realistic sport-specific tasks [4, 5, 41], a pegboard task requiring fine motor skills [2], an inverted-reversed printing task [42], finger tapping [43], keyboard pressing [12], ball catching [44], and adaptation in visuomotor rotation tasks [45]. Thus, the present study extends those findings in so far that interlimb transfer effects are observable in a ball dribbling task, which, however, are modulated by skill level.

Interestingly, transfer effects of the control groups receiving direct feedback were stronger in novice participants compared to those who were experienced. However, ball dribbling is a well-learned motor behavior for handball and basketball players, but not for nonplayers. It is well-known that motor learning undergoes several stages [46] such that the task to be executed in the present study differed in several aspects with respect to skill level. It is thought that, during the initial motor learning phase, movements are unskilled and depend strongly on feedback along with high demands on attention [47, 48]. With sustained practice, movement aspects such as accuracy and velocity increase and become more automated, while dependence on feedback becomes less important [49]. Since experienced participants might have been less dependent on feedback, one could assume that the level of attention decreased in the direct feedback modality, which in turn resulted in a lesser degree of intermanual transfer effects to the left hand compared to novice participants. However, this is a speculative view which needs further investigation of the explicit role of attention in intermanual transfer.

4.2. Mirror Visual Feedback. The present results concerning MVF are twofold since intermanual transfer effects were more pronounced through MVF compared to normal feedback only in the experienced group. Novice participants, relatively unfamiliar with basketball dribbling, did not benefit more from mirror visual feedback compared to normal (direct) feedback. The latter finding is in contrast to studies that found pronounced transfer effects in healthy participants (for an overview see [20]). However, due to study protocol and feedback modalities, only the studies by Hamzei et al. [26] and Läppchen et al. [25] are directly comparable to the present approach. They compared learning simple fine motor tasks (e.g., a pegboard task) with either direct feedback from the training hand or MVF. Clear advantages of MVF over direct feedback were found in intermanual transfer from right to left hand. Based on accompanied functional MRI data Hamzei et al. (2012) found a mirror training specific neural network, including areas that are associated with the mirror neural system. Moreover, Läppchen et al. (2012) found different excitability changes (induced by TMS) in M1 in both hemispheres after mirror training. The $M1_{left}$ (contralateral to the trained hand) of the direct feedback group had increased excitability and the mirror training group had decreased $M1_{left}$ excitability [25]. Such differential neural networks that have substantial overlap with the MNS might be one reason for augmented transfer effects compared to normal feedback [20].

Therefore, from a neurophysiological point of view, different involvement of MNS-related brain regions might be responsible for the skill-level dependent results in the current

experiment. The tasks used by [25, 26] were basic fine motor tasks that were comparable to fine motor executions that humans perform in everyday life such as putting a peg in a hole or using a teaspoon. Consequently, it might well be that those tasks become or were already familiar within the training process and had become part of the motor repertoire. Indeed, Hamzei et al. (2012) argued that observation of this embodied action (i.e., the tasks used in their study) activates MNS-related brain regions, likely due to motor simulation [26]. However, the ball dribbling task in the present study has no equivalence to the everyday life of nonplayers. Therefore, although speculative and not measured directly, one might argue that the ball dribbling task, being relatively unfamiliar for novice participants, did not activate the MNS to such an extent that it drives augmented transfer effects as suggested through MVF. In contrast, experienced ball dribblers, whose sport frequently requires ball dribbling skill, might had stronger involvement of MNS-related brain regions. Support for this interpretation comes from (motor-) expert studies. In expert dancers, as an example, different activations of the MNS with higher involvement of the MNS have been detected when observed movements are familiar, that is, part of the own motor repertoire [38, 39]. Along with the activation of ipsilateral motor areas through observing the right training hand in a mirror (i.e., illusion of a moving left hand) in accordance with the cross-activation model (cf. [8]), this resulted in performance gains of the left untrained hand which outweighed any performance gains through "common" intermanual transfer effects [6, 7].

Alternatively, considering the different task demands of ball dribbling concurrently with MVF or active feedback, it could well be that task complexity plays an essential role for our findings, which in turn is related to individual skill level [50, 51]. Thus, a simple explanation could be that for experienced players the active feedback condition was simple, while MVF was complex (or at least very unusual or more complex). In contrast, both feedback modalities were complex for novice participants. The unusual feedback through a mirror might have forced even experienced ball dribblers to direct attention more strongly back to task execution as visual feedback dependency becomes more relevant. Indeed, it has been indicated that with increasing task complexity the profit of concurrent feedback also increases [50]. The increase in attention of experienced players to task execution and thus to the illusion of the left hand might have, in accordance with the cross-activation model, increased neural involvement of ipsilateral brain areas, which in turn evoked the performance improvements of the left hand. Bearing this in mind, our results are well in line with the current knowledge and further suggest that MVF-induced transfer effects could depend on the two interrelated factors' task complexity and the individual's skill level [27, 52]. If so, mirror therapy studies in the future might consider these aspects to find the best means of motor rehabilitation.

Although the present exploratory approach requires further investigation into the role of task complexity, the role of attention, skill level, and additional comparisons to other feedback modalities, we propose that the present results support MVF as being a potential tool to support intermanual transfer effects for rehabilitation in a sport context when athletes suffer hand or arm immobilization. However, considering that the present approach is the first that attempted to transfer the mirror illusion paradigm to the sport context, the study has some limitations. First, no measurement of neural activity was implemented, so the interpretations of brain-related mechanisms are only indirect and warrant further investigation by concurrent neuroimaging techniques. Furthermore, comparisons to other feedback conditions such as purely observational feedback of a passive hand [53] or active left hand, motor imagery, and bilateral training or left handed participants have not been considered in this initial study. How far professional or high expertise players are differently affected by MVF compared to the medium expertise levels in this study would be an interesting point as well. In this line, a higher sample size including a high variance of skill levels might also reveal a possible relationship between baseline values and intermanual performance gains through MVF. Lastly, proprioceptive sensations from the hand behind the mirror when unintentionally moved might have interfered with the mirror illusion differently in the two expertise groups [54], a factor that should be systematically controlled in the future.

5. Conclusion

The present study found that mirror visual feedback facilitates intermanual transfer effects in sport, but only for participants that had experience with the movements being performed. Thus, this study introduced the role of skill level and task complexity to the field of mirror visual feedback, two interrelated factors that could provide new insights in the study of mechanisms underlying MVF.

Competing Interests

The authors declare that there are no known competing interests associated with this publication and there has been no significant financial support for this work that could have influenced its outcome.

Acknowledgments

The authors would like to thank the handball and basketball sport clubs supporting this study. The authors also thank Fabian Hanpft, Sabine Mayer, Johannes Jester, Philipp Sprott, and Florian Bönnemann for help with data acquisition.

References

[1] G. Thut, N. D. Cook, M. Regard, K. L. Leenders, U. Halsband, and T. Landis, "Intermanual transfer of proximal and distal motor engrams in humans," *Experimental Brain Research*, vol. 108, no. 2, pp. 321–327, 1996.

[2] K. Schulze, E. Lüders, and L. Jäncke, "Intermanual transfer in a simple motor task," *Cortex*, vol. 38, no. 5, pp. 805–815, 2002.

[3] N. Birbaumer, "Motor learning: passing a skill from one hand to the other," *Current Biology*, vol. 17, no. 23, pp. R1024–R1026, 2007.

[4] E. Haaland and J. Hoff, "Non-dominant leg training improves the bilateral motor performance of soccer players," *Scandinavian Journal of Medicine and Science in Sports*, vol. 13, no. 3, pp. 179–184, 2003.

[5] T. Stöckel, M. Weigelt, and J. Krug, "Acquisition of a complex basketball-dribbling task in school children as a function of bilateral practice order," *Research Quarterly for Exercise and Sport*, vol. 82, no. 2, pp. 188–197, 2011.

[6] G. Howatson, T. Zult, J. P. Farthing, I. Zijdewind, and T. Hortobágyi, "Mirror training to augment cross-education during resistance training: a hypothesis," *Frontiers in Human Neuroscience*, vol. 7, article 396, 2013.

[7] T. Zult, G. Howatson, E. E. Kádár, J. P. Farthing, and T. Hortobágyi, "Role of the mirror-neuron system in cross-education," *Sports Medicine*, vol. 44, no. 2, pp. 159–178, 2014.

[8] M. Lee, M. R. Hinder, S. C. Gandevia, and T. J. Carroll, "The ipsilateral motor cortex contributes to cross-limb transfer of performance gains after ballistic motor practice," *Journal of Physiology*, vol. 588, no. 1, pp. 201–212, 2010.

[9] G. Dreisbach, H. Haider, and R. H. Kluwe, "Preparatory processes in the task-switching paradigm: evidence from the use of probability cues," *Journal of Experimental Psychology*, vol. 28, no. 3, pp. 468–483, 2002.

[10] S. Obayashi, "Possible mechanism for transfer of motor skill learning: implication of the cerebellum," *The Cerebellum*, vol. 3, no. 4, pp. 204–211, 2004.

[11] K. L. Ruddy and R. G. Carson, "Neural pathways mediating cross education of motor function," *Frontiers in Human Neuroscience*, vol. 7, article 397, 2013.

[12] H. G. Taylor and K. M. Heilman, "Left-hemisphere motor dominance in righthanders," *Cortex*, vol. 16, no. 4, pp. 587–603, 1980.

[13] G. Rizzolatti, L. Fadiga, V. Gallese, and L. Fogassi, "Premotor cortex and the recognition of motor actions," *Cognitive Brain Research*, vol. 3, no. 2, pp. 131–141, 1996.

[14] M. Jeannerod, "Neural simulation of action: a unifying mechanism for motor cognition," *NeuroImage*, vol. 14, no. 1, pp. S103–S109, 2001.

[15] J. P. Farthing, J. R. Krentz, C. R. A. Magnus et al., "Changes in functional magnetic resonance imaging cortical activation with cross education to an immobilized limb," *Medicine and Science in Sports and Exercise*, vol. 43, no. 8, pp. 1394–1405, 2011.

[16] J. P. Farthing, J. R. Krentz, and C. R. A. Magnus, "Strength training the free limb attenuates strength loss during unilateral immobilization," *Journal of Applied Physiology*, vol. 106, no. 3, pp. 730–736, 2009.

[17] T. Hortobágyi, S. P. Richardson, M. Lomarev et al., "Interhemispheric plasticity in humans," *Medicine and Science in Sports and Exercise*, vol. 43, no. 7, pp. 1188–1199, 2011.

[18] V. S. Ramachandran and D. Rodgers-Ramachandran, "Synaesthesia in phantom limbs induced with mirrors," *Proceedings of the Royal Society of London B: Biological Sciences*, vol. 263, no. 1369, pp. 377–386, 1996.

[19] V. S. Ramachandran and E. L. Altschuler, "The use of visual feedback, in particular mirror visual feedback, in restoring brain function," *Brain*, vol. 132, no. 7, pp. 1693–1710, 2009.

[20] F. J. A. Deconinck, A. R. P. Smorenburg, A. Benham, A. Ledebt, M. G. Feltham, and G. J. P. Savelsbergh, "Reflections on mirror therapy: a systematic review of the effect of mirror visual feedback on the brain," *Neurorehabilitation and Neural Repair*, vol. 29, no. 4, pp. 349–361, 2015.

[21] C. S. McCabe, R. C. Haigh, E. F. J. Ring, P. W. Halligan, P. D. Wall, and D. R. Blake, "A controlled pilot study of the utility of mirror visual feedback in the treatment of complex regional pain syndrome (type 1)," *Rheumatology*, vol. 42, no. 1, pp. 97–101, 2003.

[22] E. L. Altschuler, S. B. Wisdom, L. Stone et al., "Rehabilitation of hemiparesis after stroke with a mirror," *The Lancet*, vol. 353, no. 9169, pp. 2035–2036, 1999.

[23] G. Yavuzer, R. Selles, N. Sezer et al., "Mirror therapy improves hand function in subacute stroke: a randomized controlled trial," *Archives of Physical Medicine and Rehabilitation*, vol. 89, no. 3, pp. 393–398, 2008.

[24] I. Nojima, T. Mima, S. Koganemaru, M. N. Thabit, H. Fukuyama, and T. Kawamata, "Human motor plasticity induced by mirror visual feedback," *The Journal of Neuroscience*, vol. 32, no. 4, pp. 1293–1300, 2012.

[25] C. H. Läppchen, T. Ringer, J. Blessin et al., "Optical illusion alters M1 excitability after mirror therapy: A TMS Study," *Journal of Neurophysiology*, vol. 108, no. 10, pp. 2857–2861, 2012.

[26] F. Hamzei, C. H. Läppchen, V. Glauche, I. Mader, M. Rijntjes, and C. Weiller, "Functional plasticity induced by mirror training: the mirror as the element connecting both hands to one hemisphere," *Neurorehabilitation and Neural Repair*, vol. 26, no. 5, pp. 484–496, 2012.

[27] G. Wulf and C. H. Shea, "Principles derived from the study of simple skills do not generalize to complex skill learning," *Psychonomic Bulletin & Review*, vol. 9, no. 2, pp. 185–211, 2002.

[28] A. Utley and S. Astill, "Motor control, learning and development," *International Journal of Sports Science and Coaching*, vol. 3, no. 2, pp. 297–299, 2008.

[29] L. Jäncke, N. J. Shah, and M. Peters, "Cortical activations in primary and secondary motor areas for complex bimanual movements in professional pianists," *Cognitive Brain Research*, vol. 10, no. 1-2, pp. 177–183, 2000.

[30] T. F. Münte, E. Altenmüller, and L. Jäncke, "The musician's brain as a model of neuroplasticity," *Nature Reviews Neuroscience*, vol. 3, no. 6, pp. 473–478, 2002.

[31] G. Schlaug, "The brain of musicians," *Annals of the New York Academy of Sciences*, vol. 930, pp. 281–299, 2001.

[32] N. Balser, B. Lorey, S. Pilgramm et al., "Prediction of human actions: expertise and task-related effects on neural activation of the action observation network," *Human Brain Mapping*, vol. 35, no. 8, pp. 4016–4034, 2014.

[33] G. Buccino, F. Lui, N. Canessa et al., "Neural circuits involved in the recognition of actions performed by nonconspecifics: An fMRI Study," *Journal of Cognitive Neuroscience*, vol. 16, no. 1, pp. 114–126, 2004.

[34] Y. Chang, "Reorganization and plastic changes of the human brain associated with skill learning and expertise," *Frontiers in Human Neuroscience*, vol. 8, no. 1, article 35, 2014.

[35] S. M. Aglioti, P. Cesari, M. Romani, and C. Urgesi, "Action anticipation and motor resonance in elite basketball players," *Nature Neuroscience*, vol. 11, no. 9, pp. 1109–1116, 2008.

[36] S. Hüttermann, D. Memmert, and D. J. Simons, "The size and shape of the attentional 'spotlight' varies with differences in sports expertise," *Journal of Experimental Psychology: Applied*, vol. 20, no. 2, pp. 147–157, 2014.

[37] R. Rienhoff, L. Fischer, B. Strauss, J. Baker, and J. Schorer, "Focus of attention influences quiet-eye behavior: an exploratory investigation of different skill levels in female basketball players," *Sport, Exercise, and Performance Psychology*, vol. 4, no. 1, pp. 62–74, 2015.

[38] B. Calvo-Merino, D. E. Glaser, J. Grèzes, R. E. Passingham, and P. Haggard, "Action observation and acquired motor skills: an fMRI study with expert dancers," *Cerebral Cortex*, vol. 15, no. 8, pp. 1243–1249, 2005.

[39] B. Calvo-Merino, J. Grèzes, D. E. Glaser, R. E. Passingham, and P. Haggard, "Seeing or doing? influence of visual and motor familiarity in action observation," *Current Biology*, vol. 16, no. 22, p. 2277, 2006.

[40] J. Cohen, *Statistical Power Analysis for the Behavior Science*, Lawrance Eribaum Association, Hillsday, NJ, USA, 1988.

[41] O. Senff and M. Weigelt, "Sequential effects after practice with the dominant and non-dominant hand on the acquisition of a sliding task in schoolchildren," *Laterality*, vol. 16, no. 2, pp. 227–239, 2011.

[42] S. E. Parlow and M. Kinsbourne, "Asymmetrical transfer of training between hands: implications for interhemispheric communication in normal brain," *Brain and Cognition*, vol. 11, no. 1, pp. 98–113, 1989.

[43] J. I. Laszlo, R. A. Baguley, and P. J. Bairstow, "Bilateral transfer in tapping skill in the absence of peripheral information," *Journal of Motor Behavior*, vol. 2, no. 4, pp. 261–271, 1970.

[44] S. M. Morton, C. E. Lang, and A. J. Bastian, "Inter- and intra-limb generalization of adaptation during catching," *Experimental Brain Research*, vol. 141, no. 4, pp. 438–445, 2001.

[45] R. L. Sainburg and J. Wang, "Interlimb transfer of visuomotor rotations: independence of direction and final position information," *Experimental Brain Research*, vol. 145, no. 4, pp. 437–447, 2002.

[46] U. Halsband and R. K. Lange, "Motor learning in man: a review of functional and clinical studies," *Journal of Physiology Paris*, vol. 99, no. 4–6, pp. 414–424, 2006.

[47] C. G. Atkeson, "Learning arm kinematics and dynamics," *Annual Review of Neuroscience*, vol. 12, pp. 157–183, 1989.

[48] R. Shadmehr and F. A. Mussa-Ivaldi, "Adaptive representation of dynamics during learning of a motor task," *Journal of Neuroscience*, vol. 14, no. 5, pp. 3208–3224, 1994.

[49] B. Preilowski, "Phases of motor-skills acquisition: a neuropsychological approach," *Journal of Human Movement Studies*, vol. 3, pp. 169–181, 1977.

[50] R. Sigrist, G. Rauter, R. Riener, and P. Wolf, "Augmented visual, auditory, haptic, and multimodal feedback in motor learning: a review," *Psychonomic Bulletin and Review*, vol. 20, no. 1, pp. 21–53, 2013.

[51] M. A. Guadagnoll and T. D. Lee, "Challenge point: a framework for conceptualizing the effects of various practice conditions in motor learning," *Journal of Motor Behavior*, vol. 36, no. 2, pp. 212–224, 2004.

[52] T. Haerem and D. Rau, "The influence of degree of expertise and objective task complexity on perceived task complexity and performance," *Journal of Applied Psychology*, vol. 92, no. 5, pp. 1320–1331, 2007.

[53] P. Reissig, R. Puri, M. I. Garry, J. J. Summers, and M. R. Hinder, "The influence of mirror-visual feedback on training-induced motor performance gains in the untrained hand," *PLoS ONE*, vol. 10, article e0141828, 2015.

[54] R. W. Selles, M. E. Michielsen, J. B. J. Bussmann et al., "Effects of a mirror-induced visual illusion on a reaching task in stroke patients: implications for mirror therapy training," *Neurorehabilitation and Neural Repair*, vol. 28, no. 7, pp. 652–659, 2014.

Hindawi Publishing Corporation
Neural Plasticity
Volume 2016, Article ID 7365609, 13 pages
http://dx.doi.org/10.1155/2016/7365609

Research Article

Neuromuscular Plasticity: Disentangling Stable and Variable Motor Maps in the Human Sensorimotor Cortex

Dominic Kraus and Alireza Gharabaghi

Division of Functional and Restorative Neurosurgery and Centre for Integrative Neuroscience, Eberhard Karls University Tuebingen, 72076 Tuebingen, Germany

Correspondence should be addressed to Alireza Gharabaghi; alireza.gharabaghi@uni-tuebingen.de

Received 11 April 2016; Revised 28 June 2016; Accepted 19 July 2016

Academic Editor: David E. Vaillancourt

Motor maps acquired with transcranial magnetic stimulation (TMS) are evolving as a biomarker for monitoring disease progression or the effects of therapeutic interventions. High test-retest reliability of this technique for long observation periods is therefore required to differentiate daily or weekly fluctuations from stable plastic reorganization of corticospinal connectivity. In this study, a novel projection, interpolation, and coregistration technique, which considers the individual gyral anatomy, was applied in healthy subjects for biweekly acquired TMS motor maps over a period of twelve weeks. The intraclass correlation coefficient revealed long-term reliability of motor maps with relevant interhemispheric differences. The sensorimotor cortex and nonprimary motor areas of the dominant hemisphere showed more extended and more stable corticospinal connectivity. Long-term correlations of the MEP amplitudes at each stimulation site revealed mosaic-like clusters of consistent corticospinal excitability. The resting motor threshold, centre of gravity, and mean MEPs across all TMS sites, as highly reliable cortical map parameters, could be disentangled from more variable parameters such as MEP area and volume. Cortical TMS motor maps provide high test-retest reliability for long-term monitoring when analyzed with refined techniques. They may guide restorative interventions which target dormant corticospinal connectivity for neurorehabilitation.

1. Introduction

Adaptive reorganization of cortical maps after brain damage is referred to as plasticity and is regarded as relevant during recovery and compensation by reflecting changes of neural circuit architecture and synaptic connectivity [1]. The connectivity of these neuronal networks is, however, also being continuously modified by use-dependent mechanisms independent of any injury or recovery. When studying changes of cortical map plasticity during disease progression or therapeutic interventions, it is therefore necessary to disentangle stable and variable map parameters. In this context, brain stimulation techniques are particularly suitable for monitoring the cortical maps, for example, to probe effective corticospinal connectivity by measuring time-locked motor evoked potentials (MEP) at target muscles. The techniques applied in animal research and human studies, for example, intracortical microstimulation or epicortical electrical stimulation, differ with regard to their level of invasiveness and spatial accuracy [2–7].

Transcranial magnetic stimulation (TMS)—albeit with significantly less spatial resolution than surgical mapping techniques—has been established as a powerful alternative mapping tool for clinical and research application [8]. When applied, for example, in the context of stroke patients, TMS mapping revealed a reduced excitability and a decreased cortical representation of the impaired movement [9, 10]. After short-term therapy, the cortical motor map and the manual dexterity increased at least temporarily [11]. Following longer interventions, clinical gains were paralleled by the recruitment of cortical motor representation in the affected hemisphere outside the primary motor cortex [9, 12, 13].

However, more recent studies have challenged these previous findings by revealing corticospinal connectivity outside the primary motor cortex in healthy subjects [14] as well as by demonstrating relevant variability of the spatial extent

of motor maps independent of any intervention [15]. This ambiguity might be related to methodological differences; in recent years, individual magnetic resonance images (MRIs) have been used in conjunction with navigated TMS (nTMS). This technique monitors the coil position, direction, and tilting, thus increasing the repeatability of both coil placement [16, 17] and orientation [18]. When the TMS coil was aligned on the basis of the individual shape of the central sulcus, the somatotopy in the primary motor hand area could be captured [19]. Navigated TMS might thus be more precise than standard TMS, for example, in capturing nonprimary motor cortex corticospinal connectivity [14], but is perhaps still not precise enough to distinguish between the natural daily or weekly fluctuations of the motor map extent [15] and lasting cortical plasticity in the course of a disease or intervention. Such a differentiation would necessitate stable cortical map parameters that are resistant to such natural fluctuations.

In this context, simulation studies have indicated that the individual gyral anatomy has a major impact on TMS-induced electrical field distributions [20–25]. The reliability of motor maps might thus be improved when accounting for interindividual differences in brain anatomy. Combining nTMS maps with individual MRIs facilitated—as a first step on the way—the analysis of group data in normalized space [15, 26, 27]. Previous nTMS approaches, however, still projected the TMS coil positions as a grid of target points on the brain surface, resembling a plane that covered both gyri and sulci, and did not account for differences in cortex morphology [15, 17–19, 28–30]. To overcome this limitation, we recently proposed a novel projection, interpolation, and coregistration technique for estimating nTMS sites onto the individual anatomy, namely, by following the surface curvature of gyri [31]. The novelty of this approach was thus not related to the application of neuronavigation to the TMS mapping procedure itself, as was the case in previous nTMS studies, but instead consisted in the application of the stereotactic information provided by nTMS to visualize the stimulation findings in relation to the specific anatomy [31]. The specific visualization of the stimulation sites, obtained by *nestling* them to the gyral curvature, was complemented by a mathematical interpolation which considered all neighboring stimulation results in a distance-weighted fashion. This technique achieved a lower variability of cortical motor maps between subjects in normalized space than standard TMS mapping [31].

In the present study, we reasoned that this refined TMS technique would also provide high test-retest reliability of cortical motor maps, although the inherent variability of TMS metrics, like other metrics representing human physiology, may be related to many biological reasons. We tested the long-term stability of nTMS in healthy subjects, not for days and weeks as tested previously but for several months, and with six instead of only two or three different measurement time points. Since these previous studies—which applied the standard TMS mapping approach—revealed low retest reliability even for these short observation periods, a repetition of this standard procedure for longer follow-up periods will not provide any further insight. We therefore focused our long-term examination on the novel approach which was recently introduced [31]. Notably, the limited reliability observed in previous studies was not related to focal mapping parameters such as *centre of gravity or hotspot* but to mapping parameters that capture the extent of the cortical motor map, such as the *map area*. We therefore addressed these classical parameters and also applied complementary measures to describe the cortical extent of the cortical motor map, such as motor maps of the *mean spatial overlap, the mean MEP amplitude, and the intraclass correlations of the MEP amplitude* in the present study.

We detected extended sensorimotor areas with high functional overlap between subjects and in the course of the mapping sessions. Therefore, long-term stable map areas could be disentangled from the more fluctuating ones by which they were surrounded. At each stimulation site, intraclass correlations of the MEP amplitudes revealed mosaic-like clusters of consistent corticospinal excitability spanning over distributed areas in the sensorimotor cortex. Moreover, and somewhat unexpectedly, relevant interhemispheric differences with more stable corticospinal connectivity in the nonprimary motor areas of the dominant hemisphere were unraveled, reflecting use-dependent plasticity.

2. Material and Methods

2.1. Subjects. Twelve right-handed subjects (mean age 24 years, range 19–28, 8 males) with verified right-handedness (EHS > 70) according to the Edinburgh Handedness Inventory [32] were studied in the course of six experiments with a mean of 14.7 days between experiments. In all subjects, cortical motor maps of the nondominant, right hemisphere were captured; in six of the participants, additional motor maps of the dominant, that is, left, hemisphere could be acquired. In three of the subjects, an additional seventh measurement was performed ~1.5 years after the sixth session. All measurements were performed at the same time of day. However, the participants were deliberately not requested to alter their daily routines. We thereby hoped to emulate real-life conditions of clinical practice as closely as possible. All participants gave written informed consent and had no contraindication to TMS [33] or a history of any neurological or psychiatric disease. The studies were approved by the local ethics committee and were in accordance with the declaration of Helsinki.

2.2. Mapping Protocol. The cortical mapping was performed by the same person in all experiments (DK) as described previously [31]: we used a navigated TMS stimulator (eXimia®, Nexstim, Helsinki, Finland) and a biphasic figure-8 coil (Nexstim, Helsinki, Finland) with a mean diameter of 50 mm and an estimated focality of 0.68 cm^2 (eXimia Focal Bipulse, Helsinki, Finland). The neuronavigation system controlled the position, orientation, and tilt angle of the TMS coil. Prior to the mapping, individual anatomical T1-weighted magnetic resonance images were acquired by a 3-Tesla Siemens TIM Trio MRI system (Siemens AG, Erlangen, Germany) using the t1-MPRAGE gradient echo, a field of view (FOV) of 256 mm and 176 sagittal slices, a voxel size of $1 \times 1 \times 1\,mm^3$, a repetition

time (TR) of 2300 ms, and an echo time (TE) of 2.98 ms. Individual MRIs were loaded into the eXimia system for coregistration with the subject's head using three anatomical landmarks (nasion + both crux helix) and nine additional points on the scalp (registration error < 2 mm). The electromyography (EMG) signal of the extensor digitorum communis (EDC) of both arms was recorded with the integrated EMG device of the eXimia system (3 kHz sampling rate, band-pass filter of 10–500 Hz) using Ag/AgCl AmbuNeuroline 720 wet gel surface electrodes (Ambu GmbH, Germany). The MEPs were acquired from relaxed muscles. The EDC was chosen for this study, since this muscle is the main target during brain-robot interface-based interventions [34–36] designed for stroke rehabilitation [37, 38]. The electrodes were placed 2 cm apart from each other on the muscle belly of the forearm [39], differently from the procedure usually applied for hand muscles.

For each subject, the cortical representation of the EDC muscle was determined using 40% of maximum stimulator output at the anatomically defined "hand knob" of the primary motor cortex (M1) as the starting position. If the initial stimulator output was not sufficient to elicit MEPs, it was increased in steps of 5%. The current waveform of the stimulator was biphasic. The orientation of the induced current in the brain was posterior-anterior for the first phase and anterior-posterior for the second phase of the stimulus as stipulated by the manufacturer. The orientation of the electric field, calculated on the basis of the individual MRI of each subject by the eXimia software, was kept perpendicular to the central sulcus, and the location with the highest MEP response was selected as the stimulation point. Having determined the "hotspot" with about 30 stimuli by moving the coil around the hand knob, we varied the orientation of the coil within an angle of approximately 90° in steps of roughly 10° and with 3 stimuli at each angle, around the original orientation. Using this method, we were able to ascertain the orientation with the highest response in this spot. This orientation was posterior-anterior in all cases with only slight (±20°) interindividual differences. The resting motor threshold (RMT) was determined using the relative frequency method, that is, selecting the minimum stimulus intensity (by changing the stimulator output in 2% steps of maximum stimulator output (MSO)) that resulted in MEPs >50 μV in the peak-to-peak amplitude in at least 5 out of 10 consecutive trials [40, 41].

The cortical map representation was acquired at 110% RMT with the same coil orientation as was applied at the hotspot. This map was extended in random order around the hotspot with evenly distributed stimuli until MEPs could no longer be evoked in the EDC. Despite some interindividual variability, this procedure was sufficient to cover the entire cortical representation of the EDC in all subjects [31]. A visual grid (5 mm × 5 mm × 5 mm), predefined in the navigation software, was used for guidance during the mapping procedure, applying 2-3 stimuli per cell and resulting in an average of 10 stimuli per 1 cm^2. Specifically, two stimuli were applied per cell; when one of them did not result in a response, a third stimulus was applied. The actual navigation coordinates of each stimulus were then used for data analysis, resulting in a spacing of approximately 3 mm, due to the small variability of the stimulation sites within each cell. Stimulation sites were visualized on the surface at a depth of 20 mm to ensure that the stimuli were located within the cortex in all subjects (range of scalp to cortex distance: 13–18.5 mm). This procedure was chosen due to the fact that the manufacturer allows adjustments to be made in steps of 5 mm only, that is, at 15 mm, 20 mm, and 25 mm. This TMS protocol thus resulted in stimulation sites 20 mm below the scalp and spaced approximately 3 mm apart with their coordinates located in individual MRI space.

2.3. Data Processing. Data were analyzed using Matlab R2010b (MathWorks GmbH, Ismaning, Germany) with a custom-built code, the Toolbox SPM8 (Wellcome Trust Centre for Neuroimaging, London, UK), the FreeSurfer Software Suite (Martinos Centre for Biomedical Imaging, Charlestown, USA), and SPSS V21 (IBM GmbH, Ehningen, Germany).

For data analyses, we then used the actual navigation coordinates (i.e., the MRI coordinates within the reference frame of the eXimia system) of each stimulus, resulting in an interstimulus spacing of approximately 3 mm. Finally, these spots were interpolated for visualization, sampled on a 1 × 1 × 1 mm grid to close the gap between stimulation sites, and then projected onto the gyral anatomy following the procedure described below [31]. Importantly, this interpolation technique increased the reliability of every single stimulus by considering all its neighboring stimulation results in a distance-weighted way. This technique also provides a higher level of focality than the conventional approach of treating each stimulus as a discrete event. The level of focality is thus higher than the actual area activated by the stimulation pulse.

Please note that this interpolation procedure resulted formally in a volume (mm^3) instead of the conventional surface (mm^2) to describe the extension of the cortical map. Since the *calculated* value (mm^3) was proportional to the *real* surface area (mm^2) and was always calculated in the same way for all sessions, it provided a suitable measure for determining the test-retest reliability. During the mapping, about 100 stimuli were applied, with some subject-to-subject variability due to the individual cortical representation of the EDC [31]. Recent findings indicate that reliable motor maps could be created with around 60 stimuli [42]. During this study, the respective map could also be captured with less than 100 stimuli in subjects who had a small cortical representation of the EDC, while in others, more stimuli were required. Such variability of individual cortical maps has already been shown in detail elsewhere [31]. The procedure lasted for ~15 minutes and the subjects were instructed to keep their muscles relaxed during this time. During offline analysis, the EMG data were visually inspected and any trials in which muscle preactivation was detected were discarded (<1% of all trials had to be removed due to EMG activation).

2.3.1. nTMS Processing. Since the stereotactic information provided by the nTMS (eXimia, Nexstim, Helsinki, Finland) refers to the coil position outside the head only, additional calculations are necessary to translate this information

beyond the coil and onto the brain. We therefore used the coordinates of the TMS coil to project all stimulation points of the map onto the cortex in the direction of the magnetic field between the two coil windings [31]. The coil coordinates acquired via the navigation system were thereby transferred to the individual MR image of each subject at a depth of ~20 mm (see previous section).

Thereafter, the mean MEP amplitude and the centre of gravity (CoG) of each map were determined. Due to the uncertainty of the exact stimulation depth using TMS, the CoG is usually calculated in two dimensions only. Moreover, we applied individual space (and not normalized space) to analyze the reliability of the CoG so as to enable us to compare it with the literature. The maximum amplitude-weighted stimulation point was calculated using the following formula [43]:

$$\mathrm{CoG} = \frac{\sum a_i * x_i}{A}, \frac{\sum a_i * y_i}{A} \quad (1)$$

with a_i as the MEP amplitude at positions x_i (medial-lateral) and y_i (anterior-posterior) and A as the sum of all MEP amplitudes.

The MEP amplitudes of all stimuli were then projected onto a $1 \times 1 \times 1$ mm grid and *interpolated* by taking all neighboring stimulation results into account in a distance-weighted way. This resulted in a three-dimensional map area with *mean MEP amplitude* for each grid cell. The sum of active grid cells (with MEPs > 50 μV) subsequently resulted in the map area and the map volume (area $*$ mean map MEP), that is, the MEP amplitude-weighted area, for each measurement. Please note that this *mean MEP amplitude* is different from the *mean Map MEP amplitude* (Table 2) which captures all the *noninterpolated* stimulation amplitudes of one session.

The individual MRI volumes and coregistered MEP maps were spatially normalized to MNI space, using SPM8 for further group analysis [44].

2.3.2. FreeSurfer Processing. The MNI normalized MRI images were then imported into the FreeSurfer software [31], which aligned the individual central sulci, and a cortical surface structure was reconstructed using the inbuilt functions [45]. An average brain surface with >160k mesh points was then created by coregistration of the cortical surface structures [44]. The coregistered MEP maps were first projected onto the individual surface structures with the inbuilt function *mri_vol2surf* of FreeSurfer and then transferred onto the average surface structure with *mri_surf2surf*. As a result, all maps were projected onto the same surface coordinate system, enabling us to gain further statistics for each mesh point of the cortical surface.

This procedure enabled us to calculate the mean MEP amplitude over all measurements and subjects, the mean overlap of all subjects in the course of the experiments (in percent), and the intraclass correlation (ICC) values for the MEP amplitudes at each mesh point.

2.3.3. Statistical Analysis. A repeated measure ANOVA (rmANOVA) with Greenhouse-Geisser correction was performed to determine differences in TMS parameters between sessions. Intraclass correlation was applied to compute the test-retest reliability [46] for mean map MEP, map area, map volume, RMT, coordinates of the CoG, and the MEP amplitudes at each stimulation site, that is, surface mesh point.

A two-way random average measure (ICC(2, k)) was chosen in SPSS according to McGraw and Wong [47] for the map parameters. In addition, we calculated an ICC(1, k) value for each surface mesh point using the MEP amplitude in that coordinate. ICC values usually range from 0 to 1 but can become negative if the variance in the subject is higher than the group variance. Values above 0.75, between 0.5 and 0.75, and below 0.5 are regarded as reflecting high, moderate, and poor test-retest reliability, respectively [46].

3. Results

3.1. Group Data of TMS Parameters. The data of all experimental sessions was acquired and analyzed without any dropouts and no significant mean differences of TMS parameters between sessions were revealed in the rmANOVA. The original TMS parameters of each hemisphere are summarized on the group level in Tables 1 and 2 and on the single subject level in Figures 1 and 2, respectively.

3.2. Reliability of TMS Parameters. In the nondominant, right hemisphere, ICC values over six sessions showed high reliability for the RMT (ICC = 0.989; 95% Confidence Interval CI: 0.975 to 0.996, Figure 1(a)), the medial-lateral (ICC = 0.947; 95% CI: 0.882 to 0.983, Figure 1(b)) and anterior-posterior CoG (ICC = 0.98: 95% CI: 0.955 to 0.933, Figure 1(c)), and the mean map MEP amplitude, that is, the average of all MEP amplitudes of the cortical map (ICC = 0.869; 95% CI: 0.711 to 0.956, Figure 1(d)). The map volume (ICC = 0.695; 95% CI: 0.32 to 0.899, Figure 1(f)) and map area (ICC = 0.178; 95% CI: −0.879 to 0.73, Figure 1(e)) showed moderate and poor reliability, respectively.

In the dominant, left hemisphere, ICC values over six sessions revealed high reliability for the RMT (ICC = 0.990; 95% CI: 0.970 to 0.998, Figure 2(a)), the medial-lateral (ICC = 0.979; 95% CI: 0.927 to 0.997, Figure 2(b)) and anterior-posterior CoG (ICC = 0.972; 95% CI: 0.914 to 0.996, Figure 2(c)), and the mean map MEP amplitude (ICC = 0.855; 95% CI: 0.566 to 0.977, Figure 2(d)). The map volume (ICC = 0.152; 95% CI: −0.130 to 0.535, Figure 2(f)) and map area (ICC = −0.056; 95%: −0.173 to 0.403, Figure 2(e)) revealed poor reliability.

In three subjects, a seventh session (highlighted in red, Supplementary Figure 1 (a–f) in Supplementary Material available online at http://dx.doi.org/10.1155/2016/7365609) could be acquired for the nondominant hemisphere. The high reliability of the RMT (ICC = 0.995; 95% CI: 0.976 to 1), medial-lateral CoG (ICC = 0.973; 95% CI: 0.878 to 0.999) and anterior-posterior CoG (ICC = 0.892; 95% CI: 0.537 to 0.997), and the mean map MEP amplitude (ICC = 0.928; 95% CI: 0.664 to 0.998) in the previous six sessions could be preserved in the seventh measurement, that is, ~1.5 years after the sixth session.

Table 1: Right hemisphere: original group data of TMS parameters (resting motor threshold, the coordinates of the centre of gravity, mean map MEP amplitude, map area, and map volume) for six experimental sessions in the right, nondominant hemisphere of twelve subjects.

	Session					
	Session 1	Session 2	Session 3	Session 4	Session 5	Session 6
RMT (% MSO)	43.1 ± 8.0	44.1 ± 8.6	44.2 ± 8.8	44.1 ± 8.4	43.0 ± 8.2	43.1 ± 8.4
CoG m-l (mm)	60.7 ± 6.4	61.3 ± 3.8	60.9 ± 5.4	60.9 ± 4.3	60.7 ± 4.6	60.0 ± 4.4
CoG a-p (mm)	109.0 ± 8.4	108.9 ± 9.7	108.0 ± 8.9	107.3 ± 10.6	107.2 ± 9.6	105.7 ± 10.9
Mean map MEP amplitude (μV)	255.6 ± 155.3	240.7 ± 147.9	165.3 ± 48.3	227.5 ± 177.7	190.9 ± 144.7	227.5 ± 118.1
Map area (mm^3)	1795.6 ± 1006	2291.4 ± 1118.3	2306.8 ± 1979.8	1958.4 ± 1597.6	1522.7 ± 969.4	2299.5 ± 1125.5
Map volume ($mm^3 * \mu$V)	512772.6 ± 475433.5	650398.9 ± 579946.1	405527.8 ± 380330.5	678479.5 ± 1120122.4	331512.3 ± 345943.7	579769.2 ± 444784.6

Mean ± SD.

Table 2: Left hemisphere: original group data of TMS parameters (resting motor threshold, the coordinates of the centre of gravity, mean map MEP amplitude, map area, and map volume) for six experimental sessions in the left, dominant hemisphere of six subjects.

	Session					
	Session 1	Session 2	Session 3	Session 4	Session 5	Session 6
RMT (% MSO)	42.3 ± 7.9	44.7 ± 7.4	44.7 ± 7.8	43.7 ± 7.9	44.3 ± 10.2	43.7 ± 8.7
CoG m-l (mm)	134.5 ± 6.2	135.5 ± 5.9	135.3 ± 7.2	133.9 ± 8.2	132.2 ± 7.2	131.0 ± 7.3
CoG a-p (mm)	108.9 ± 11.3	109.4 ± 9.5	106.9 ± 8.5	111.7 ± 8.2	112.4 ± 7.7	111.3 ± 8.9
Mean map MEP amplitude (μV)	242.5 ± 98.9	269.6 ± 106.8	275.5 ± 142.7	227.9 ± 122.7	209.5 ± 140.9	179.4 ± 53.1
Map area (mm^3)	1726.8 ± 1359.7	1805 ± 839.8	2134.0 ± 1530.9	1616.3 ± 1132.3	1818.5 ± 667.4	1491.5 ± 614.9
Map volume ($mm^3 * \mu$V)	442868.3 ± 470689.2	468965.8 ± 268648.9	531075.8 ± 324023.0	448895.9 ± 498086.2	381524.2 ± 239264.6	258593.3 ± 100338.3

Mean ± SD.

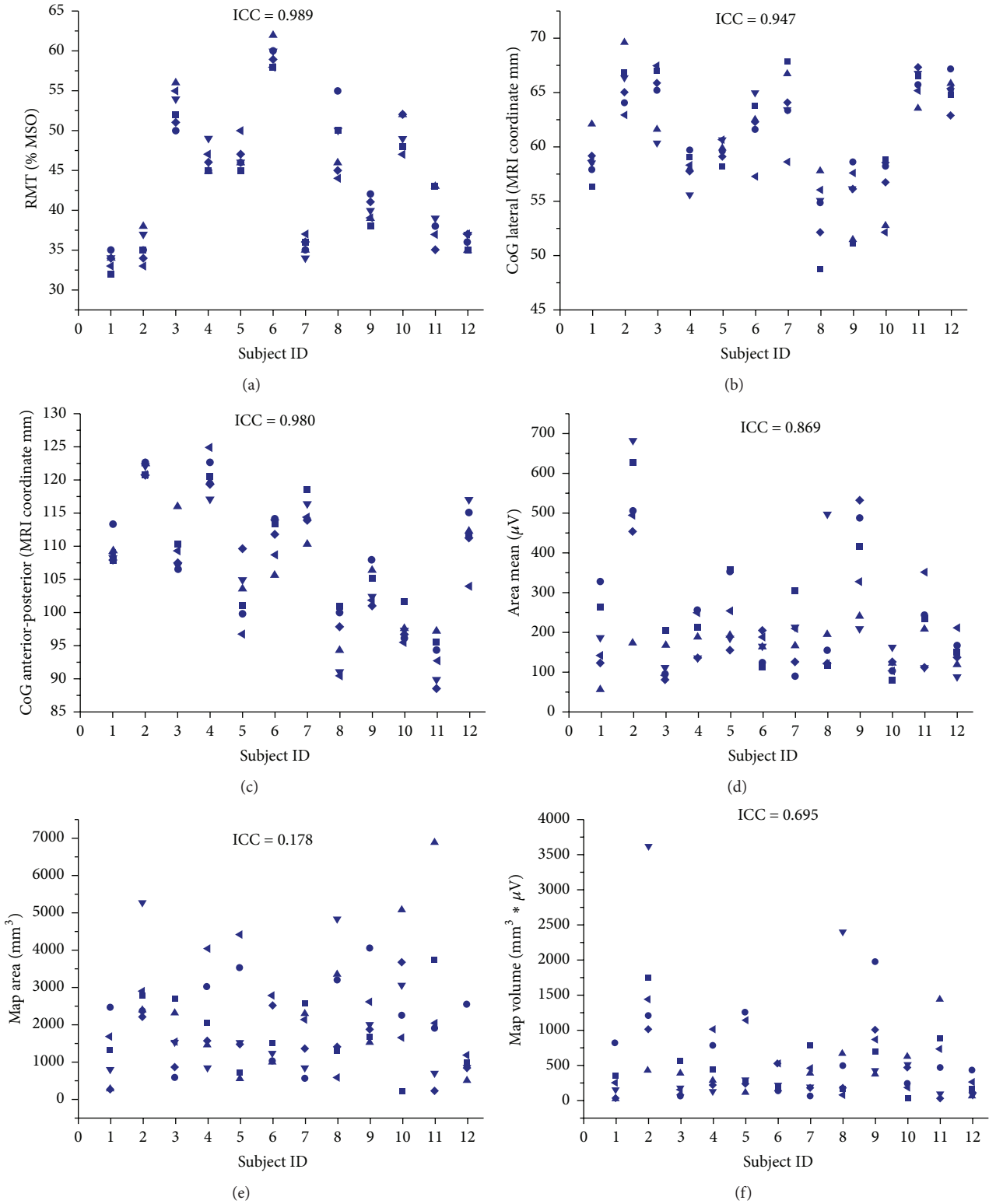

Figure 1: Intrasubject distribution of original data for six experimental sessions (■: Session 1; ●: Session 2; ▲: Session 3; ▼: Session 4; ◆: Session 5; ◂: Session 6) in the right, nondominant hemisphere of twelve subjects for RMT (a), medial-lateral CoG (b), anterior-posterior CoG (c), mean map MEP amplitude (d), map area (e), and map volume (f).

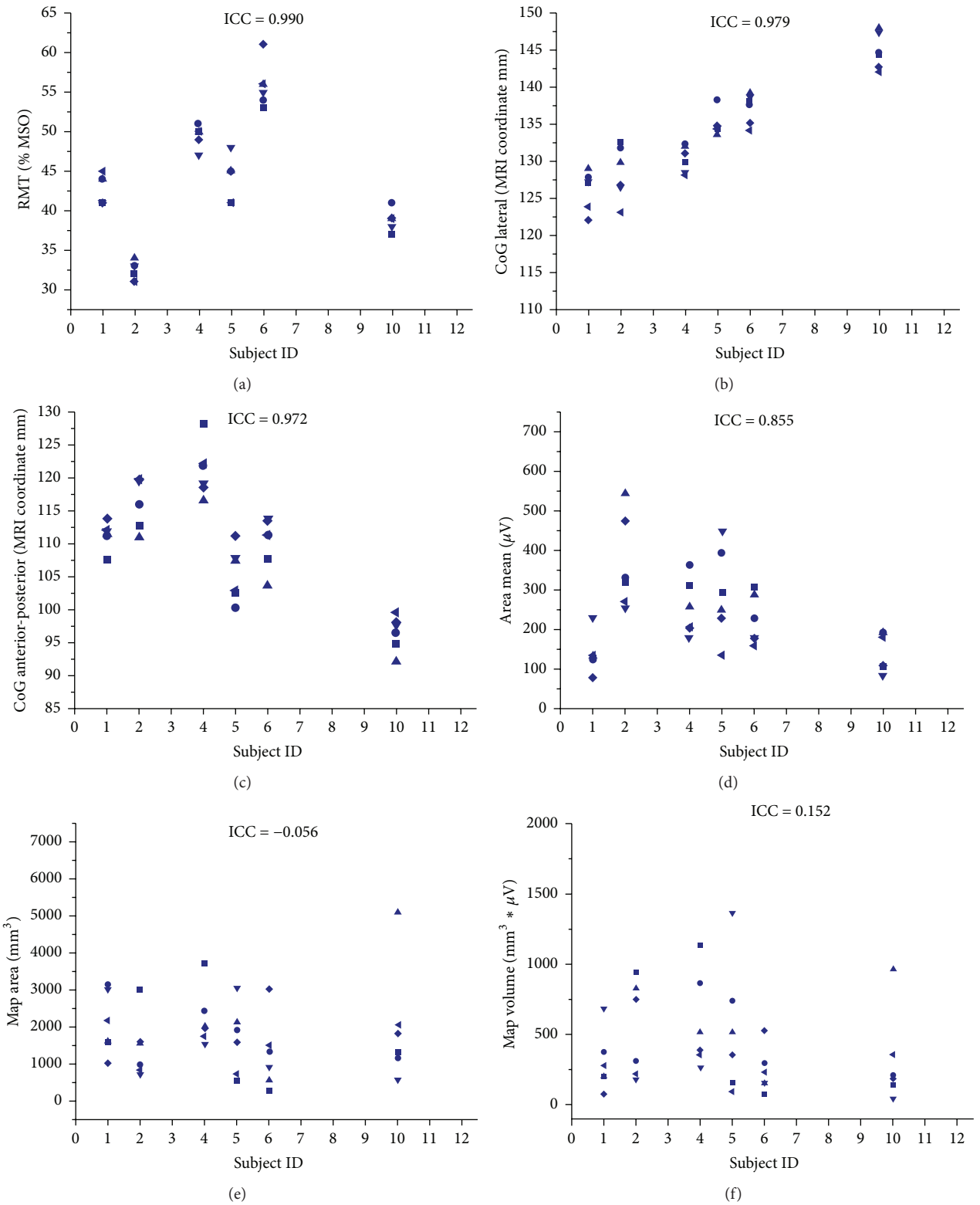

Figure 2: Intrasubject distribution of original data for six experimental sessions (■: Session 1; ●: Session 2; ▲: Session 3; ▼: Session 4; ◆: Session 5; ◂: Session 6) in the left, dominant hemisphere of six subjects for RMT (a), medial-lateral CoG (b), anterior-posterior CoG (c), mean map MEP amplitude (d), map area (e), and map volume (f).

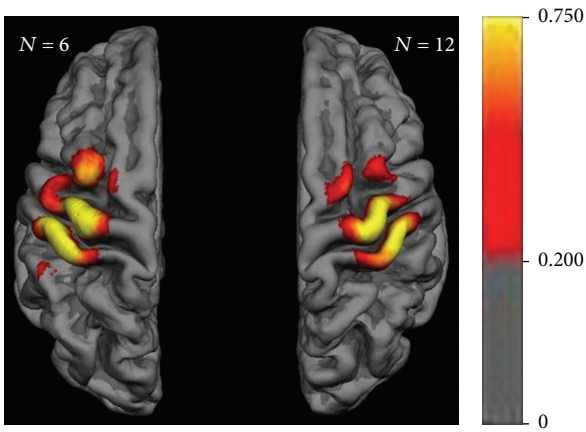

Figure 3: Motor map group data of individual means over time with mean overlap percentage. Color bar indicates percent of subjects presenting with MEPs > 50 μV throughout the experimental sessions.

3.3. Motor Map Group Data. The mean overlap percentage revealed a high spatial overlap over the hand area of M1 and the corresponding somatotopic sensory (S1) area of both hemispheres; that is, in these regions (indicated in yellow) at least 75% of the subjects presented with MEPs > 50 μV. This core area was surrounded by a fringe area (indicated in red) extending medially and laterally on M1 and S1 and anteriorly on the premotor (PM) cortex. In this fringe area, less than 75% of the subjects presented with MEPs > 50 μV (Figure 3).

The mean MEP amplitude depicted a smaller activation area than the previous overlap map; that is, activation was confined to those cortical areas in which all subjects had mean MEPs > 100 μV (indicated in yellow) and >50 μV (indicated in red) (Figure 4). Notably, this area covered a large part of M1 and S1 and extended towards the PM cortex in the left, dominant hemisphere, while it remained fairly restricted to the hand knob of M1 and the corresponding S1 in the right, nondominant hemisphere. These interhemispheric differences remained stable, even when the right cortical map was restricted to the very same six subjects who were analyzed for the left cortical map (Supplementary Figure 2).

3.4. Motor Map Reliability. The intraclass correlation (ICC) values for the MEP amplitudes at each mesh point confirmed the previous cortical maps (of the mean MEP amplitude), showing the same interhemispheric differences and revealing moderate to high reliability (up to >0.75) of the MEP amplitude in the course of the six experiments (Figure 5). Interestingly, these long-term correlations of the MEP amplitude at each stimulation site presented mosaic-like clusters of consistent corticospinal excitability spanning over distributed areas in the sensorimotor cortex.

4. Discussion

This study introduces complementary and highly consistent measures for capturing the extent of the cortical motor map with transcranial magnetic stimulation (TMS) and demonstrates the high test-retest reliability of these maps for

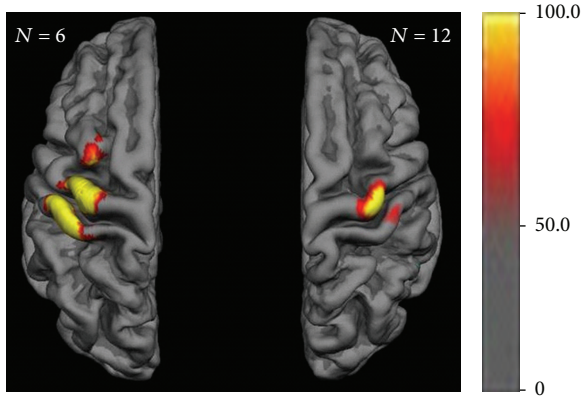

Figure 4: Motor map group data of individual means over time with mean MEP amplitude. Color bar indicates mean MEP amplitude in μV throughout the experimental sessions.

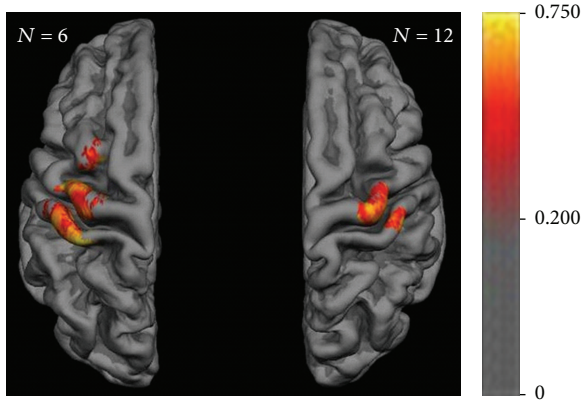

Figure 5: Motor map reliability with intraclass correlation (ICC) for the MEP amplitudes > 50 μV at each mesh point. Color bar indicates ICC value of repeatability in the course of the six experiments revealing mosaic-like clusters of consistent corticospinal excitability.

long observation periods by considering the individual gyral anatomy. We examined motor-evoked potentials (MEPs) of the extensor digitorum communis muscle of healthy subjects over a period of twelve weeks with six biweekly acquired TMS motor maps, whereas previous studies on TMS test-retest reliability spanned observation periods of one to six weeks with a total of two to three measurements only [15, 48–54]. The demonstrated consistency of the acquired motor map parameters over several months qualifies them as biomarkers for monitoring disease progression or the effects of therapeutic interventions, for example, in the context of neurorehabilitation. However, these results need to be extrapolated carefully to individuals with brain damage since patients might have more variable cortical physiology. Particular attention should be paid to the specific TMS parameters chosen for long-term monitoring. Like previous studies, but for longer observation periods, we were able to disentangle the highly stable TMS parameters, that is, the resting motor threshold (RMT), centre of gravity (CoG), and mean MEPs across all TMS sites, from the more variable ones, that is, the map area. We, therefore, suggest not transferring

the classical motor map parameters, *map area* and *volume*, to patients but rather the complementary ones introduced and tested in this study, that is, motor maps of the *mean spatial overlap*, the *mean MEP amplitude*, and the *intraclass correlations of the MEP amplitude* (see paragraphs below).

More specifically, the high reliability, captured by the intraclass correlation (ICC), of the RMT and mean map MEP amplitude confirmed previous findings following shorter observation periods [49–53]. Former findings on the consistency of the CoG were more variable [15, 48, 51, 53] than the high reliability in the present study for observation periods of up to 1.5 years.

When it came to the cortical representation area of corticospinal connectivity, the findings were more variable. With regard to the classical parameter *map area*, this study demonstrated poor reliability in the course of six sessions. This finding agrees with previous observations of decreasing reliability of the map area from moderate/high [51, 52] to poor/moderate [15] when increasing the length of the observation period and the number of measurements from two to three. These findings are probably related to the individual conditions of the subjects over time, that is, reflecting the natural daily or weekly fluctuations of the motor map extent [15]. To differentiate them from lasting cortical plasticity in the course of a disease or intervention, more stable cortical map parameters that are resistant to such natural fluctuations would be necessary.

Accordingly, complementary measures for capturing the extent of the cortical motor map were suggested in the present study and revealed spatially specific areas of high reliability throughout the whole observation period of twelve weeks: motor maps of the mean spatial overlap, the mean MEP amplitude, and the ICC of the MEP amplitude enabled us to disentangle a highly reliable core from the surrounding fringe areas of corticospinal connectivity. Future studies may test whether the demonstrated reliability of these complementary motor map parameters will persist when acquired with fixed coil positions (e.g., lateromedial, posteroanterior) or monophasic stimulation.

The overlap map of the present study revealed a core over the hand area of M1 and S1, surrounded by less consistent findings that extended medially and laterally on the sensorimotor cortex and anteriorly on the premotor cortex (Figure 3). These observations were confirmed by the two other motor maps, that is, maps of the mean MEP amplitude and the ICC of the MEP amplitude. However, both of these covered a smaller cortical area than the overlap map. Notably, the maps of the mean (Figure 4) and ICC (Figure 5) of the MEP amplitude in particular revealed relevant interhemispheric differences. In the left, dominant hemisphere, these maps covered a large area of M1 and S1 and extended towards the PM cortex, whereas they remained fairly restricted to the hand knob of M1 and the corresponding S1 in the right, nondominant hemisphere. Moreover, the ICC map unraveled mosaic-like clusters of consistent corticospinal excitability spanning over distributed areas in the sensorimotor cortex and intermingling with spots of decreased reliability.

We interpret the spatial differences between the overlap maps and the mean MEP amplitude maps as a reflection of the high variability of the classical TMS parameter *map area*. More specifically, we propose that the map area represents the instantaneous cortical representation, that is, the natural daily or weekly fluctuations of the motor map extent, and that the mean MEP amplitude map (Figure 4) reflects a stable motor map that is more resistant to this variability.

Rapid functional plasticity of the map area has already been described during different learning processes. Comparing implicit versus explicit motor learning could show an increase of the motor map during the implicit learning period, which was reversed to baseline as soon as explicit knowledge was gained [55]. In another study with Braille readers, the cortical map area varied with the activity of the hand, that is, showing a larger map area during working days than at weekends [56].

By contrast, the stable interhemispheric differences of the mean MEP amplitude map and the ICC map in this study were very probably related to the right-handedness of the participants. This implied a lifelong higher use of the right hand in activities of daily living and therefore a persistent use-dependent reorganization and more extended (towards premotor and somatosensory areas) cortical representation area of this hand in the left, dominant hemisphere [54, 57]. However, further studies with more subjects are necessary to draw definite conclusions.

The present study confirmed earlier animal experiments [58–61] and human studies [14, 39, 62–64], which indicated that corticospinal connections are not limited to the primary motor cortex but extend to different regions of the sensorimotor system. Approximately half of the primate brain's pyramidal tract neurons are located in postcentral areas, for example, the primary somatosensory cortex, sharing functional properties with regard to movement-related activity and discharge patterns as a function of muscle strength with precentral pyramidal tract neurons [31, 65–67]. In the present study, we confirmed this extended corticospinal connectivity of the somatosensory cortex and demonstrated marked interhemispheric differences, that is, highly reliable MEPs elicited from the left S1 of the dominant hemisphere, in healthy subjects. However, due to the rather nonfocal nature of TMS, a complementary explanation of these findings might be possible. Even if the centre of the TMS coil is over the primary somatosensory cortex, this does not necessarily mean that somatosensory cortex stimulation produces the descending volley. It could mean that neurons located rather posterior in the motor cortex, but still anterior to the somatosensory cortex, are activated by the magnetic stimulation delivered to S1 [39]. Therefore, we clearly acknowledge that it is not possible for this type of study to draw conclusions regarding the precise site of cortical stimulation. On the other hand, intraoperative electrical stimulation in humans with both mono- and bipolar focal stimulation of the premotor and somatosensory cortex also elicited MEPs [39, 63], supporting the hypothesis of direct corticospinal connectivity of nonprimary motor cortex areas.

Despite the fact that they have considerably less spatial resolution than surgical mapping techniques, the TMS maps unraveled mosaic-like clusters of consistent corticospinal excitability. This is consistent with the findings

of intracortical microstimulation in nonhuman primates which demonstrated that identical movements are elicited by the stimulation of multiple and noncontiguous sites [39, 60]. Although previous studies have already suggested that TMS maps are suitable for reproducing these experimental microstimulation findings in humans [15, 52], the present examination is the first to demonstrate the long-term reliability of this specific cortical pattern and to characterize the extended topographic distribution in the sensorimotor cortex intermingled with spots of decreased reliability. We consider this pattern to be evidence of the specific activation of neuronal pools in the respective cortical areas, for example, S1 or PM, thus rendering the alternative explanation, that is, the current spread to distant areas such as to M1 and the pyramidal tract, rather unlikely. These findings therefore underline the TMS technique presented here as a powerful and precise mapping tool for clinical and research application.

Interestingly, this study is the first to demonstrate the long-term retest reliability of corticospinal connectivity of the premotor cortex, for the left, dominant hemisphere in particular. The right, nondominant hemisphere showed a larger fluctuation of the PM corticospinal connectivity, suggesting that this pathway is a dormant reserve for compensatory activation, for example, when the nondominant hand is used more frequently or when lesions of the M1 corticospinal connections, for example, after stroke, necessitate alternative pathways. Along the same lines, recent neurofeedback interventions have explored the plasticity of the nondominant, right hemisphere in the healthy [39] and lesioned brain [37, 68]. These findings indicate that combining motor imagery-related β-band event-related desynchronization with proprioceptive feedback in a brain-robot interface environment [69, 70] might be sufficient to unmask latent corticospinal connectivity [37], redistribute sensorimotor connectivity patterns, and enhance corticospinal pathways of both the S1 and PM cortex [39, 71]. Moreover, pilot data applying this concept demonstrated operant conditioning of the targeted brain state and provided a direct brain-behavior relationship [72] with functional gains after stroke, which were specific for the trained task [68].

5. Conclusion

We demonstrated the high test-retest reliability of the applied TMS mapping technique for long observation periods. This study revealed the long-term reliability of motor maps with relevant interhemispheric differences, that is, more extended and stable corticospinal connectivity in the sensorimotor cortex and nonprimary motor areas of the left, dominant hemisphere. Different cortical maps allowed the disentangling of stable cortical reorganization from more rapid plastic fluctuations. Mosaic-like clusters of consistent corticospinal excitability spanning over distributed areas in the sensorimotor cortex indicated functionally specific and spatially precise activation of neuronal pools by TMS. Moreover, these findings may guide restorative interventions addressing dormant corticospinal connectivity for neurorehabilitation.

Competing Interests

The authors report no competing interests.

Acknowledgments

Dominic Kraus was supported by the Graduate Training Centre of Neuroscience, International Max Planck Research School for Cognitive and Systems Neuroscience, Tuebingen, Germany. The authors thank Dr. Robert Bauer for his statistical advice and Seyed A. Nicksirat for his help with the figures. Alireza Gharabaghi was supported by grants from the German Research Council [DFG GH 94/2-1, DFG EC 307] and from the Federal Ministry of Education and Research [BFNT 01GQ0761, BMBF 16SV3783, BMBF 0316064B, and BMBF 16SV5824].

References

[1] C. Xerri, "Plasticity of cortical maps: multiple triggers for adaptive reorganization following brain damage and spinal cord injury," *The Neuroscientist*, vol. 18, no. 2, pp. 133–148, 2012.

[2] R. J. Nudo and G. W. Milliken, "Reorganization of movement representations in primary motor cortex following focal ischemic infarcts in adult squirrel monkeys," *Journal of Neurophysiology*, vol. 75, no. 5, pp. 2144–2149, 1996.

[3] S. B. Frost, S. Barbay, K. M. Friel, E. J. Plautz, and R. J. Nudo, "Reorganization of remote cortical regions after ischemic brain injury: a potential substrate for stroke recovery," *Journal of Neurophysiology*, vol. 89, no. 6, pp. 3205–3214, 2003.

[4] D. Ramanathan, J. M. Conner, and M. H. Tuszynski, "A form of motor cortical plasticity that correlates with recovery of function after brain injury," *Proceedings of the National Academy of Sciences of the United States of America*, vol. 103, no. 30, pp. 11370–11375, 2006.

[5] G. Di Pino, G. Pellegrino, G. Assenza et al., "Modulation of brain plasticity in stroke: a novel model for neurorehabilitation," *Nature Reviews Neurology*, vol. 10, no. 10, pp. 597–608, 2014.

[6] H. G. T. Becker, T. Haarmeier, M. Tatagiba, and A. Gharabaghi, "Electrical stimulation of the human homolog of the medial superior temporal area induces visual motion blindness," *The Journal of Neuroscience*, vol. 33, no. 46, pp. 18288–18297, 2013.

[7] H. Duffau, "Lessons from brain mapping in surgery for low-grade glioma: insights into associations between tumour and brain plasticity," *The Lancet Neurology*, vol. 4, no. 8, pp. 476–486, 2005.

[8] P. M. Rossini, D. Burke, R. Chen et al., "Non-invasive electrical and magnetic stimulation of the brain, spinal cord, roots and peripheral nerves: basic principles and procedures for routine clinical and research application. An updated report from an I.F.C.N. Committee," *Clinical Neurophysiology*, vol. 126, no. 6, pp. 1071–1107, 2015.

[9] R. Traversa, P. Cicinelli, A. Bassi, P. M. Rossini, and G. Bernardi, "Mapping of motor cortical reorganization after stroke: a brain simulation study with focal magnetic pulses," *Stroke*, vol. 28, no. 1, pp. 110–117, 1997.

[10] C. M. Bütefisch, R. Kleiser, and R. J. Seitz, "Post-lesional cerebral reorganisation: evidence from functional neuroimaging and transcranial magnetic stimulation," *Journal of Physiology-Paris*, vol. 99, no. 4–6, pp. 437–454, 2006.

[11] J. Liepert, H. Bauder, W. H. R. Miltner, E. Taub, and C. Weiller, "Treatment-induced cortical reorganization after stroke in humans," *Stroke*, vol. 31, no. 6, pp. 1210–1216, 2000.

[12] J. Liepert, W. H. R. Miltner, H. Bauder et al., "Motor cortex plasticity during constraint-induced movement therapy in stroke patients," *Neuroscience Letters*, vol. 250, no. 1, pp. 5–8, 1998.

[13] D. P. Carey, S. Della Sala, and M. Ietswaart, "Neuropsychological perspectives on eye-hand coordination in visually-guided reaching," *Progress in Brain Research*, vol. 140, pp. 311–327, 2002.

[14] S. Teitti, S. Määttä, L. Säisänen et al., "Non-primary motor areas in the human frontal lobe are connected directly to hand muscles," *NeuroImage*, vol. 40, no. 3, pp. 1243–1250, 2008.

[15] C. Weiss, C. Nettekoven, A. K. Rehme et al., "Mapping the hand, foot and face representations in the primary motor cortex—retest reliability of neuronavigated TMS versus functional MRI," *NeuroImage*, vol. 66, pp. 531–542, 2013.

[16] C. Schönfeldt-Lecuona, A. Thielscher, R. W. Freudenmann, M. Kron, M. Spitzer, and U. Herwig, "Accuracy of stereotaxic positioning of transcranial magnetic stimulation," *Brain Topography*, vol. 17, no. 4, pp. 253–259, 2005.

[17] P. Julkunen, L. Säisänen, N. Danner et al., "Comparison of navigated and non-navigated transcranial magnetic stimulation for motor cortex mapping, motor threshold and motor evoked potentials," *NeuroImage*, vol. 44, no. 3, pp. 790–795, 2009.

[18] S. Schmidt, R. Bathe-Peters, R. Fleischmann, M. Rönnefarth, M. Scholz, and S. A. Brandt, "Nonphysiological factors in navigated TMS studies; confounding covariates and valid intracortical estimates," *Human Brain Mapping*, vol. 36, no. 1, pp. 40–49, 2015.

[19] E. Raffin, G. Pellegrino, V. Di Lazzaro, A. Thielscher, and H. R. Siebner, "Bringing transcranial mapping into shape: sulcus-aligned mapping captures motor somatotopy in human primary motor hand area," *NeuroImage*, vol. 120, pp. 164–175, 2015.

[20] P. T. Fox, S. Narayana, N. Tandon et al., "Column-based model of electric field excitation of cerebral cortex," *Human Brain Mapping*, vol. 22, no. 1, pp. 1–14, 2004.

[21] F. S. Salinas, J. L. Lancaster, and P. T. Fox, "3D modeling of the total electric field induced by transcranial magnetic stimulation using the boundary element method," *Physics in Medicine and Biology*, vol. 54, no. 12, pp. 3631–3647, 2009.

[22] A. Thielscher and F. A. Wichmann, "Determining the cortical target of transcranial magnetic stimulation," *NeuroImage*, vol. 47, no. 4, pp. 1319–1330, 2009.

[23] A. Opitz, M. Windhoff, R. M. Heidemann, R. Turner, and A. Thielscher, "How the brain tissue shapes the electric field induced by transcranial magnetic stimulation," *NeuroImage*, vol. 58, no. 3, pp. 849–859, 2011.

[24] A. Opitz, W. Legon, A. Rowlands, W. K. Bickel, W. Paulus, and W. J. Tyler, "Physiological observations validate finite element models for estimating subject-specific electric field distributions induced by transcranial magnetic stimulation of the human motor cortex," *NeuroImage*, vol. 81, pp. 253–364, 2013.

[25] A. Opitz, N. Zafar, V. Bockermann, V. Rohde, and W. Paulus, "Validating computationally predicted TMS stimulation areas using direct electrical stimulation in patients with brain tumors near precentral regions," *NeuroImage: Clinical*, vol. 4, pp. 500–507, 2014.

[26] E. Niskanen, P. Julkunen, L. Säisänen, R. Vanninen, P. Karjalainen, and M. Könönen, "Group-level variations in motor representation areas of thenar and anterior tibial muscles: navigated transcranial magnetic stimulation study," *Human Brain Mapping*, vol. 31, no. 8, pp. 1272–1280, 2010.

[27] S. Diekhoff, K. Uludağ, R. Sparing et al., "Functional localization in the human brain: gradient-echo, spin-echo, and arterial spin-labeling fMRI compared with neuronavigated TMS," *Human Brain Mapping*, vol. 32, no. 3, pp. 341–357, 2011.

[28] S. Ngomo, G. Leonard, and C. Mercier, "Influence of the amount of use on hand motor cortex representation: effects of immobilization and motor training," *Neuroscience*, vol. 220, pp. 208–214, 2012.

[29] M. van de Ruit and M. J. Grey, "The TMS map scales with increased stimulation intensity and muscle activation," *Brain Topography*, vol. 29, no. 1, pp. 56–66, 2016.

[30] J. Meincke, M. Hewitt, G. Batsikadze, and D. Liebetanz, "Automated TMS hotspot-hunting using a closed loop threshold-based algorithm," *NeuroImage*, vol. 124, pp. 509–517, 2016.

[31] D. Kraus and A. Gharabaghi, "Projecting navigated TMS sites on the gyral anatomy decreases inter-subject variability of cortical motor maps," *Brain Stimulation*, vol. 8, no. 4, pp. 831–837, 2015.

[32] R. C. Oldfield, "The assessment and analysis of handedness: the edinburgh inventory," *Neuropsychologia*, vol. 9, no. 1, pp. 97–113, 1971.

[33] S. Rossi, M. Hallett, P. M. Rossini et al., "Safety, ethical considerations, and application guidelines for the use of transcranial magnetic stimulation in clinical practice and research," *Clinical Neurophysiology*, vol. 120, no. 12, pp. 2008–2039, 2009.

[34] M. Vukelić, R. Bauer, G. Naros, I. Naros, C. Braun, and A. Gharabaghi, "Lateralized alpha-band cortical networks regulate volitional modulation of beta-band sensorimotor oscillations," *NeuroImage*, vol. 87, pp. 147–153, 2014.

[35] M. Vukelić and A. Gharabaghi, "Oscillatory entrainment of the motor cortical network during motor imagery is modulated by the feedback modality," *NeuroImage*, vol. 111, pp. 1–11, 2015.

[36] M. Vukelić and A. Gharabaghi, "Self-regulation of circumscribed brain activity modulates spatially selective and frequency specific connectivity of distributed resting state networks," *Frontiers in Behavioral Neuroscience*, vol. 9, 2015.

[37] A. Gharabaghi, D. Kraus, M. T. Leão et al., "Coupling brain-machine interfaces with cortical stimulation for brain-state dependent stimulation: enhancing motor cortex excitability for neurorehabilitation," *Frontiers in Human Neuroscience*, vol. 8, article 122, 2014.

[38] A. Gharabaghi, G. Naros, F. Khademi et al., "Learned self-regulation of the lesioned brain with epidural electrocorticography," *Frontiers in Behavioral Neuroscience*, vol. 8, article 429, 2014.

[39] D. Kraus, G. Naros, R. Bauer, M. T. Leão, U. Ziemann, and A. Gharabaghi, "Brain-robot interface driven plasticity: distributed modulation of corticospinal excitability," *NeuroImage*, vol. 125, pp. 522–532, 2016.

[40] S. Groppa, A. Oliviero, A. Eisen et al., "A practical guide to diagnostic transcranial magnetic stimulation: report of an IFCN committee," *Clinical Neurophysiology*, vol. 123, no. 5, pp. 858–882, 2012.

[41] U. Ziemann, S. Lönnecker, B. J. Steinhoff, and W. Paulus, "Effects of antiepileptic drugs on motor cortex excitability in humans: A Transcranial Magnetic Stimulation Study," *Annals of Neurology*, vol. 40, no. 3, pp. 367–378, 1996.

[42] M. van de Ruit, M. J. L. Perenboom, and M. J. Grey, "TMS brain mapping in less than two minutes," *Brain Stimulation*, vol. 8, no. 2, pp. 231–239, 2015.

[43] E. M. Wassermann, L. M. McShane, M. Hallett, and L. G. Cohen, "Noninvasive mapping of muscle representations in human motor cortex," *Electroencephalography and Clinical Neurophysiology*, vol. 85, no. 1, pp. 1–8, 1992.

[44] J. Ashburner and K. J. Friston, "Unified segmentation," *NeuroImage*, vol. 26, no. 3, pp. 839–851, 2005.

[45] A. M. Dale, B. Fischl, and M. I. Sereno, "Cortical surface-based analysis. I. Segmentation and surface reconstruction," *NeuroImage*, vol. 9, no. 2, pp. 179–194, 1999.

[46] L. G. Portney and M. P. Watkins, *Foundations of Clinical Research: Applications to Practice*, Prentice Hall, Upper Saddle River, NJ, USA, 2000.

[47] K. O. McGraw and S. P. Wong, "Forming inferences about some intraclass correlation coefficients," *Psychological Methods*, vol. 1, no. 1, pp. 30–46, 1996.

[48] M.-T. Forster, M. Limbart, V. Seifert, and C. Senft, "Test-retest reliability of navigated transcranial magnetic stimulation of the motor cortex," *Neurosurgery*, vol. 10, no. 1, pp. 51–55, 2014.

[49] A. Cacchio, M. Paoloni, N. Cimini et al., "Reliability of TMS-related measures of tibialis anterior muscle in patients with chronic stroke and healthy subjects," *Journal of the Neurological Sciences*, vol. 303, no. 1-2, pp. 90–94, 2011.

[50] A. Cacchio, N. Cimini, P. Alosi, V. Santilli, and A. Marrelli, "Reliability of transcranial magnetic stimulation-related measurements of tibialis anterior muscle in healthy subjects," *Clinical Neurophysiology*, vol. 120, no. 2, pp. 414–419, 2009.

[51] M. P. Malcolm, W. J. Triggs, K. E. Light, O. Shechtman, G. Khandekar, and L. J. Gonzalez Rothi, "Reliability of motor cortex transcranial magnetic stimulation in four muscle representations," *Clinical Neurophysiology*, vol. 117, no. 5, pp. 1037–1046, 2006.

[52] P. Mortifee, H. Stewart, M. Schulzer, and A. Eisen, "Reliability of transcranial magnetic stimulation for mapping the human motor cortex," *Electroencephalography and Clinical Neurophysiology/Evoked Potentials Section*, vol. 93, no. 2, pp. 131–137, 1994.

[53] K. M. McGregor, H. Carpenter, E. Kleim et al., "Motor map reliability and aging: a TMS/fMRI study," *Experimental Brain Research*, vol. 219, no. 1, pp. 97–106, 2012.

[54] S. L. Wolf, A. J. Butler, G. I. Campana et al., "Intra-subject reliability of parameters contributing to maps generated by transcranial magnetic stimulation in able-bodied adults," *Clinical Neurophysiology*, vol. 115, no. 8, pp. 1740–1747, 2004.

[55] A. Pascual-Leone, J. Grafman, and M. Hallett, "Modulation of cortical motor output maps during development of implicit and explicit knowledge," *Science*, vol. 263, no. 5151, pp. 1287–1289, 1994.

[56] A. Pascual-Leone, E. M. Wassermann, N. Sadato, and M. Hallett, "The role of reading activity on the modulation of motor cortical outputs to the reading hand in Braille readers," *Annals of Neurology*, vol. 38, no. 6, pp. 910–915, 1995.

[57] H. R. Siebner and J. Rothwell, "Transcranial magnetic stimulation: new insights into representational cortical plasticity," *Experimental Brain Research*, vol. 148, no. 1, pp. 1–16, 2003.

[58] S.-Q. He, R. P. Dum, and P. L. Strick, "Topographic organization of corticospinal projections from the frontal lobe: motor areas on the lateral surface of the hemisphere," *Journal of Neuroscience*, vol. 13, no. 3, pp. 952–980, 1993.

[59] S.-Q. He, R. P. Dum, and P. L. Strick, "Topographic organization of corticospinal projections from the frontal lobe: motor areas on the medial surface of the hemisphere," *The Journal of Neuroscience*, vol. 15, no. 5 I, pp. 3284–3306, 1995.

[60] G. W. Huntley and E. G. Jones, "Relationship of intrinsic connections to forelimb movement representations in monkey motor cortex: a correlative anatomic and physiological study," *Journal of Neurophysiology*, vol. 66, no. 2, pp. 390–413, 1991.

[61] E. G. Jones and S. P. Wise, "Size, laminar and columnar distribution of efferent cells in the sensory-motor cortex of monkeys," *The Journal of Comparative Neurology*, vol. 175, no. 4, pp. 391–437, 1977.

[62] T. Kombos, T. Pietilä, B.-C. Kern et al., "Demonstration of cerebral plasticity by intra-operative neurophysiological monitoring: report of an uncommon case," *Acta Neurochirurgica*, vol. 141, no. 8, pp. 885–889, 1999.

[63] T. Kombos, O. Suess, B.-C. Kern et al., "Comparison between monopolar and bipolar electrical stimulation of the motor cortex," *Acta Neurochirurgica*, vol. 141, no. 12, pp. 1295–1301, 1999.

[64] S. Schmidt, R. Fleischmann, R. Bathe-Peters, K. Irlbacher, and S. A. Brandt, "Evolution of premotor cortical excitability after cathodal inhibition of the primary motor cortex: a sham-controlled serial navigated TMS study," *PLoS ONE*, vol. 8, no. 2, Article ID e57425, 2013.

[65] J. R. Russel and W. DeMyer, "The quantitative corticoid origin of pyramidal axons of Macaca rhesus. With some remarks on the slow rate of axolysis," *Neurology*, vol. 11, pp. 96–108, 1961.

[66] E. A. Murray and J. D. Coulter, "Organization of corticospinal neurons in the monkey," *The Journal of Comparative Neurology*, vol. 195, no. 2, pp. 339–365, 1981.

[67] C. Fromm and E. V. Evarts, "Pyramidal tract neurons in somatosensory cortex: central and peripheral inputs during voluntary movement," *Brain Research*, vol. 238, no. 1, pp. 186–191, 1982.

[68] G. Naros and A. Gharabaghi, "Reinforcement learning of self-regulated β-oscillations for motor restoration in chronic stroke," *Frontiers in Human Neuroscience*, vol. 9, article 391, 2015.

[69] R. Bauer, M. Fels, M. Vukelić, U. Ziemann, and A. Gharabaghi, "Bridging the gap between motor imagery and motor execution with a brain-robot interface," *NeuroImage*, vol. 108, pp. 319–327, 2015.

[70] M. Fels, R. Bauer, and A. Gharabaghi, "Predicting workload profiles of brain-robot interface and electromygraphic neurofeedback with cortical resting-state networks: personal trait or task-specific challenge?" *Journal of Neural Engineering*, vol. 12, no. 4, article 046029, 2015.

[71] D. Kraus, G. Naros, R. Bauer et al., "Brain state-dependent transcranial magnetic closed-loop stimulation controlled by sensorimotor desynchronization induces robust increase of corticospinal excitability," *Brain Stimulation*, vol. 9, no. 3, pp. 415–424, 2016.

[72] G. Naros, I. Naros, F. Grimm, U. Ziemann, and A. Gharabaghi, "Reinforcement learning of self-regulated sensorimotor β-oscillations improves motor performance," *NeuroImage*, vol. 134, pp. 142–152, 2016.